University of New Hampshire
University of New Hampshire Scholars' Repository

Doctoral Dissertations | Student Scholarship

Fall 1977

MIXING IN INTERMESHING TWIN SCREW EXTRUDERS

JAGDISH MAHESHRI MAHESHRI
University of New Hampshire, Durham

Follow this and additional works at: https://scholars.unh.edu/dissertation

Recommended Citation
MAHESHRI, JAGDISH MAHESHRI, "MIXING IN INTERMESHING TWIN SCREW EXTRUDERS" (1977). *Doctoral Dissertations*. 2370.
https://scholars.unh.edu/dissertation/2370

This Dissertation is brought to you for free and open access by the Student Scholarship at University of New Hampshire Scholars' Repository. It has been accepted for inclusion in Doctoral Dissertations by an authorized administrator of University of New Hampshire Scholars' Repository. For more information, please contact nicole.hentz@unh.edu.

INFORMATION TO USERS

This material was produced from a microfilm copy of the original document. While the most advanced technological means to photograph and reproduce this document have been used, the quality is heavily dependent upon the quality of the original submitted.

The following explanation of techniques is provided to help you understand markings or patterns which may appear on this reproduction.

1. The sign or "target" for pages apparently lacking from the document photographed is "Missing Page(s)". If it was possible to obtain the missing page(s) or section, they are spliced into the film along with adjacent pages. This may have necessitated cutting thru an image and duplicating adjacent pages to insure you complete continuity.

2. When an image on the film is obliterated with a large round black mark, it is an indication that the photographer suspected that the copy may have moved during exposure and thus cause a blurred image. You will find a good image of the page in the adjacent frame.

3. When a map, drawing or chart, etc., was part of the material being photographed the photographer followed a definite method in "sectioning" the material. It is customary to begin photoing at the upper left hand corner of a large sheet and to continue photoing from left to right in equal sections with a small overlap. If necessary, sectioning is continued again — beginning below the first row and continuing on until complete.

4. The majority of users indicate that the textual content is of greatest value, however, a somewhat higher quality reproduction could be made from "photographs" if essential to the understanding of the dissertation. Silver prints of "photographs" may be ordered at additional charge by writing the Order Department, giving the catalog number, title, author and specific pages you wish reproduced.

5. PLEASE NOTE: Some pages may have indistinct print. Filmed as received.

University Microfilms International
300 North Zeeb Road
Ann Arbor, Michigan 48106 USA
St. John's Road, Tyler's Green
High Wycombe, Bucks, England HP10 8HR

77-23,648

MAHESHRI, Jagdish Maheshri, 1947-
MIXING IN INTERMESHING TWIN SCREW EXTRUDERS.

University of New Hampshire,
Ph.D., 1977
Engineering, chemical

Xerox University Microfilms, Ann Arbor, Michigan 48106

MIXING IN INTERMESHING TWIN SCREW EXTRUDERS

by

JAGDISH MAHESHRI
B.S., University of Bombay, 1970
M.S., University of New Hampshire, 1972

A DISSERTATION

Submitted to the University of New Hampshire
In Partial Fulfillment of
The Requirement for the Degree of

Doctor of Philosophy
Graduate School
Engineering Ph.D. Program
Transport Phenomena
September, 1977

This thesis has been examined and approved.

Charles E. Wyman

Thesis director, Charles E. Wyman
Assistant Professor of Chemical Engineering

Stephen S.T. Fan

Stephen S.T. Fan
Professor of Chemical Engineering

S. S. Kuo

Shan S. Kuo
Professor of Mathematics

John A. Wilson

John A. Wilson
Associate Professor of Mechanical Engineering

Frank L. Pilar

Frank L. Pilar
Professor of Chemistry

May 25, 1977

Date

ACKNOWLEDGEMENTS

I am in deep gratitude to my advisor, Professor Charles E. Wyman, for his valuable guidance and continued encouragement in completing this work. His careful reading and important comments on the original draft of this thesis have contributed a great deal in shaping the final manuscript. I sincerely appreciate his time and patience; and the series of discussions we had proved to be very beneficial to me.

During the course of this work, discussions with the research personnel of the North American Bitruder Company in Springfield, Vermont, helped me in understanding various practical aspects of twin screw extruders. Mr. Paul Nobel, Mr. George Tremblay, and Mr. Ralph Weisse of the North American Bitruder Co. deserve special mention for their valuable suggestions.

The excellent help provided by Mr. Gregory Jones and Mr. Ken Palmer in building the experimental simulation unit is sincerely appreciated. Mr. Warren Celli deserves thanks for his timely help on diagrams for this thesis.

During my Ph.D. years, the Department of Chemical Engineering provided me with a financial support in the form of a teaching assistantship and money for supplies for which I express my gratitude. I am thankful to Professor Fan, our Department Chairman, for being concerned and encouraging me during my graduate years. The experimental analysis was

made possible by the Central University Research Fund of the University of New Hampshire.

My wife Pushpa deserves very special credit and thanks for her continued support, patience, and understanding without which this work would not be possible. I express my gratitude to my brothers for their moral support.

TABLE OF CONTENTS

LIST OF TABLES

LIST OF FIGURES

ABSTRACT

Mixing in Intermeshing Twin Screw Extruders

by

Jagdish Maheshri

In this work, three models are studied to describe Newtonian, isothermal, steady laminar flow in the melt conveying channel of an intermeshing twin screw extruder. Since the primary aim of this thesis is to analyze flow in the end regions where both screw intermesh and the helical geometrical configuration of the system and the associated boundary conditions pose serious difficulties in solving the equation of motion, only the middle of the channel width is considered and the cross channel velocity component is ignored. Thus, the equation of motion is solved for the down channel and channel depth velocity components. Using the stream function, these equations for the two components of velocity are reduced to an elliptic fourth order partial differential equation, a biharmonic equation.

As a result of the rapidly varying pressure gradients in the end regions of the channel, the exact analytical solution for the equation of motion is not possible. To solve the biharmonic equation, two finite difference numerical methods are considerd, and their relative merits

are critically examined on a test problem. The biharmonic equation in cylindrical coordinates for a zero helix angle twin screw channel is solved by a coupled pair of Poisson equations, while the direct iterative method is employed for the models in rectangular coordinates.

An experimental simulation unit was built to test the zero helix angle twin screw models. Motion pictures of polywax particles in 1000 cp silicone oil were taken to obtain experimental velocity profiles, and the results compared well with those obtained by the cylindrical model. The descrepancies in these results due to leakage of fluid in and out of the channel were analysed by fitting the experimental velocity data by least squares and calculating the flow rate based upon the experimental velocity profile.

The cylindrical model is compared with the flat plate models for a zero helix angle case, and the curved boundary flat plate model is then extended to a nonzero helix angle twin screw extruder channel. Numerical results are obtained for 0, 15, 30, and 45 degree helix angle channels in the co-rotating as well as counter-rotating mode of operation. From the predicted velocity profiles, the total shear strain distribution across the channel depth is calculated by following several streamlines, and based on these results, mixing in a twin screw extruder is analyzed.

In order to compare mixing in a single screw to that in a twin screw extruder, the middle part of the channel width and length is considered. For a twin screw channel, a

uniform strain distribution is found as opposed to the widely varying strain distribution in a single screw extruder and is probably responsible for the better mixing in twin screw extruders. Also, a phenomenon called "splitting" is found which greatly improves mixing in twin screw extruders by providing a dividing and combining action for the fluid.

I INTRODUCTION

Extrusion is one of the most important forming techniques of polymer processing. More thermoplastics are converted into useful products by extrusion than by any other method [24]. Plastic film, pipe, rod, and plastic coated wire and paper are a few examples of commercially important products manufactured by extrusion processes.

The word "extrude" originates in the Latin words "ex" (out) and "trudere" (to thrust), and thus, it closely describes the process itself as "shaping by forcing through an exit opening called the die" [36]. This is accomplished, generally, by a screw rotating in a cylindrical barrel. The feed to the extruder may be solid or it may sometimes be liquid. When fed by a solid, it is called as a plasticating extruder while if it is fed by a liquid, it is termed a melt extruder. For a plasticating extruder, solid feed may be composed of homopolymers, copolymers, or polymer blends. The feed is introduced at one end of the extruder, and as it advances along the extruder length, it is melted, homogenized (or reacted if the extruder is used as a reactor), and transported to the die at high pressure and temperature for forming into product.

In a plasticating extruder, as the feed advances along the extruder length towards the die, it passes through the

three distinct zones (Fig:1.1). The first zone, the solid conveying zone, begins at the feed inlet; and solid feed moves forward in the form of a plug. In doing so, the frictional forces between the barrel surface and the solid plug subject the solid particles to considerable shear; and they are consequently crushed to smaller size. The solid conveying zone extends to a point where the solid particles just begin to melt. Then, the next zone, where the solid polymer and its melt coexists, begins. This zone extends over a major part of the extruder and is called the melting zone or the transition zone. Melting of the solid particles is caused by thermal energy applied to the polymer by conduction through the hot barrel surface from external heaters and by conversion of mechanical energy to heat through viscous dissipation in the viscous melts. The melting zone is very important since the behavior of the polymer in this region has a profound effect on both the extruder performance and the extrudate quality. The last zone, the melt conveying zone or the metering zone, begins at the point where all solid particles are completely melted and extends to the outlet of the extruder, the die. In this zone, the melt is homogenized and delivered to the die at high pressure and temperature for forming into a finished product. Of course, for a melt extruder, the melt conveying zone extends from the feed end all the way up to the die of the extruder since there is no solid present [36].

Until the early nineteen forties, the design of

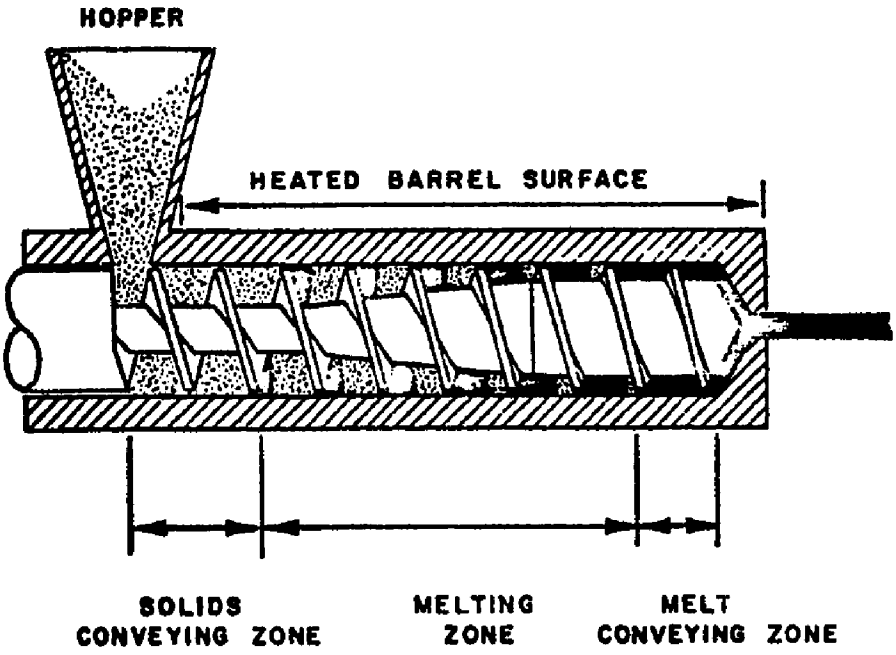

FIGURE I.1 SCHEMATIC PICTURE OF A PLASTICATING SINGLE SCREW EXTRUDER

extruders remained a mechanical art. With rapidly expanding plastic markets and rising labor and processing costs, a great deal of interest developed among scientists, engineers, and process workers in understanding the principles of extrusion operation; and consequently, modern extrusion theory was developed [6]. At least part of the plasticating process can now be described by mathematical relationships through the application of theories developed in rheology, thermodynamics, and fluid dynamics.

Early plastic extrusion was almost exclusively carried out by single screw machines. Most of the fluid in the melt conveying zone of a single screw is contained in the channel formed between the bottom (the screw root) and sides of the screw channel (the flights) and the barrel surface (Fig:1.1). Because of the rotation of the screw, the fluid is contained within a system that has both a moving boundary (the screw root and the channel flights) and a stationary boundary (the barrel surface); hence drag flow is established in the fluid due to its viscosity. It is this drag flow which enables the single screw extruder to transport the viscous material from the feed end to the die. The flow through the extruder can be reduced by restricting the die which results in a "back flow" or pressure flow of the fluid. This pressure flow opposes the drag flow and thus alters the velocity profile in the channel with a net effect of decreasing the flow rate and increasing the mixing. When the die is completely closed, the pressure

flow equals the drag flow and the net discharge becomes zero [24].

The fluid particles on the barrel surface and on the screw root for any degree of pressure flow do not move in the axial direction at all, while those contained in the space between the barrel surface and the screw root do. Except for the no net discharge condition, the maximum axial velocity occurs at the center. Thus, the fluid particles between the barrel surface and the screw root have a wide variety of residence times so that the heat and work treatment to the fluid particles varies over a wide range. Thus, it is very difficult to produce a homogeneous product. Also, heat sensitive material requiring a very short residence time with a narrow distribution can not be effectively processed in a single screw device [26]. Another important limitation of single screw extruder is that for good mixing the die has to be closed to some degree, thus sacrifycing the throughput rate [36].

With the enormous growth of the plastic industry, new tougher, and specialized materials - homopolymers, copolymers, and various blends - have to be processed at conditions enabling very accurate temperature control, uniform residence time, and better mixing [26]. A different type of extruder, the twin screw extruder offers all of these processing capabilities; and consequently they have become more important in the plastic industry for production of high quality products. The increased popularity of twin

screw extruders is demonstrated by the statistical analysis of extrusion machines in use today in the United States [29]. According to this survey, twin screws have been replacing single screws in many extrusion processes including manufacturing sheets, pipe, rods and profiles, wire and cable coatings, textile fiber, lay flat or quenched film, blown film, pelletizing, extrusion coating and flexible tubing.

In the twin screw device, instead of a single screw rotating in a tightly fitted barrel, two screws rotate in a tightly fitted figure "8" shaped barrel (Fig:1.2). There are different kinds of twin screw extruders in use today which can be classified into two major groups - intermeshing and nonintermeshing. In an intermeshing twin screw extruder (Fig:1.3), the land (the flight crest) of either screw virtually contacts the screw root of the other; while in a nonintermeshing twin screw extruder the lands of one screw just clear the lands of the other. Each of these two major groups can be further subdivided as to the mode of rotation of the two screws. When both screws rotate in the same direction, they are termed co-rotating while if they rotate in opposite directions, they are referred to as counter-rotating (Fig:1.3). Co-rotating can be either for both screws moving clockwise or anticlockwise while counter-rotating can be either with one screw turning clockwise and the other anticlockwise, or vice a versa. The differences between the co-rotating and the counter-rotating

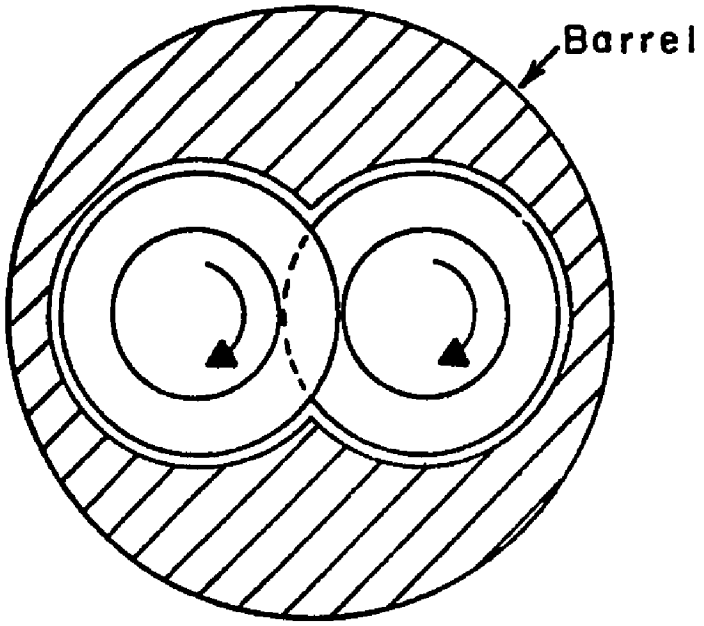

CO-ROTATING TWIN SCREW
(cut away view)

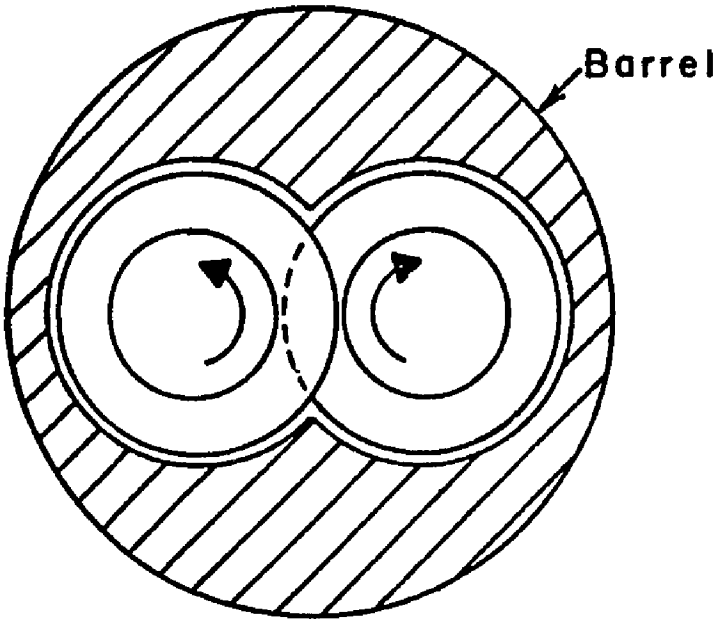

COUNTER-ROTATING TWIN SCREW
(cut away view)

FIGURE 1.2

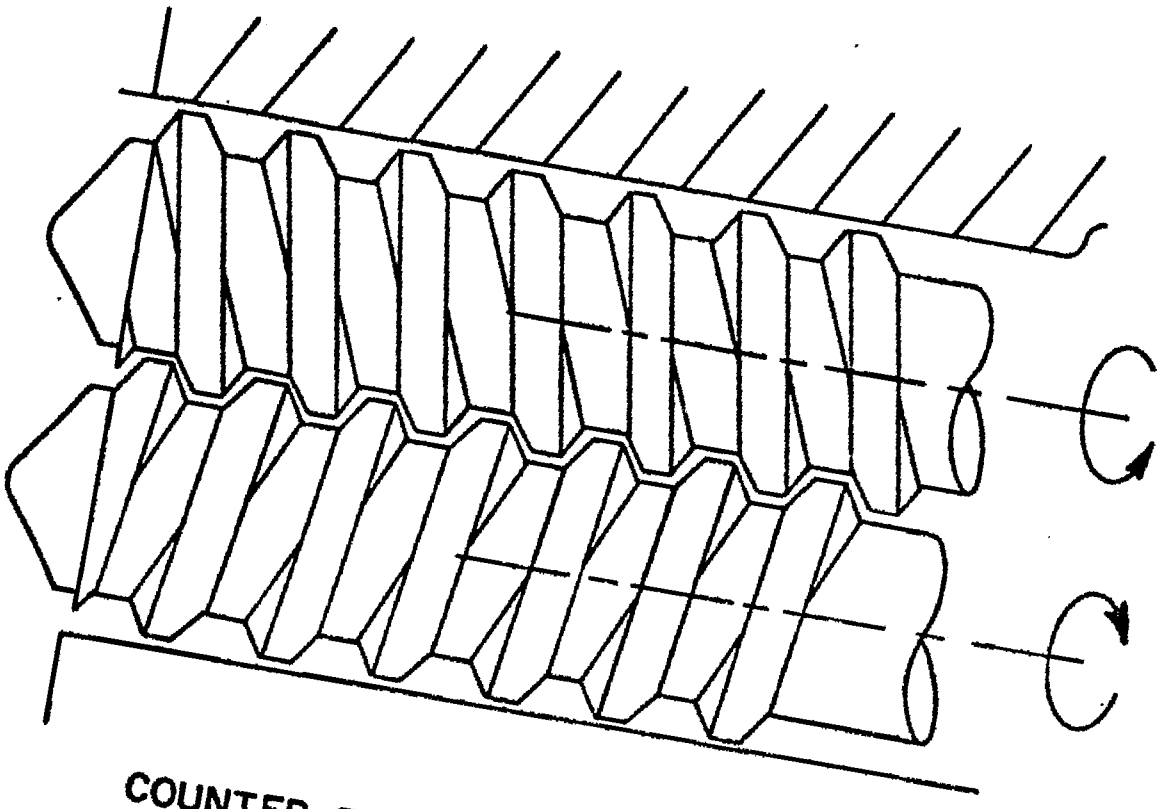

COUNTER-ROTATING TWIN SCREWS
(cut away view)

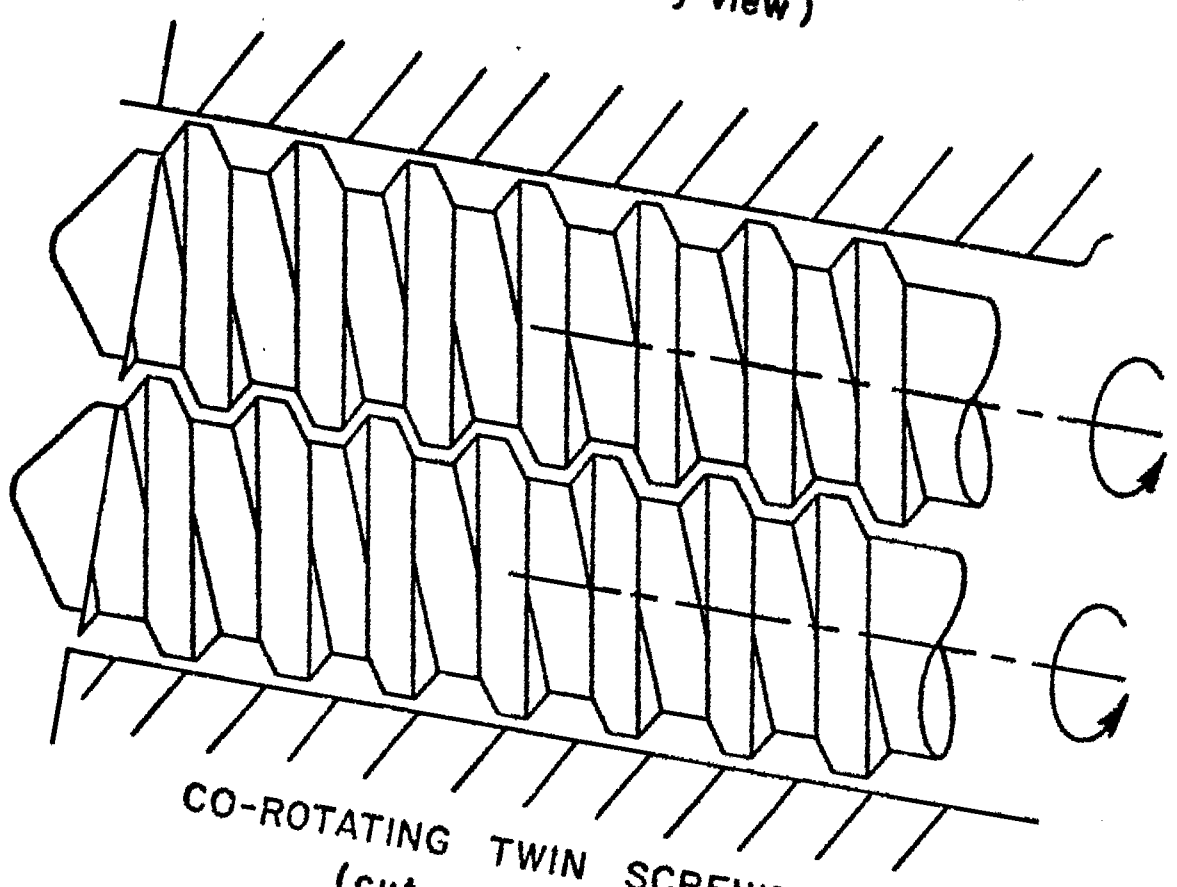

CO-ROTATING TWIN SCREWS
(cut away view)

FIGURE 1.3

twin screw extruders from the processing point of view will be considered later in this chapter.

Since there is more interest in using intermeshing twin screw extruders in industiral processes as compared to the nonintermeshing ones, the intermeshing twin screw extruders will only be considered here. In an intermeshing twin screw, the channel formed between the screw flights is virtually sealed off by the land of the second screw at the points of intersections of the two and by the surrounding barrel on the outside. Because of these confined channels, as one screw rotates all particles locked in its channel are pushed forward continuosly and uniformly by the lands of the second screw at the intermeshing point. The melt, for a nonleakage case, can not stick to the screw root because one screw continuosly wipes the other. In the single screw, on the other hand, a continuos helix shaped chamber or channel exists over the entire screw length, and as described earlier, fluid particles sitting on the screw root and on the barrel surface do not move in the axial direction at all.

Prause [26] pointed out the difference between intermeshing twin screw and single screw extruders very clearly by giving an example of a steel ball. When placed in the feed opening of a single screw with the feed end raised and the screw stationary, the ball rolls through the helix channel all the way down to the die without being obstructed. If the same experiment is repeated with the

feed end lowered enough and the screw rotating, the ball never moves up the extruder. In a twin screw, on the other hand, when the feed end is slightly raised and the screws are stationary, the ball rolls down the channel of one screw only one screw turn, its motion being interrupted at the point where the second screw intermeshes with the first. Thus the ball travels the length of one pitch or lead. Now, if the twin screw feed end is lowered and the screws are rotated, the steel ball can not roll back due to gravity because it is pushed forward by the intermeshing lands of the second screw towards the raised die.

This difference in extrusion principle has important consequences for mixing. As described by Todd [37], in a single screw extruder, the material next to the barrel is heated to its melting point and further scrapped and accumulated by the leading edge of the screw flight. This action provides some blending of ingredients. After melting is complete, the screws drag material forward and develop the pressure required for flow through the die. This pressure flow leads to an increased energy requirement and a nonuniform product temperature which may be detrimental to the polymer. Higher temperatures also cause a lower viscosity with less efficient utilization of shear forces for dispersion. Thus the dispersion in a single screw extruder is largely due to the high shear forces during melting and the relative motion of screw and the barrel. Furthermore, because the residence time distribution varies

from a very low value for some particles to an almost infinite value for those next to the root and the barrel surface, uniform mixing of all ingredients can not be achieved effectively. In a twin screw extruder, however, material moves back and forth from one half of the "8" shaped barrel to the other, twice each revolution, thereby providing a dividing and combining action for effective compounding.

Because of the positive conveying action caused by the land of one screw intersecting the root of the other, there are no dead zones or corners in an intermeshing twin screw extruder. This means that nearly all particles spend approximately the same amount of time travelling through the twin screw extruder, and the resulting narrow residence time distribution of fluid particles offers a number of processing benefits. First, all fluid particles receive the same work and heat treatment and the final product is more homogeneous than would result in a single screw extruder with its continuous channel. In addition, during the extrusion operation, volatile materials contained in the polymer are often removed through a small hole in the barrel called the ventport; due to the nature of these confined channels of a twin screw extruder, only the material in the channel under the ventport is in the decompression zone [1], so that the barrel venting operation can be controlled effectively. In a single screw, on the other hand, the helix shaped channel, and therefore the decompression zone,

runs over the entire screw length,so that the barrel venting operation can not be so easily controlled. The closed channel of a twin screw extruder also means that the melt viscosity and the die pressure do not affect the melt movement, and hence the melt discharge is practically surge free. Furthermore the extrusion operation can be carried out successfully over a wide range of melt viscosities. In a single screw, the continuous helix shaped chamber results in the melt movement being sensitive to both the back pressure and the melt viscosity [1].

Good mixing of fluid particles of a material or materials is known to be dependent upon the amount of shear strain [36] exerted on the fluid particles, where the shear strain is the total product of shear rate and the corresponding time intervals over which the shear is imposed upon a fluid particle. A mixing process in which a fluid particle is reduced to smaller size particles is called a microscopic mixing process while one in which materials are mixed together due to a blending action is termed a macroscopic mixing process [26,27]. The mixing action in a single screw unit depends mainly upon the back pressure and the resulting back flow in the metering section. In the twin screw machine, however, additional mixing occurs at points where the screws intermesh and since the material encounters the high shear rates there which are responsible for the microscopic mixing or dispersion action [26,27]. In addition to the microscopic mixing at the intermeshing

point, material is also being exchanged from one screw to the other so that blending or macroscopic mixing is also achieved. Because of the combined microscopic as well as macroscopic mixing, twin screw extruders provide a better opportunity of minimizing the need for removal of excess frictional heat [1]. Therefore, in many mixing processes, the input power requirement is significantly less in a twin screw system than for a single screw machine [1].

The process of compounding is a result of microscopic as well as macroscopic mixing in which various ingredients are simultaneously dispersed and blended together to form a homogeneous mixture on some definable small scale. Effective compounding can be achieved by supplying just enough energy so that a uniform product quality is maintained. Since a twin screw extruder offers an excellent opportunity for microscopic as well as macroscopic mixing, it has become increasingly popular as an effective continuous compounding machine for many industrial applications [14]. For instance, for glass reinforced thermoplastic compounds where homogeneity is the most important requirement, twin screw extruders successfully handle this task. Gras [14] and Todd [37] pointed out the important benefits that twin screws offer relative to single screw machines for reinforced plastic compounding. Furthermore, they are replacing roll mills on which thermosets were previously processed. Alloying of different polymers which are structurally dissimilar or incompatible

requires substantial shear for blending at closely controlled uniform temperature condition, and a narrow residence time distribution. Single screws can not meet these requirements while twin screw compounders can handle alloying processes successfully by providing controlled shear and heat exposure times which can be limited to a few seconds and also by providing shear rates as high as 20,000 sec -1 .

In addition to compounding, there are many other areas, as reported by Mack [23], and Gras [14], where twin screws offer important benefits. The positive conveying action, improved kinetics and heat transfer, and completely self wiping operation of twin screw extruders offer improved homogenization of resins and fibers, better wetting of fibers, dependable volatile removal, and close, accurate control of glass content. Reclamation of polyesters and nylon fiber scraps based on twin screw technology resulted in significant savings for producers of plastic fibers and films. Generation of high extrusion pressures with a very short backup length is another feature of twin screw extruders providing processing flexibility. Thus, for instance, in a well designed twin screw system, extrusion pressures of 3000 to 5000 psi can be easily generated over a screw length of 2-3 diameters.

In addition to the benefits of twin screw extruders discussed in the preceding paragraphs,there are also some limitations. The most obvious one is that they are much

more expensive than single screws because of the complex design of the screws themselves and the thrust bearings [28,14,26]. Other limitations include susceptibility to quicker loading, low bulk density of preblended material influencing the throughput rate, and low speeds. To overcome some of these shortcomings, manufacturers of twin screw machines have simplified the design and increased the throughput rates by vacuum venting to remove entrapped air from feed stock [14].

As discussed previously, there are two major types of twin screw extruders, co-rotating and counter-rotating twin screws (as shown in Fig: 1.2). Many workers have pointed out major differences between these types and some of them disagree with each other on certain points. Since little definitive theoretical work has been developed, it is very difficult to clearly understand the differences between the co-rotating and counter-rotating twin screw extruders. Nonetheless, major differences as pointed out by workers in the field and others are summarized.

Prause [27] stated that from the processing standpoint, counter-rotating screws produce a better mixing effect than co-rotating screws, while co-rotating screws provide a better self cleaning action because of the wiping of one screw by the other. The direction of rotation does not alter the processing action for co-rotating screws but for the counter-rotating screws, some experts feel that screws rotating away from the center help prevent clogging in the

ventport if cre is needed. When the screws rotate inwards towards the center, material may tend to accumulate or pile up on the top of the screw in the ventport area thus decreasing the ventport action or possibly clogging the vent. On the other hand, according to Prause, some experts feel inward rotating screws tend to push solid feed material more forcefully into the barrel than do outward rotating screws. These statements are based primarily on a consensus of experts backed by observation of material flow behavior in twin screw machines.

Adams [1] agrees with Prause on the fact that higher shear stresses are exerted by material passing through the nip of the two screws for counter-rotating twin screw systems, while comparatively low shear stresses are exerted on material in the nip region for co-rotating twin screw systems. Consequently, a higher input power is required for the counter-rotating twin screw systems in which higher pressures are generated in the gap, but wear problems become significant. For co-rotating twin screw systems, the material follows an "8" shaped path along the entire barrel length [1]; and therefore, statistically the chances are better that all the fluid particles will receive uniform treatment than in a counter-rotating system. Also, because of the self wiping action in co-rotating system, there is a better control over residence time distribution and hence temperature.

In order to quantitatively characterize the important

differences in mixing capabilities and velocity distributions between the co-rotating and the counter-rotating twin screw machines as well as between single screw and twin screw machines, the present work is undertaken. In the following chapter, the theoretical background of single and twin screw extruders is reviewed so that the significance of the present work is clarified.

II THEORETICAL BACKGROUND

As described before, a single screw extruder consists of a screw rotating in a tightly fitted barrel. Polymer which may be fed as a solid, a mixture of solid and melt, or just a melt moves from one end of the screw to the other, confined in a helix shaped chamber formed by the screw root, the screw flights on either side, and the inner barrel surface. In Fig 2.1a, the geometry and the descriptive symbols pertaining to a double flighted single screw are given, although they could apply equally well to any number of flights. The inside diameter of the barrel is Db; the radial distance between the screw root and the inner surface of the barrel or the channel depth is H; the radial clearance between the crest of the screw flight and the inner barrel surface is δ_f; the axial distance of one full turn or the screw lead is L; the channel width or the perpendicular distance between the flights is W; the width of the screw flight is e; and the angle formed between the flight and the plane normal to the screw axis is the helix angle, ϕ. The channel width W and the helix angle ϕ vary with channel depth slightly, while the channel depth H and the screw lead L are normally constants but may vary in the axial direction depending upon the screw section (e.g. a tapered section).

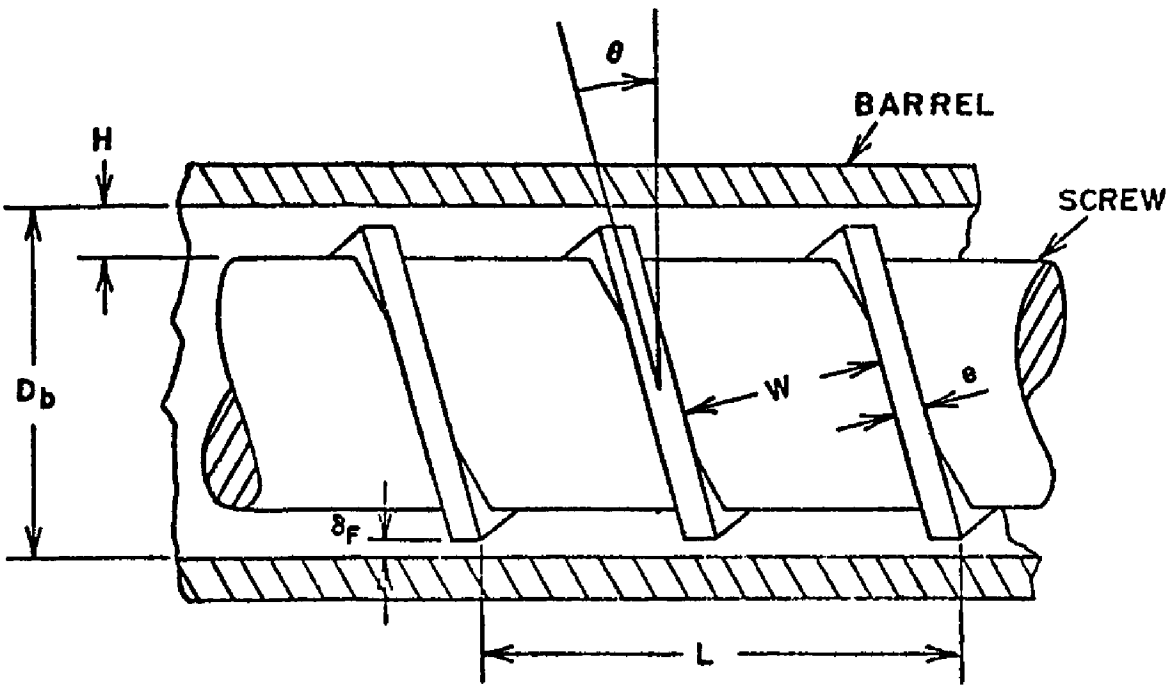

Fig. 2.1a: Geometry of a Double Flighted Single Screw Extruder(Cut Away View)

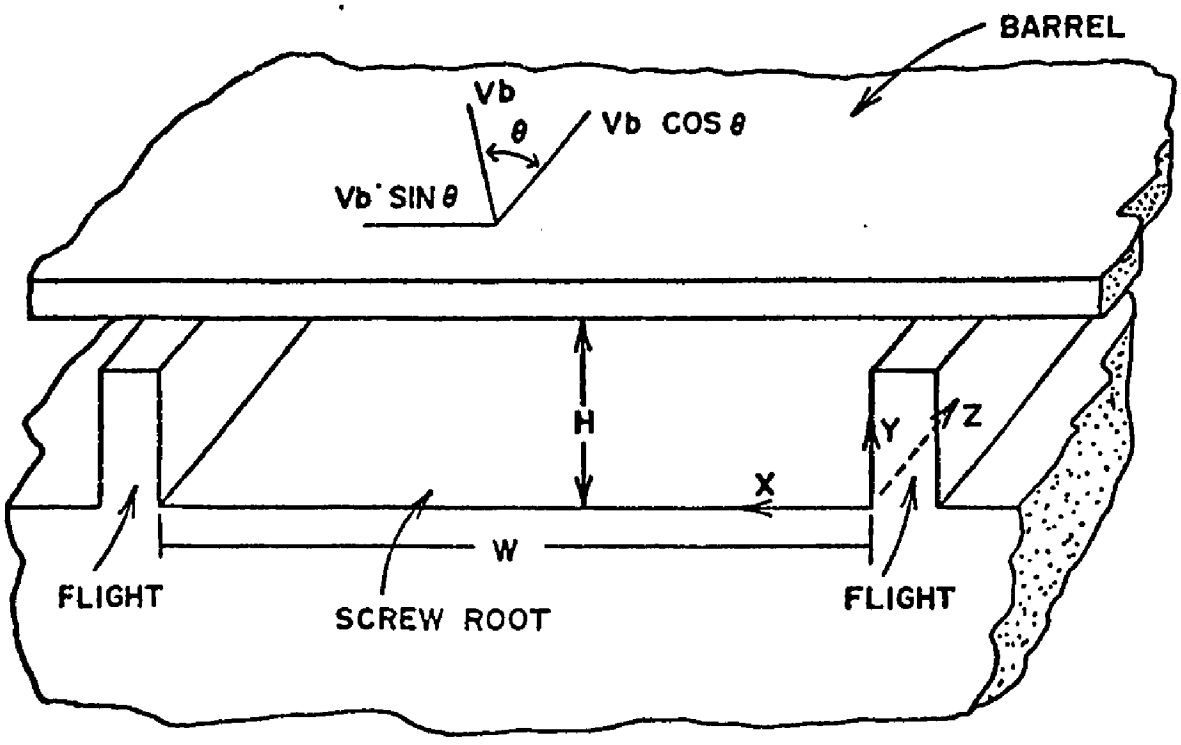

Fig. 2.1b: Unwound Channel of a Single Screw Extruder

It is difficult tc analyse the flow behavior of material in a plasticating extruder based on the real geometry cf the screw so the barrel and the screw root are usually unwound to form twc flat plates as shown in Fig 2.1b. Furthermore, by considering the device as a rotating barrel and a staticnary screw, it is easier to visualize and analyse the extrusion mechanism [24,36]; and coupled with the flat plate model, this moving barrel becomes an infinite flat plate sliding cn the top of the channel and moving at constant velccity Vb at an angle θ, the helix angle, with respect to the down channel direction. The screw root forms the base plate with a flight at either side as shown in Fig 2.1b. Thus, fcr the flat plate model, a rectangular coordinate system can be applied with axes x, y, and z, as shown in Fig 2.1b, which lie along the cross channel direction, radially frcm the screw root, and in the down channel directicn respectively. The origin of the axes may be chosen at any pcint on the screw root, although it is usually chosen at a pcint cn the screw root next to a screw flight.

Mckelvey [24], Tadmcr [36], and others have developed flow models based cn the flat plate assumption in the melt conveying zcne of a single screw extruder, and Mckelvey showed that less than a 4% error is introduced by neglecting the curvature when Rc/Ri is less than 1.3 for a Newtonian fluid. In crder to simplify the flow analysis, certain assumptions were made which include an incompressible

Newtonian fluid; steady state, laminar, fully developed isothermal flow; negligible slight effects; no slip at the wall; and negligible inertial and gravitational forces compared to the viscous and pressure forces. Furthermore, the y component of velocity was neglected, and the cross channel and the down channel pressure gradients were treated as constants. Based on these simplifying assumptions, the three components of the velocity were determined by the equation of motion [5] to obtain the velocity profiles in the cross channel direction, Vx, and in the down channel direction, Vz,

$$V_x = V_b \sin\theta \, (y/H)(2 - 3\, y/H) \tag{2.1}$$

$$V_z = V_b \cos\theta \left(y/H + 3 \frac{Q_p}{Q_d} (y/H)(1 - y/H) \right) \tag{2.2}$$

The pressure gradient in the cross channel direction, $\partial P/\partial x$, was obtained by utilizing the fact that the net flow in the cross channel direction is zero, while the pressure gradient in the down channel direction, $\partial P/\partial z$, would depend upon the net down channel flow possible for the die condition. Thus,

$$\frac{\partial P}{\partial x} = - \frac{6 \mu V_b \sin\theta}{H^2} \tag{2.3}$$

$$\frac{\partial P}{\partial z} = - \frac{6 \mu V_b \cos\theta}{H^2} \left(\frac{Q_p}{Q_d} \right) \tag{2.4}$$

where the terms Qp and Qd in the above expressions are the down channel pressure flow and the drag flow rates respectively, and the boundary conditions used to model the

system are Vx and Vz equal zero at the screw root while Vx is equal to $-V_b \sin\theta$ and Vz equals $V_b \cos\theta$ at the barrel surface. The moving barrel rotates with speed N revolutions per unit time so that the barrel velocity Vb is $N\pi D_b$.

The velocity profile in the axial direction l, Vl, was obtained by summing the axial components of the cross channel and the down channel velocities and can be given as:

$$V_l = V_x \cos\theta + V_z \sin\theta$$

$$\text{or,} \qquad V_l = 3 V_b \sin\theta\cos\theta \left(1 + \frac{Q_P}{Q_d}\right)(y/H)(1-y/H) \qquad (2.5)$$

Tadmor [36], Mckelvey, and others [24,22] have shown that these velocity profiles can be used to describe mixing in a single screw extruder. According to their analysis, mixing for laminar flow systems depends upon the total strain, γ, exerted on a fluid particle during its stay in the metering zone. The total strain for a fluid particle in a steady state system depends upon the sum of all the shear rates experienced times the time, t, of exposure to that shear rate as well as the total time required for it to travel through the system, and in an extruder, both these factors depend upon the initial location of the fluid particle in the channel. By calculating these variables as a function of initial location in the channel, it is possible to calculate the total strain experienced by the fluid particles as a function of their initial position, i.e. the total strain distribution across the channel.

This analysis, of course, holds only at points far from the flights, where the velocity profiles, equations 2.1 and 2.2, are valid. In addition, since the net cross channel flow is zero, the fluid must "turn over" at the flights, so that a fluid particle in a single screw extruder alternately moves on two levels in the channel with a different velocity in each. Thus, the relation between any given plane and its so-called complementary plane after it "turns over" must be also known to compute the time and velocity history of a fluid particle in each plane as it moves through an extruder. Then, the strain can be determined.

In Fig 2.2, the motion of a particle in the cross channel direction of a single screw extruder is shown. The fractional heights a and a* of a plane and its complementary plane respectively are determined from the fact that the net flow in the cross channel direction is zero [24],

$$a = \frac{1 - a^* + (1 + 2a^* - 3a^{*2})^{0.5}}{2} \qquad (2.6)$$

If the time required to move between the planes is neglected, the time that the fluid particle spends in either plane is calculated by dividing the channel width W by the velocity in that plane, and the total time in one complete cycle is the sum of the times for a plane and its complement. Then, the fraction of the time spent by the fluid particle in the upper or the lower plane is calculated by dividing the respective time by the total time in one

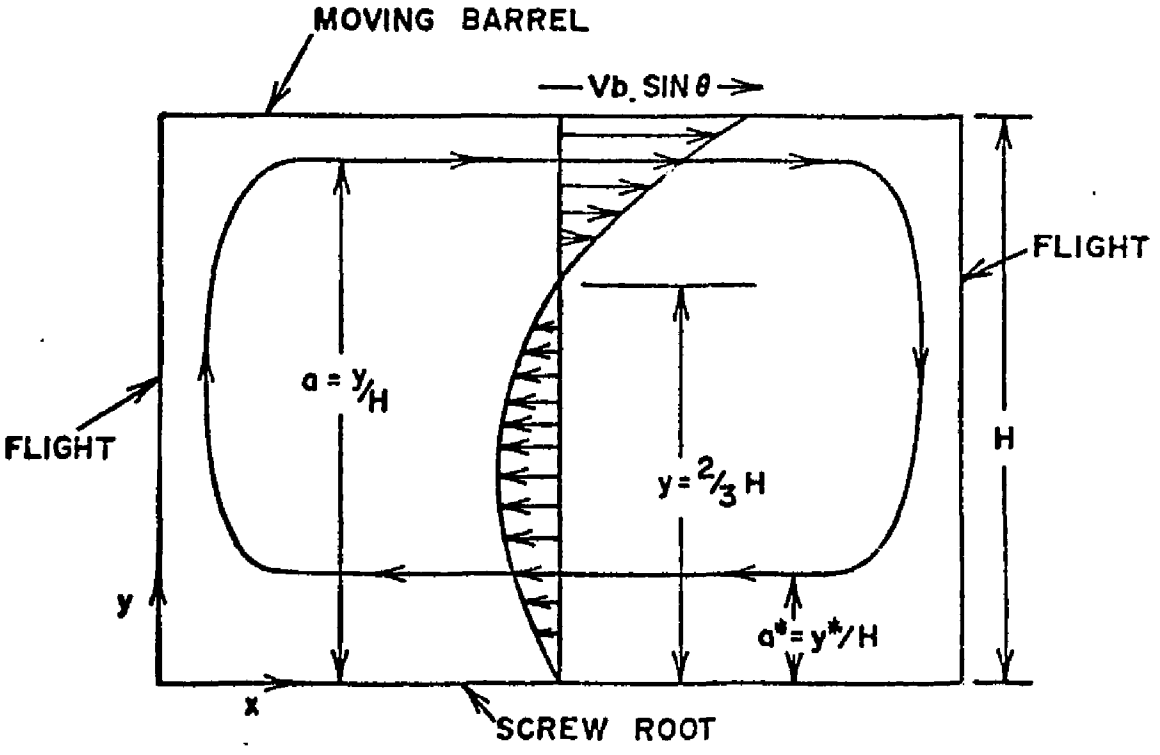

Fig. 2.2: A Fluid Particle Motion in the Cross Channel of a Single Screw Extruder

cycle. Thus, the time fraction in the upper portion, tf, is:

$$t_f = \frac{1}{1 - \frac{a(2-3a)}{a^*(2-3a^*)}} \qquad (2.7)$$

The residence time, t, of the fluid particle in the extruder is the axial length of the channel, l, divided by the average velocity of the fluid particle in the axial direction, $\overline{Vl}$, where $\overline{Vl}$ is computed as:

$$\overline{V_l} = V_l(a)\, t_f + V_l(a^*)(1-t_f) \qquad (2.8)$$

Vl(a) and Vl(a*) are the axial velocities in the upper and the lower planes respectively and are calculated from equation 2.5. The residence time, t, of any such fluid particle is then given by [36]:

$$t = \frac{1}{3\, Vb\left(1+\frac{Qp}{Qd}\right)\left[a^*(1-a^*) + t_f(a-a^*)(1-a-a^*)\right]\sin\theta\cos\theta} \qquad (2.9)$$

In order to calculate the total strain on a fluid particle, its average shear rate must be first evaluated. There are two procedures to calculate the average shear rates. Mohr et al [43] calculated it in the cross channel direction by computing the average velocity as:

$$\overline{V_x} = t_f\, V_x(a) + (1-t_f)\, V_x(a^*) \qquad (2.10)$$

while the average shear rate in the x direction was defined as:

$$\bar{\dot{\gamma}}_x = \frac{d\overline{V_x}}{dy^*} \qquad (2.11)$$

On the other hand, the expressions employed by Mckelvey to calculate $\bar{\dot{\gamma}}_x$ and $\bar{\dot{\gamma}}_z$ are:

$$\bar{\dot{\gamma}}_x = |\dot{\gamma}_x| t_f + |\dot{\gamma}_x^*| (1-t_f) \qquad (2.12)$$

$$\bar{\dot{\gamma}}_z = |\dot{\gamma}_z| t_f + |\dot{\gamma}_z^*| (1-t_f) \qquad (2.13)$$

Mckelvey compared his method with that of Mohr et al [43] in detail and pointed out that the difference between the methods for the calculation of $\bar{\dot{\gamma}}_x$, is only a numerical factor. In the case of $\bar{\dot{\gamma}}_z$, however, Mckelvey's method leads to the logical conclusion, as Tadmor [36] describes it, that $\bar{\dot{\gamma}}_z$, is a function of the ratio Qp/Qd, while in Mohr et al's method it is independent of this ratio. Furthermore, Tadmor [36] pointed out that since the fluid particles "roll over" at the flights, the absolute values of the strains rather than their directions will be decisive.

In calculating the total strain, γ, Mckelvey [24] calculated the strain in the x and y directions as:

$$\gamma_x = \bar{\dot{\gamma}}_x t \qquad (2.14)$$

$$\gamma_z = \bar{\dot{\gamma}}_z t \qquad (2.15)$$

and then simply adds the magnitudes of the strain components, so:

$$\gamma = \gamma_x + \gamma_z \qquad (2.16)$$

Another approach [36] used to calculate the total strain,

γ, is tc add the average shear rate components vectorially and then weigh them by the residence time t as,

$$\dot{\gamma} = (\dot{\gamma}_x^2 + \dot{\gamma}_z^2)^{1/2} \qquad (2.17)$$

$$\dot{\gamma}^* = (\dot{\gamma}_x^{*2} + \dot{\gamma}_z^{*2})^{1/2} \qquad (2.18)$$

$$\gamma = [\dot{\gamma} t_f + \dot{\gamma}^*(1-t_f)]\, t \qquad (2.19)$$

In this case, $\dot{\gamma}$ and $\dot{\gamma}^*$ represent the average shear rate experienced by the fluid particle in the upper and lower parts of the channel respectively rather than in the cross flow and in the down channel flow as in equations 2.14, 2.15, 2.16. Figures 2.3 and 2.4 show the results of these two methods of determining total strains for various values of θ and Qp/Qd.

The calculated strain distibutions provide no indicatic cf the ccnsequences of the high and the low strain levels to the overall product quality from the extruder since the relative significance of the total strain observed in a particular regicn depends not only on the level of strain itself but also on the fraction of the flow rate experiencing that level of strain, i.e. the residence time distributicn function. For a single screw extruder, the residence time distributicn is given by [36]:

$$F(t)\,d(t) = F(a)\,da = \frac{3a(1-a+(1+2a-3a^2)^{0.5})}{(1+2a-3a^2)^{0.5}}\,da \qquad (2.20)$$

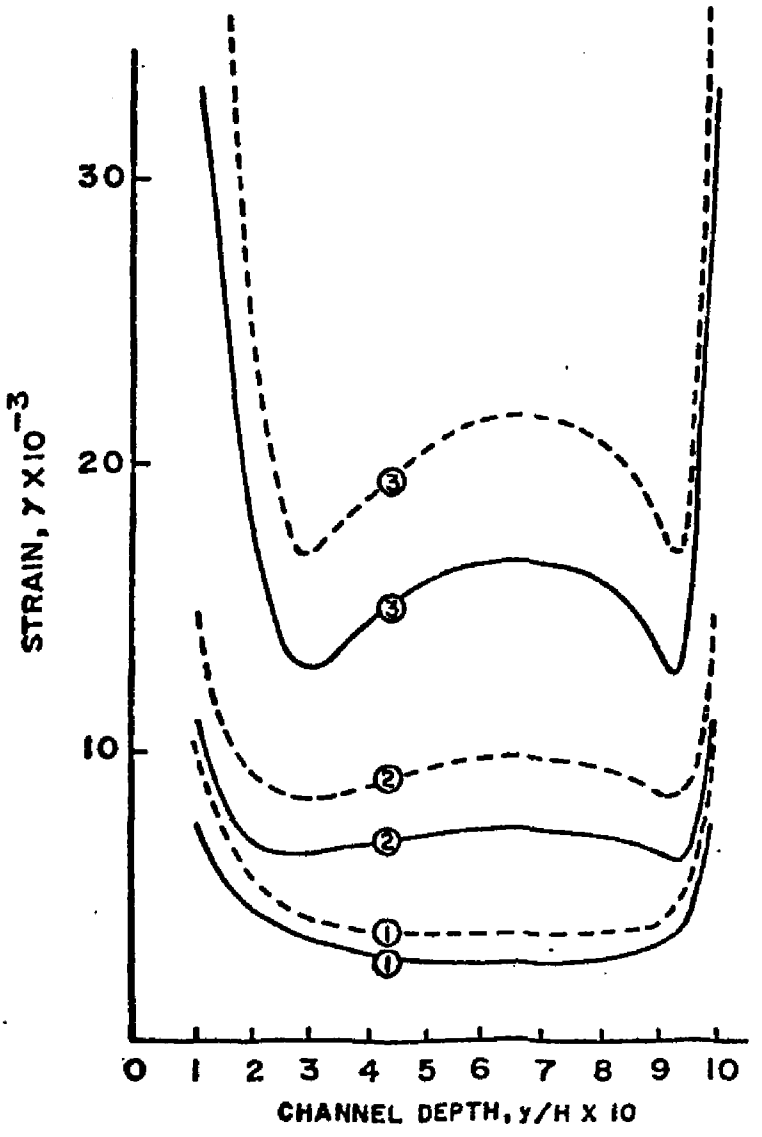

Fig. 2.3: Total Strain in a Single Screw Extruder as a Function of Initial Position. Calculations are Based on a Total Extruder Length of 100", Channel Depth of 0.2" and 20° Helix Angle
——— Calculations Based on Equation 2.19
- - - - - Calculations Based on Equation 2.16
(1) Qp/Qd = 0 (2) Qp/Qd = 0.5 (3) Qp/Qd = 0.75

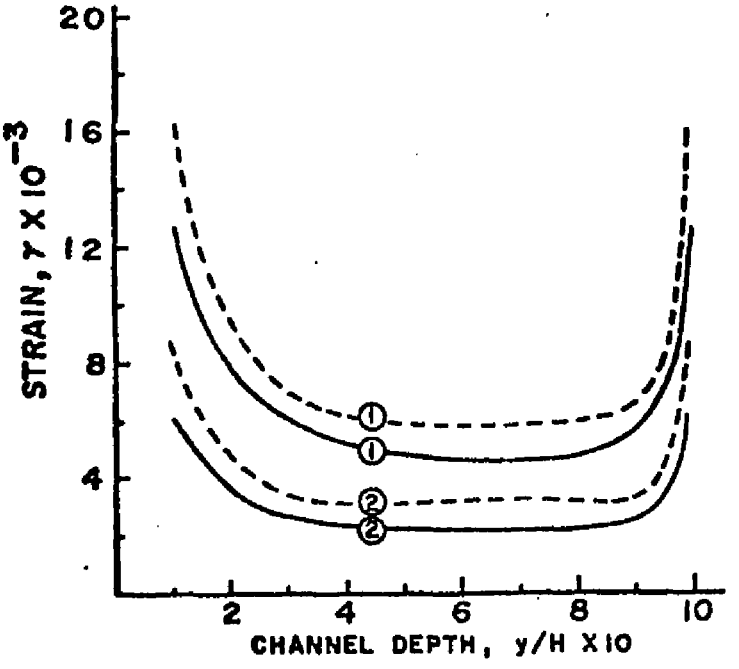

Fig. 2.4: Total Strain in a Single Screw Extruder as a Function of Initial Position and the Helix Angle θ for No Pressure Flow

———— Calculations Based on Equation 2.19

- - - - - Calculations Based on Equation 2.16

(1) $\theta = 0^{o}$ (2) $\theta = 30^{o}$

Combining the total strain distribution, γ, with the residence time distribution, F(t)d(t), Tadmor [36] defined the weighted average total strain, $\bar{\bar{\gamma}}$, as follows:

$$\bar{\bar{\gamma}} = \int_{t_o}^{\infty} \gamma F(t) dt = \int_{2/3}^{1} \gamma F(a) da \qquad (2.21)$$

where t_o is the minimum residence time possible in the extruder which occurs at a height which is 2/3 of the channel depth.

It can be seen from Fig 2.5 and Fig 2.6 that $\bar{\bar{\gamma}}$ varies moderately with respect to helix angle θ for the range used in practice and also varies with the ratio of the pressure flow to the drag flow, Qp/Qd. A sharp increase in $\bar{\bar{\gamma}}$ is only evident when pressure flow opposes the drag flow and attains values above 40% of the drag flow. Thus, mixing improves with increasing opposition of pressure flow to drag flow. The results shown for pressure flow reinforcing drag flow are only of theoretical interest since only positive pressure gradients are possible in single screw extruders. Tadmor et al [36] showed that $\bar{\bar{\gamma}}$ is a function of 1, H, Qp/Qd, and the helix angle θ.

Lidor et al [22] calculated the residence time distribution function theoretically for a shallow single screw extruder based on the solid conveying, melting, and melt conveying models. Their analysis almost exclusively deals with the melting zone of the single screw extruder.

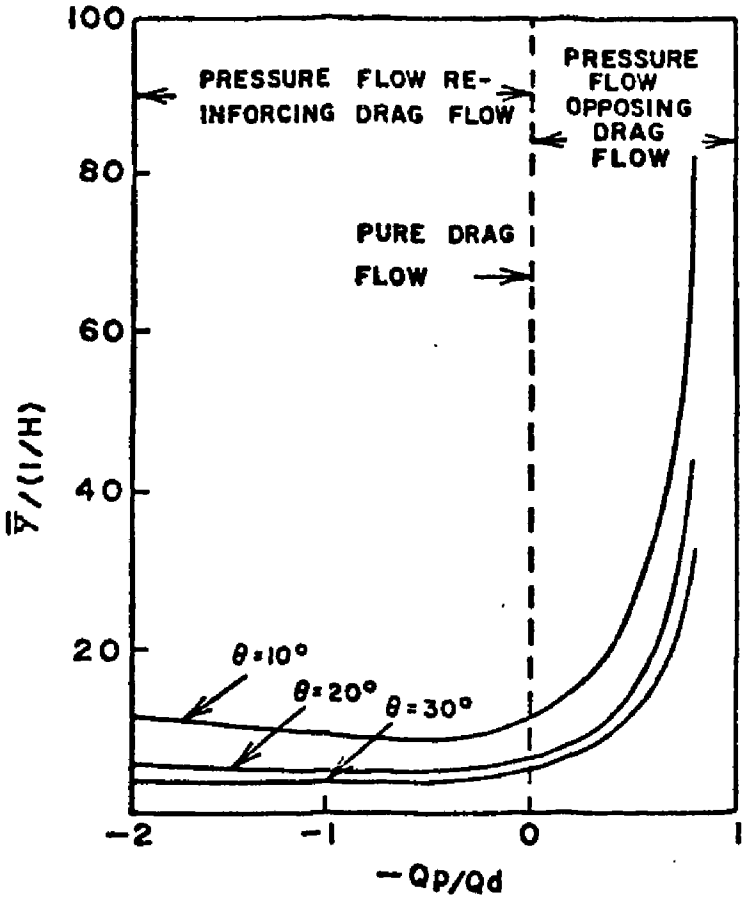

Fig. 2.5: Weighted Average Total Strain $\bar{\bar{\gamma}}$ vs Qp/Qd

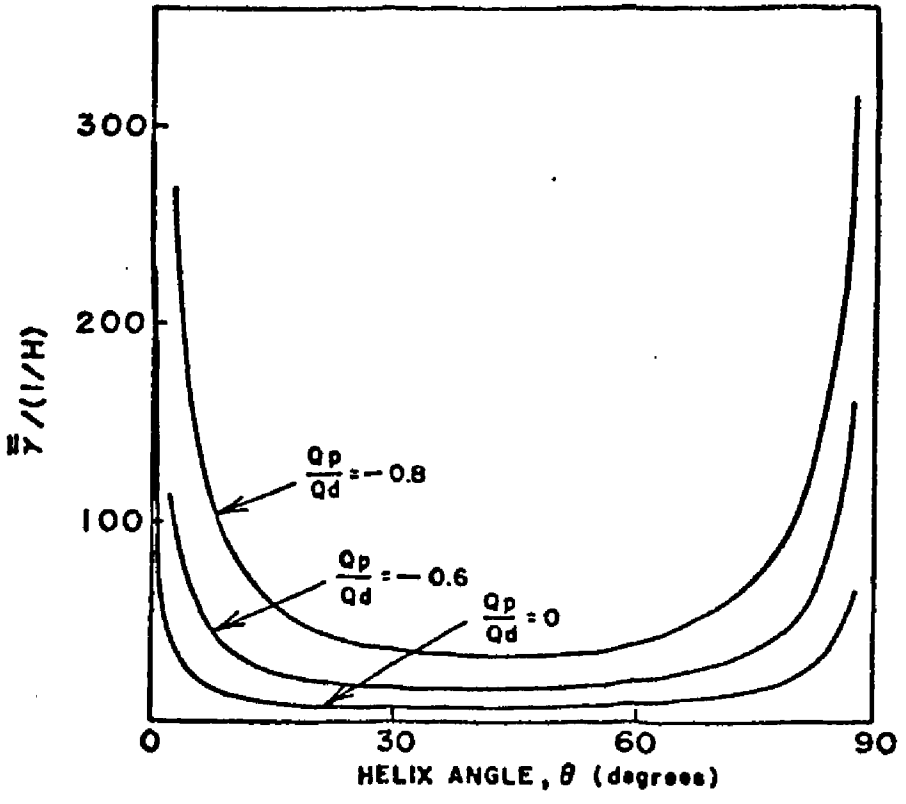

Fig. 2.6: Weighted Average Total Strain vs the Helix Angle, θ

In addition to the residence times, the total strain imposed upon the fluid particles was also calculated; and the strain distribution function was developed for the entire single screw extruder. The method of strain calculation in the melt conveying zone is identical to that described earlier [36].

Kaplan et al [18] have shown that the results of single screw extrusion theory can be easily extended to nonintermeshing twin screw extruders by introducing a geometric factor to account for the interaction of the two screws. They developed a simplified three flat plate model similar to a single screw two plate model to obtain flow expressions for Newtonian viscous flow. The total pressure drop and volumetric flow rate were calculated and compared with a single screw extruder for identical screw speeds and geometries, and the model was then extended to account for leakage and non-Newtonian fluids. Nonintermeshing screw devices, as they described it, have their own merits in feeding, venting, and devolatilizing operations.

Unlike noninterneshing twin screw extruders, the flow behavior in intermeshing twin screw machines as developed by the few articles on the subject can not be simplified by applying the corresponding single screw extrusion theory. Wyman [40] developed a theoretical confining plate model to describe the down channel velocity profiles for intermeshing twin screw extruders with shallow channels. The flow analysis was simplified by considering viscous flow of an

incompressible, Newtonian fluid under isothermal conditions. For a shallow channel, as he described it, the extruder can be pictured as two flat plates, one the screw root, being stationary while the other, the barrel, moves with a velocity Vb at an angle θ, the helix angle. The second screw lands which project down through the barrel wall to contact the stationary screw root are pictured as large rotating cylinders between segments of barrel plate as shown in Fig 2.7. In simplifying the analysis, he neglected the curvature of the cylinders formed by the second screw lands by replacing them with flat plates perpendicular to screw root and the barrel, thus closing the channel completely, as shown in Fig 2.8. These confining plates extend at regular intervals through the barrel wall and contact the stationary root and the flights. They are parallel to the x,y plane and move with the velocity $V_b/\cos\theta$ in the down channel direction.

Taking into account the fact that the net flow rate in the down channel direction is due the positive displacement action of the screw, analytical expressions were developed for the down channel drag and pressure flows in the middle part of the channel where the pressure gradient, $\partial P/\partial z$, is constant. Thus the down channel velocity Vz for a twin screw of N turns and the barrel diameter D, becomes:

$$V_z = \pi DN\cos\theta\left\{(Y/H)\left(\frac{6}{\cos^2\theta}-2\right)+6(Y/H)^2\left(\frac{1}{2}-\frac{1}{\cos^2\theta}\right)\right\} \quad (2.22)$$

while the constant pressure gradient in the z direction,

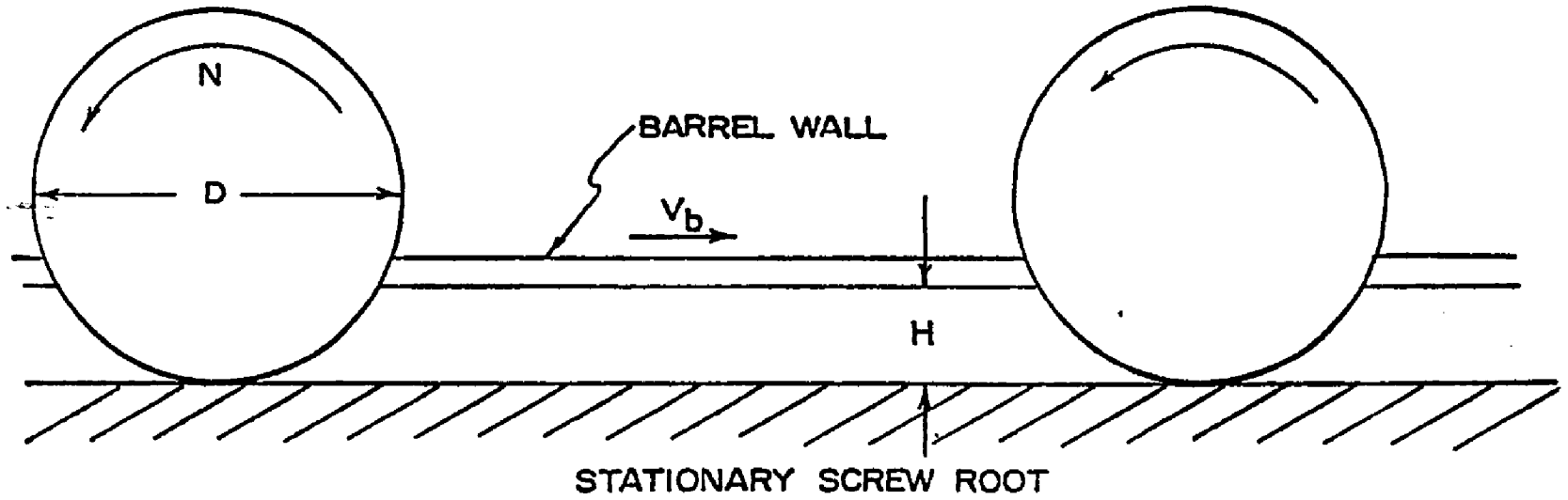

Fig. 2.7: Cross Sectional View of the Unwound Channel with Two of the Rotating Cylinders shown for a Co-rotating Twin Screw Extruder

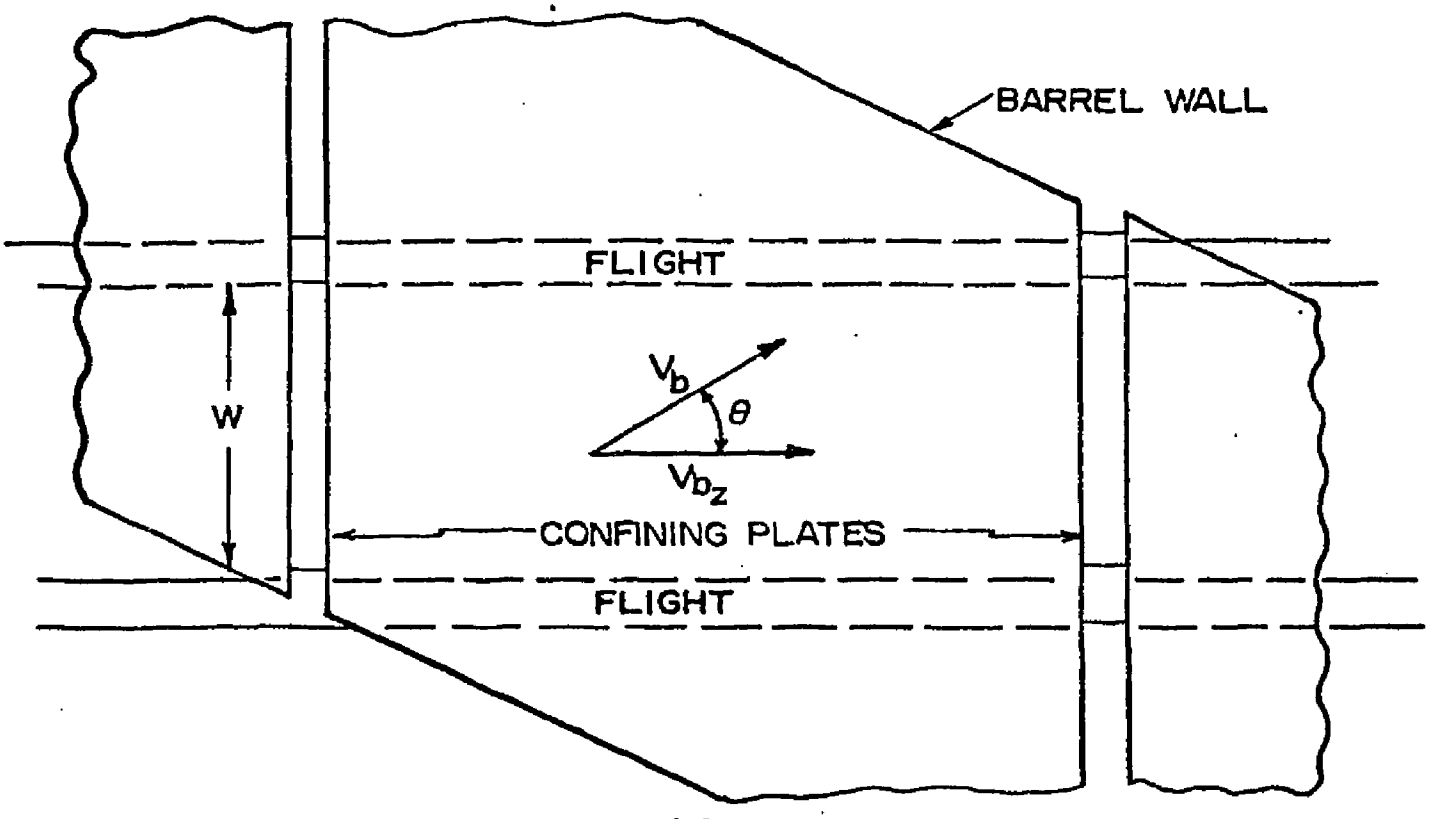

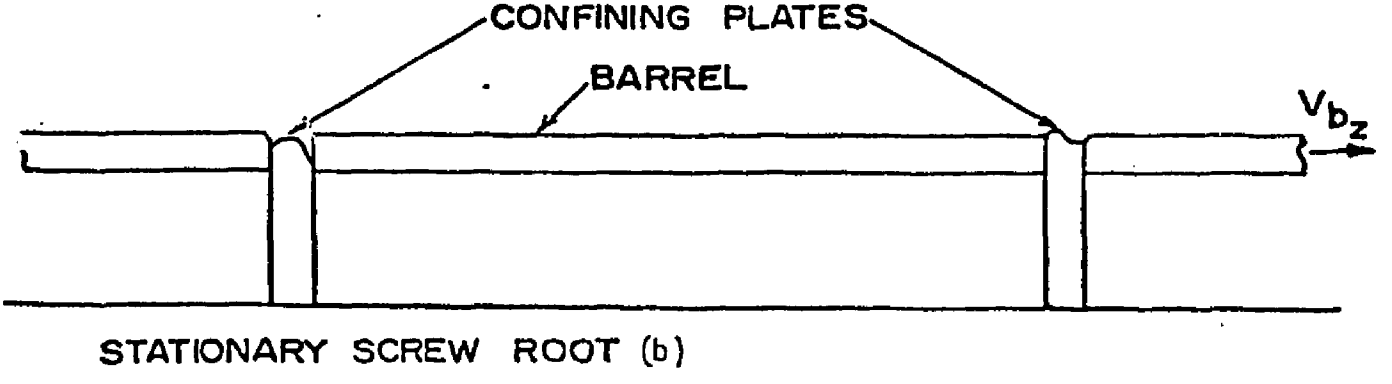

Fig. 2.8: The Confining Plate Model
(a) Overhead View of Channel
(b) View Parallel to Screw Flights

$\partial P/\partial z$, is given by the following equation:

$$\frac{\partial P}{\partial z} = \frac{12\mu\pi DN}{H^2}\left[\frac{\cos\theta}{2} - \frac{1}{\cos\theta}\right] \qquad (2.23)$$

Since the pressure gradient is always negative, the pressure should decrease along the down channel direction so that the pressure flow reinforces the drag flow.

Using equations 2.22 and 2.23 for low helix angles ($\theta=0$), Wyman [40] compared the twin screw down channel velocity profile to that in a single screw with no net flow, and he concluded that the shear rate profile due to the down channel velocity in the twin screw machine is the inverted image of that in a single screw with no discharge. Thus, the highest shear rate occurs near the barrel wall for the single screw extruder but near the screw root of a twin screw extruder. However, as one screw root slips under the confining screw land of the latter, material next to the root must "turn over" towards the barrel wall while material at the trailing edge of the screw land is moving from the wall towards the high shear root. In addition to this action, the cross channel component of flow forces material to circulate from the root to the barrel wall and back so a sigrificant percentage of the material experiences a high shear rates in a twin screw extruder. This is not possible in a single screw extruder unless the discharge is closed, an impractical situation.

Kim, Skatschkow, and Jewmenow [17,19,20] developed a theoretical model for determination of the velocity profiles

in the middle part of a twin screw channel. The model assumed that the velocity components are functions of the x and y coordinates only, and the pressure gradients $\partial P/\partial x$, $\partial P/\partial y$, and $\partial P/\partial z$ were assumed constant. Thus, the velocity components Vx, Vy, and Vz were found from the three components of the equation of motion for Newtonian, incompressible, steady flow of a viscous fluid under isothermal conditions. The cross channel pressure gradient $\partial P/\partial x$ was calculated from the fact that the net flow in the cross channel direction is zero while the vertical pressure gradient $\partial P/\partial y$ must be such that the cross channel flow from the screw root to a certain channel height half way across the channel is equal to the flow in the y direction from either flight to the midpoint of the channel at the same channel height. As a result, $\partial P/\partial x$ and $\partial P/\partial y$ were found to be functions of x and y respectively; and although the authors do not discuss it further, this is in direct contradiction to their original assumptions. Finally, $\partial P/\partial z$ had to be specified rather than being calculated by equating the net down channel flow to that due to positive displacement action of the screw as determined by Wyman [40].

In analysing the mixing process in the twin screw channel, Kim et al [17,19,20] calculated nine components of the shear rate tensor and then averaged them by integrating across the channel depth. The average shear strain for each component was found by multiplying the shear rate by the residence time of the extruder, and these values were

combined to obtain an expression for the average total strain times the melt viscosity. Thus, the criteria used to describe mixing by this model depends upon the amount of the average total strain. The results obtained by this model were experimentally confirmed [7,19].

In the preceding paragraphs, the analytical models developed by Wyman [40] and Kim, Skatschkow, and Jewmenow [17,19,20] were discussed. The confining plate model of Wyman treats only the down channel velocity in the middle portion of the channel; while the model by Kim et al treats the channel extending from flight to flight across the channel but only the middle portion in the down channel direction. The expressions for the velocity components obtained by Kim et al are functions of x and y only, and based on these expressions, mixing criteria were developed in terms of the average total shear strain. These models neglect the end zones in the z direction where the lands of the second screw touch the screw root of the first. Higher pressure gradients should be developed in these end zones to account for the turning of the material flow; and the resulting shear energy should yield higher shear stresses for the material passing through these regions. In addition, both of these models assumed there is no leakage from the channel.

The mixing criterion developed by Kim et al [17,19] does not take into account the fact that the material contained in any y-plane can pass to one of two different

y-planes depending upon whether the material ends its travel in a plane due to the cross channel velocity Vx or the down channel velocity Vz. However the mixing process is very complex; and to theoretically describe the complete mixing action in a twin screw extruder, all velocity components must be determined before the shear rate can be calculated for a fluid particle as it moves over the entire channel during its stay in the extruder. Furthermore, the total shear strain distribution must be found by integrating the shear rate over that time span and the result may be a function of all three coordinates x, y, and z. In addition to this, leakage should be considered to make the analysis complete.

For the present work, the twin screw extruder channel is analysed over the entire channel length between the points of intersection with the moving second screw lands. Therefore, the significance of the mode of rotation of the second screw on the velocity profiles and mixing capabilities of a twin screw extruder can be assessed, and the results can be compared to the performance of a single screw machine. However, to simplify the analysis, the effects of the screw flights and the cross channel velocity component are neglected so only the z and y directions and the respective components of the velocity are involved.

III THE SYSTEM MODELS

The end and side views of a co-rotating and a counter-rotating twin screw extruder are shown in Fig 1.2 and 1.3. The two screws have identical frequencies of rotation and are positioned such that the land of either one just clears the root of the other. If the geometries of the two screws are identical, the flow description for one screw channel provides a complete flow description of both. However, if the two screws are different in their geometrical configuration, then each one must be analysed separately.

In principle, a complete model of the system under consideration for melt conveying in intermeshing twin screw extruders should allow calculation of the velocity components along with the pressure, temperature, shear stress, and shear strain distributions. The flow equations provided by such model should take into account the pertinent physical properties, the geometry of the screws and barrel, and the operating conditions. Considering the complexity of the screw and barrel configuration, the problem of leakage, and the non-Newtonian, time dependent nature of most polymer melts, the accomplishment of such comprehensive objectives is very difficult and not warranted at this stage of our understanding of these devices.

Therefore, based on the equation of motion, an attempt is made here to develop a simplified, steady, isothermal, Newtonian fluid model describing the flow behavior of the material contained in the screw channel of a twin screw extruder. Attention is primarily devoted to the end regions of a twin screw channel where the intermeshing land of the second screw intersects with the channel of the first.

In order to obtain velocity profiles in the twin screw confined channel, the equation of motion in cylindrical coordinates should be employed. From Fig 1.2 and 1.3, the shape of the helical confined channel starting from one point of intersection of the two screws to the next can be visualized. The boundary conditions will be applied along the extruder flights which are helical and not along a single cylindrical coordinate axis alone; therefore, it is very difficult to solve the equation of motion in the cylindrical coordinate system. Although Tung and Laurence [50] developed a coordinate representation of fluid motion in a helical configuration, they did not apply it to any problem; and it is difficult to apply to the twin screw channel. In addition, the nonorthogonal axes used would complicate obtaining shear rate and shear strains. Therefore, more simplified approaches are sought in the present work to develop flow models that describe an intermeshing twin screw extruder. These models are first developed for a hypothetical zero helix angle twin screw extruder to compare the theoretical results to an

experimental simulation unit. Then, some of the models are extended to describe flow in actual twin screw extruders with nonzero helix angles.

For a zero helix angle case, the model which best describes flow in the confined channel is of course the one which treats the actual geometrical configuration of the system under consideration. When the helix angle is brought to zero, the same land of the second screw seals both ends of the extruder channel as shown in Fig 3.1 for a zero helix angle co-rotating twin screw extruder. The screws rotate with angular velocity $2\pi N$ radians per unit time. The confined channel ABCDAA'A is the region of interest for the present work. The root of screw 1 of radius b is rotating in the clockwise direction with speed $2\pi bN$ while the barrel BCD of radius a is stationary. Thus the confined channel is formed by the moving screw root AA'A, the stationary barrel BCD, and the lands of the rotating second screw DAB touching the root of the first screw from the top. The second screw lands are of radius a and move with velocity $2\pi aN$.

Let the point O be the origin and the θ direction originate from point A in the positive clockwise direction. The angle AOE between the point of intersection of the second screw land with the first screw root and barrel respectively is called α, and let $P(r',\theta)$ be any point on the second screw land EAB. The velocity components Vr and V_θ on the boundaries of the screw root and the barrel are:

$$V_r = 0 \quad ; \quad V_\theta = 2\pi bN \qquad \text{at } r = b \qquad 2\pi \geq \theta \geq 0 \tag{3.1}$$

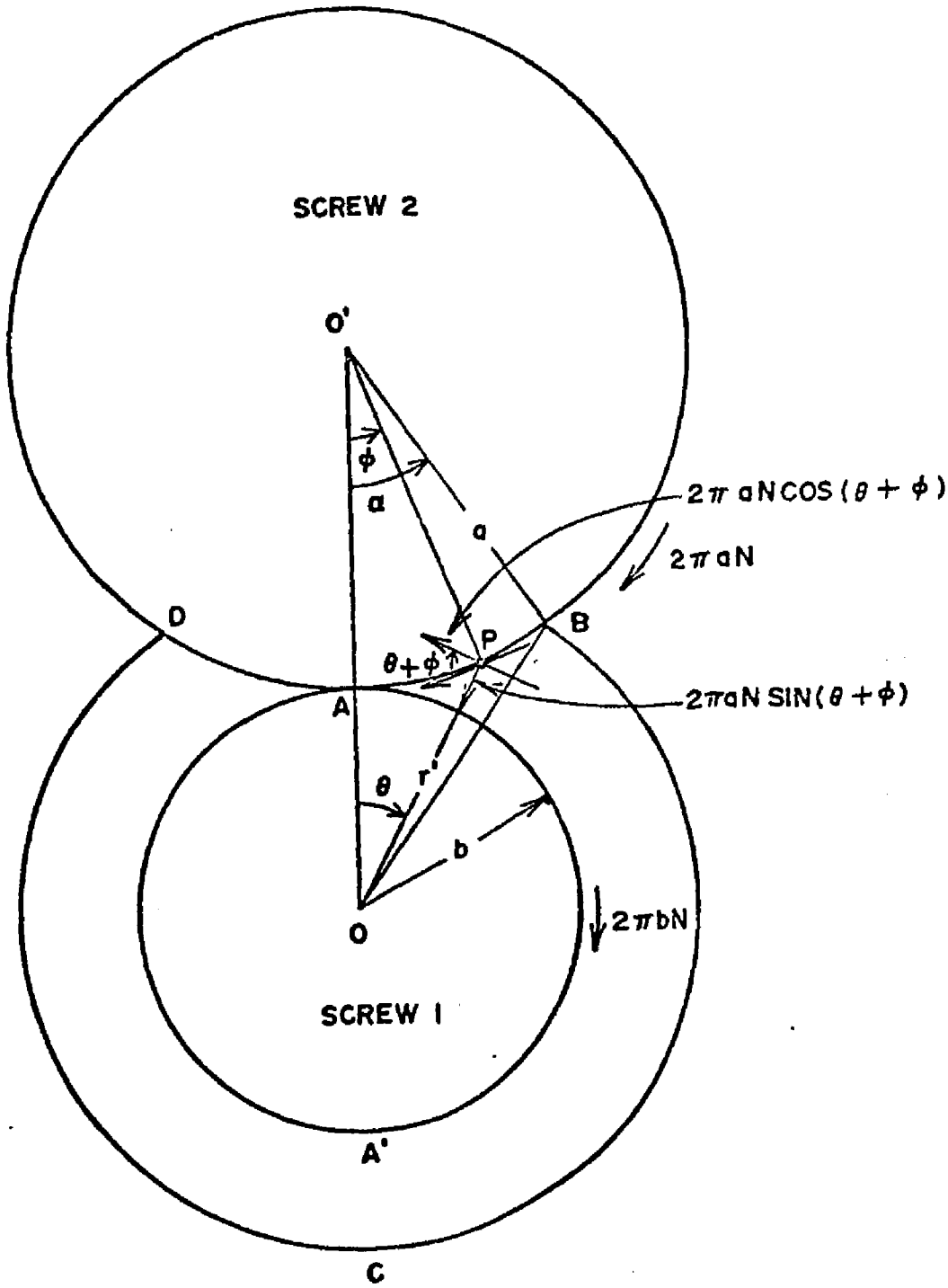

Fig. 3.1: Two Clockwise Co-Rotating Screws of Radii a and b Touching Each Other at Point A, and a partially cut barrel BCD Surrounding the Lower Screw and just Touching the Upper Screw at Points B and D

$$V_r = 0 \; ; \quad V_\theta = 0 \qquad \text{at } r = a \quad (2\pi-\alpha) \geq \theta \geq \alpha \tag{3.2}$$

and on the boundary DAE, formed by the second screw land,

$$V_r = -2\pi a N \sin(\theta+\phi) \qquad \alpha \geq \theta \geq 0 \tag{3.3}$$

$$V_r = 2\pi a N \sin(\theta+\phi) \qquad 2\pi \geq \theta \geq (2\pi-\alpha) \tag{3.4}$$

$$V_\theta = -2\pi a N \cos(\theta+\phi) \qquad \alpha \geq \theta \geq (2\pi-\alpha) \tag{3.5}$$

where the angles θ and ϕ are as shown in Fig 3.1 and the radial coordinate r' on the boundary DAB can be shown to be related to these angles according to relations:

$$\theta = \cos^{-1}\left[\frac{r'^2 + b^2 + 2ab}{2r'(a+b)}\right] \tag{3.6}$$

$$\phi = \cos^{-1}\left[\frac{a^2 + (a+b)^2 - r'^2}{2a(a+b)}\right] \tag{3.7}$$

For any point P(r', θ) on the boundary DAB, r' is known if θ is given or vice versa from equation 3.6, and the angle ϕ then can be determined from equation 3.7. Thus knowing θ and ϕ, V_θ and Vr can be determined from equations 3.3 through 3.5. It is assumed that there is no motion in the z direction which is perpendicular to the plane of the paper in Fig 3.1.

In order to solve the equation of motion for the zero helix angle case, the following assumptions are made: the material is incompressible and behaves as a Newtonian fluid; steady, isothermal, laminar flow is assumed; inertial and gravitational effects are negligible due to the high

viscosity of the fluid material; there is no flow in the axial direction; and the confined channel is leakproof. Thus, with these assumptions the general equation of motion in cylindrical coordinates reduces to [5]:

$$\frac{\partial P}{\partial r} = \mu\left[\frac{\partial}{\partial r}\left(\frac{1}{r}\frac{\partial}{\partial r}(rV_r)\right) + \frac{1}{r^2}\frac{\partial^2 V_r}{\partial \theta^2} - \frac{2}{r^2}\frac{\partial V_\theta}{\partial \theta}\right] \qquad (3.8)$$

$$\frac{1}{r}\frac{\partial P}{\partial \theta} = \mu\left[\frac{\partial}{\partial r}\left(\frac{1}{r}\frac{\partial}{\partial r}(rV_\theta)\right) + \frac{1}{r^2}\frac{\partial^2 V_\theta}{\partial \theta^2} + \frac{2}{r^2}\frac{\partial V_r}{\partial \theta}\right] \qquad (3.9)$$

where μ is the fluid viscosity. Since the pressure gradients $\partial P/\partial r$ and $\partial P/\partial \theta$ are not constant, a direct analytical solution of equations 3.8 and 3.9 is not possible. However, an approximate solution can be developed using finite difference numerical methods for which the complete procedure is developed in chapters IV and V.

Another approach to develop flow models describing fluid motion in a twin screw extruder is to unwind the confined channel so that the barrel surface and the screw root now are represented by flat plates. In order to clarify this approach, certain assumptions are made, the first being to treat one of the screws as stationary, while the barrel rotates around it. The second screw moves around the stationary screw as well since it is attached to a fixed position on the barrel. Due to the intermeshing nature of the two screws, the second screw must also turn on its own axis with the same angular speed as the barrel so that it will not be forced to move axially as it rotates. A picture

of this system is shown in Fig 3.2.

Wyman [40] clarified this treatment by giving the example of a small spider running up the channel formed by the flights (side walls), a ceiling (the barrel wall), and a floor (the screw root) so that he is completely trapped in the confined channel. When the twin screw machine starts rotating, the spider sees the ceiling (barrel) moving at an angle θ (the helix angle) with respect to the stationary flight walls; and in a while he sees the wall of the other cylinder rolling along the channel (counter-rotating) or against the channel (co-rotating) towards him. Thus, he will be pushed ahead by this moving wall if he tries to stay stationary on the root, and therefore, he must run to keep ahead of the wall. If he runs too fast, he will be stopped by the other wall moving in front of him. Thus, he must run in the confined channel until he reaches the extruder die, the total time of his imprisonment in the confined channel being called the residence time of the extruder. In a single screw extruder, the spider could relax on the stationary root as long as he wished.

As pointed out by Wyman [40], this model can be simplified further by considering the intermeshing second screw lands as flat plates perpendicular to screw root and the barrel. This representation is designated as the confining flat plate model [40]. According to this model as described in the preceding chapter and also in Fig 2.8, these plates are spaced equally along the screw channel from

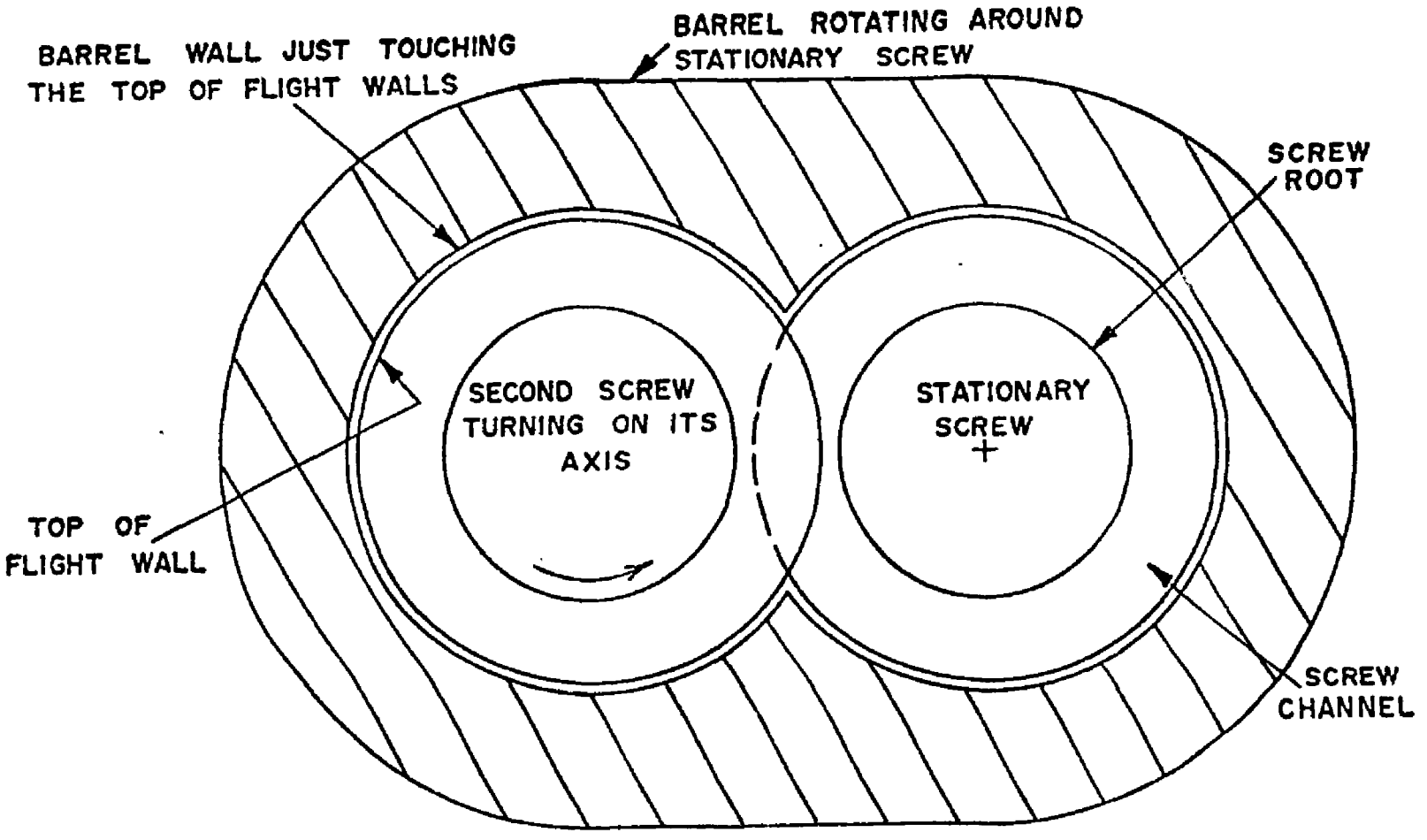

Fig. 3.2: Cross Sectional View of a Co-Rotating Twin Screw Extruder Perpendicular to the Screw Axis with the Barrel and the Second Screw Rotating Around the Stationary Screw and with the Second Screw Rotating on its Axis

one end tc the cther with their number equal to the number of times the interneshing seccnd screw lands contact the root of the first. They move in the down channel direction with the velccity Vb/cosθ . Since this work is concerned with the influence cf the end regions on mixing in twin screw extruders, the flat plates will be considered to move in the directicn perpendicular to the screw root with the velccity cf their rctation, Vb.

The ctter flat plate model, the curved boundary flat plate model, is ctained by unwinding the original helical shaped channel as described abcve but the unwinding is now done in a manner such that the loss of curvature is minimized as explained later. In Fig 3.3a, a spiral shaped ccnfined channel ACICEGA is shown as a channel projected on a plane perpendicular to the extruder axis. The channel is unwcund by cutting the extruder along the line DECF and the left hand pcrtion cf the channel including point B is pulled around and trought tc the right hand side from below so that the original staticnary screw root spiral becomes the flat plate CC of the sane length $\pi Dr/cos\theta$. The initial spiral length cf the barrel, AGB, however, becomes the moving flat plate A'B' which is smaller in length as a result of the unwinding than the actual length of the barrel spiral. The amcunt of shrinkage invclved fcr barrel is calculated in the Appendix A. Thus, the actual spiral shaped confined channel CAGBC beccmes the ccnfined channel CCB'A' after unwinding.

The curved boundary ACB in the initial helical confined

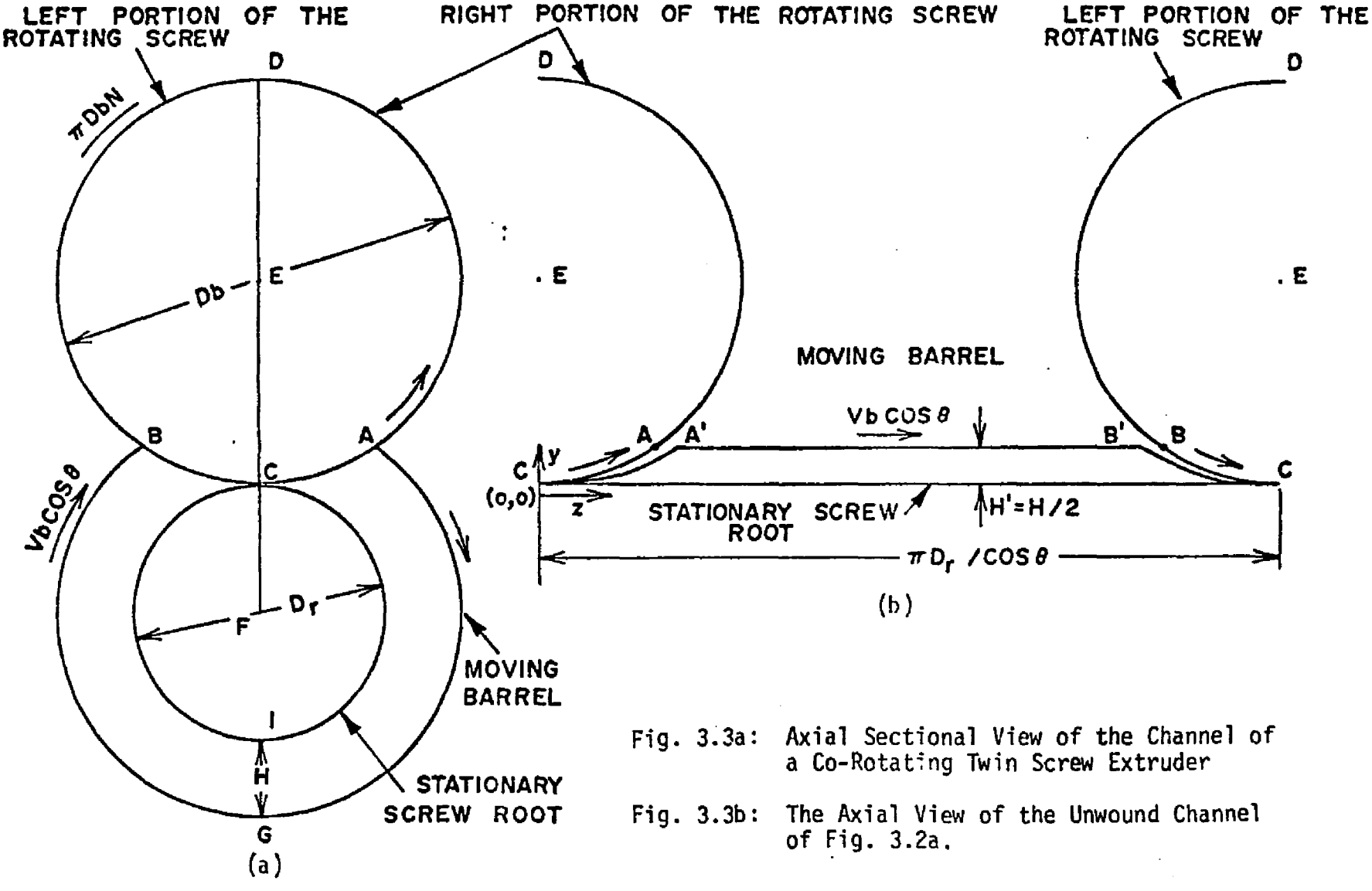

Fig. 3.3a: Axial Sectional View of the Channel of a Co-Rotating Twin Screw Extruder

Fig. 3.3b: The Axial View of the Unwound Channel of Fig. 3.2a.

channel is cut into two equal arcs AC and CB which remain unchanged after unwinding the channel and rotate with the velocity πDtN as shown in Fig 3.2. However, in the plane along the channel depth and the down channel direction, the actual geometry of these curved arcs AC and CB are represented by arcs CA' and CB' respectively in Fig 3.3b such that arcs AC and CB in fig 3.3a represent axial projections of the arcs CA' and CB'. In other words, the down channel coordinate of the point A' in Fig 3.3b will be the down channel coordinate of the point A in Fig 3.3b times the the factor $1/\cos\theta$, and thus, for zero helix angle case, the point A' coincides with the point A.

The transferred channel depth H' can be shown to be equal to half of the original channel depth H. The shrinking of the channel depth and the barrel length after unwinding is necessary since it aids in simplifying the flow analysis and minimizes the effects of curvature in going from the actual screw geometry to the rectangular geometry of the model under consideration. Although the channel depth is reduced to half its original size, it will not affect the velocity profile since we will be dealing with the dimensionless velocity profiles and dimensionless channel height. In calculating shear rate, however, the calculated shear rate will be corrected by introducing an appropriate correction factor which is 0.5. Although the values of shear rate so obtained may deviate from the actual ones in the region where the down channel coordinate tends

to a value zero or $\pi Dr/\cos\theta$, this deviation is assumed to be negligible and its effect will be discussed later in chapter VIII.

The rectangular coordinate axes y and z as shown in Fig 3.3b are in the direction of the channel depth and the down channel direction respectively. In order to compare this model with the zero helix angle model in the cylindrical coordinates, it is necessary to take into account shrinkage and transform the location of a point from the rectangular coordinates y and z to the cylindrical coordinates r and θ and vice versa. A complete derivation of the method of transformation is described in detail in Appendix A.

The barrel A'E' moves in the z direction, the down channel direction, with velocity Vb $\cos\theta$ [40]. The curved portions or the arcs CA' and B'C of the second screw also move in the down channel direction in addition to their angular motion of N revolution per unit time around the center E. However, their down channel velocity Vp varies across the channel depth from Vr/$\cos\theta$ at the screw root to Vb/$\cos\theta$ at the barrel wall where Vr equals NπDr and Vb equals NπDb. Thus, the velocity Vp can be represented by Vr(D/Dr)/$\cos\theta$ where D, the diameter with respect to the stationary screw, varies from Dr at the screw root to Db at the barrel wall.

Now, if the arcs CA' and E'C are considered not to move in the down channel direction although they rotate at N revolutions per unit time, then the barrel will move in the

down channel direction with a velocity Vb cosθ-Vb/cosθ (equivalent tc -Vb sinθtanθ) while the screw root will move in the down channel direction with a velocity -Vr/cosθ. Making the velccities dimensicnless with respect to velocity Vr and the distances with respect to the screw root diameter Dr, the model simplifies tc the one described in Fig 3.4 for a co-rctating case. The dimensionless screw root length is now π/cosθ while the channel depth H' is (Db-Dr)/(4Dr). The z cccrdinate of the pcint A', $Z_{A'}$, is given by

$$Z_{A'} = \left[H' \left\{ \frac{Db}{Dr} - H' \right\} \right]^{0.5} / \cos\theta \qquad (3.10)$$

and the arcs CA' and E'C rotate in the axial plane with the linear velocity Vr which in its dimensionless form becomes Db/Dr. The y and z ccmpcnents of Vr at any point R(y,z) on the arc CA' are given by the following expressions:

$$V_{ry} = \frac{V_r z \cos^2\theta}{\left[\left(\frac{Db}{2Dr}\right)^2 - z^2 \sin^2\theta \cos^2\theta \right]^{0.5}} \qquad (3.11)$$

$$V_{rz} = \frac{V_r \cos\theta \left[\left(\frac{Db}{2Dr}\right) - y \right]}{\left[\left(\frac{Db}{2Dr} - y\right)^2 \sin^2\theta + \left(\frac{Db}{2Dr}\right)^2 \cos^2\theta \right]^{0.5}} \qquad (3.12)$$

and the relaticn between the y and z coordinate for a point R(y,z) cn the arc CA' is,

$$\left(\frac{Db}{2Dr}\right)^2 = z^2 \cos^2\theta + \left[\left(\frac{Db}{2Dr}\right) - y \right]^2 \qquad (3.13)$$

For the arc E'C, the velccity component Vrz remains the same as that fcr the arc CA' but the other component of velocity,

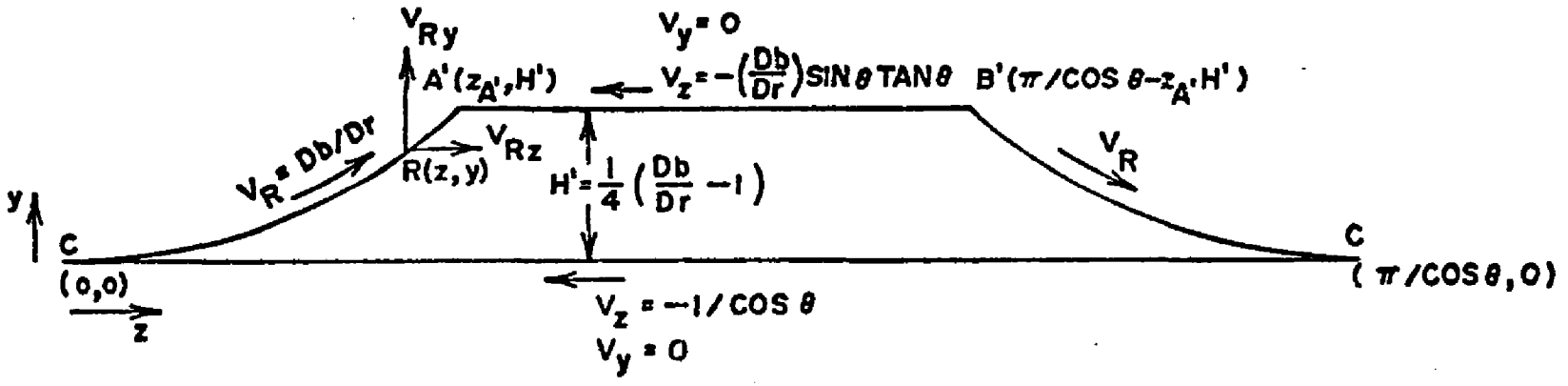

Fig. 3.4: Dimensionless Form of the Curved Boundary Flat Plate Model for a Co-Rotating Twin Screw Channel.

Vry, changes its sign.

For the curved boundary flat plate model just developed, the boundary conditions for this model can now be summarized. The velocity components on the boundaries are:

$$V_y = 0 \; ; \quad V_z = -1/\cos\theta \qquad \text{at } y = 0 \tag{3.14a}$$

$$V_y = 0 \; ; \quad V_z = -\frac{V_b}{V_r}\sin\theta\tan\theta \qquad \text{at } y = H' \tag{3.14b}$$

$$V_y = V_{ry} \; ; \quad V_z = V_{rz} \qquad \text{on the arc } CA' \tag{3.14c}$$

$$V_y = -V_{ry} \; ; \quad V_z = V_{rz} \qquad \text{on the arc } B'C \tag{3.14d}$$

where the velocity components Vry and Vrz are given by equations 3.11 and 3.12.

This model, the curved boundary flat plate model, differs from the confined plate model of Wyman [40] or from the 'S' forming flow model of Jewmenow and Kim [17] in that the curvature and rotation of the second screw lands at the end of the channel are not neglected. To further simplify the analysis, the following assumptions are made: the material is incompressible and behaves as a Newtonian fluid, the flow is laminar and isothermal, steady state behavior is assumed, entrance and exit effects are neglected, inertial and gravitational effects are negligible, and the confined channel is leakproof. Thus, with these assumptions the three components of the equation of motion in rectangular coordinate system reduce to [5]:

$$\frac{\partial^2 V_x}{\partial x^2} + \frac{\partial^2 V_x}{\partial y^2} + \frac{\partial^2 V_x}{\partial z^2} = \frac{1}{\mu}\left(\frac{\partial P}{\partial x}\right) \tag{3.15}$$

$$\frac{\partial^2 V_y}{\partial x^2} + \frac{\partial^2 V_y}{\partial y^2} + \frac{\partial^2 V_y}{\partial z^2} = \frac{1}{\mu}\left(\frac{\partial P}{\partial y}\right) \qquad (3.16)$$

$$\frac{\partial^2 V_z}{\partial x^2} + \frac{\partial^2 V_z}{\partial y^2} + \frac{\partial^2 V_z}{\partial z^2} = \frac{1}{\mu}\left(\frac{\partial P}{\partial z}\right) \qquad (3.17)$$

The complete flow behavior of material in the channel is influenced by the three velocity components Vx, Vy, and Vz; and the geometric configuration of the channel makes the boundary conditions difficult to apply. Since this study is aimed at understanding the influence of the intermeshing second screw land on the fluid motion in the confined channel of the first, the flow analysis is simplified by treating the y,z plane half way across the channel width but over the entire channel length where velocity components involved are only Vy and Vz. The channel is considered to be wide enough so that the velocities under consideration are not functions of the channel width X, and the equations of motion reduce to:

$$\frac{\partial^2 V_y}{\partial y^2} + \frac{\partial^2 V_y}{\partial z^2} = \frac{1}{\mu}\left(\frac{\partial P}{\partial y}\right) \qquad (3.18)$$

$$\frac{\partial^2 V_z}{\partial y^2} + \frac{\partial^2 V_z}{\partial z^2} = \frac{1}{\mu}\left(\frac{\partial P}{\partial z}\right) \qquad (3.19)$$

Since the pressure gradients $\partial P/\partial y$ and $\partial P/\partial z$ are not constants, the analytical solution of equations 3.18 and 3.19 is not possible. However, an approximate solution can be developed using finite difference numerical methods for

which the complete procedure is developed in the chapter V.

IV NUMERICAL METHODS

In this chapter various numerical methods that can be used to obtain the desired approximate solutions of the momentum equation are examined and compared. If the equations for velocity components, equations 3.18 and 3.19, were expressed directly in their finite difference forms, the result would contain the three unknowns Vy, Vz, and P, so one more equation would be needed to obtain the complete solution. This relation comes from the equation of continuity [5]:

$$\frac{\partial V_z}{\partial z} + \frac{\partial V_y}{\partial y} = 0 \qquad (4.1)$$

Thus, with three equations and three unknowns (dependent variables), the approximate solution should be possible [44].

One solution procedure is to consider the unsteady equation of motion so that equations 3.18 and 3.19 will now include first order time derivative terms [44]. An initial pressure distribution P is calculated from assumed values of the velocities Vy and Vz by substituting the unsteady state equations 3.18 and 3.19 into 4.1. Then, the velocity components Vy and Vz are computed for the initial time increment Δt by equations 3.18 and 3.19 from the pressure value just found. Next, the pressure P is recomputed based

on the latest velocities. The time is then advanced by its increment Δt and all the steps mentioned above are repeated. This procedure is continued until P, Vy, and Vz remain unchanged through successive steps, i.e. until the steady state values of the P, Vy, and Vz are obtained. Since in this approach the solution of the unsteady state equations of motion is obtained by solving a set of parabolic equations, the method takes a large number of iterations to reach the steady state solution. In addition, some problems may arise with satisfying the continuity equation if the computer program is not carefully written [54].

Another approach to solve equations 3.18 and 3.19 along with the continuity equation 4.1 is to combine them into one equation involving only one dependent variable through use of the stream function ψ [5]. Let the stream function ψ be defined by:

$$V_z = -\frac{\partial \psi}{\partial y} \qquad (4.2)$$

$$V_y = \frac{\partial \psi}{\partial z} \qquad (4.3)$$

so that the continuity equation 4.1 is always satisfied. Combining equations 3.18, 3.19, 4.2, and 4.3 and further eliminating the pressure gradient terms, the following expression, the biharmonic equation [13], is obtained.

$$\frac{\partial^4 \psi}{\partial y^4} + 2\frac{\partial^4 \psi}{\partial y^2 \partial z^2} + \frac{\partial^4 \psi}{\partial z^4} = 0$$

or, $$\nabla^4 \psi = 0 \qquad (4.4)$$

The stream function approach is straightforward compared to the method dealing with three dependent variables simultaneously as it deals with only one dependent variable ψ. In addition, with the stream function approach, the boundary conditions are simplified; and the streamlines can be used as an indication of particle tragectories in steady laminar flow, a useful result for the experimental analysis. Therefore, a procedure is developed to find the stream functions, and consequently the velocity components Vy and Vz, using finite difference numerical methods.

Two basic methods for the solution of the biharmonic equation in rectangular coordinates have received a great deal of attention. In the first, the biharmonic equation is solved directly, and Gclub [45] derived an algorithm for the solution of the discrete biharmonic equation in rectangular regions which was examined experimentally by Walker [46] and Ehrlich [11]. Application of block Gaussian elimination to this problem was described by Bauer and Reiss [47] and Angel and Bellman [48]. Iterative methods applied directly to the biharmonic difference equations were investigated by Fox [13], Fairweather, Gourley and Mitchell [49], and Hadjidimos [15]. Zlamal analysed discretization and error estimates for fourth order elliptic boundary value problems [41]. Smith [33] and Ehrlich and Gupta [10] claim that iterative

methods applied directly to the biharmonic difference equations are not very satisfactory since they do not yield a highly accurate solution and require a large number of iterations. One of the important problems involved in the application of finite difference methods to the solution of boundary value problems by the direct iterative method is in the estimation of discretization error [41,42].

The second technique is an iterative method that treats the biharmonic equation 4.4 as a coupled pair of Poisson equations, and it has been examined by Ehrlich [10,11], Greenspan and Schultz [51], Gupta [52], Gupta and Manohar [53], Mclaurin [25], and Smith [33,34,35]. One of the important reasons for using the coupled pair of equations is that the accumulation of rounding errors is substantially reduced [10]. In addition, there is already extensive literature for second order differential equations (Poisson equations), while there are only a few papers that deal with higher order elliptic equations. The reason, as Zlamal describes [41], is that we have a very useful and simple tool for second order equations, the maximum principle, which holds both for differential equations and their finite difference analogs while there does not exist such a simple tool for higher order equations. Ehrlich and Gupta [10] support this fact by stating that the two second order (a coupled pair) boundary value problems can be solved using one of the fast Poisson solvers that are available even for nonrectangular domains.

In spite of the claim made by many workers that a coupled pair of Poisson equations is more advantageous and simpler for solving the biharmonic equation than the direct iterative method, it is surprising that no article brings out the differences in these two methods. Therefore, the biharmonic equation is solved here by both methods on rectangular boundaries to find out the relative merits and demerits of each.

In order to compare the direct iterative method with the coupled pair of Poisson equations, a model problem is chosen. As shown in Fig 4.1, four belts which extend infinitely in the direction perpendicular to the paper form a rectangular isolated region of length π and height H equal to 0.125 containing a viscous fluid. The belt AB moves in the positive z direction with unit velocity, belts AC and BD move in the y direction with velocities -1.5 and 1.5 respectively, and belt CD is stationary. This system also describes the confining plate model. Since the belts completely enclose the rectangular channel, the stream function on all the boundaries must be the same and is chosen as zero.

$$\psi = 0 \quad \text{at} \quad z = 0, \pi \tag{4.5}$$

$$\psi = 0 \quad \text{at} \quad y = 0, H \tag{4.6}$$

The velocity components Vy and Vz on the boundaries are:

$$V_y = 0 \; ; \quad V_z = 1.0 \quad \text{at} \quad y = 0 \tag{4.7}$$

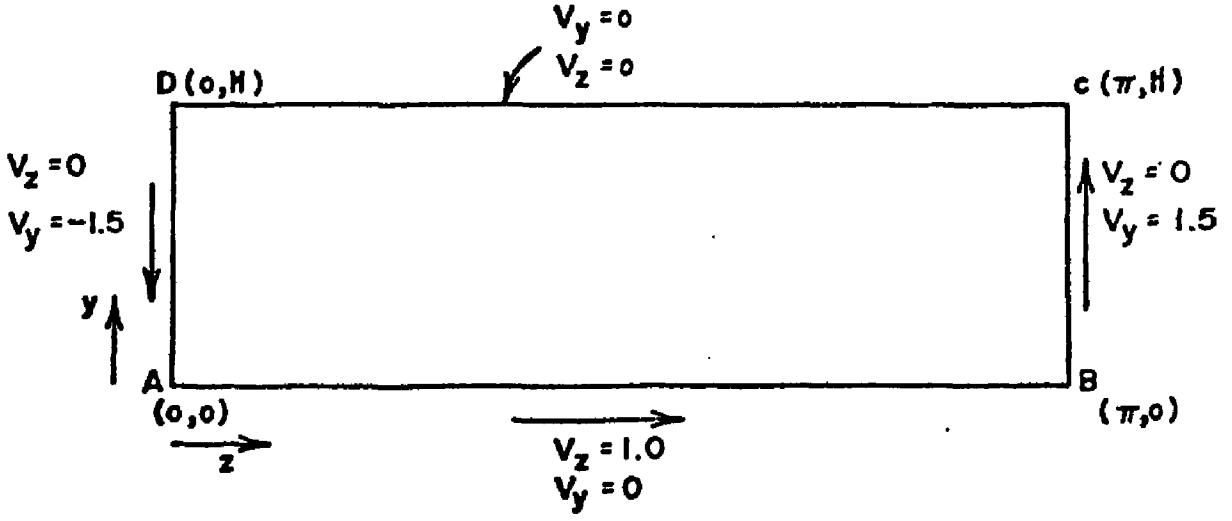

Fig. 4.1: Boundary Conditions for the Model Problem in Rectangular Coordinates

$$V_y = 0 \; ; \quad V_z = 0 \qquad \text{at } y = H \tag{4.8}$$

$$V_y = -1.5 \; ; \quad V_z = 0 \qquad \text{at } z = 0 \tag{4.9}$$

$$V_y = 1.5 \; ; \quad V_z = 0 \qquad \text{at } z = \pi \tag{4.10}$$

and equations 4.2 and 4.3 allow us to express the stream functions in terms of these velocity components.

In order to check the convergence of the numerical solution in the middle part of the rectangular boundary region of the model problem (at $z = \pi/2$), the steady state value of the stream function can be obtained analytically from equation 3.21. Since the flow is fully developed in the middle part of the region under consideration, the velocity component Vz is function of the y coordinate only and the pressure gradient $\partial P/\partial z$ is constant. From the continuity equation, it can be shown that the velocity component Vy in the middle part reduces to zero. Since the boundary is completely enclosed, the net flow rate in the z direction should be zero; and consequently, applying the boundary corditions represented by equations 4.7 and 4.8, it can be shown that [24]:

$$V_z = (a-1)(3a-1) \tag{4.11}$$

where $a = y/H$. To obtain the expression for the stream function corresponding to equation 4.11, advantage is taken of the fact that the stream function ψ, in general, can be expressed as:

$$d\psi = \left(\frac{\partial \psi}{\partial y}\right)_z dy + \left(\frac{\partial \psi}{\partial z}\right)_y dz \tag{4.12}$$

Since in the middle portion of the boundary region Vy=0, i.e. $\partial\psi/\partial z=0$, therefore,

$$d\psi = \left(\frac{\partial\psi}{\partial y}\right)_z dy = -V_z\, dy \qquad (4.13)$$

Combining equations 4.11 and 4.13 and integrating with appropriate limits leads to:

$$\psi = -aH(a-1)^2 \qquad (4.14)$$

Smith, Ehrlich and others [7,10,11,12,25,33,34,35] treated the biharmonic equation, as pointed out earlier, as a coupled pair of Poisson equations. Since the biharmonic equation describing the test system can be expressed as:

$$\nabla^2(\nabla^2\psi) = 0 \qquad (4.15)$$

then with;

$$\omega = \nabla^2\psi \qquad (4.16)$$

equation 4.15 can be written as:

$$\nabla^2\omega = 0 \qquad (4.17)$$

Thus, equations 4.16 and 4.17 form a pair of coupled equations representing the biharmonic equation 4.15. The quantity ω, in this case, is the vorticity defined as $\nabla^2\psi$ [5,44].

Let the increment in the z direction Δz, be h and that

in the y direction Δy, be k so that:

$$z = jh \tag{4.18}$$

$$y = ik \tag{4.19}$$

where the integers i and j correspond to row i and column j respectively of the rectangular finite difference grid. Using the central difference approximation, equations, 4.16 and 4.17 are represented by their finite difference forms as follows [21,30]:

$$\psi_{i,j} = \frac{\left[(k/h)^2(\psi_{i,j+1}+\psi_{i,j-1})+(\psi_{i+1,j}+\psi_{i-1,j})-k^2\omega_{i,j}\right]}{2\left[(k/h)^2+1\right]} \tag{4.20}$$

$$\omega_{i,j} = \frac{\left[(k/h)^2(\omega_{i,j+1}+\omega_{i,j-1})+\omega_{i+1,j}+\omega_{i-1,j}\right]}{2\left[(k/h)^2+1\right]} \tag{4.21}$$

Introducing the accelerating factors α_1 and α_2, equations 4.20 and 4.21 are modified to give the latest value of the stream function and vorticity for an iteration step based on their values from the preceding step and that computed by equations 4.20 and 4.21 as,

$$(\psi_{i,j})_{\substack{\text{new}\\\text{value}}} = \alpha_1(\psi_{i,j})_{\substack{\text{from}\\\text{equation 4.20}}} + (1-\alpha_1)(\psi_{i,j})_{\substack{\text{preceding}\\\text{value}}} \tag{4.22}$$

$$(\omega_{i,j})_{\substack{\text{new}\\\text{value}}} = \alpha_2(\omega_{i,j})_{\substack{\text{from}\\\text{equation 4.21}}} + (1-\alpha_2)(\omega_{i,j})_{\substack{\text{preceding}\\\text{value}}} \tag{4.23}$$

which allows calculation of the stream functions, and consequently the velocity profiles, for the entire channel.

Since the optimum accelerating factors are not known for a rectangular boundary case involving the coupled pair of Poisson equations, several sets of accelerating factors were tried; and the optimum accelerating factors for the model problem under investigation were found to both be 0.8. To obtain an approximate solution by the coupled set of second order equations, initial values of stream function and vorticity at all mesh points were set to -0.01 and 0.0 respectively. Then, the stream functions were calculated at all mesh points from equation 4.22 while the w's were computed at all mesh points by equation 4.23. These two steps were repeated successively until the ψ's at all mesh points converge to their steady state values, and these were tested against the corresponding analytical values of the stream function given by equation 4.14 in the middle part of the channel. The method used for elimination of the fictitious mesh points is direct or explicit since their values at any step were computed based upon the known values of the nonfictitious mesh points obtained in the preceding stage. The computer program "TWOSEC" describing the computational steps and procedures is included in the Appendix E-1.

The approximate solution for the stream function

obtained by the coupled pair of Poisson equations was found to be almost independent of the initial assumed values of the stream function and vorticity. Also, a little deviation in the value of the optimum accelerating factor did not make a significant difference in the rate of convergence. However, the optimum accelerating factor was found to be dependent upon the mesh size and the boundary conditions used. In order to obtain the approximate solution , the channel was divided into 30 by 30 mesh grid giving a total of 29 by 29 interior mesh points. 750 iterations were required before the iterative solution converged to their steady state values with the time per iteration 0.12 seconds giving a total time of 85 seconds. The accuracy of convergence was 99.7%, and the rate of convergence of the stream function values in the middle region is shown in Fig 4.2.

Fox [13] was the first to consider the case of the direct solution of the biharmonic difference equation for rectangular as well as curved boundaries involving derivative boundary conditions. He discussed the general principles of the suggested method and established the relevant firite difference formulae. A numerical example was solved for a problem with rectangular boundaries, and curved boundary problems were briefly discussed. His solution technique, however, was based upon relaxation methods [13,30].

For the direct iterative method with the central

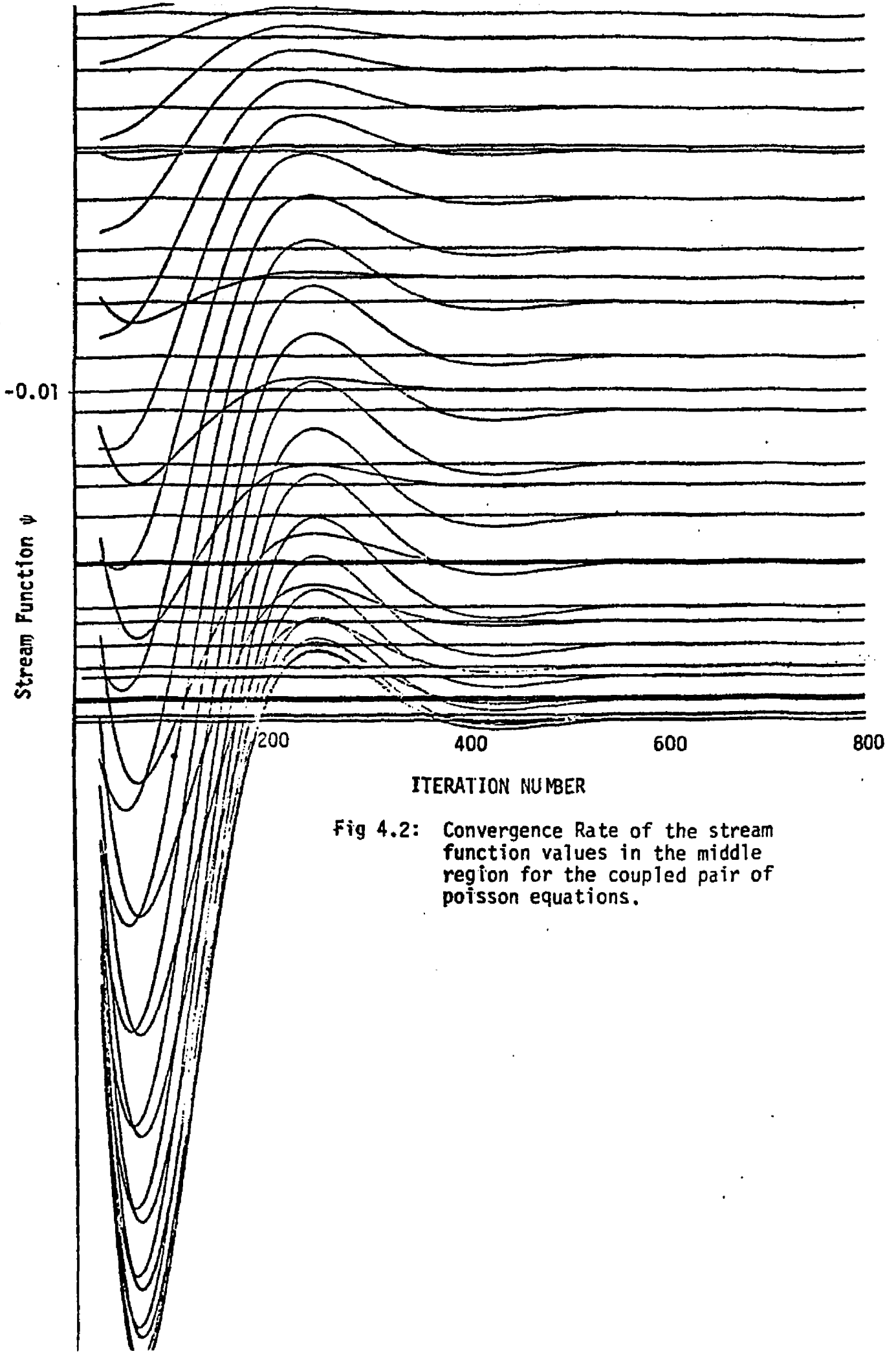

Fig 4.2: Convergence Rate of the stream function values in the middle region for the coupled pair of poisson equations.

difference approximation, the biharmonic equation 4.4 is expressed as a finite difference equation involving 13 mesh points. Letting R be equal to k/h, the resulting biharmonic difference equation is represented as:

$$\psi_{i-2,j} + 2R^2\psi_{i-1,j-1} - 4(1+R^2)\psi_{i-1,j} + 2R^2\psi_{i-1,j+1} + R^2\psi_{i,j-2}$$
$$-4(R^2+R^4)\psi_{i,j-1} + (6+6R^4+8R^2)\psi_{i,j} - 4(R^2+R^4)\psi_{i,j+1} + R^4\psi_{i,j+2}$$
$$+ 2R^2\psi_{i+1,j-1} - 4(1+R^2)\psi_{i+1,j} + 2R^2\psi_{i+1,j+1} + \psi_{i+2,j} = 0$$

or,
$$\sum_{n=1}^{13} A_n \psi_n = 0 \qquad (4.24)$$

The computational molecule [13,30] representation of the equation 4.24 is shown in Fig 4.3.

The general procedure to obtain the approximate solution for the rectangular boundary problem is to satisfy equation 4.24 at every internal mesh point. The mesh points lying outside the boundary, the fictitious mesh points, are eliminated in terms of the internal mesh points using derivative boundary conditions such as the known velocity components on the boundaries which are derivatives of the stream function as shown in equations 4.2 and 4.3. For higher accuracy, For recommended use of accurate derivative boundary conditions where differences of orders up to at least fourth should always be retained in Gregory-Newton's interpolation formula [13,30], although up to sixth order would often be advantageous to minimize the number of

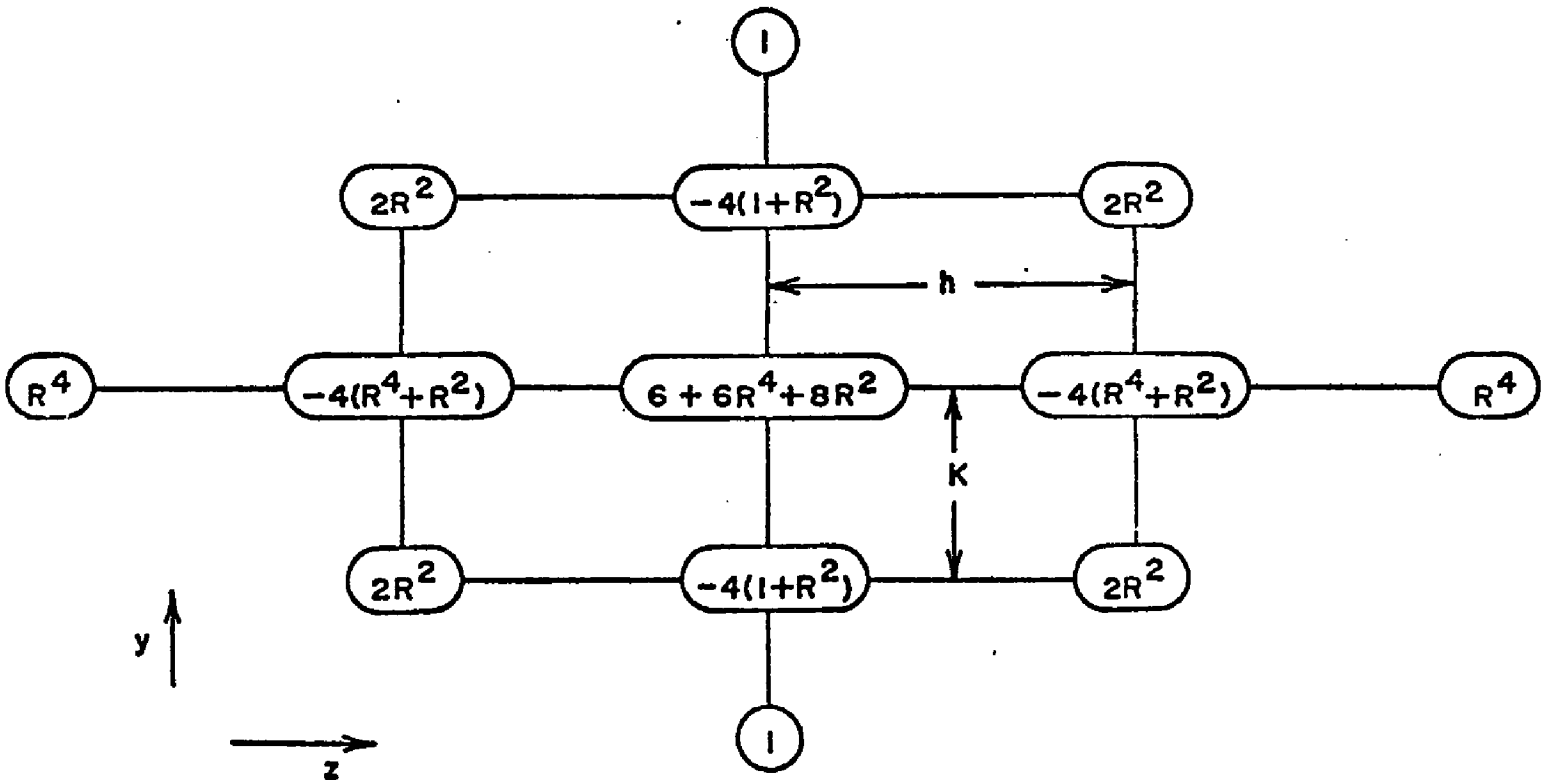

Fig. 4.3: The Computational Molecule of Equation 4.24; R is equal to k/h, the Ratio of Unit Mesh Length in the y direction, k, to the Unit Mesh Length in the z direction, h.

iterations. According to his method of relaxation, an additional term Δ is used in the finite difference biharmonic equation 4.24 which includes differences up to the sixth order in the Taylor's series expansion. This term, Δ, is expressed as follows:

$$\Delta = -\frac{1}{9}\left[h^2 \frac{\partial^6 \psi}{\partial z^6} + k^2 \frac{\partial^6 \psi}{\partial y^6} \right] = -\frac{1}{9}\left[\frac{\delta^6_{o,z}}{h^4} + \frac{\delta^6_{o,y}}{k^4} \right]$$

$$\text{or,} \quad k^4 \Delta = -\frac{1}{9}\left[R^4 \delta^6_{o,z} + \delta^6_{o,y} \right] \qquad (4.25)$$

where R equals k/b. Using the central difference approximations, the quantities $\delta_{o,z}$ and $\delta_{o,y}$ are expressed as:

$$\delta^6_{o,z} = \psi_{i,j+3} - 6\psi_{i,j+2} + 15\psi_{i,j+1} - 20\psi_{i,j} + 15\psi_{i,j-1} - 6\psi_{i,j-2} + \psi_{i,j-3} \qquad (4.26)$$

$$\delta^6_{o,y} = \psi_{i+3,j} - 6\psi_{i+2,j} + 15\psi_{i+1,j} - 20\psi_{i,j} + 15\psi_{i-1,j} - 6\psi_{i-2,j} + \psi_{i-3,j} \qquad (4.27)$$

Thus, incorporation of the term Δ in equation 4.24 leads to the expression involving 17 mesh points:

$$\sum_{n=1}^{13} A_n \psi_n + \Delta = 0 \qquad (4.28)$$

Fox first neglected the term Δ and solved the set of simultaneous equations by relaxation methods. Then, he computed the term Δ by equations 4.25 through 4.27 and the result was substituted back into equation 4.28. Now, he

could recompute new ψ's and repeat the procedure until the ψ's did not change significantly.

In the present procedure for the direct iteration method, the term Δ is included in the finite difference biharmonic equation. The method of successive overrelaxation and the concept of accelerating factor were not developed at the time of Fox's work, but it is employed here to accelerate the rate of convergence and to minimize the number of iteration cycles. The derivative boundary conditions employ Gregory-Newton's interpolation formulae involving forward and backward differences up to the sixth order and can be described as follows:

$$\psi_{i,j-2} = -6h\left(\frac{\partial \psi}{\partial z}\right)_{i,j-1} - 7.7\,\psi_{i,j-1} + 15\,\psi_{i,j} - 10\,\psi_{i,j+1} + 5\,\psi_{i,j+2} - 1.5\,\psi_{i,j+3} + 0.2\,\psi_{i,j+4} \qquad (4.29)$$

$$\psi_{i,j+2} = 6h\left(\frac{\partial \psi}{\partial z}\right)_{i,j+1} - 7.7\,\psi_{i,j+1} + 15\,\psi_{i,j} - 10\,\psi_{i,j-1} + 5\,\psi_{i,j-2} - 1.5\,\psi_{i,j-3} + 0.2\,\psi_{i,j-4} \qquad (4.30)$$

$$\psi_{i-2,j} = -6k\left(\frac{\partial \psi}{\partial y}\right)_{i-1,j} - 7.7\,\psi_{i-1,j} + 15\,\psi_{i,j} - 10\,\psi_{i+1,j} + 5\,\psi_{i+2,j} - 1.5\,\psi_{i+3,j} + 0.2\,\psi_{i+4,j} \qquad (4.31)$$

$$\psi_{i+2,j} = 6k\left(\frac{\partial \psi}{\partial y}\right)_{i+1,j} - 7.7\,\psi_{i+1,j} + 15\,\psi_{i,j} - 10\,\psi_{i-1,j} + 5\,\psi_{i-2,j} - 1.5\,\psi_{i-3,j} + 0.2\,\psi_{i-4,j} \qquad (4.32)$$

where $\partial\psi/\partial y$ and $\partial\psi/\partial z$ are located at the mesh points lying on the boundary, while the terms on the left hand sides of equations 4.29 through 4.32 lie on mesh points one length beyond the boundary. Before these mesh points were

eliminated, the values of the stream function two mesh lengths beyond the boundary are eliminated in terms of the interior mesh points by employing Gregory-Newton's interpolation formula in a similar manner.

For the computational procedure, all sides of the rectangular channel were divided into 30 increments to solve the biharmonic equation 4.4 so that the total number of interior mesh points for the biharmonic equation was 29 by 29. The fictitious mesh points beyond the boundary were eliminated in terms of the internal mesh points using derivative boundary conditions retaining differences up to second order for the coupled pair of Poisson equations and up to sixth order for the direct iterative method. In contrast to the coupled pair of Poisson equation method, however, indirect or implicit elimination of fictitious mesh point was used in which its value was replaced in terms of the nonfictitious mesh points which include the current unknown value of the central mesh point.

In order to obtain the approximate solution, initial stream function values at all mesh points were set equal to -0.01. Unfortunately, the optimum accelerating factor estimation criteria for this method is not available in the literature [41,42]. At first, different sets of accelerating factors, α, were assumed; and the stream functions were computed using equations 4.28 in the accelerating factor expressions:

$$(\psi_{i,j})_{\substack{\text{new}\\\text{value}}} = \alpha\,(\psi_{i,j})_{\substack{\text{calculated}\\\text{by equation 4.28}}} + (1-\alpha)(\psi_{i,j})_{\substack{\text{preceding}\\\text{value}}} \qquad (4.33)$$

The accelerating factcr was varied from 1 to 2. It was found that there did nct exist one particular value of the accelerating factcr for which the convergence was fastest for all mesh pcints. In cther words, higher values of the accelerating factor were favored by some mesh points while lower values were favored by cthers, and the overall effect of the accelerating factor on the rate of convergence of all mesh pcints tc their steady state values was found to be complex and ccnfusing. For instance, when the accelerating factor value was 1.75, it tcok over 4000 iteration cycles before the 99% ccnvergence was achieved. However, not all mesh points were converging at the same speed. Some of them oscillated as they quickly reached their steady state values, cthers ccnverged very slcwly, and the rest converged at a rate somewhat in between.

The next step was to see if the optimum accelerating factor is a functicn cf position. Several empirical forms of the accelerating factor which varied from one mesh point to ancther were investigated. The most efficient one found for the model under consideration was a function of the y coordinate cnly and is given by the following set of equations:

$$\left.\begin{aligned} \alpha &= 2 - B(3a)^C \qquad 0 \le a \le 1/3 \\ \alpha &= 2 - B + B\left(\frac{3a-1}{2}\right)^D \qquad \frac{1}{3} \le a \le 1 \end{aligned}\right\} \qquad (4.34)$$

In order to determine empirical constants B, C, and D, several possible combinations were attempted; and the convergence pattern in each case was studied. A computer plot of the stream function over the channel depth vs the number of iteration cycles was made for the down channel position at $z = \pi/2$ and the stream function behavior was observed. From these observations, a relation between the constants C and D was found.

From equation 4.14, a plot of Ψ/H versus a is shown in Fig 4.4. Areas A_1 and A_2 as shown in Fig 4.4 can be determined by integrating equation 4.14 with the proper limits as,

$$A_1 = \int_0^{1/3} (\Psi/H)\, da = -11/324 \qquad (4.35)$$

$$A_2 = \int_{1/3}^{1} (\Psi/H)\, da = -16/324 \qquad (4.36)$$

The ratio of A_1 to A_2, R_ψ, is obtained as:

$$R_\psi = A_1/A_2 = 11/16 \qquad (4.37)$$

Now if a plot of the accelerating factor α is made against a as shown in Fig 4.5, areas A_1' and A_2' can be determined by integrating the expressions for α, equation 4.34, with respect to a between the appropriate limits,

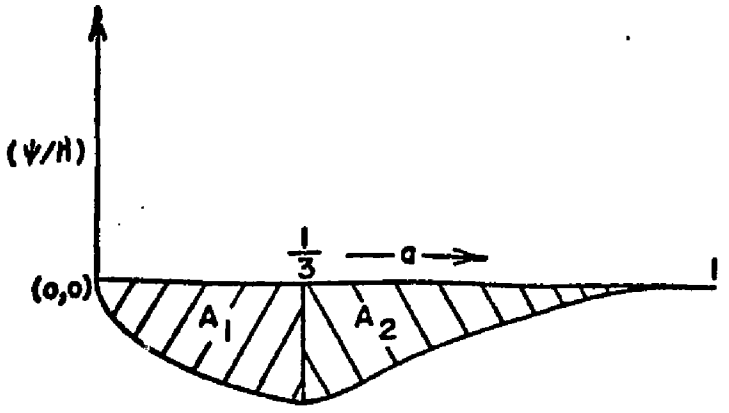

Fig. 4.4: A Plot of (ψ/H) vs a

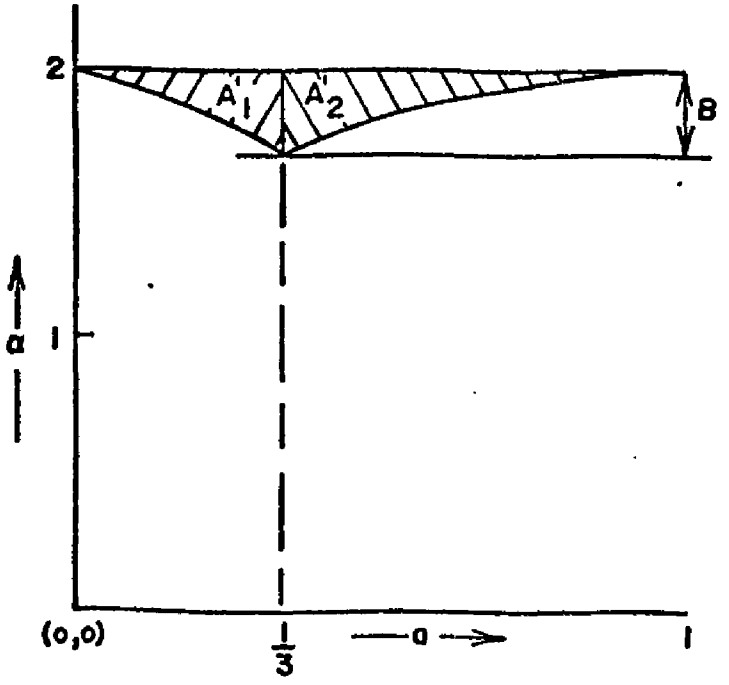

Fig. 4.5: A Plot of the Accelerating Factor α vs a

$$A_1' = \int_0^{1/3} B(3a)^C da = \frac{B}{3(C+1)} \qquad (4.38)$$

$$A_2' = \int_{1/3}^{1} B - B\left(\frac{3a-1}{2}\right)^D da = \frac{2BD}{3(D+1)} \qquad (4.39)$$

Thus, the ratio of A_1' to A_2', R_α, becomes:

$$R_\alpha = A_1'/A_2' = \frac{D+1}{2D(C+1)} \qquad (4.40)$$

For the optimum convergence, it was found that R_ψ and R_α become equal which, on further simplification, yields:

$$C = \frac{8-3D}{11D} \qquad (4.41)$$

The next step is to determine the constants B and C (or D), but no relation was found between them despite a number of attempts. However, the following procedure seems to lead in the right direction to obtain a form for optimum accelerating factor. First the constant D is assumed, and the constant C is found from the equation 4.41. Then a value for the constant B is assumed, and the convergence checked. The procedure is repeated by changing the value of the constant B until the least number of iteration cycles is required for convergence. The entire procedure is now repeated with another value of the constant D, and the corresponding best value of the constant B is obtained for the least number of iteration cycles. Thus, the best values of the constants B and D are determined to give the best possible convergence rate. The above method and the form of

the accelerating factcr, equation 4.34, however may still not be the true cptimum ones to obtain the fastest convergence rate.

As a result of the abcve procedure, the constants B, C, and D fcr tke best ccnvergence rate were found to be B=0.7092, C=E.2834, D=0.C85; and 400 iteration cycles were required to cktair complete convergence. The time per iteratien was C.16 second, thus giving a total time of 64 seconds. The accuracy cf convergence was over 99.99%. The convergence rate of the stream function values in the middle part of the channel versus the iteration number is shown in Fig 4.6. The ccmputer program describing all computational details, "FCUETH", is included in the Appendix E-2.

Numerical solutions were cbtained by both the explicit and the implicit elimination of fictitious mesh points as discussed kefcre, and the highest value of the accelerating factor α that could be employed before unstable oscillatiens kegan were 1.3 and 2.0 respectively. The number of iteration cycles required for convergence for the explicit elimiratien cf fictitious mesh point approach was about 8 to 9 times higher than that for the other approach; therefore, tke implicit elimination of the fictitious mesh points was adopted fcr the direct iterative method.

For the direct iterative procedure, the approximate solution was fcund to be sensitive to the initial stream function values; and a little deviation in the value of the accelerating factcr is found to affect the rate of

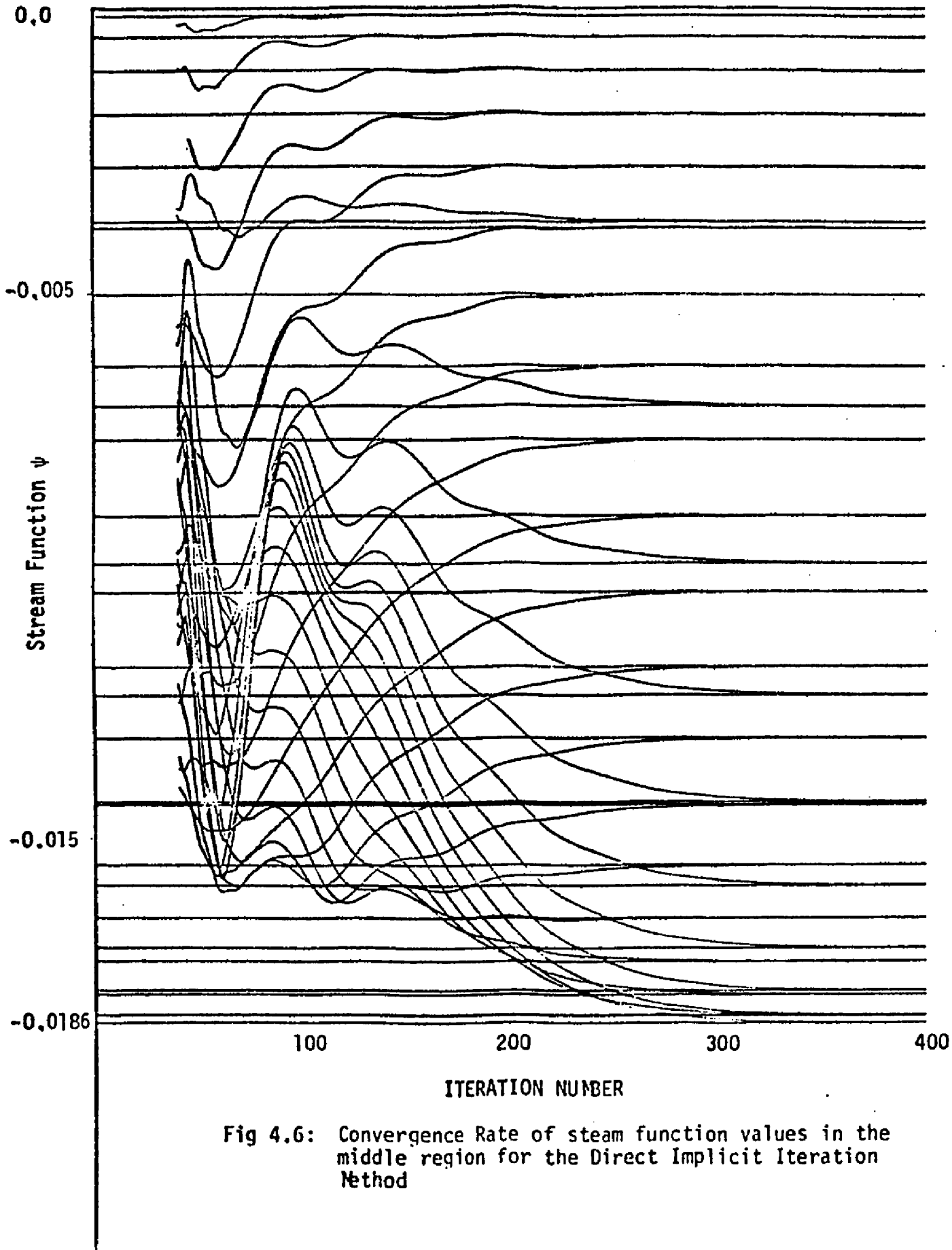

Fig 4.6: Convergence Rate of steam function values in the middle region for the Direct Implicit Iteration Method

convergence significantly. The optimum accelerating factor was alsc found to be a strong function of mesh size, boundary conditions, and the ccnstants B, C, and D which appear in eguaticn 4.34. Thus, in this method, estimation of the cptimum accelerating factor and the computational procedures invclved are not straightforward as they are for the coupled pair of Poisson equations. However, the accuracy cf convergence is fcund to be better than that in the coupled pair of Poisson equation approach.

For the curved boundary problem which is discussed in the chapter V, the direct iterative method is employed. The estimaticn of the optimum accelerating factor in that case is simplified by emplcying a form of α which is the function cf current value cf the stream function itself, and is given as:

$$\alpha_{i,j} = 2 - B\,|\,\psi_{i,j}\,| \qquad (4.42)$$

The constant B can be determined by few trials starting with a lowest value and would depend upon the magnitude of the stream functior values involved. When equation 4.42 was emplcyed for the mcdel rectangular boundary problem, it was found to be 30 percent less efficient than the use of equation 4.34. However, the loss in efficiency in convergence rate must be tclerated for the curved boundary system since eguaticn 4.34 does not apply.

V NUMERICAL SOLUTIONS FOR THE SYSTEM MODELS

In chapter III, three models were developed, one for a zero helix angle case in the cylindrical coordinate system called the cylindrical model and the other two for any helix angle in rectangular cocrdinates called the curved boundary flat plate and the ccnfining flat plate models. Since the model problem in chapter IV corresponds to the confining flat plate ncdel, the numerical solution for the latter is already kncwn. In the present chapter, the numerical procedures used tc ctain the approximate solutions for other twc ncdels are described since direct analytical solution cf equaticns 3.8 and 3.9 was not possible.

The Cylindrical Model

The appicximate sclution cf equations 3.8 and 3.9 in cylindrical ccordinates is cbtained by introducing the stream functicn, ψ, defined by [5]:

$$V_r = \frac{1}{r}\frac{\partial \psi}{\partial \theta} \qquad (5.1)$$

$$V_\theta = -\frac{\partial \psi}{\partial r} \qquad (5.2)$$

so that the ccntinuity equaticn in cylindrical coordinate system is satisfied. Ncw, eliminating the pressure gradient

terms from equations 3.8 and 3.9 in the manner similar to that used in obtaining the biharmonic equation 4.4 in chapter IV, the resulting biharmonic equation in cylindrical coordinates becomes:

$$\nabla^4\psi = \frac{\partial^4\psi}{\partial r^4} + \frac{2}{r}\frac{\partial^3\psi}{\partial r^3} - \frac{1}{r^2}\frac{\partial^2\psi}{\partial r^2} + \frac{1}{r^3}\frac{\partial\psi}{\partial r} + \frac{2}{r^2}\frac{\partial^4\psi}{\partial r^2\partial\theta^2}$$
$$- \frac{2}{r^3}\frac{\partial^3\psi}{\partial r\partial\theta^2} + \frac{4}{r^4}\frac{\partial^2\psi}{\partial\theta^2} + \frac{1}{r^4}\frac{\partial^4\psi}{\partial\theta^4} = 0 \qquad (5.3)$$

In the preceding chapter two approaches were studied for obtaining the solution of the biharmonic equation in rectangular coordinates. The direct iterative method will be employed to solve the biharmonic equation 4.4 in rectangular coordinates for the curved boundary flat plate model. However, equation 5.3 is solved using a pair of second order Poisson equations, because the behavior of accelerating factor for the direct iterative method in the cylindrical coordinate system is not known, while the coupled pair of Poisson equations solution is straightforward.

Equations 4.16 and 4.17 in cylindrical coordinate form provide the desired pair of second order equations, and if h and k are the increments in the θ and r directions respectively, these equations can be represented in their finite difference forms based on the central difference approximation as follows [21,30]:

$$\psi_{i,j} = \frac{\left[\left(\frac{1}{k^2}+\frac{1}{2rk}\right)\psi_{i+1,j} + \left(\frac{1}{k^2}-\frac{1}{2rk}\right)\psi_{i-1,j} + \frac{1}{h^2r^2}\left(\psi_{i,j+1}+\psi_{i,j-1}\right) - \omega_{i,j}\right]}{2\left(\frac{1}{k^2}+\frac{1}{r^2h^2}\right)} \tag{5.4}$$

$$\omega_{i,j} = \left[\left(\frac{1}{k^2}+\frac{1}{2rk}\right)\omega_{i+1,j} + \left(\frac{1}{k^2}-\frac{1}{2rk}\right)\omega_{i-1,j} + \frac{1}{h^2r^2}\left(\omega_{i,j+1}+\omega_{i,j-1}\right)\right] \tag{5.5}$$

where integers i and j correspcnd to row i and column j respectively cf the finite difference grid in cylindrical coordinates. The accelerating factors α_1 and α_2, as described in the preceding chapter, can be introduced to speed up the ccnvergence rate. Thus, the newest values of the stream functions and vorticities are computed for an iteration step based cn their values from the preceding step and that ccmputed by equations 5.4 and 5.5 in a manner analogous tc equations 4.22 and 4.23.

Eliminaticn of fictitious mesh points beyond the boundaries for a region $\alpha \leq \theta \leq (2\pi-\alpha)$ is straightforward. However, for the curved boundary regions, all the interior mesh points are nonfictitious, and the fictitious external points are eliminated using the boundary conditions described by equaticns 3.3 and 3.5. To eliminate the stream function cn an external mesh pcint in equation 5.4, a second order interpclaticn formula [13] is employed that uses the stream function value on the curved boundary; while to compute the vorticity, the external point is eliminated using the derivative bcundary condition [13].

The computational procedure employed for a coupled pair

of Poisson equations is similar to that described in chapter IV. A 30 by 30 mesh grid was used, and the stream function and the vorticity values at all the interior mesh points were set equal to -0.02 and 0.0 respectively. The accelerating factors which provided the best convergence were both 0.6 with the convergence stability a strong function of the values chosen. The number of iterations required to obtain the approximate solution for the entire channel or a part of it ranged from 3000 to 4000, and the time per iteration was 0.17 seconds. The convergence accuracy, as tested against equation 7.3, the known analytical solution in the middle part of the channel, was 99.8 percent.

The Curved Boundary Flat Plate Model

In order to obtain the approximate solution of equation 4.24 for the curved boundary flat plate model, the entire channel CC'E'A', as shown in Fig 3.4, was transformed into a grid of mesh points such that mesh length in the z direction was 1/30 th of the length CC' and that in the y direction was 1/30 th of the transformed channel depth H'. Equation 4.24 was satisfied at every internal mesh point which was at least one mesh length inside the boundaries. Fictitious mesh points which were outside the boundaries or less than one mesh length inside the boundaries, were eliminated using

Gregory-Newton's interpolation formulae involving accurate derivative boundary conditions [13]. These formulae will be described in detail later in this chapter.

The elimination procedure for fictitious mesh points was implicit since direct algebraic substitution for the fictitious point was made in equation 4.24 using the boundary condition to produce an equation involving only nonfictitious points with their latest values. The elimination of the fictitious mesh points can be illustrated by applying the finite difference biharmonic equation 4.24 at the mesh point P, as shown in Fig 5.1. The internal mesh points T and Q as well as the external fictitious mesh points E,S and R are among the 13 mesh points involved in equation 4.24. The mesh points S and T are eliminated in terms of the internal mesh points of the same row, i.e. U,V,W,X, etc, by applying Gregory-Newton's forward interpolation formulae for both the boundary condition involving the known stream function and that for its derivative with respect to z at the point a where the line ST cuts the boundary. Similarly, mesh points S and Q can be eliminated in terms of the internal nonfictitious mesh points of the same column, i.e. L,M,N, etc, by applying Gregory-Newton's interpolation formulae for both the boundary condition of the known stream function and that for its derivative with respect to y at the point b, where the line SQ cuts the boundary. Since the mesh point S is eliminated twice in these steps, only the arithmetic average

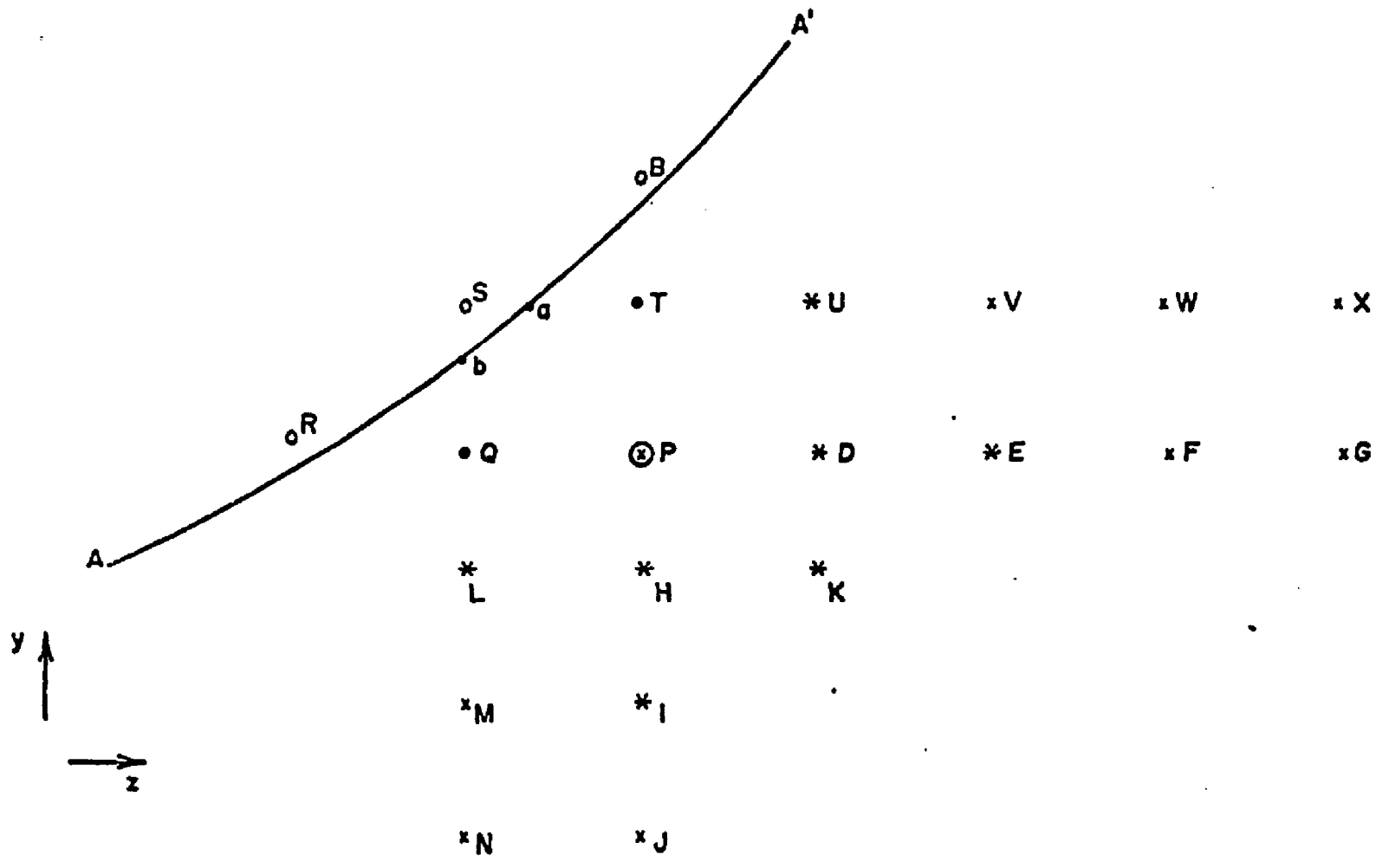

Fig. 5.1: Equation 4.24 as Applied at the Mesh Point P. Points B, S and R lie outside the Curved Boundary AA' and thus are External Fictitious Mesh Points; while Points T and Q are internal Fictitious Mesh Points.

value of S will be eliminated. In other words, half of the mesh point S will be eliminated in the positive z direction and the other half will be eliminated in the negative y direction as explained above. The mesh point B will always be eliminated in the negative y direction in terms of the nonfictitious mesh points P,H,I,J, etc; and the mesh point R will always be eliminated in the positive z direction in terms of the nonfictitious mesh points P,D,E,F, etc. Thus, the biharmonic difference equation only contains internal nonfictitious mesh points; and iterations were performed at every such point on the grid until convergence was achieved.

Gregory-Newton's interpolation formulae for implicit elimination of external as well as internal fictitious mesh points are described by equations 5.6 and 5.7, using forward and backward differences respectively. These formulae can also be used for extrapolation [13].

$$\psi(a+fh) = \left[1 + f\Delta + f(f-1)\Delta^2 + \cdots\cdots \right] \psi(a) \qquad (5.6)$$

$$\psi(a-fh) = \left[1 - f\nabla + f(f-1)\nabla^2 - \cdots\cdots \right] \psi(a) \qquad (5.7)$$

The Δ and ∇ in these equations are the forward and backward difference operators respectively operating on $\psi(a)$ the stream function value at a mesh point a. h is the distance between two successive evenly spaced mesh points in the direction of interest, while f is a fraction such that the boundary is at a distance of fh from the mesh point at

the point a.

Consider the forward difference interpolation formula, equation 5.6, for the case shown in Fig 5.2. The points A and B are such that they are less than one mesh length, h, from the curved boundary. Let $\psi'(A)$ and $\psi(O)$ be the stream function values at the mesh point A and at the point O on the boundary respectively as shown in Fig 5.2. Thus, from Fig 5.2, AO=hf and OC=2h-hf; and equation 5.6 for point O can be written as:

$$\psi(O) = \left[1 + f\Delta + f\frac{(f-1)}{2!}\Delta^2 + \cdots\cdots \right] \psi_A \qquad (5.8)$$

Since z=fh, dz=hdf, differentiating equation 5.8 with respect to f yields the following expression:

$$\left(\frac{\partial\psi}{\partial f}\right)_O = h\left(\frac{\partial\psi}{\partial z}\right)_O = \left[\Delta + \frac{(2f-1)}{2}\Delta^2 + \cdots \right] \psi_A \qquad (5.9)$$

$(\partial\psi/\partial z)_O$ is the y component of velocity at the point O on the boundary which is given by equation 3.11 and therefore equation 5.9 becomes:

$$h V_r \left[\frac{2\cos^2\theta}{\left(\left(\frac{Db}{2Dr}\right)^2 - z^2\sin^2\theta\cos^2\theta\right)^{0.5}} \right] = \left[\Delta + \frac{(2f-1)}{2}\Delta^2 + \cdots \right] \psi_A \qquad (5.10)$$

where V_r equals Db/Dr as desribed in chapter III.

Equations 5.8 and 5.10 form a pair of equations for elimination of fictitious mesh points A and B. These can be further simplified while retaining up to sixth order

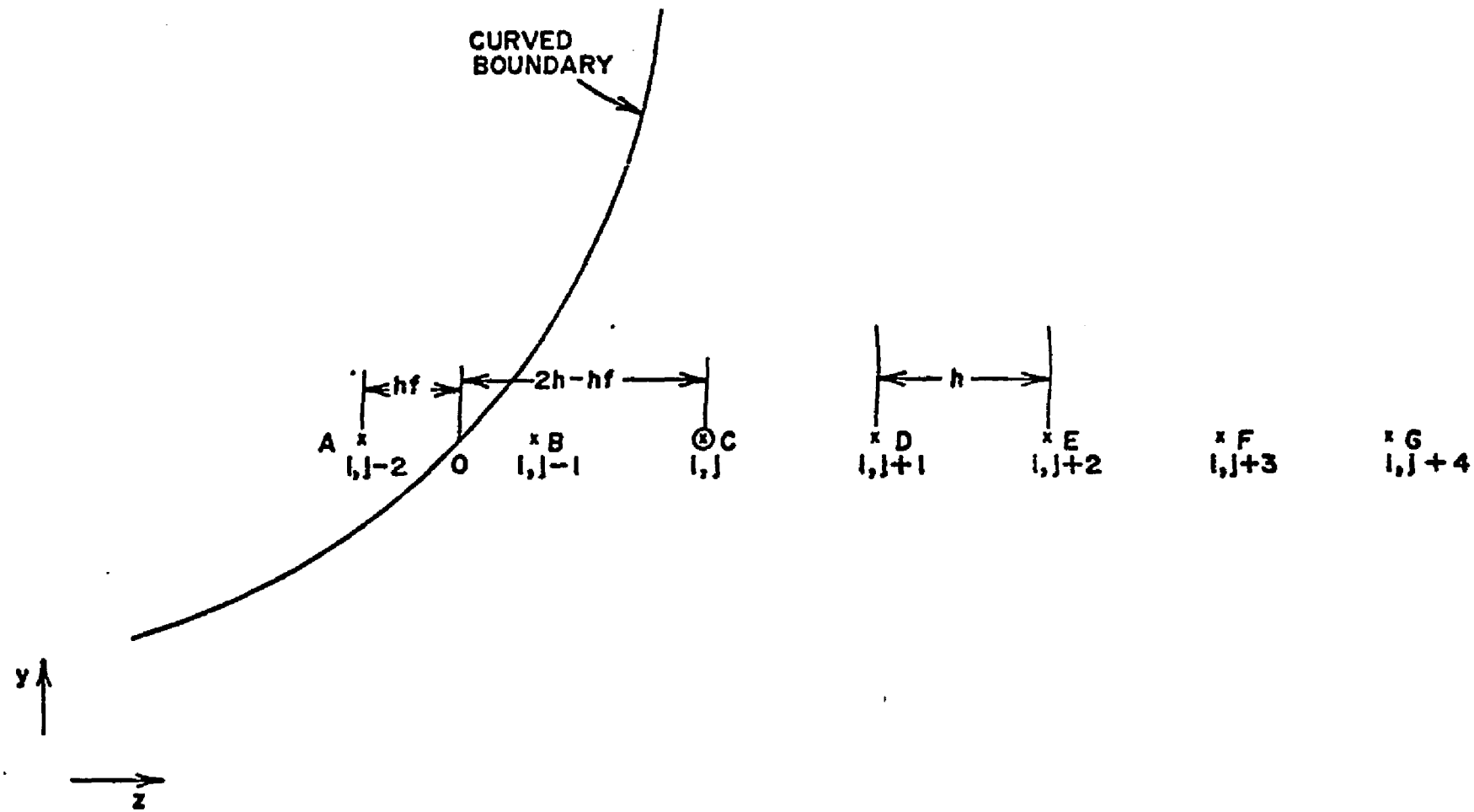

Fig. 5.2 Application of Gregory-Newton's Interpolation Formula for Elimination of Fictitious Mesh Points in the Positive z-direction

differences and sclved for pcints A and B to give,

$$\psi_A = a_1\psi_C + b_1\psi_D + c_1\psi_E + d_1\psi_F + e_1\psi_G + f_1$$

$$\text{or, } \psi_{i,j-2} = a_1\psi_{i,j} + b_1\psi_{i,j+1} + c_1\psi_{i,j+2} + d_1\psi_{i,j+3} + e_1\psi_{i,j+4} + f_1 \quad (5.11)$$

$$\psi_B = \psi_{i,j-1} = a_2\psi_{i,j} + b_2\psi_{i,j+1} + c_2\psi_{i,j+2} + d_2\psi_{i,j+3} + e_2\psi_{i,j+4} + f_2 \quad (5.12)$$

where the coefficients a_1, b_1, ... f_1 and a_2, b_2, ...f_2 result from the simultaneous solution of equations 5.8 and 5.10. Similarly, starting frcm equation 5.7, a pair of equations can be derived to eliminate two fictitious mesh points in the y direction in which one lies outside the boundary while the other is just inside but less than one mesh length away. Thus as shown in Fig 5.3,

$$\psi_{i+2,j} = a_3\psi_{i,j} + b_3\psi_{i-1,j} + c_3\psi_{i-2,j} + d_3\psi_{i-3,j} + e_3\psi_{i-4,j} + f_3 \quad (5.13)$$

$$\psi_{i+1,j} = a_4\psi_{i,j} + b_4\psi_{i-1,j} + c_4\psi_{i-2,j} + d_4\psi_{i-3,j} + e_4\psi_{i-4,j} + f_4 \quad (5.14)$$

A pair cf equaticns for elimination of two fictitious mesh points in the negative z direction for the right curved boundary can be obtained starting from the equation 5.7 to yield (as shcwn in Fig 5.4):

$$\psi_{i,j+2} = a_5\psi_{i,j} + b_5\psi_{i,j-1} + c_5\psi_{i,j-2} + d_5\psi_{i,j-3} + e_5\psi_{i,j-4} + f_5 \quad (5.15)$$

$$\psi_{i,j+1} = a_6\psi_{i,j} + b_6\psi_{i,j-1} + c_6\psi_{i,j-2} + d_6\psi_{i,j-3} + e_6\psi_{i,j-4} + f_6 \quad (5.16)$$

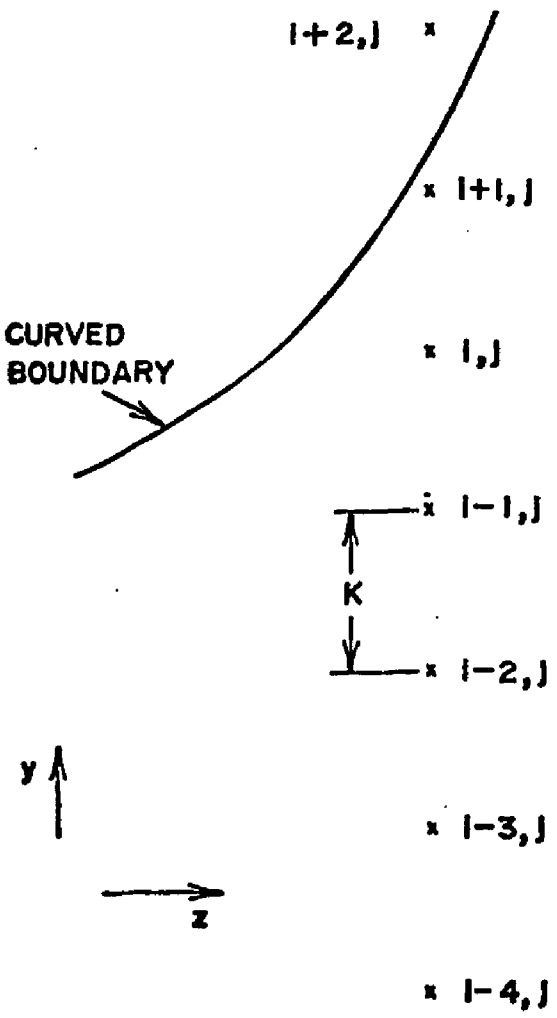

Fig. 5.3: Elimination of Fictitious Mesh Points in the Negative y-direction

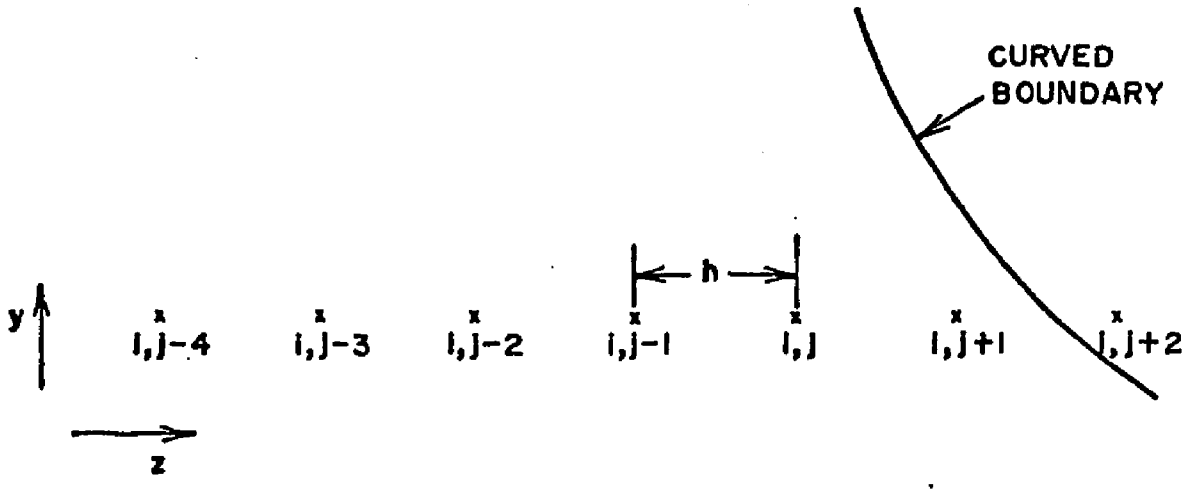

Fig. 5.4: Elimination of Fictitious Mesh Points in the Negative z-direction

The coefficients a_3, b_3, ...a_6, b_6, c_6, ...,f_6 can be computed in the manner described earlier.

After the elimination of fictitious mesh points is completed, there may be more fictitious mesh points which were not included in the 13 point formula but were introduced by Gregory-Newton's interpolation formulae retaining up to sixth order differences. These were eliminated in the same manner in terms of their respective interior mesh points.

In general, the process of elimination of fictitious mesh points is very complex. The nature of the curved boundary and mesh size in either direction are the important factors that influence the number of fictitious mesh points which must be eliminated. Furthermore, depending upon the order of the differences retained in the Gregory-Newton's interpolation formulae, additional fictitious mesh points may be involved which must be eliminated before attempting the solution at the mesh point under consideration. Again some of the fictitious mesh points must be simultaneously eliminated in both the y and z directions. The complexity of the problem can be realized when all these aspects are considered at once, and a step-by-step process is required which will satisfy all the required conditions and still make it possible to compute a solution at the mesh point under consideration. The complete procedure of elimination of fictitious mesh points is described in detail in Appendix

B.

The computational procedure was initiated by setting all of the values of the stream function at all mesh points equal to -0.01, and the accelerating factor used was in accordance with equation 4.42. The value of the constant B in equation 4.42 was found to be higher for the counter-rotating case and to increase as the down channel mesh size, Δz, decreased. For the co-rotating case, the value of the constant B was 15, while for the counter rotating case it was 20 for the same mesh size, Δz, which is 1/30 th of the bottom boundary. When Δz was decreased by a factor of 5 to include only the end region, the value of B for the co-rotating case rose to 30; and the rate of convergence dropped. Thus, the accelerating factor values were low when the numerical solution for an end segment of the channel was determined. In addition, the acceptable value of the accelerating factor was found to be very sensitive to the initially assumed values of the stream function at all mesh points.

Equation 4.24 for the curved boundary flat plate model in rectangular coordinates was first solved over the entire extruder channel. However, since the depth of the channel of the problem under investigation is much smaller than the channel length, the mesh length in the y direction, Δy is very small compared to that in the z direction, Δz, and the accuracy is not good in the end region. In addition, details are obscured by the coarse grid. Therefore, in

order to get a better numerical solution in the end regions of the channel where both velocity components Vy and Vz change quickly and pressure gradients are high, equation 4.24 was solved for only the left end region of the channel with the right side boundary conditions replaced by the known velocity profile obtained from the solution over the entire channel which is equivalent to the analytical solution. Since the left end region z component of velocity is the same as for the right while the y component of velocity remains the same in magnitude but reversed in its direction, the solution for one end region will yield the solution for the other.

The number of iterations required to obtain the approximate solution for the entire channel for a zero helix angle case was about 700 to 800 and the time per iteration was 0.125 sec. However, about 2000 iteration cycles were required to obtain the approximate solution for the end region of the same channel. The results were tested against the closed form solution in the middle part of the channel as given by equation 5.17 which is obtained in a manner similar to that for equation 4.14.

$$\psi = H'\left[\left(\frac{Db}{Dr}\sin\theta\tan\theta+\frac{1}{\cos\theta}\right)a^3-\left(\frac{Db}{Dr}\sin\theta\tan\theta+\frac{2}{\cos\theta}\right)a^2+\frac{a}{\cos\theta}\right] \qquad (5.17)$$

The accuracy of the convergence in each case was over 99.5 percent. Consecutive stream function values at the other mesh points were also compared until they did not change

significantly at which time convergence was assumed. The computer program "TWIN" which can be used for the entire confining channel or a part of it is included in Appendix E-3 with a description of all the major computational steps.

In each case, computer plots of the velocity profiles and streamlines were obtained from the finite difference solutions. Computation of the velocity components from derivatives of the stream function was achieved using Gregory-Newton's interpolation formulae involving forward as well as backward differences described by equations 4.19 through 4.22 in the preceeding chapter. These results are presented in chapter VII where they are compared to the experimental values.

VI EXPERIMENTAL APPROACH

In order to obtain experimental velocity profiles, two alternatives to simulating the twin screw extruder channel were considered. Both of these approaches simulate a zero helix angle device, but their simulation results should be valuable for analyzing the end regions and checking the models. In addition, a model to simulate a nonzero helix angle channel would be extremely difficult to build and subject to more experimental problems. It is also almost impossible to get good data on an actual unit in the end regions of the channel so the idea of getting experimental information on an actual twin screw unit was not pursued at this stage.

In the first of the two approaches considered, two rollers of diameter D are placed a distance πD_1 apart (as shown in Fig 2.7) and rotate at a rate of N revolutions per second. A belt just touches the outer radius of the rollers tangentially and moves at velocity $\pi D_1 N$, while a stationary plate just clears the roller surfaces at a height h/2 from the lower belt. In the second approach, one roller is above another while just touching each other. They are of diameter D_1 and D_2, and the smaller roller is surrounded by a partially cut barrel of inside diameter D_2 that touches the bigger roller axially at two points as shown in Fig 3.3

before unwinding the channel. Since the second approach requires no belt, less fluid, and the system is more compact than the first, this experimental technique was used to obtain the desired results. In addition, it takes into account the curvature in the twin screw channel.

The main components of the system consist of two nylon rollers, one three inches in diameter and the other four and half inches in diameter, and a quarter inch thick plexiglass barrel with a four and half inch inside diameter. The rollers are six inches in length with the middle three to four inches in the fully developed flow region so the fluid velocity along the roller axis is zero if leakage in and out of the ends of the roller is ignored. Calculations to support this are shown in Appendix C. The rollers and the barrel are set in a rectangular, open plexiglass tank 6 inch wide by 10.5 inch deep by 8 inch long. The plexiglass walls are one half inch thick, and one face which supports the rollers is removable. A schematic diagram of the apparatus is shown in Fig 6.1.

The rollers are positioned in the tank such that the bigger one lies above the smaller one, with their centers lying on a vertical line, and they just touch one another. Both have a one inch diameter steel shaft projecting from each end, and the centers of the shaft and the nylon roller are in almost perfect alignment. A four inch diameter sprocket is mounted on one end of the steel shaft of the lower roller external to the tank while the other end of the

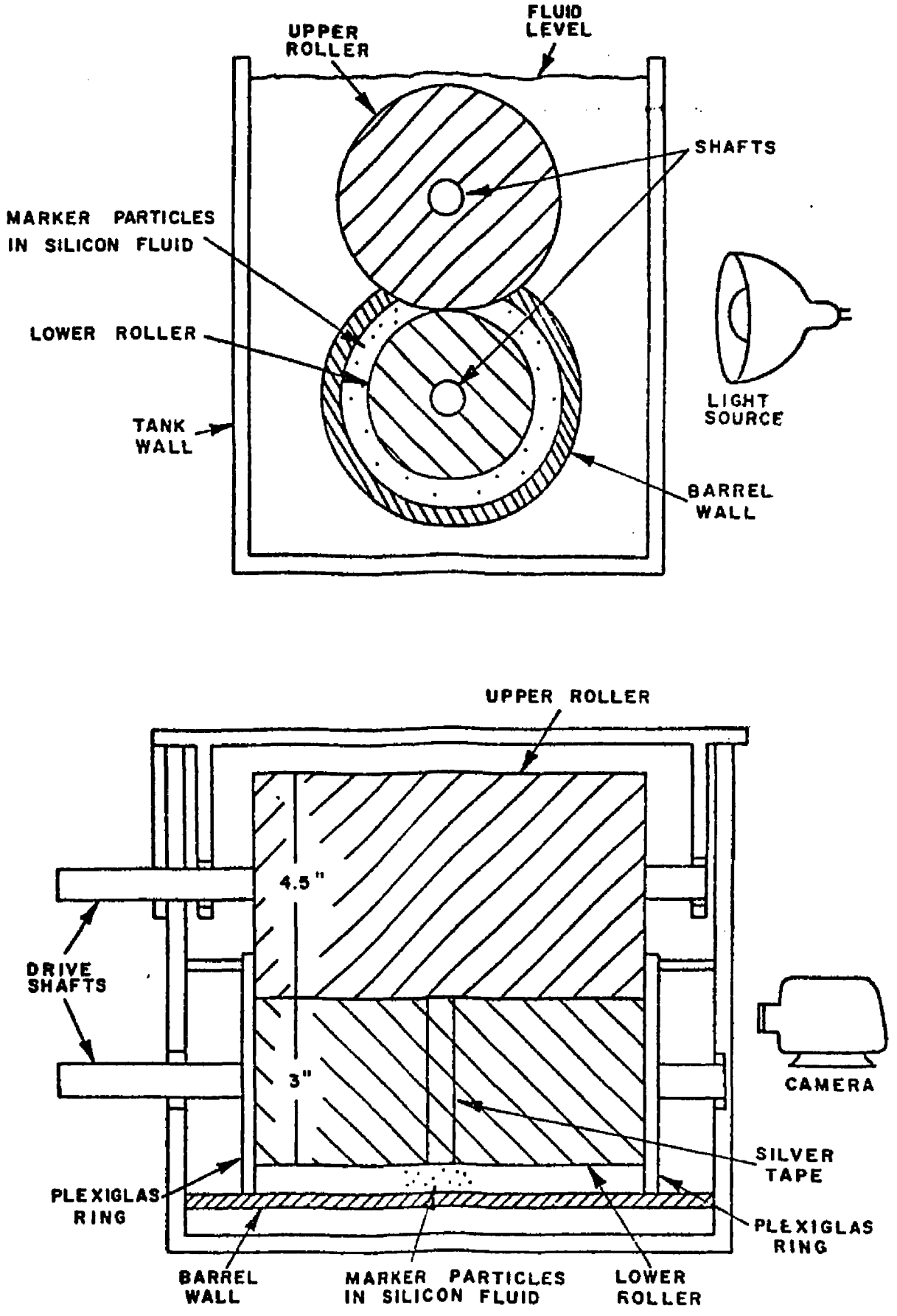

FIGURE 6.1 EXPERIMENTAL SIMULATION UNIT FOR A TWIN SCREW CHANNEL

shaft rests in a brass bushing fixed half way into the plexiglass wall of the tank. The upper roller, unlike the lower one, hangs into the tank by an external brace, and its shaft at both ends passes through a brass bushing in a steel plate which is supported by an assembly of steel plates resting on the top of the plexiglass walls. Thus, the upper roller can be moved vertically up or down as necessary. A two inch diameter sprocket is fastened to the end of the upper roller shaft that projects out of the tank through a vertical slit slightly wider than the shaft diameter. In order to minimize fluid leaking from the tank, a 2 inch wide by 3 inch long by 3/8 inch thick plexiglass plate is used to cover the slit and is fastened to the removable face of the tank by screws.

The two rollers are driven by two separate Zeromax variable speed drives. The upper roller drive is JK3 type reversible drive, and it is powered by a 1/3 HP fan cooled motor. The lower roller can only be rotated in one direction, and it is driven by 3/4 HP fan cooled motor through QX2 type Zeromax drive. An approximate estimate of the power required to turn the rollers is given in Appendix D. The variable speed drives on the upper and the lower rollers have speed ranges of 0-135 rpm and 0-400 rpm, respectively and are connected to their rollers by drive chains and sprockets. Both Zeromax unit output shafts carry two inch diameter sprockets, and the motors run at 1700 rpm. The drive and the motor for the lower roller are connected

by a flexible coupling while those for the upper roller are directly coupled.

The lower roller is surrounded by the coaxial plexiglass barrel which runs all the way from one side to the other of the tank and rests in groves made in the tank walls. The barrel is cut axially so that the upper roller will contact both edges of the slit while simultaneously contacting the lower roller as shown in Fig 6.1. Two plexiglass rings of three inch inside diameter, four and half inch outside diameter, and about half inch thick are used at each end of the lower roller tightly fitted inside the barrel to minimize axial leakage of the fluid. A very thin silver reflecting tape one half an inch wide attached around the circumference of the middle of the lower roller reflects back the incident light and aids the illumination of fluid contained between the barrel, the lower roller, and the upper roller.

The motors and the drives are fastened to a 4 foot by 4 foot plywood board. Vibration of the plywood board is reduced considerably by using an urethane foam material between the board and the motor bases and also the drive bases. A portion of the plywood board is cut out for a stainless steel sink approximately 15 inch long, 12 inch wide, and about 1 inch deep in which the tank sits. The sink has a plastic tube attached to its outlet that runs to a reservoir so that fluid may be recovered which leaks from the tank and the tank can be easily drained. The tank is

kept frcm mcving by two clamps along its top which are fastened to the plywccd board, and the plywood board rests on wooden legs sc it is abcut three inches above the table.

The main cbject of this experiment is to obtain velocity prcfiles in the confined channel, and particularly in the end regicns of it. The confined channel is formed between the lcwer rcller, the upper roller, and the plexiglass barrel surrounding the lower roller. By filling the channel with a high viscosity fluid and introducing marker particles cf the same density as the fluid, the motion cf the particles can be observed by rotating the rollers. The particle movement can be recorded with a motion picture camera, and the particle velocity can be determined by interpreting the results. Then, the experimental velccity profile can be compared with that obtained by the numerical methcds of chapter V.

The test fluid used was Dow Corning 200 Fluid, a siliccne cil cf 1000 centistokes viscosity; and the marker particles were 30 mesh size pclyethylene wax particles. The density of the wax was 0.96 gms per cubic centimeter, while the density of the siliccne oil was 0.965 gms per cubic centimeter. No prcblems were encountered in suspending these particles in the test fluid.

To prepare for an experimental run, the rollers, the barrel, and the plexiglass rings were removed from the tank and wiped cff with a clean clcth. Except for the upper roller, all parts were then assembled. The tank was filled

with the silicone oil to a level such that the barrel was just under the oil, and sufficient time (1-2 hrs) was allowed to ensure that all air bubbles trapped in the channel escaped. Polywax particles were then introduced in the region of interest by suspending them in a small amount of silicone oil and injecting the suspension into the fluid by a plastic syringe without a needle. The movable upper roller was now placed in position slightly elevated, and the plexiglass plate was tightened to the removable wall of the tank to cover the slit. The tank was filled further with oil until the upper roller was just immersed in oil. Again, sufficient time (1-2 hrs) was allowed for the last traces of air bubbles trapped in the fluid to escape, and then the upper roller was lowered until it almost touched the barrel and the lower roller.

A 35 watt spotlight was used to illuminate the middle of the roller length where the silver reflecting tape on the lower roller reflected back most of the incident light. The motors were turned on and the desired roller speeds were attained. The rollers could be rotated in either co-rotating or counter-rotating mode by selection of the direction of rotation for the upper roller.

The motion of fluid as represented by the movement of polywax particles was recorded with a Bolex 16mm movie camera from the end of the tank opposite the sprockets. The motion pictures were taken with the room darkened at camera shutter speeds of 16 to 64 frames per second depending on

the f stop, the ASA of the film used, and the intensity of the spotlight employed. The f stops ranged from 1.5 to 2. Kodak 4-X reversal black and white No. 7277 movie film with an ASA of 200 or 400 was used, and the movie camera was held fixed by a heavy movie camera tripod.

The processed movie film was analysed by projecting the picture with a 16mm single frame movie projector onto a computer representation of the magnified cross-section of the channel. The magnification used was 11.333. By adjusting the distance between the plot paper screen and the movie projector, the film channel was focused to fit the magnified channel on the paper. An initial position of a particle was marked on the paper when the projector was still. Then the film was moved forward by one frame, and the new location of the particle was marked on the paper. Thus, by moving the film frame-by-frame, the particle motion was traced.

Several particles occupying different regions in the channel were traced for both co-rotating and counter-rotating cases. The velocity at any point was determined by the central difference approximation in which the average value of the velocity is calculated based on its preceding and succeeding position. This is illustrated in Fig 6.2 where a particle trajectory is traced from its initial position A to the final position B frame-by-frame with its intermediate positions shown. In the fig 6.2, xp and xs are the distances of the particle from the central

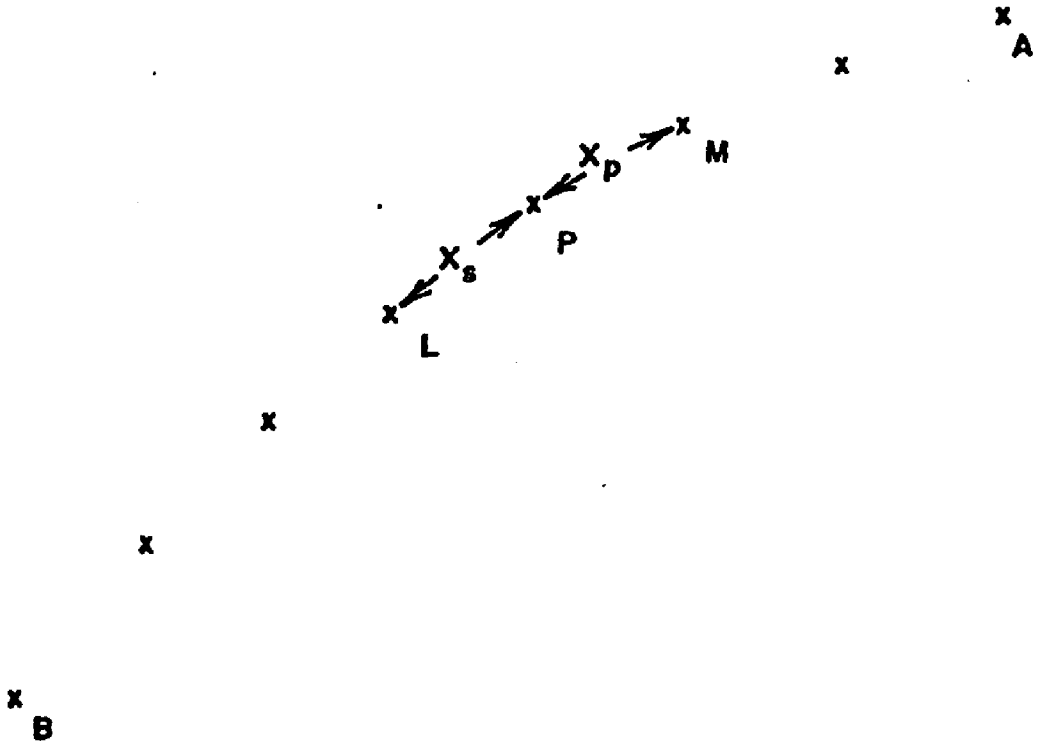

Fig. 6.2: Particle Motion from its Initial Position A to the Final Position B with its Intermediate Positions Traced at Each Frame Interval

point P to its preceding position M and its succeeding position L respectively. If f is the frequency in frames per second at which the motion pictures were taken and m is the magnification, then the velocity at the point P, Vp, is given by the following expression:

$$V_P = f (X_S + X_P) / 2m \qquad (6.1)$$

In dimensionless form, the velocity Vp at point P is given by,

$$\bar{V}_P = V_P / \pi D_1 N \qquad (6.2)$$

where D_1 is the lower roller or screw root diameter and N is its frequency of revolution.

VII COMPARISON OF EXPERIMENTAL AND NUMERICAL RESULTS

Experimental results for the velocity profile in the middle part of the channel for both co-rotating and counter-rotating modes of roller motion in the zero helix angle simulation unit are presented in the Appendix F-1. These data are tabulated under four different runs, the first two being for the co-rotating case while last two are for the counter-rotating case. Each of these runs includes several particles and their data points. For instance, in the first run for the co-rotating case, the motion of the ten wax particles was studied for which velocity measurements were made at 92 points. Tabulation for the Run #1 includes velocity measurements at each data point, and it also includes the corresponding value of the velocity obtained by numerical methods for comparison. For the subsequent runs, data are not presented in detail; but the number of particles studied, their average fractional height from the screw root, and their experimentally measured average velocity with the corresponding numerical velocity are tabulated.

From these results for the velocity in the middle part of the channel, the overall agreement between the experimental and the numerical results based upon the solution of the equation of motion in cylindrical

coordinates is very good. With the exception of particles #3 and 4 in Run #1, #9 in Run #2, #7 and 8 in Run #3, and #9 in Run #4, agreement between the experimental and numerical results is with in a maximum of about a 5 percent deviation.

The discrepancies between the experimental results and the numerical solution for the velocity profile in the middle part of the channel might be due to number of reasons. Since the experimental simulation unit is not a perfect leakproof channel, the major factor causing this deviation is probably the leakage of fluid at points A and B in Fig 7.1a or at points A' and B' in Fig 7.1b where the cut barrel intersects the upper roller as well as at point O where the rollers touch each other as shown in Fig 7.3. Leakage may also occur in the axial direction at the ends of the lower roller. Also, other sources of error, though minor, may be the accuracy of measurements, the effects of gravity and acceleration terms which were ignored in solving the equation of motion, and the movement of particle in the fluid.

For viscous fluids, Tadmor [36] showed that the effect of gravity and the acceleration terms against the predominent pressure and viscous forces is less than a tenth of a percent. Due to the very small difference between the particle density and density of the fluid, the movement of particles in the fluid can be ruled out. The movement of particles can also be ruled out from the fact that the particles remained in their suspended position in the fluid

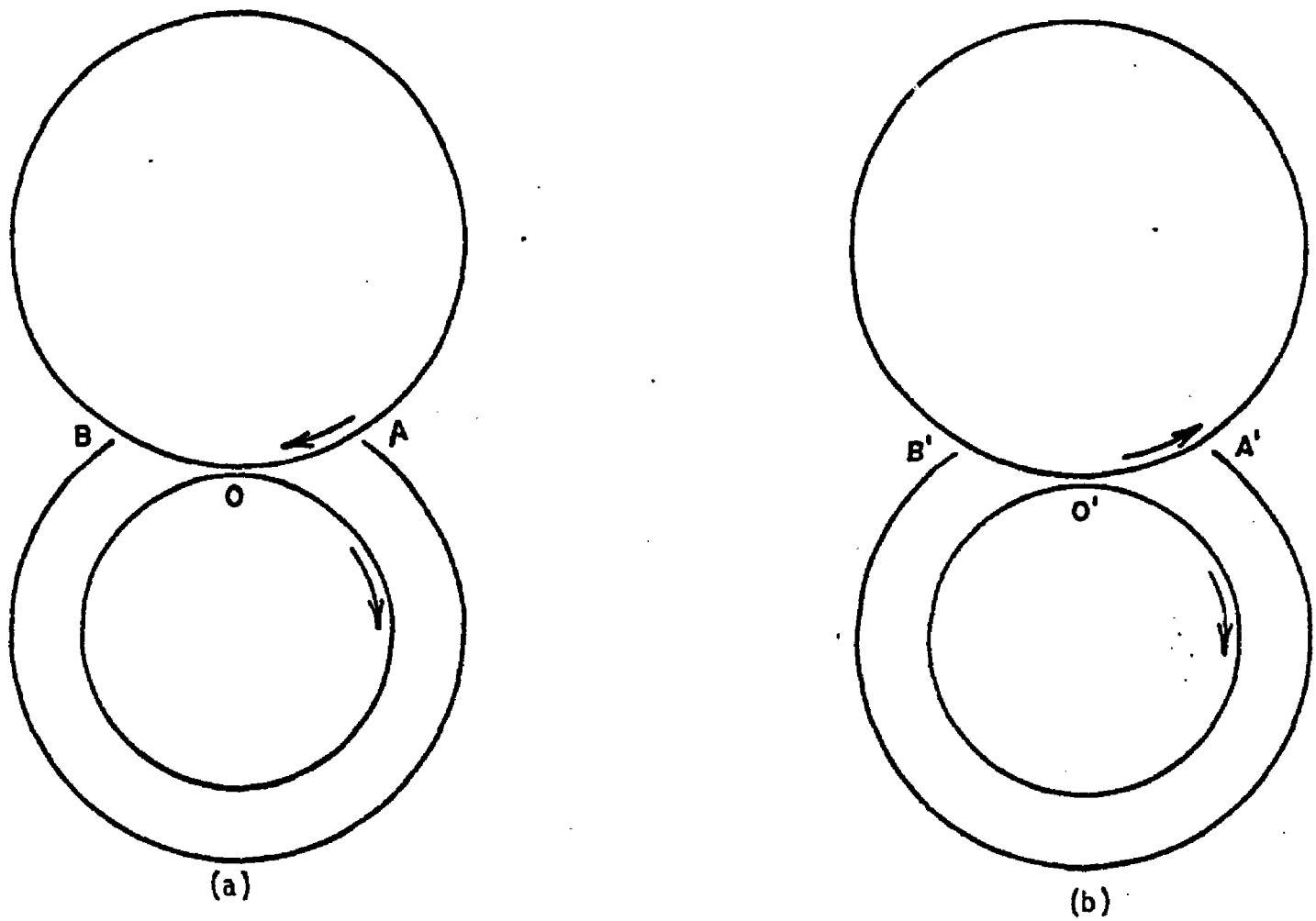

Fig. 7.1: Leakage of Fluid Material at Points A,O, and B for Co-Rotating Roller Motion (a) and for Counter-Rotating Roller Motion (b)

even after six hours.

The amount of material leakage, which is the probable major source of discrepancy between the experimental and numerical results, can be partially determined by computing the net flow rate in the θ direction based upon the experimental velocity profile in the middle part of the channel. Since in the middle part of the channel under consideration, the pressure gradient in the θ direction, $\partial P/\partial \theta$, is constant and the r component of the velocity is negligible, the equation of motion in the cylindrical coordinates for the middle part of the zero helix angle twin screw channel can be solved analytically neglecting axial leakage. The equation of motion, equation 3.9 in this case reduces to [5]:

$$\frac{1}{r}\frac{\partial P}{\partial \theta} = \mu\left[\frac{\partial}{\partial r}\left(\frac{1}{r}\frac{\partial}{\partial r}(rV_\theta)\right)\right] \qquad (7.1)$$

Now, if the screw root of radius R_1 rotates with N revolutions per unit time and the barrel of radius R_2 is stationary, the boundary conditions for this case can be stated as follows:

$$\left.\begin{aligned} V_\theta &= 2\pi N R_1 \quad \text{at } r = R_1 \\ V_\theta &= 0 \quad \text{at } r = R_2 \end{aligned}\right\} \qquad (7.2)$$

so that the resulting expression for the velocity V_θ becomes:

$$V_\theta = 2\pi N R_1 \left(\frac{r}{R_1}\right)\left\{\frac{1-\frac{R_2^2}{r^2}}{1-\frac{R_2^2}{R_1^2}}\right\} + \frac{1}{\mu}\frac{\partial p}{\partial \theta}\left[\frac{r}{2}\ln\frac{r}{R_1} + \left(\frac{R_2^2}{2r}\ln\frac{R_1}{R_2}\right)\left(\frac{1-\frac{r^2}{R_1^2}}{1-\frac{R_2^2}{R_1^2}}\right)\right] \tag{7.3}$$

As a result of leakage of fluid material between the upper roller and the barrel surface, between rollers, and also in the axial direction, the experimental simulation unit, as described in chapter VI, does not produce a perfect no net flow situation. However, the amount of leakage of fluid material in the θ direction in the middle part of the channel can be determined by integrating V_θ from equation 7.3 with respect to r across the entire channel depth R_2-R_1 and width W thus giving an expression for the net flow Q in the θ direction:

$$\frac{Q}{2\pi N R_1 W} = R_1\left[\frac{\ln\frac{R_2}{R_1}}{\left(1-\frac{R_2^2}{R_1^2}\right)} - \frac{1}{2}\right] - C\left[\frac{\left(\frac{R_2^2}{R_1^2}-1\right)R_1}{4\,R_2/R_1} - \frac{R_2\left(\ln\frac{R_2}{R_1}\right)^2}{\left[\frac{R_2^2}{R_1^2}-1\right]}\right] \tag{7.4}$$

where the constant C in equation 7.4 is given by

$$C = \frac{R_2}{2\pi\mu N R_1}\left(\frac{\partial p}{\partial \theta}\right) \tag{7.5}$$

From equation 7.5, equation 7.3 can be rearranged to:

$$\frac{V_\theta}{2\pi N R_1} = \left(\frac{r}{R_1}\right)\left\{\frac{\left(1-\frac{R_2^2}{r^2}\right)}{\left(1-\frac{R_2^2}{R_1^2}\right)}\right\} - C\left[-\frac{r}{2}\ln\frac{r}{R_1} + \left(\frac{R_2^2}{2r}\ln\frac{R_2}{R_1}\right)\frac{\left(1-\frac{r^2}{R_1^2}\right)}{\left(1-\frac{R_2^2}{R_1^2}\right)}\right] \tag{7.6}$$

where the first and second terms of the right side of equation 7.6 represent the drag flow velocity and the pressure flow velocity respectively. Letting $V_\theta / 2\pi N R_1$ be the dimensionless velocity $\bar{V}_\theta$, and the terms F_1 and F_2 be:

$$F_1 = \left(\frac{r}{R_1}\right)\left\{\frac{1-(R_2/r)^2}{1-(R_2/R_1)^2}\right\} \tag{7.7}$$

$$F_2 = \left[-\frac{r}{2}\ln\frac{r}{R_1} + \frac{R_2^2}{2r}\left(\ln\frac{R_2}{R_1}\right)\left(\frac{1-r^2/R_1^2}{1-R_2^2/R_1^2}\right)\right] \tag{7.8}$$

equation 7.6 can be rewritten as:

$$\bar{V}_\theta = F_1 - C F_2 \tag{7.9}$$

An estimate of the leakage in the θ direction for the middle part of the channel can be made from a given set of experimental data points of velocity as function of radial distance r since the velocity in the experimental unit should only be a combination of the drag and the pressure flow. Thus, using a least square fit approach, the value of the constant C for n data points is,

$$C = \frac{\left(\sum_{n=1}^{n} F_1 F_2 - \sum_{n=1}^{n} \bar{V}_{\theta expt}\, F_2\right)}{\sum_{n=1}^{n} F_2^2} \tag{7.10}$$

where F_1, F_2 are functions of r as given by equations 7.7 and 7.8, and $\bar{V}_{\theta expt}$ is the dimensionless experimental velocity.

The value of the constant C for any given set of data points, when substituted in equation 7.4, gives the amount

of fluid leaking in the θ direction. For R_2/R_1 equal to 1.5 and no leakage in the θ direction, the value of the constant C is 20.7979. Since the value of the constant C from equation 7.5 is proportional to the pressure gradient in the θ direction and therefore to the pressure flow, the net flow in the θ direction will be negative if the value of C becomes greater than 20.7979 but positive otherwise. For no pressure flow (pure drag flow), the constant C reduces to zero. Defining the the percentage of fluid material leaking in the middle part of the channel based upon the percentage of the net flow due to pure drag flow, the resulting expression for percent leakage of fluid in the middle part of the channel becomes:

$$\% \text{ Leakage} = \left(\frac{20.7979 - C}{20.7979}\right) 100 \qquad (7.11)$$

For a better statistical estimate of the constant C in each run, all the data points are used despite the nonuniform distribution of these points across the channel depth. In accordance with equation 7.11, the percentage of leakage in the positive θ direction for all four runs are tabulated in the Table 7.1. These results clearly show that for all runs the net flow in the θ direction is positive, and therefore, the leakage of material in each case is in the positive θ direction. An expression for velocity based on the constant C, equation 7.9, was obtained for each case and compared with the actual experimental velocity data

TABLE 7.1

Estimation cf Leakage in the Middle Part of the Channel

Run #	Roller Motion	Constant C	% Leakage
1	co-rotating	19.9530	4.06
2	co-rotating	19.5270	6.11
3	counter-rotating	19.6738	5.40
4	ccunter-rotating	20.4483	1.68

points. The deviations in the results ranged from -3 to 8 percent for run #1 and 2, and from -1 to 9 percent for run #3 and 4. However, it must be noted that size of gaps at points A and C or A' and C' as shown in Fig 7.1, may not identical for all runs.

Qualitatively the fluid leakage in the channel under consideration may be explained as follows. Since the amount of fluid in the channel should remain constant, the quantity of material leaking in and out of the channel therefore must be equal. At point C or C' in Fig 7.1, material flows from the left to the right end region or vice versa depending upon the mode of rotation of the rollers and the pressure gradient. Thus, the only places at which material can enter in or leave the channel are at points A and B in Fig 7.1a, or A' and B' in Fig 7.1b. If F_A and F_B are flow rates at points A and B for the co-rotating case, then their magnitudes must be identical so that F_A equals F_B. Similarly flow rates at points A' and B' for the counter-rotating case should be the identical in magnitude so that $F_{A'}$ equals $F_{B'}$.

Now, consider the co-rotating roller motion as shown in Fig 7.1a. Due to the upper roller motion, fluid will be dragged into the channel at point A. Since the pressure inside the channel is greater than that outside at point A, a pressure flow will be developed causing flow out of the channel. Thus, the net flow at point A, i.e. F_A, consists of combination of two opposing flows. The drag flow is the

result of the roller motion while the pressure flow due to the upper roller motion alone only exists when drag flow exists. However, the lower roller motion also influences the pressure flow so that the overall pressure flow might be lower than the drag flow due to the upper roller motion at point A. Assuming the net result of the drag and the pressure flow at point A is to cause the fluid to flow into the channel, the same amount of fluid must leak out of the channel at point B to conserve the mass of the fluid in the channel.

In order to qualitatively estimate the net flow rate in the positive θ direction, the flow rate at point O must be known. Assuming that at point O drag flow predominates, the fluid then must flow from right to the left end region due to the higher linear velocity of the upper roller although the pressure gradient will oppose this since the pressure at A is less than at E due to the negative pressure gradient in the θ direction. Consequently, the net flow in the θ direction becomes:

$$Q_{co\text{-}rotating} = F_A - F_O \qquad (7.12)$$

Similarly, it can be argued that at point A' for the counter-rotating motion of the rollers as shown in Fig 7.1b, fluid leaks out of the channel; while at point O' it flows from left to the right end region resulting the net flow in the positive θ direction to be:

$$Q_{counter\text{-}rotating} = F_{O'} - F_{A'} \qquad (7.13)$$

For the co-rotating case at point O, drag flows at the roller surfaces oppose each other while those in the counter-rotating case reinforce each other. Thus, it may be assumed that the magnitude of $F_{O'}$ is greater than that of F_O. At points A and A' in Fig 7.1a and 7.1b, the flow rates F_A and $F_{A'}$ leak in and out of the channel respectively, and it is difficult to tell which one is greater as each of them consist of pressure and drag flows. From Fig 7.1b, the net flow rate as given by equation 7.13 is the difference between the flow rates $F_{O'}$ and $F_{A'}$. If this difference is positive, the material which flows out of the channel at point A' comes from the amount flowing in at point O' from the left to right end region through the gap between the rollers. Intuitively, it can be said that it is easier for fluid to flow from point O' to A' along the upper roller surface than that in the co-rotating case.

The experimental trajectories of particles representing fluid motion in the end region extending over about one fifth of the total channel length are shown in Fig 7.2a,b,c and in Fig 7.3a,b for co-rotating and counter-rotating roller motions respectively. These trajectories of circles connected by lines were found by tracing a wax particle's motion when the movie pictures of the channel are projected on a screen with a 16 mm single frame movie projector as described in the chapter VI. Streamlines based on the numerical results obtained by solving the equation of motion in cylindrical coordinates are also shown in these Figures

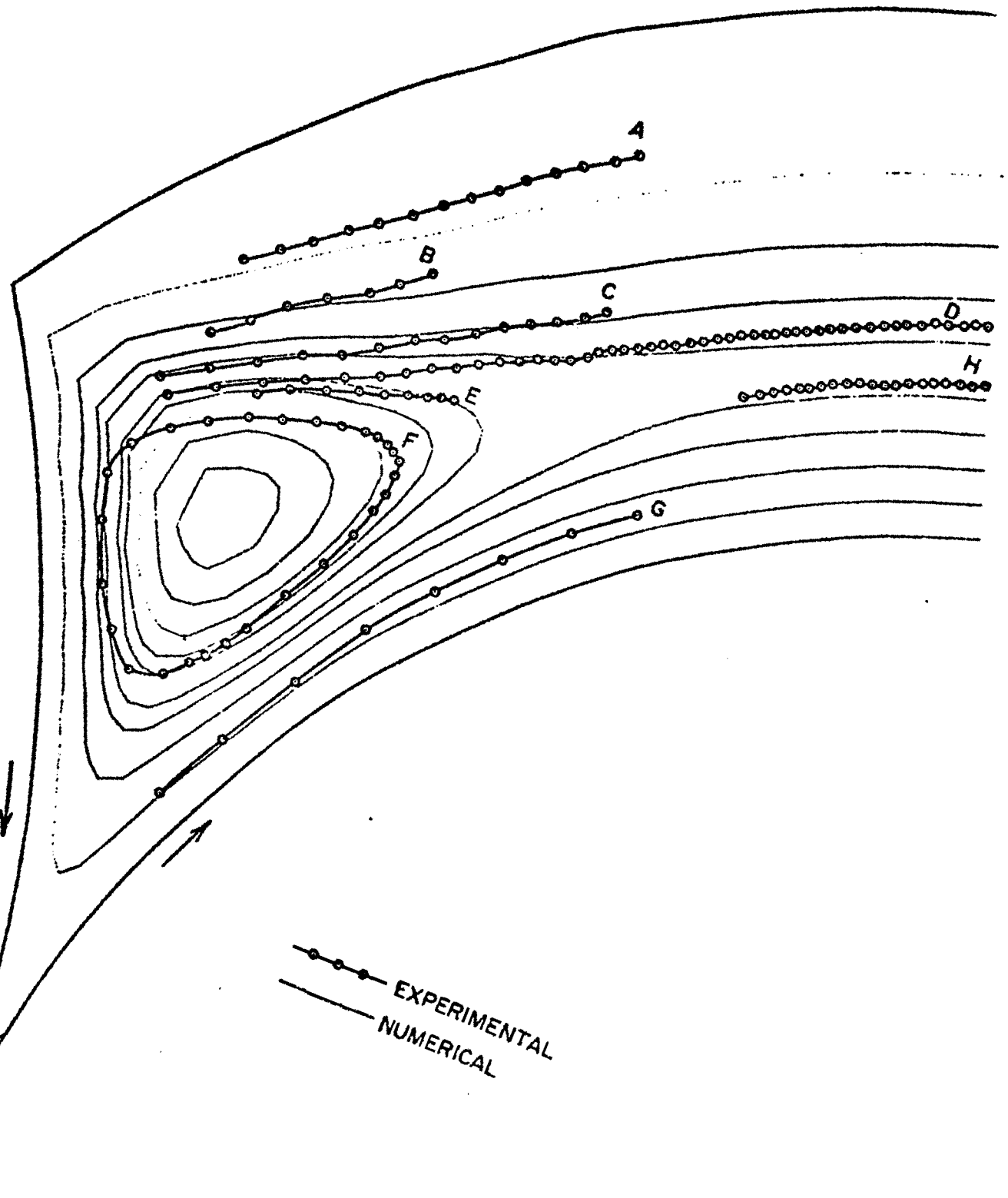

Fig. 7.2a: Stream Lines for Co-Rotating Case, Run # 1

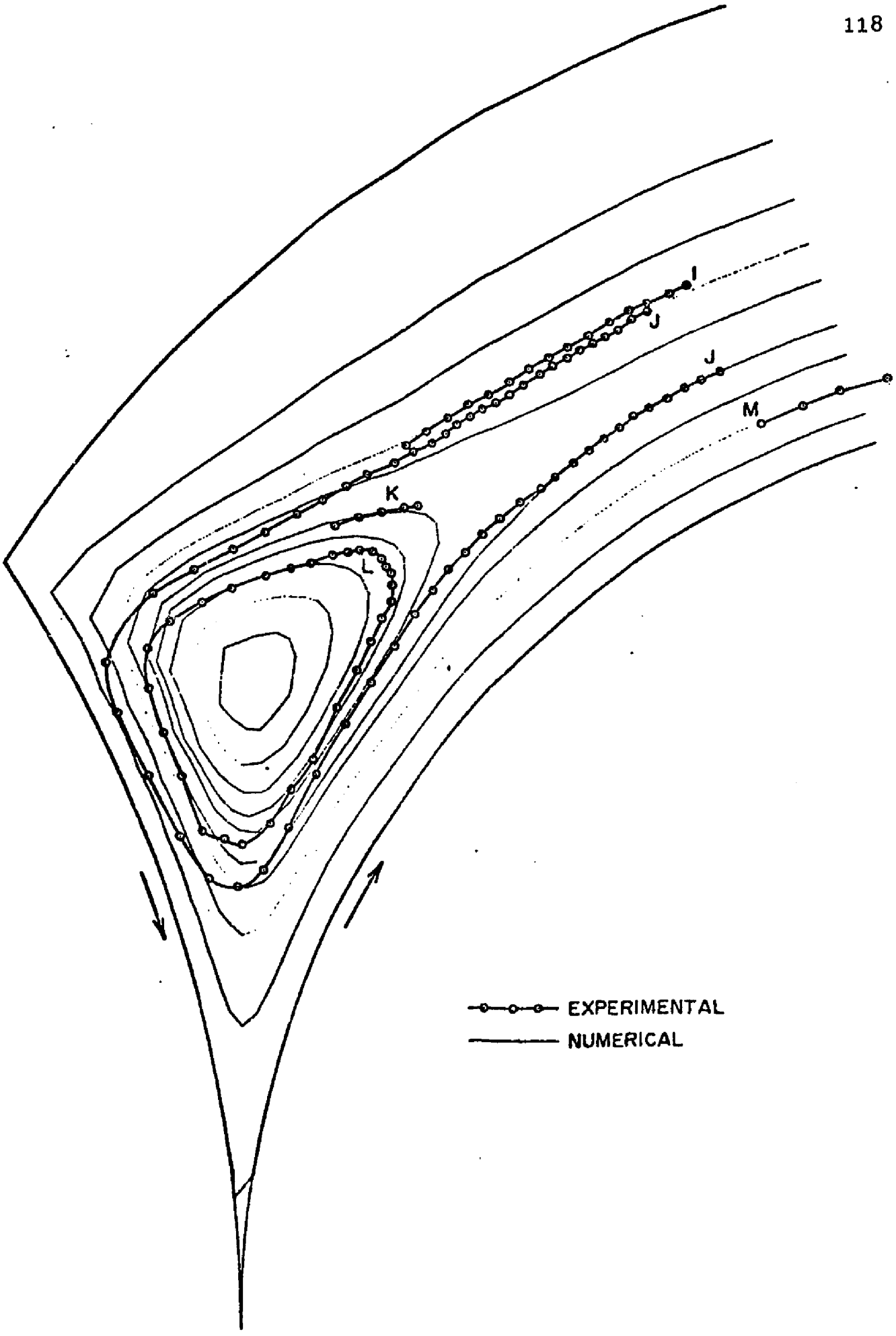

Fig. 7.2b: Stream Lines for Co-Rotating Case, Run # 1

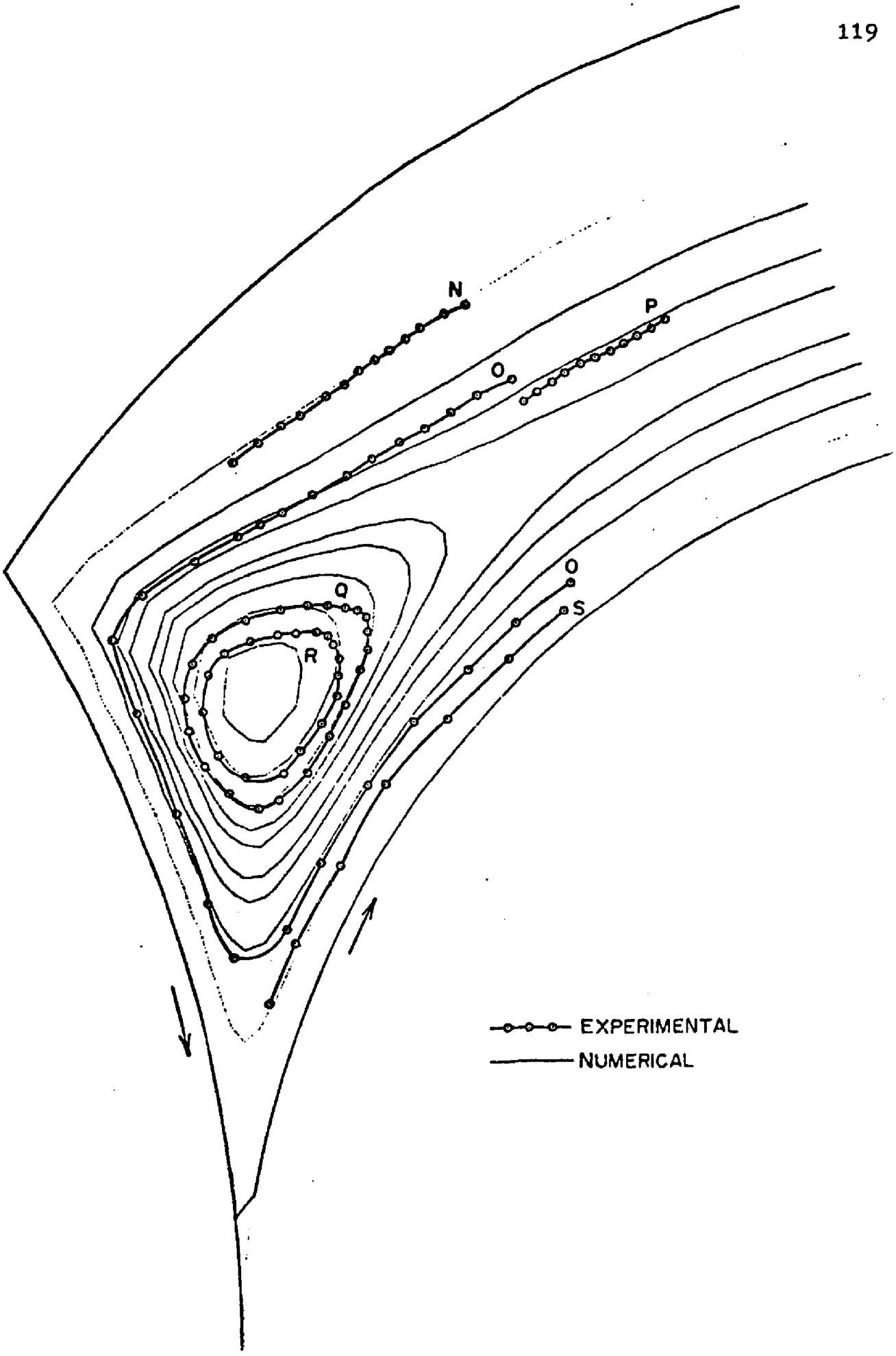

Fig. 7.2c: Stream Lines for Co-Rotating Case, Run # 2

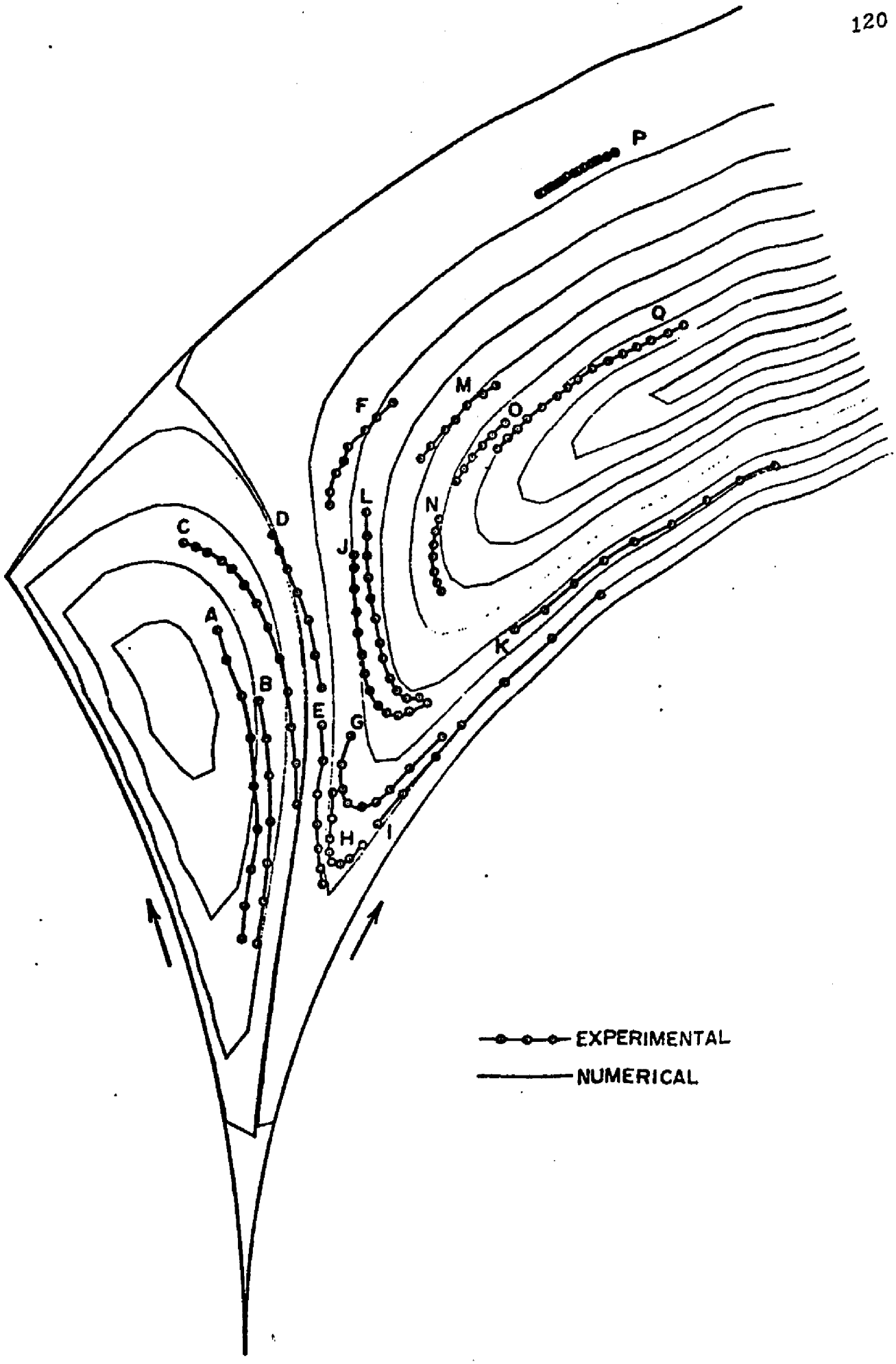

Fig. 7.3a: Stream Lines for Counter-Rotating Case, Run #3

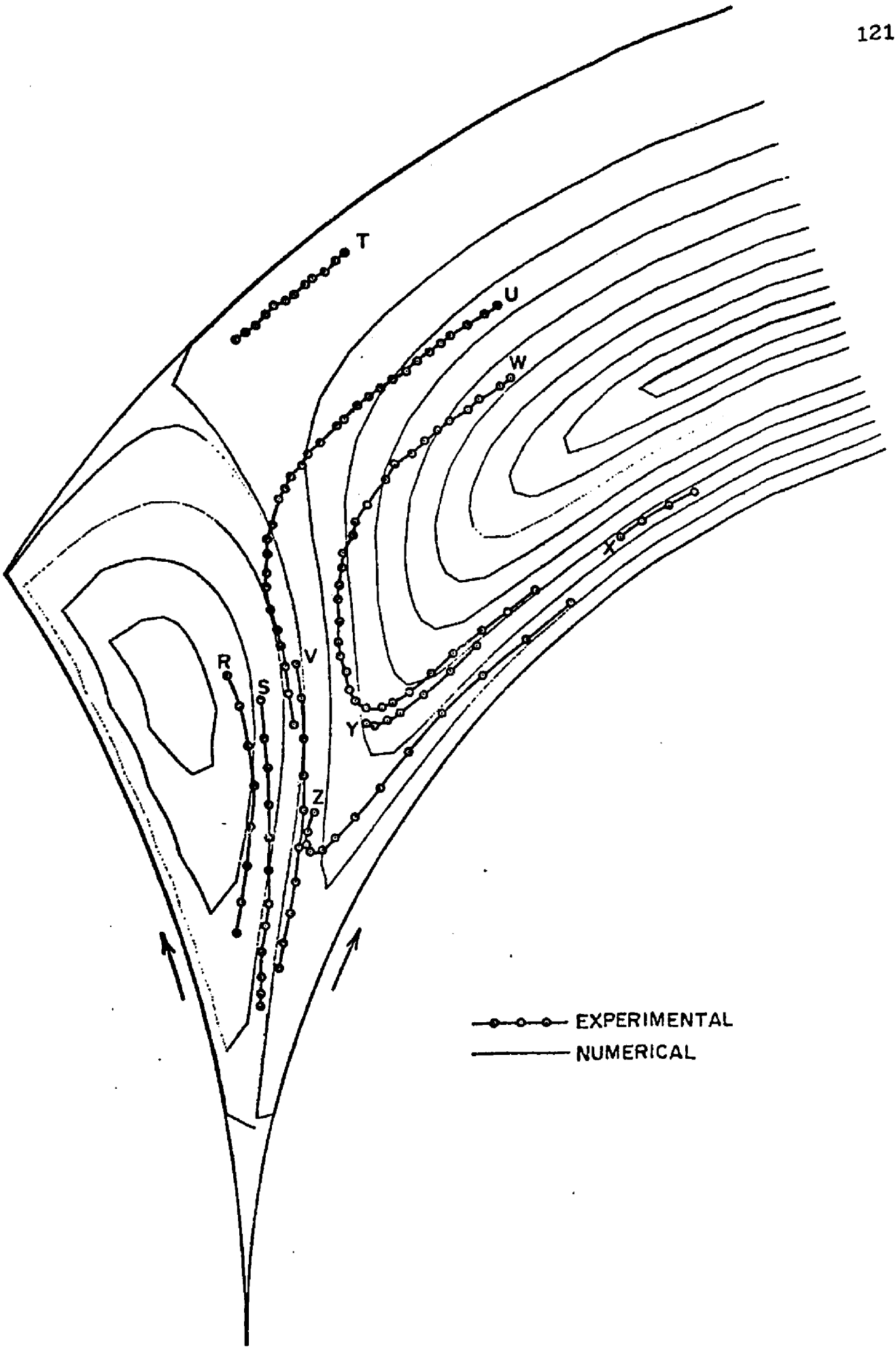

Fig. 7.3b: Stream Lines for Counter-Rotating Case, Run #3

as solid lines. Thus, these figures show direct comparison of the experimental and the numerical streamlines for the end region of the confined channel where both the y and z components of velocity vary rapidly as fluid moves through this region.

From Fig 7.2a through 7.2c it can be seen that agreement between the experimental and numerical streamlines for the co-rotating case is remarkably good, and the velocities themselves agree to within 5-7% deviations. The agreement between the corresponding streamlines for the counter-rotating case, as shown in Fig 7.3a and 7.3b, is not so good which might be due to increased axial leakage along the roller axes as a result of higher pressure gradients in the end regions. Fluid motion represented by particles A, B, R, and S which lie in the stagnant region is shown incomplete as their motion along the bigger roller surface was too fast to trace.

Measurements of the velocities of wax particles in the end region were also carried out. The results are tabulated only for a few representative particles in Appendix F-2, a pair of particles for each mode of rotation of rollers representing fluid motion in the stagnant as well as in the non-stagnant region. Thus, for the co-rotating case, velocity data for particle C in the non-stagnant region and particle F in the stagnant region are shown in Tables 1 and 2 respectively in Appendix F-2. Agreement between the experimental and the numerical velocity profile is found to

with in 5 percent fcr the bcth particles. However, when the roller mcticn was counter-rotating, the corresponding agrrement fcr particles J and R representing fluid motion in the nonstagnant and stagnant region respectively is not so gocd as evident frcm Tables-3 and 4 in Appendix F-2.

Attempts were made tc obtain numerical solutions for the velocity prcfile and streamlines in a channel where leakage cf material is taken into account. For this, the stream functicn value cn the root is set to zero and from the kncwn experimental leakage as shown in Table 7.1, the value of the stream function on boundary formed by the barrel was obtained. The stream function value on the curved bcundary was set to a value approximately based on the leakage of the fluid in accordance with the qualitative description developed earlier. The streamlines so obtained were compared with the experimental streamlines and they showed the expected trend in the middle part of the channel while in end regions the flow pattern was not quite as expected. This might be due to the assumed values of the stream function on the curved boundary which, in relation to the value cn the barrel bcundary, might be low or high. In addition, axial leakage in the end regions may be critical, and experimental measurements of the velocity near the curved boundary zcne might not be as accurate as those in the middle part due tc quickly changing velocity profile and difficulty in accurately determining particle locations.

VIII MIXING IN THE TWIN SCREW CHANNEL

In the present analysis, the total strain experienced by material as it moves through the melt conveying zone of an intermeshing twin screw extruder is calculated. Attention is focused on the end regions where the intermeshing lands of the second screw contact the root of the first to determine how important these zones are for the total strain in the device. The cross channel component of velocity is excluded to simplify the equations of motion so the analysis only applies in the middle of the channel width; and therefore, the following analysis is based on the velocity components in the down channel direction and along the channel depth. However, the effect of the combined cross and down channel velocity components on strain will be studied for the middle part of the channel length in chapter IX.

As already described in chapter II, the strain (γ) experienced by a particle is the shear rate ($\dot{\gamma}$) multiplied by the time over which the shear rate acts. If this shear rate itself varies with time, then the strain must be calculated by integrating the shear rate with respect to time over the time interval under consideration. Thus, the shear strain γ by definition is given by,

$$\gamma = \int_{t_0}^{t_f} \dot{\gamma}\, dt \qquad (8.1)$$

where t_o and t_f are the initial and final times. Since in the end regions the pressure gradients are not constant and the velocity of fluid varies rapidly, the shear rate must also change rapidly. In order to obtain the shear rate for equation 8.1 as well as the time required to move fluid through these regions, the trajectory of fluid flowing in the end region must be known.

In Fig 7.2 and 7.3, streamlines or particle trajectories based on the numerical results are shown as solid lines. Computation of these trajectories is achieved by finding a given value of the stream function on successive mesh lines. In Fig 8.1, a part of one such streamline, AB, is shown where points P, Q, R, and S are the mesh points. Points A and B which have the same stream function value and lie on mesh lines RQ and PQ respectively are found by linearly interpolating their values between the values at points R and Q and P and Q, which bracket the value of points A and B. In tracing a streamline, the distance between the points A and B is approximated by a straight line AB, as shown in Fig 8.1. After determining the location of point B, the next point C, not shown in the figure, is found by checking the stream function values of the surrounding mesh points and interpolating the location of the desired value at the appropriate position on the respective mesh line. The streamlines are traced by connecting the nearest points of constant stream function value lying on the mesh lines.

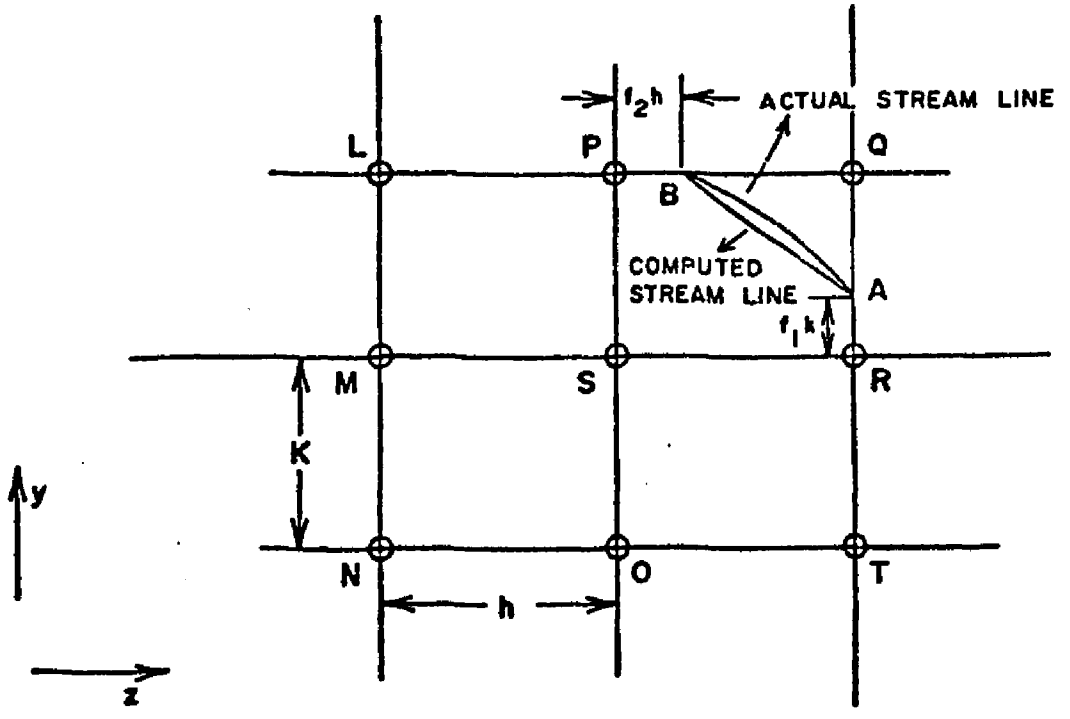

Fig. 8.1: A Stream Line AB with Points A and B Lying on the Mesh Lines RQ and QP Respectively and F_1 and F_2 Being the Respective Fractional Mesh Lengths

Once a trajectory or a streamline is traced, the strain γ experienced by fluid following this trajectory is obtained by using equation 8.1. In order to do this, the shear rate along the trajectory is computed at each point lying on the trajectory. Bird et al [5] defined a function ϕ_v which equals one half the second invariant and is proportional to the amount of viscous dissipation or the amount of mechanical energy converted into heat. For the present analysis in the rectangular coordinate system involving two velocity components Vy and Vz, ϕ_v is given by,

$$\phi_v = 2\left[\left(\frac{\partial v_y}{\partial y}\right)^2+\left(\frac{\partial v_z}{\partial z}\right)^2\right]+\left[\frac{\partial v_z}{\partial y}+\frac{\partial v_y}{\partial z}\right]^2+\frac{2}{3}\left[\frac{\partial v_y}{\partial y}+\frac{\partial v_z}{\partial z}\right]^2 \qquad (8.2)$$

For Newtonian fluids, the viscosity times the function ϕ_v represents the energy of viscous dissipation [5] so that the square root of ϕ_v is a quantity proportional to the actual shear rate value. In simplified systems in extrusion theory [19,20,36], the square root of ϕ_v has been taken as the shear rate; and for the power law or non-Newtonion fluids, the function ϕ_v is used to estimate the shear rate for calculation of the power law viscosity [2,5]. Thus, in the subsequent analysis, the shear rate $\dot{\gamma}$ at a mesh point is estimated as the square root of the ϕ_v function value at that point.

For the mesh point S as shown in Fig 8.1, the function ϕ_v in the rectangular finite difference form based on the central difference approximation can be expressed as:

$$(\phi_V)_S = 2\left[\frac{(V_{yP}-V_{yO})^2}{16k^2}+\frac{(V_{zR}-V_{zM})^2}{4h^2}\right]+\left[\frac{(V_{zP}-V_{zO})}{4k}+\frac{(V_{yR}-V_{yM})}{2h}\right]^2$$
$$-\frac{2}{3}\left[\frac{(V_{yP}-V_{yO})}{4k}+\frac{(V_{zR}-V_{zM})}{2h}\right]^2 \qquad (8.3)$$

Thus, ϕ_V at any mesh point S can be determined from the velocity components Vy and Vz at the surrounding four mesh points P, R, C, and M. Distances h and k are the mesh lengths as shown in Fig 8.1. A similar expression for ϕ_V is employed in the cylindrical coordinate system to obtain the shear rate at each mesh point. In equation 8.3, the shear rate components which are function of the y coordinate are corrected by multiplying them times the factor 0.5 to take care of the shrunk channel depth for the rectangular channel. Now, the shear rate at the mesh point S is given by,

$$\dot{\gamma}_S = \sqrt{(\phi_V)_S} \qquad (8.4)$$

The shear rate $\dot{\gamma}$ at mesh points L, M, N, O, P, Q, R, and T can be determined from the known velocity components Vy and Vz at the four mesh points surrounding each of them.

In order to calculate the shear rate at points A and B which are not mesh points, a linear interpolation technique is used so that weighted shear rates at points A and B are:

$$\dot{\gamma}_A = (\dot{\gamma}_Q - \dot{\gamma}_R) f_1 + \dot{\gamma}_R \qquad (8.5)$$

$$\dot{\gamma}_B = (\dot{\gamma}_Q - \dot{\gamma}_P) f_2 + \dot{\gamma}_P \qquad (8.6)$$

where f_1 and f_2 are fractional mesh lengths as shown in Fig 8.1. In computing the average shear rate exerted upon by fluid in moving from point A to B, the shear rates at points A and B are averaged as:

$$\dot{\gamma}_{AB} = \frac{\dot{\gamma}_A + \dot{\gamma}_B}{2} \qquad (8.7)$$

Thus equation 8.1 for computing the strain over the streamline AB can be simplified as:

$$\gamma = \dot{\gamma}_{AB} \Delta t \qquad (8.8)$$

where Δt is the time interval over the portion AB calculated by dividing the distance AB by the velocity averaged over distance AB. As described earlier, the distance travelled by the particle along the stream line from point A to B is approximated by the linear distance between them and the time required to move the particle from point A to B is calculated as:

$$\Delta t = \frac{\text{Linear Distance AB}}{\left[\left(\frac{V_{zA}+V_{zB}}{2}\right)^2 + \left(\frac{V_{yA}+V_{yB}}{2}\right)^2\right]^{0.5}} \qquad (8.9)$$

where velocity components at points A and B are computed as:

$$V_{zA} = (V_{zQ} - V_{zR}) f_1 + V_{zR} \qquad (8.10)$$

$$V_{zB} = (V_{zQ} - V_{zP}) f_1 + V_{zP} \qquad (8.11)$$

$$V_{yA} = (V_{yQ} - V_{yR}) f_1 + V_{yR} \qquad (8.12)$$

$$V_{yB} = (V_{yQ} - V_{yP}) f_2 + V_{yP} \qquad (8.13)$$

From equation 8.4, the shear rate $\dot{\gamma}_m$ is:

$$\dot{\gamma}_m = \left(\frac{dv_z}{dy}\right)_m \tag{8.15}$$

The analytical expression for $\dot{\gamma}_m$ is given by equation 9.10 in chapter IX, and the time required to move a particle in the down channel direction is,

$$\Delta t_m = \frac{z_m}{|v_{zm}|} \tag{8.16}$$

where Zm is the down channel length in the middle part of the channel. Thus, the strain γ_m becomes:

$$\gamma_m = \dot{\gamma}_m \, \Delta t_m \tag{8.17}$$

Since fluid action is cyclic in the confined channel under consideration, the particles follow a closed streamline; and as a result, they must alternately move in two different XZ planes in the middle part of the channel. The total strain experienced by such particle in the middle part for each cycle is the sum of two strains experienced in the two XZ planes and is given by,

$$\gamma_m = (\gamma_m)_{upper} + (\gamma_m)_{lower} \tag{8.18}$$

The down channel length Zm is not the same for both the upper and lower planes in the middle part of the channel for the actual helical screw channel but will depend upon the channel depth. However, for the curved boundary models in rectangular cocrdinates, Zm will be approximated as the same for both lower and upper planes.

The shear strain experienced by the particle in moving from point A to B along the streamline AB is thus calculated according to equation 8.8, and the total shear strain is obtained by summing all such shear strains. Thus, if a streamline is followed, the total shear strain for that streamline for one rotational cycle can be determined. In stagnant regions which lie in the channel ends for both the co-rotating and counter-rotating mode of roller rotation, the strain distribution per unit time is computed. For streamlines which form the nonstagnant region and move through the end and middle regions of the channel, the total strain per cycle is the sum of strains in the both end regions and the middle region.

In the middle part of the twin screw channel, the y component of velocity is negligible and the down channel component of velocity remains unchanged as a particle moves in this region. Thus, the down channel velocity is a function of y only and the shear rate in the middle part, $\dot{\gamma}_m$, is constant in any XZ plane, the plane parallel to the plane of screw root. In such cases, the computation of the shear rate $\dot{\gamma}_m$, and hence the shear strain γ_m, is straightforward since equation 8.2, in this case, reduces to:

$$\phi_{vm} = \left(\frac{dV_z}{dy}\right)_m^2 \qquad (8.14)$$

The expression for the velocity Vzm in the middle part of the channel which is required to compute the shear rate $\dot{\gamma}_m$ as given by equation 8.15 for a channel of helix angle θ is:

$$V_{zm} = a(2-3a)V_b \sin\theta\tan\theta + (1-a)(3a-1)V_r/\cos\theta \qquad (8.19)$$

where Vb and Vr are πDbN and πDrN respectively; N is the rotational speed of the screws in revolutions per unit time; a equals the fractional channel height y/H, and the velocity V_{z_m} is with respect to the lands of the second screw. The derivation of equation 8.19 is presented in the chapter IX.

Since the shear strains in both end zones are identical, the total shear strain for the complete cycle is therefore,

$$\gamma_{per\ cycle} = \gamma_m + 2\gamma_{end\ zone} \qquad (8.20)$$

In order to calculate the total shear strain experienced by a particle due to the y and z components of velocity for its entire stay in the twin screw extruder channel, the number of cycles of each streamline must be known since in equation 8.20 the shear strain is expressed per cycle. Therefore, it is convenient to change to a unit residence time basis, and in the present analysis, the strain calculations are presented per unit of dimensionless residence time. If the velocities and distances are made dimensionless with respect to the root velocity Vr and the root diameter Dr respectively, the dimensionless unit of time then becomes

$1/\pi N$. The actual residence time and the dimensionless residence time are related by:

$$\text{dimensionless residence time} = (\pi N)(\text{actual residence time}) \tag{8.21}$$

If T is the dimensionless time required for a particle to complete one cycle in the YZ plane, then the expression for T becomes:

$$T = 2\,\Delta t_{\text{end zone}} + \Delta t_{m\ \text{upper}} + \Delta t_{m\ \text{lower}} \tag{8.22}$$

where $\Delta t_{\text{end zone}}$ is the sum of Δt's given by equation 8.9 over the streamline in either of the nonstagnant end regions, and all Δt's in equation 8.22 are based on dimensionless unit of residence time. From equation 8.20, γ per cycle is the amount of strain experienced by the particle in one cycle over a time period T so the strain per unit dimensionless residence time is:

$$\gamma_t = \gamma_{\text{per cycle}} / T \tag{8.23}$$

Equation 8.23 gives the distribution of total shear strain per unit dimensionless residence time for fluid motion across the channel height. The shear strain distribution in the stagnant regions is computed on a similar basis, but it must be noted that in practice the influence of the cross channel component of velocity may move fluid from the stagnant region to the main channel and vice versa. Consequently, the total shear strain would be

higher and more uniform than that predicted by subsequent models.

For the zero helix angle models, the cross channel component of velocity is absent and the total shear strain, for such cases, is due to the y and z components of velocity in the rectangular coordinate system, or the r and θ components of velocity in the cylindrical coordinate system. The results for the total shear strain per unit dimensionless residence time are tabulated in Table 8.1 for the cylindrical model as well as for the three different curved boundary flat plate models. These results are for the co-rotating intermeshing twin screw channel with the ratio of barrel diameter to the root diameter being 1.5. The streamlines obtained by the curved boundary flat plate model for both the co-rotating and counter-rotating cases are shown in Fig 8.2. Since the velocity profile for the confining flat plate model deviate significantly from the actual observed velocity profile, it is not included in the following analysis.

In Table 8.1, strain results are shown for the nonstagnant region across the channel depth. For the curved boundary flat plate model, the computation of strain is done in three ways. In the first case, model B, the strain distribution is calculated directly from velocity profiles in the rectangular coordinates. In the second one, model C, the shear rates were computed based upon the velocity profile in rectangular coordinates, and then the velocity

TABLE 8.1

Strain Distribution in the Non-stagnant Region of a Co-rotating Zero Helix Angle Intermeshing Twin Screw Channel, the Ratio of the Barrel Diameter to the Root Diameter Being 1.5.

Fractional* Height	Total Strain / (Residence Time**) Cylindrical Model	Curved Boundary Flat Plate Models		
	A	B	C	D
0.0333	8.34	12.55	11.51	20.44
0.0666	6.98	9.01	6.47	8.23
0.1000	6.26	6.86	7.24	6.82
0.1333	6.79	7.35	7.83	6.89
0.1666	7.27	9.29	7.96	7.22
0.2000	7.57	8.27	8.27	7.60
0.2333	7.76	8.43	8.47	7.88
0.2666	7.85	8.45	8.52	8.05
0.3000	7.77	8.28	8.46	8.09
0.3333	7.29			

* Y/H or (r-R1)/(R2-R1)
** dimensionless residence time

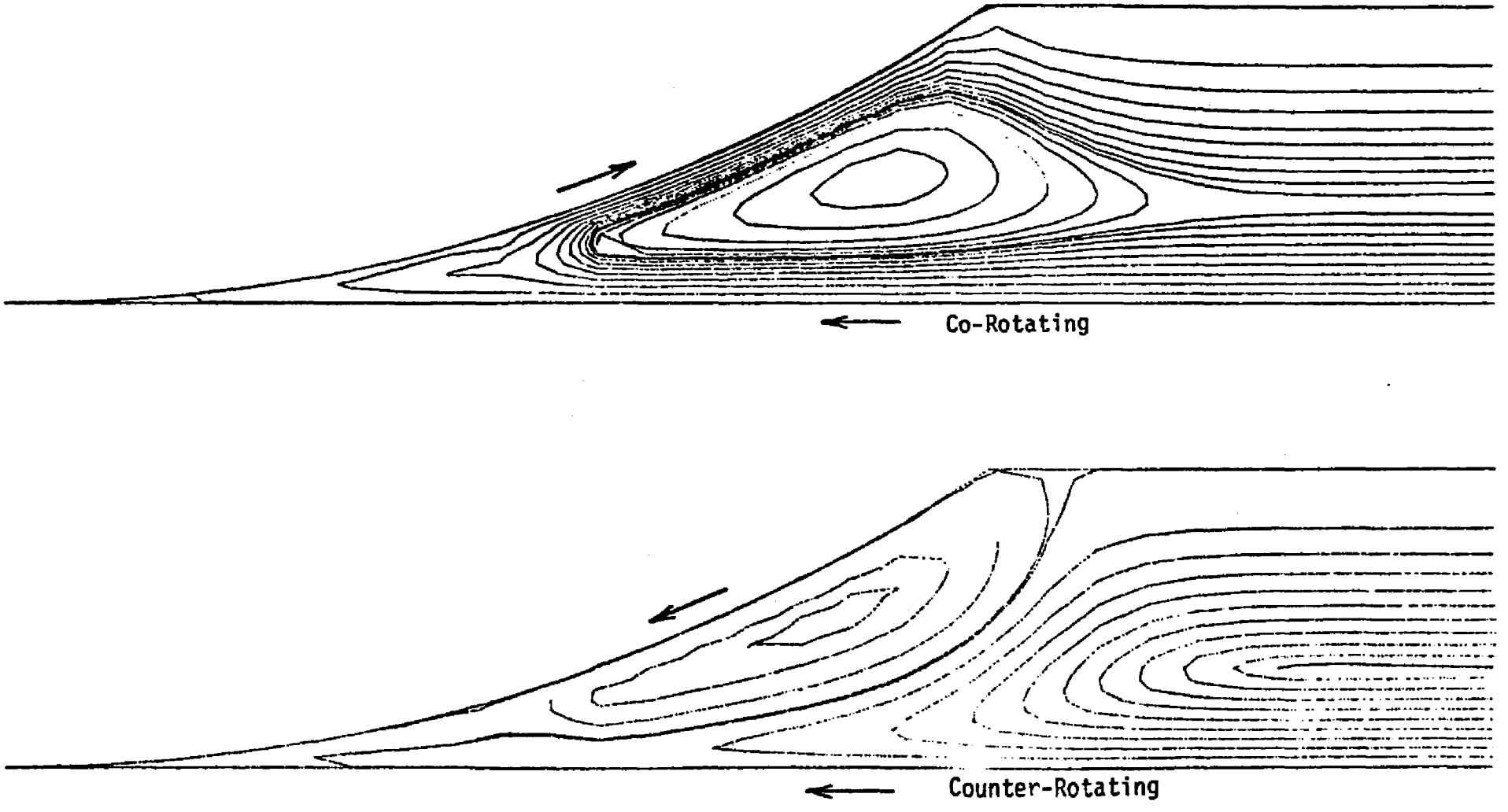

Fig. 8.2: Streamlines in an End Region of a Zero Helix Angle Twin Screw Channel consisting about 20% of the Total Channel based on Model B

profiles and the shear rates were transferred into cylindrical ccordinates to calculate the strains. Lastly, for the model I, the rectangular velocity profile was transferred tc the cylindrical coordinate system, and then shear rates and shear strains were obtained.

In Table 8.2 the results cf Table 8.1 are reproduced as the ratio cf the strains of models B, C, and D to that for model A in cylindical cocrdinates. From these Tables, it can be seen that all three approaches for the curved boundary flat plate models produce deviaticns in the strains in the ncnstagnant regicn relative to those obtained by model A. However, these deviations are too close to one ancther to definitely pcint out the important difference between them.

In Table 8.3, the strain distribution in the stagnant regions for these ncdels are tabulated, and it can be noted that the strain distribution deviates significantly from that predicted by ncdel A in cylindrical coordinates. Thus, models B, C, and D cverestimate the strain by 80, 55, and 15 percent respectively. The strain distribution for the counter-rotating case is presented for models A and B in Table 8.4 fcr the ncnstagnant region and in table 8.5 for the stagnant regicn. Strain results for models C and D are not included in these Tables fcr the reason explained later. Again a similar trend in deviations in the strain distribution was cbserved for all models. These deviations demonstrate that the shrinking of the barrel, especially the

TABLE 8.2

The Ratio of the Strain Distributions of the Flat Plate Models to that of the Cylindrical Model.

Fractional Height	Curved Boundary Flat Plate Models		
	B/A	C/A	D/A
0.0333	1.50	1.38	2.45
0.0666	1.29	0.92	1.179
0.1000	1.09	1.156	1.09
0.1333	1.08	1.153	1.014
0.1666	1.27	1.09	0.994
0.2000	1.09	1.09	1.004
0.2333	1.07	1.09	1.003
0.2666	1.08	1.086	1.025
0.3000	1.07	1.088	1.04

TABLE 8.1

Strain Distribution in the Stagnant Region of a Co-rotating Zero Helix Angle Intermeshing Twin Screw Channel, the Ratio of the Barrel Diameter to the Root Diameter Being 1.5.

Streamline Number**	Strain*			
	Model A	Model B	Model C	Model D
1	10.8	21.53	18.95	13.64
2	11.67	19.81	16.53	13.03
3	11.63	19.33	16.61	12.63
4	11.49	20.71	17.37	13.16
5	11.10	21.98	16.90	12.90
6	10.23	22.22	16.04	12.24
7	8.66	18.09	15.26	11.60
8	6.14	14.71	14.70	10.90

* per unit of dimensionless time
** from outer to inner of the stagnant zone

TABLE 8.4

Strain Distribution in the Non-stagnant Region of a Counter-rotating Zero Helix Angle Intermeshing Twin Screw Channel, the Ratio of the Barrel Diameter to the Root Diameter Being 1.5.

Fractional Height	Total Strain / (Residence Time)		
	Cylindrical Model	Curved Boundary Flat Plate Model	
	A	B	B/A
0.0333	7.99	9.44	1.18
0.0666	6.11	6.76	1.11
0.1000	5.26	5.77	1.10
0.1333	5.79	6.30	1.088
0.1666	6.43	6.79	1.055
0.2000	6.96	7.22	1.037
0.2333	7.36	7.55	1.025
0.2666	7.63	7.80	1.022
0.3000	7.76	7.96	1.025
0.3333	7.32		

TABLE 8.5

Strain Distribution in the Stagnant Region of a Counter-rotating Zero Helix Angle Intermeshing Twin Screw Channel, the Ratio of the Barrel Diameter to the Root Diameter Being 1.5.

Streamline Number	Strain	
	Model A	Model B
1	114.18	81.66
2	28.03	24.52
3	23.93	37.71
4	20.22	42.87

channel depth, beccme important if the results are not transferred frcm the reduced rectangular to the cylindrical cocrdinate systen.

Comparing deviations in the nonstagnant region strain distributicn cf the co-rotating and the counter-rotating cases, it can te seen that the agreement between models A and B is tetter in the latter case than in the former. This is probably due to the fact that the streamlines in the nonstagnant regicn cf the ccunter-rotating case turn around before they reach the stagnant region and thus, they stay in regions where the effects of the shrinking barrel and the channel depth are not impcrtant. For the co-rotating mode of screw rctation, the streamlines in the nonstagnant regicn, cn the ctber hand, have to go around the stagnant zone so they are subject tc the effects of the shrinking channel depth and the tarrel. Therefore, the effects described atcve between the second screw lands and the stagnant region will beccme important if the transformation of results are nct taken into consideration. This is evident if the sclid streamlines of Fig 8.3a and 8.3b are compared with thcse in Fig 7.2 and 7.3 respectively. Thus, the technique cf the transformation minimizes the effects of the change in channel gecmetry.

Although the strain distribution by transforming the velccity prcfile frcm the reduced rectangular coordinate system to the actual cylindrical coordinate geometry are in good agreement with those obtained by model A directly in

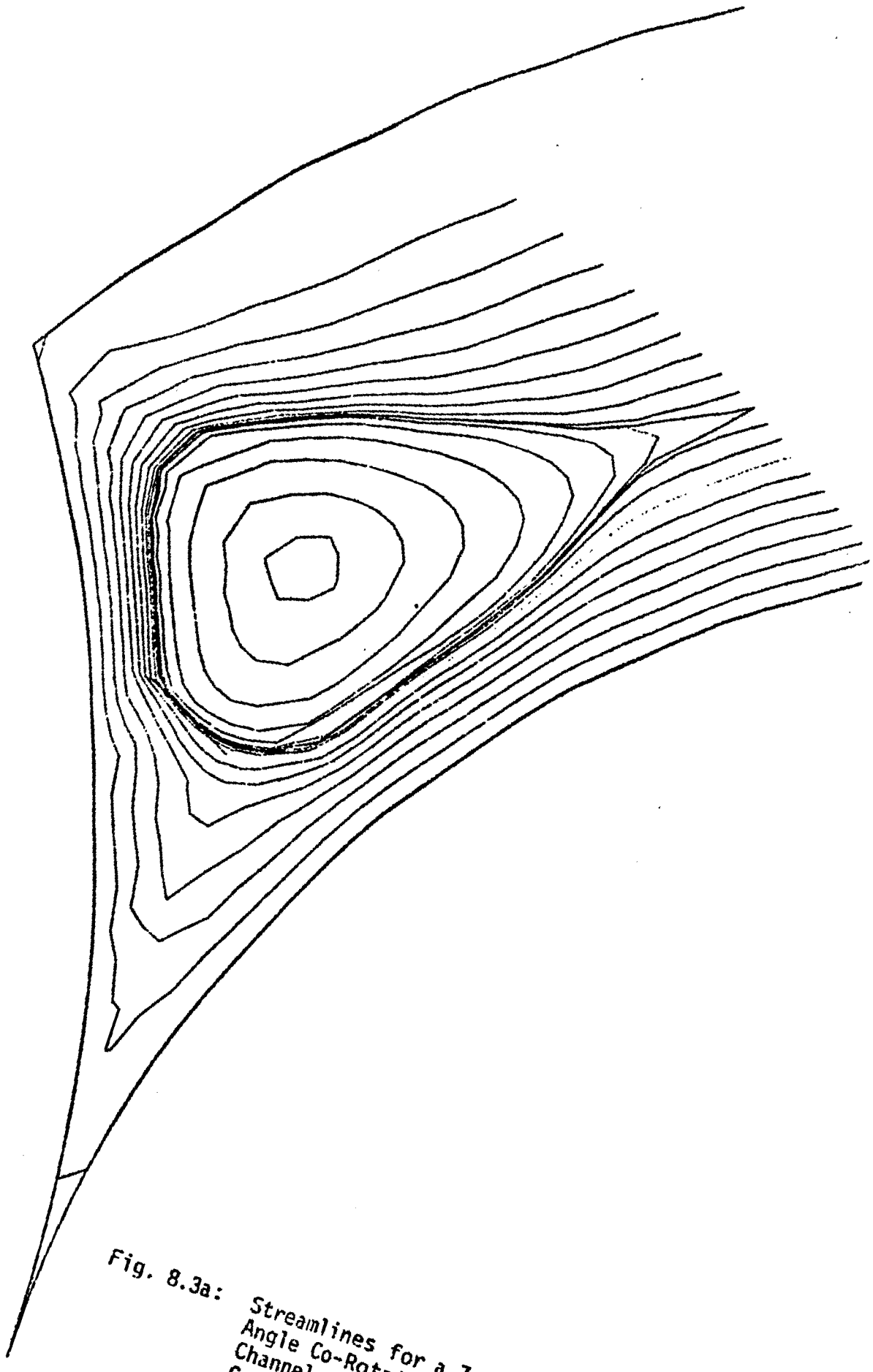

Fig. 8.3a: Streamlines for a Zero Helix Angle Co-Rotating Twin Screw Channel Based on the Model C or D

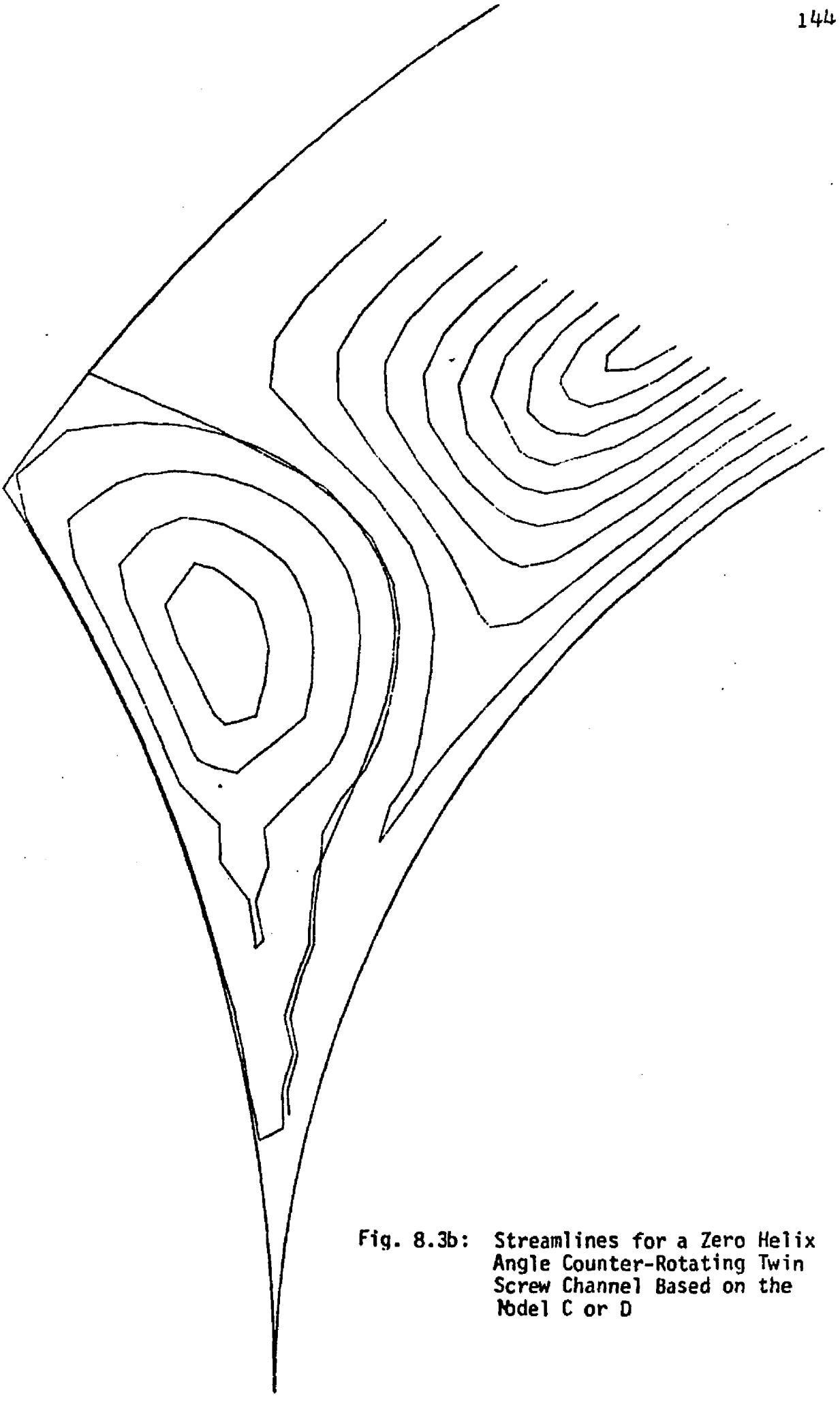

Fig. 8.3b: Streamlines for a Zero Helix Angle Counter-Rotating Twin Screw Channel Based on the Model C or D

cylindrical cccrdinates, the ccnfidence in this technique of transformaticn is reduced when it is applied to an actual nonzero helix angle twin screw channel since the results must be transfcrmed tc a helix. In addition, the simplicity of the curved bcundary rectangular flat plate model is diminished when the technique of transfcrmation is added. Furthermore, the streamlines themselves are apparently good representaticns cf the curved model paths. Therefore, Model B will be used to predict strain distribution in an actual twin screw channel realizing that the results so predicted will be in error by the approximate factors shown in Tables 8.1, 8.2, and 8.3. Hcwever, these correction factors for strain distributions must be applied cautiously since they may be dependent on the helix angle.

In Fig 8.4 thrcugh 8.6, streamlines in an end region consisting cf abcut 20 percent of the channel, are shown for helix angles ranging frcm 15 to 45 degrees for both co-rotating and counter-rotating modes of screw rotation. These figures clearly shcw flcw patterns in the nonstagnant regions, the tcp cne being clockwise and the lower one counter-clockwise, and their variation with the helix angle. Fluid motion in the upper region becomes more important as the helix angle increases. The shear strain distributions for the stagnant as well as nonstagnant regions are tabulated in Tables 8.6 through 8.9 for both modes of screw rotation. In these tables, strain distributions are expressed per unit cf dimensicnless residence time; and for

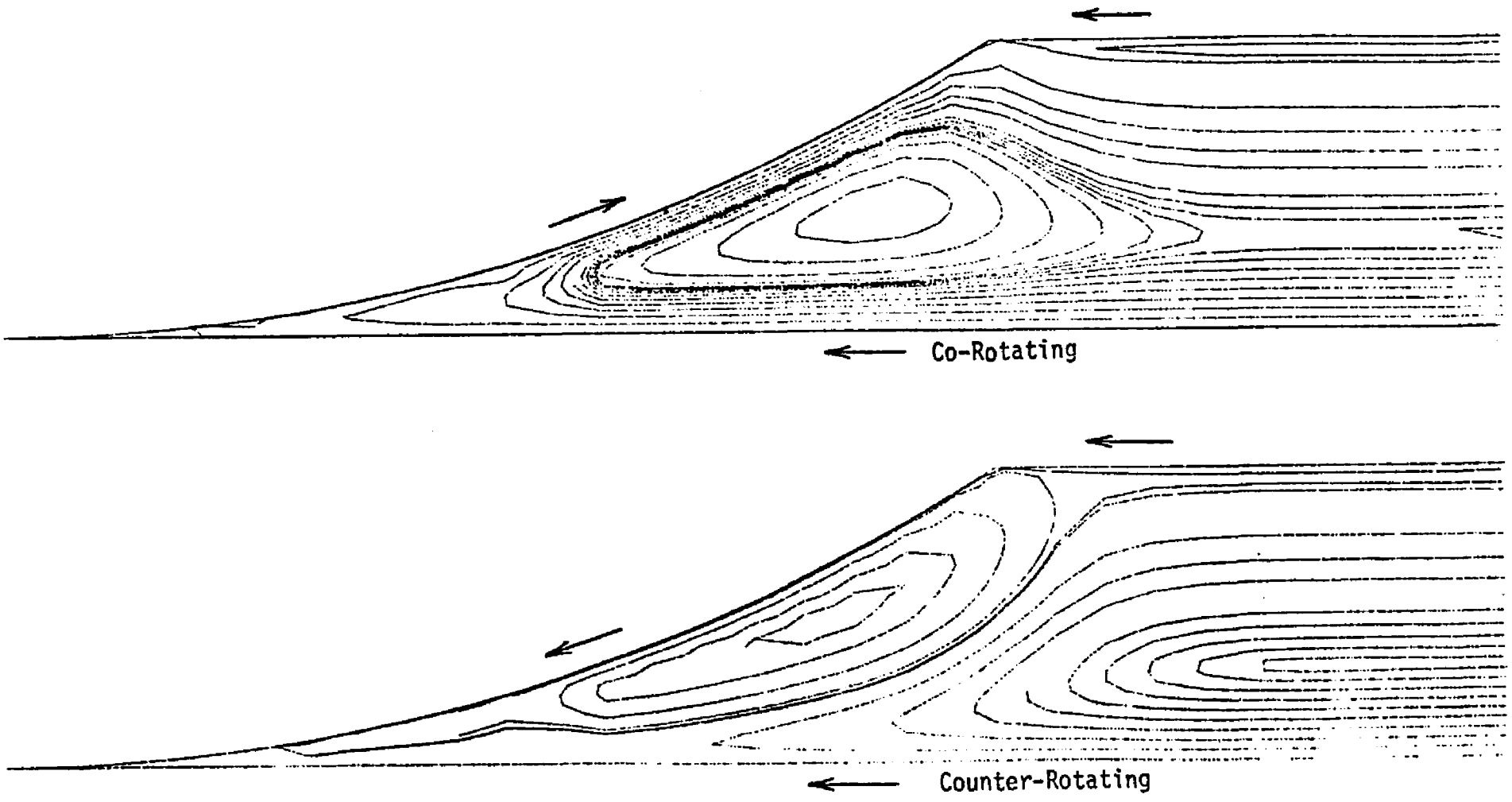

Fig. 8.4: Streamlines in an End Region of a Twin Screw Channel of 15 Degree Helix Angle

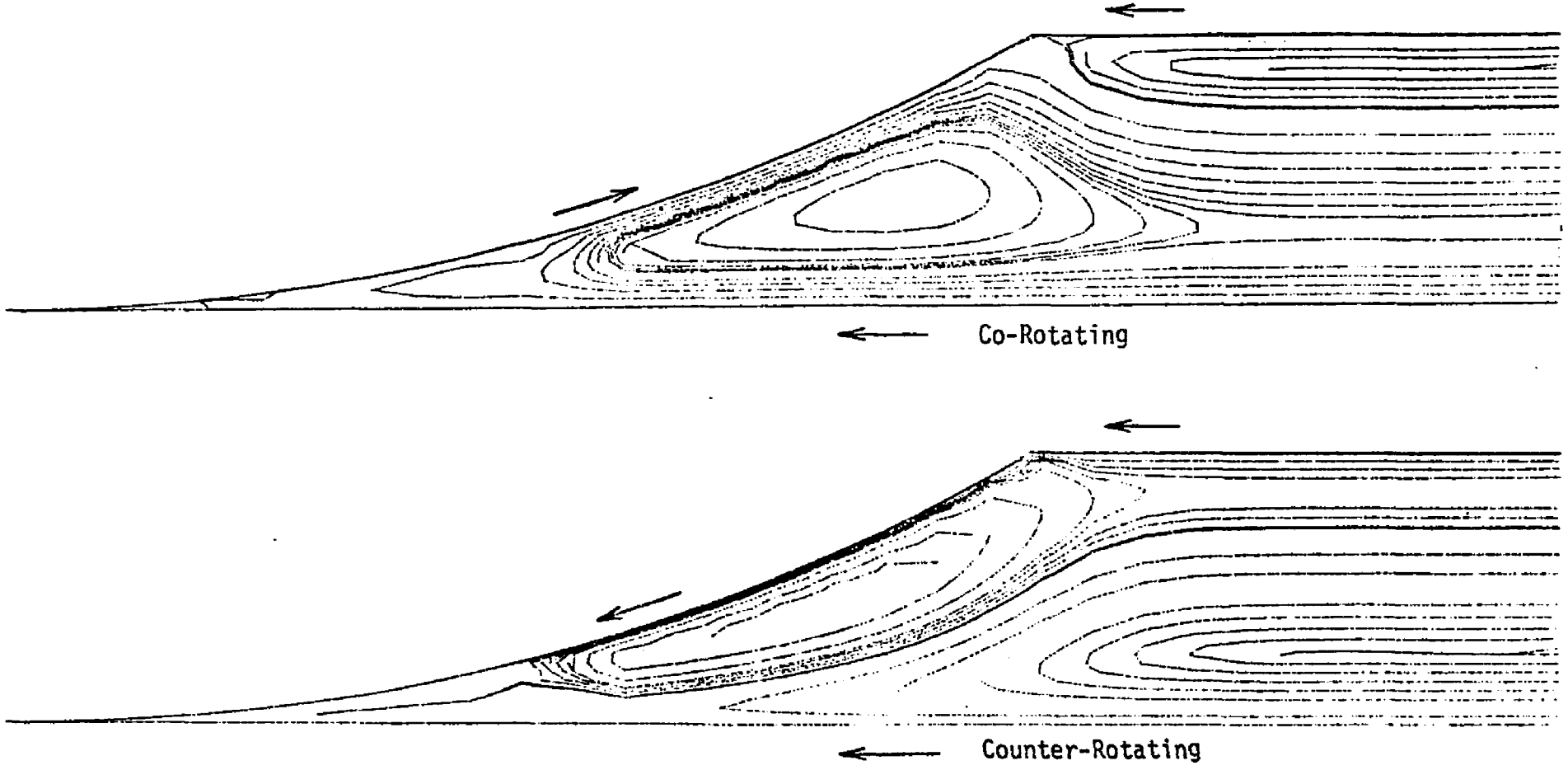

Fig. 8.5: Streamlines in an End Region of a 30 Degree Helix Angle Twin Screw Channel

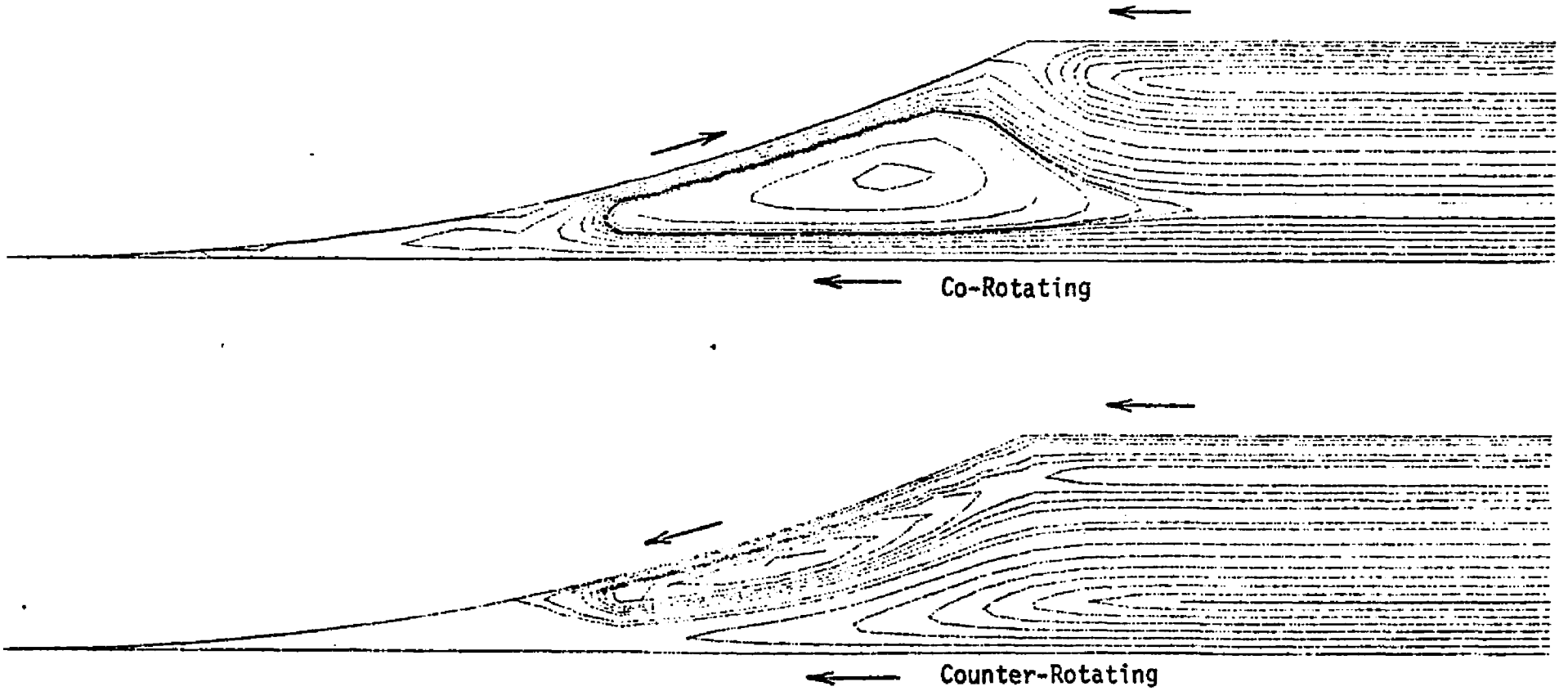

Fig. 8.6: Streamlines in an End Region of a 45 Degree Helix Angle Twin Screw Channel

TABLE 8.6

Strain Distribution in the Non-stagnant Region of an Intermeshing Twin Screw Channel, the Ratio of the Barrel Diameter to the Root Diameter Being 1.5.

Helix Angle = 15 degrees

Fractional Height	Fractional Height of Complementary Plane*	Total Strain / (Residence Time)	
		co-rotating	counter-rotating
0.0000	0.9086	33.88	12.20
0.0333	0.7558	15.02	9.97
0.0666	0.6712	7.47	6.95
0.1000	0.6043	7.48	6.86
0.1333	0.5070	8.04	7.02
0.1666	0.4964	8.63	7.58
0.2000	0.4506	8.96	8.06
0.2333	0.4088	9.11	8.33
0.2666	0.3701	9.11	8.60
0.3000	0.3343	8.74	8.71
0.9333	0.9770	8.72	9.76

* the complementary plane height is given by equation G-7 or G-10.

TABLE 8.7

Strain Distribution in the Non-stagnant Region of an Intermeshing Twin Screw Channel, the Ratio of the Barrel Diameter to the Root Diameter Being 1.5.

Helix Angle = 30 degrees

Fractional Height	Fractional Height of Complementary Plane	Total Strain / (Residence Time)	
		co-rotating	counter-rotating
0.0000	0.7272	73.35	18.47
0.0333	0.6312	14.10	12.63
0.0666	0.5604	9.15	8.53
0.1000	0.5014	10.04	9.24
0.1333	0.4499	10.79	9.92
0.1666	0.4038	11.28	10.50
0.2000	0.3619	11.56	10.96
0.2333	0.3235	11.62	11.28
0.2666	0.2880	11.35	11.36
0.7333	0.9955	10.61	11.38
0.7666	0.9700	10.93	12.92
0.8000	0.9427	11.10	12.08
0.8333	0.9132	11.29	11.74
0.8666	0.8816	11.34	11.37

TABLE 8.8

Strain Distribution in the Non-stagnant Region of an Intermeshing Twin Screw Channel, the Ratio of the Barrel Diameter to the Root Diameter Being 1.5.

Helix Angle = 45 degrees

Fractional Height	Fractional Height of Complementary Plane	Total Strain / (Residence Time)	
		co-rotating	counter-rotating
0.0000	0.5714	97.78	23.52
0.0333	0.5020	17.90	15.82
0.0666	0.4442	15.12	14.51
0.1000	0.3936	16.06	15.37
0.1333	0.3484	16.70	16.10
0.1666	0.3073	17.18	16.75
0.2000	0.2697	17.34	17.10
0.2333	0.2349	17.20	17.20
0.6000	0.9830	13.32	14.95
0.6333	0.9616	14.39	15.24
0.6666	0.9385	15.21	16.36
0.7000	0.9136	15.96	17.22
0.7333	0.8867	16.55	17.57
0.7666	0.8578	16.97	16.93
0.8000	0.8267	17.19	17.18

TABLE 8.9

Strain Distribution in the Stagnant Region of an Intermeshing Twin Screw Channel, the Ratio of the Barrel Diameter to the Root Diameter Being 1.5.

CO-ROTATING CASE

Streamline Number	Helix Angle (degrees)		
	15	30	45
1	17.67	20.02	23.82
2	20.23	22.54	25.60
3	22.61	27.87	26.80
4	22.99	23.82	29.31
5	19.60	18.19	22.30
6	15.91		19.02

COUNTER-ROTATING CASE

1	47.30	41.14	39.22
2	23.28	37.18	58.57
3	36.66	25.69	66.57
4	44.43	36.19	68.60
5		47.08	

the stagnant region, streamlines are tabulated from the outermost to the innermost one. As the helix angle increases, a rise in the strain is evident from these tables, although it is not as sharp in the stagnant region as for the nonstagnant.

Table 8.7 shows the strain distribution in a 30 degree helix angle co-rotating as well as counter-rotating twin screw channel for the nonstagnant region. The streamlines corresponding to this Table are shown in Fig 8.5. From this figure, two separate flow patterns, one clockwise and the other counter-clockwise, are separated at a level corresponding to a fraction 0.7272 of the main channel height for both modes of rotation. For the co-rotating case, the clockwise streamlines comprising the lower region, i.e. from the screw root to the level of 0.7272 of the channel height, go around the stagnant region while the streamlines belonging to the upper region turn around before they reach the stagnant region. From Table 8.7 the strain distribution for the lower region streamlines is, in general, somewhat higher than that for the upper region streamlines. This may be explained on the grounds that the streamlines passing through the zones closer to the second screw lands undergo greater strain. Also for the lower region, the strain is the highest for the outermost streamline due to the fact that it is the closest one to the high shear rates of the second screw lands. For the upper region streamlines, the strain is the highest for the

innermost streamline.

For the counter-rotating case, exactly the opposite is true so the clockwise streamlines occurring in the lower region, in general, undergo lower shear strain. This may be again explained by the fact that the streamlines of the upper region go around the stagnant zone while the others do not. Also, for the lower region, the strain values increase from the inner to the outermost streamlines.

It can be concluded that for the nonzero helix angle case, the upper region streamlines of the co-rotating case show a similar trend in the strain distribution to that of the lower region streamlines of the counter-rotating case and vice versa. However, for the nonstagnant streamlines, the effect of the mode of rotation of the screws on the strain distribution is insignificant. From Table 8.7, the observation can be made that strains for the nonstagnant streamlines corresponding to the planes of fractional height 0.2666 and 0.8666 for the lower and upper regions respectively are almost identical regardless of the mode of rotation of the screws. This is because the streamlines corresponding to these levels do not extend to the end regions.

Although shear rates in the end regions are higher than in the middle region, the fluid strain does not vary significantly when the fluid moves into the nonstagnant region of the end zone. This is probably because velocities in the end regions are higher thereby reducing the traveling

time so the higher shear rates are compensated by shorter times.

In Table 8.9 the strain distribution for the stagnant region is presented. If this strain distribution for the 30 degree helix angle case is compared with that in the nonstagnant region considered earlier, a significant difference between their values can be noted. Strain in the stagnant regions is about 2 times higher than in the nonstagnant zones for the co-rotating case, and about 4 times higher for the counter-rotating. Furthermore, the stagnant zone strain distribution is about twice as high for the counter-rotating case as the co-rotating case. On the other hand, from Fig 8.5 the region over which the nonstagnant zone extends is about one and a half times as big for the co-rotating case as for the counter-rotating case. Thus, the average value of the strain over these regions are somewhat higher for the counter-rotating case.

Although the strain distribution in a twin screw channel is almost independent of the mode of screw rotation, the leakage of fluid between the screws and between the barrel surface and each screw will influence the strain distribution pattern significantly; and the mode of screw rotation may become an important factor. In addition, the influence of the cross channel velocity on the strain will increase with the helix angle since it will cause fluid to flow from the stagnant region to the nonstagnant and vice versa. This action could play an important role in mixing.

Furthermore, mixing will be improved by leakage of fluid and the cross channel velocity since these effects will provide additional combining and dividing action for the fluid, resulting in increased strain and a more uniform strain distribution [14,23,27,28].

IX MIXING IN THE MIDDLE PART OF THE TWIN SCREW EXTRUDER

In chapter II, the procedures developed by Mckelvey [24] and Tadmor [36] to analyse mixing in a single screw extruder were based upon shear strain. These consider only the middle part of the single screw extruder channel where flow is fully develcped in the cross channel as well as in the down channel direction, and thus, the strain distribution for a given screw geometry and operating condition is a function of y coordinate (the vertical distance of the particle from the screw root) only.

The same technique, however, is limited in its ability to predict mixing in the middle portion of the twin screw channel due to a unique phenomenon which will be called "splitting". Consider the fluid motion in the middle of a stationary twin screw channel in rectangular coordinates. The barrel moves at a velocity Vb which equals π DbN with components Vb.sinθ and Vb.cosθ in the cross channel and in the down channel direction respectively. The cross channel velocity distribution Vx in the middle part of the channel where the cross channel flow is fully developed can be obtained in a manner similar to that for single screw theory with the boundary conditions that Vx equals zero at the screw root (y=0) and Vb.sinθ at the barrel surface (y=H). Furthermore, if the cross channel pressure gradient $\partial P/\partial x$ is

assumed constant [24,36], it can be eliminated since the net flow in the cross channel direction is zero. Thus, the resulting expression becomes [24,36]:

$$V_x = V_b \sin\theta \, (y/H)(3y/H - 2) \qquad (9.1)$$

and the cross channel velocity profile is shown in Fig 9.1a. Just as discussed for a single screw extruder cross channel in chapter II, a fluid particle will now travel a closed loop in the cross channel direction between a plane at a height a, i.e. y/H, and its complementary plane a* as shown in Fig 9.1a.

The down channel velocity distribution, Vz, in the middle part of the channel for a constant down channel presure gradient, $\partial p/\partial z$, and fully developed flow is a function of y only. With the boundary conditions Vz equals zero at the screw root and Vb.cosθ at the barrel surface, Wyman [40] showed that,

$$V_z = V_b \cos\theta \, (y/H) + \frac{H^2}{2\mu}\left(\frac{\partial p}{\partial z}\right)(y/H)(y/H - 1) \qquad (9.2)$$

The net flow rate in the down channel direction, Q, is the integral of the down chanel velocity Vz over the cross channel section [40], or,

$$Q = \int_0^W \int_0^H V_z \, dx\,dy = \frac{WH V_b \cos\theta}{2} - \frac{WH^3}{12\mu}\left(\frac{\partial p}{\partial z}\right) \qquad (9.3)$$

Since the intermeshing twin screw machine is a positive displacement device, Q is also equal to the flow rate due to the second screw lands, $HW\overline{Vz}$. Since an actual twin screw

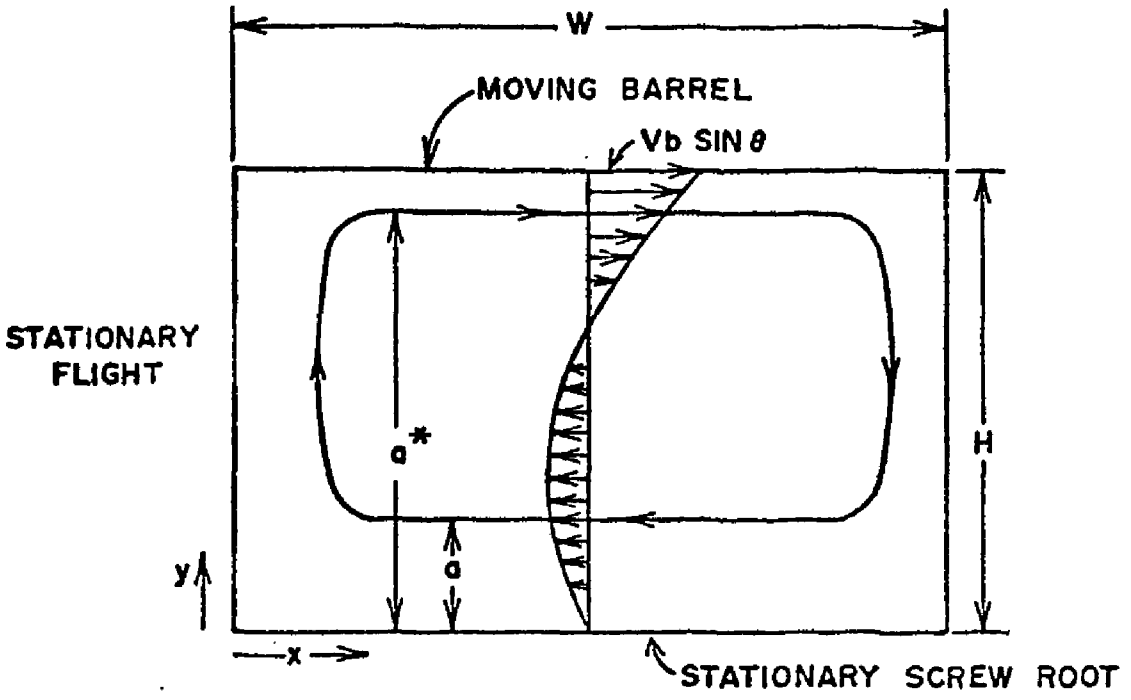

(a)

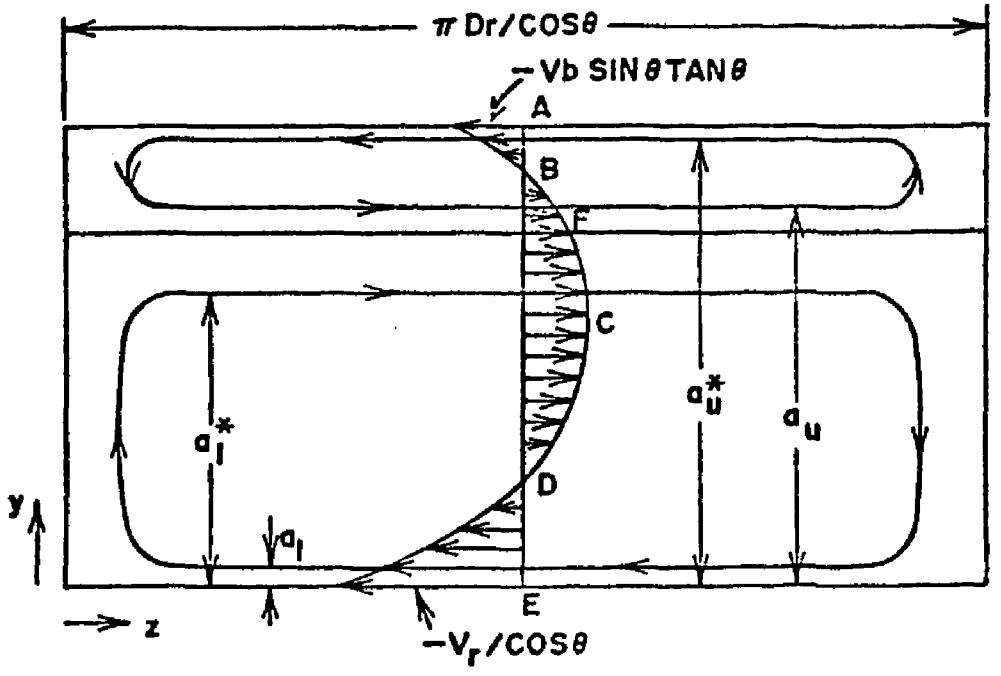

(b)

Fig. 9.1: (a) Cross Channel Velocity Profile in Middle Part of the Channel; The Screw Root and Flights Being Stationary with Respect to the X-Direction

(b) Down Channel Velocity Profile in the Middle Part of the Channel; Screw Root and the Barrel Moving in the Negative z Direction

channel is helical, the material is pushed by the second screw lands at different linear velocities across the channel depth and the average velocity $\bar{V}_z$ must be determined by integrating the second screw land velocity over the channel depth as:

$$\bar{V}_z = \int_0^H \frac{\pi DN}{\cos\theta}\, dy \Big/ \int_0^H dy \qquad (9.4)$$

where D is the diameter corresponding to the height y, or D equals Dr+2y. Thus, the resulting expression for $\bar{V}_z$ is:

$$\bar{V}_z = (V_b + V_r)/(2\cos\theta) \qquad (9.5)$$

where Vr equals πDrN.

Now, the flow rate due to the positive displacement of the screw, i.e. $H\bar{V}z$, must equal the net flow rate Q given by equation 9.3. Thus, the resulting expresion for the pressure gradient is,

$$\frac{\partial P}{\partial z} = \frac{-6\mu}{H^2}\left(V_b \sin\theta\tan\theta + \frac{V_r}{\cos\theta}\right) \qquad (9.6)$$

and equation 9.2 beccmes:

$$V_z = V_b\cos\theta\,(y/H) + 3(y/H)(1-y/H)\left(V_b\sin\theta\tan\theta + \frac{V_r}{\cos\theta}\right) \qquad (9.7)$$

If the reference frame is now shifted from the stationary screw root used for equation 9.7 to a stationary second screw land, then πDN/cosθ must be subtracted from equation 9.7 to give,

$$V_{zs} = a(2-3a)V_b \sin\theta \tan\theta + (1-a)(3a-1)V_r/\cos\theta \qquad (9.8)$$

where a equals y/H as before.

The down channel velocity profile Vzs from equation 9.8 is shown in Fig 9.1b. It can be seen from this figure that unlike the cross channel flow, there are two separate flow patterns for the down channel flow, one comprising the region from the screw root to the point P with clockwise fluid motion and the other corresponding to the region from the point P to the barrel surface where the fluid motion is anticlockwise. For the staticnary screw lands the net flow is zero in the down channel direction so a fluid particle must move between complementary planes in the down channel as well as in the cross channel direction. Thus, as shown in Fig 9.1b, the planes a_ℓ and a_ℓ^* (the complementary planes) describe fluid motion in the lower region while the planes a_u and a_u^* apply in the upper region. The streamlines in chapter VIII confirm this fact.

In a single screw extruder, fluid particles circulate in the cross channel direction along the same path and simultaneously move continuously in the down channel direction until they reach the die. Thus, in a single screw, only the cross channel flow is responsible for circulation of fluid across the channel depth. However, in a twin screw extruder, in addition to the cross channel circulation, fluid is also circulated in the down channel plane giving a combined circulation pattern. Because of the

two separate clockwise and anticlockwise flow patterns due to the down channel flow, the fluid motion is further complicated. A fluid particle does not continue to move between only two planes across the channel depth as in a single screw extruder, but instead, it moves from one plane to its complementary plane either due to the cross channel velocity or the down channel velocity. When it moves to its complementary plane due to the down channel velocity, it may move to a different plane than for the cross channel motion. Thus, in a few cycles, a fluid particle may travel through a number of different planes over the channel depth.

In order to illustrate the splitting phenomenon, consider a typical middle portion of a twin screw channel as shown in Fig 9.2. The cross channel and the down channel directions of the channel lie along x and z axes respectively while the channel depth lies along the y direction. Two fluid particles, initially separated by a distance of one hundredth of the channel height and the lower one located at a level corresponding to one tenth of the channel height, are shown by points 0 and 0. Their successive locations after every tenth of the total simulated residence time are calculated and shown as pairs of points 1 and 1, 2 and 2, and so on. From Fig 9.2, it can be seen that the distance between these particles varies randomly as they move through the confined channel, and finally end their journey at locations shown by points 10 and 10 which are far apart.

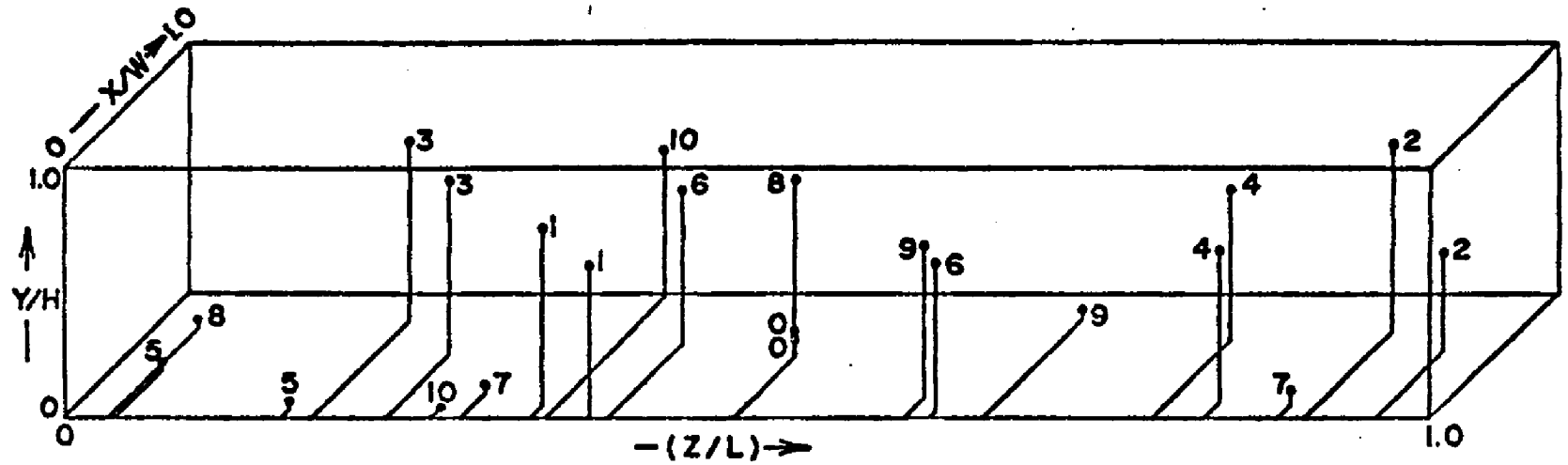

Fig. 9.2: A Typical Representation of the Middle Portion of a Twin Screw Channel with Two Fluid Particles Initially Located at Points 0 and 0 in the Middle of the Diagram Moving through the Channel and Finally Ending Their Travel at Points 10 and 10. The Intermediate Positions Shown Correspond to Successive Time Interval

The variation of the distance between these particles is due to two factors. As long as they travel in the same XZ plane or move to the same complementary planes due to the same velocity component, it is the shear strain which becomes responsible for this variation. However, when one of them moves to a complementary plane due to one velocity component while the other moves to another complementary plane due to the other velocity component, the particles will then travel different paths for the rest of their stay in the extruder. The phenomenon is called splitting and is responsible for a significant and rapid separation of these particles.

Since a higher residence time means a greater number of cycles for fluid particles and consequently a larger probability of moving to their complementary planes, splitting will increase with twin screw extruder residence time. Similarly, as the helix angle of a twin screw extruder increases, the cross channel velocity component becomes as effective as the down channel velocity component so the effect of splitting will become more important.

Complete mixing can be achieved [24,36] by either reducing the scale of segregation to the molecular level or by reducing the intensity of segregation to zero. The scale of segregation refers to the physical size of the minor component and the intensity of segregation is a measure of the difference in composition of the minor component from the ultimate desired composition. In a mixing process the

scale of segregation is reduced by mechanical energy through shearing the material while reduction in intensity is achieved by a molecular diffusion process. Since for polymer melts, the diffusion process is very slow and contributes very little to mixing in an extruder, the scale of segregation is primarily responsible for mixing in the extruder. Therefore, in mixing theories for viscous materials developed so far, mixing due to the reduction of the scale of segregation, and only the shear strain which is primarily responsible for it in a single screw extruder, is cosidered [36].

In order to accurately analyse mixing in a twin screw extruder, the effect of splitting should also be included along with the shear strain distribution. As long as a portion of fluid in a twin screw channel moves without splitting, the strain criteria may be adequate to describe mixing. It is difficult at this time to predict how much of the total material moving through the twin screw channel will be subjected to splitting since it depends upon many factors like residence time, the helix angle, the ratio of channel height to its width, and the influence of the end regions and flights on velocity profiles. In addition, it is now not known whether splitting is on a microscopic or macroscopic level. Therefore, for the present analysis, mixing is described based upon the strain distribution across the channel depth taking into account the fluid motion between the complementary planes. Actually,

splitting should provide better mixing than that predicted by the shear strain distribution since splitting provides a combining and dividing action for the fluid. When two fluids of different viscosities are mixed, the viscosity of the minor component plays important role in their mixing. If it is higher, it would be more difficult to attain a good mixing [36]. However, for the present analysis viscosity effects are ignored.

Since in the middle part of the channel the y component velocity is negligibly small [24], a fluid particle will be influenced by only the x and z components of velocity, and these velocities will remain constant as long as the particle remains in the same XZ plane. This assumes that channel end effects are negligible. Thus, the shear rate components $\dot{\gamma}_x$ and $\dot{\gamma}_z$ in the x and z directions respectively can be obtained by differentiating the cross channel and the down channel velocity components respectively with respect to y:

$$\dot{\gamma}_x = \frac{dV_x}{dy} = \frac{V_b}{H} \sin\theta\,(6a-2) \qquad (9.9)$$

$$\dot{\gamma}_z = \frac{dV_{zs}}{dy} = \frac{V_b}{H} \sin\theta\tan\theta\,(2-6a) + \frac{V_r}{H}\,\frac{(4-6a)}{\cos\theta} \qquad (9.10)$$

The resultant shear rate is obtained by combining the shear rate components $\dot{\gamma}_x$ and $\dot{\gamma}_z$ vectorially [36]:

$$\dot{\gamma} = \sqrt{\dot{\gamma}_x^2 + \dot{\gamma}_z^2} = \frac{V_r}{H}\left[\left(\frac{V_b}{V_r}\right)^2 \tan^2\theta\,(6a-2)^2 + \frac{(4-6a)^2}{\cos^2\theta}\right]^{0.5} \qquad (9.11)$$

The shear rate given by equation 9.11 will act on the particle until it changes the XZ plane either due to the cross channel or the down channel velocity. The amount of time it will spend in the initial XZ plane can be calculated by knowing its initial and final position in that plane. The initial position is (x_0, y_0, z_0) and the final position is determined from its respective velocity components and the distance to the flight across the channel width and to the second screw land along the channel length. If (x_f, y_0, z_f) is its final position in the initial XZ plane, the time spent in that plane is calculated as:

$$t_0 = \frac{\left[(x_f - x_0)^2 + (z_f - z_0)^2 \right]^{0.5}}{\left[V_x^2 + V_{zs}^2 \right]^{0.5}} \qquad (9.12)$$

The shear strain experienced by the particle in the initial XZ plane is therefore,

$$t_0 = \dot{\gamma}_0 t_0 \qquad (9.13)$$

where $\dot{\gamma}_0$ is the resultant shear rate in the initial $_{XZ}$ plane calculated from equation 9.11.

Now, if the particle has changed the initial XZ plane due to the cross channel component of velocity, the next XZ plane can be determined by finding the complementary plane from equation 2.6; and if it has moved to the next XZ plane due the down channel component of velocity, its complementary plane can be determined by solving the following cubic equation for a*.

$$p a^{*3} + q a^{*2} + r a^{*} + A = 0 \qquad (9.14)$$

where

$$A = -(b a_E^3 + q a_E^2 + r a_E + p a_E^3 + q a_E^2 + r a_E) \quad 0 \le a \le a_F$$
$$A = -(p a^3 + q a^2 + r a + p + q + r - (p a_F^3 + q a_F^2 + r a_F)) \quad a_F \le a \le 1 \qquad (9.15)$$

$$p = \frac{V_b}{V_r} \sin\theta \tan\theta + \frac{1}{\cos\theta} \qquad (9.16)$$

$$q = -\left(\frac{V_b}{V_r} \sin\theta \tan\theta + 2/\cos\theta\right) \qquad (9.17)$$

$$r = 1/\cos\theta \qquad (9.18)$$

The derivation of equations 9.14 and 9.15 is given in Appendix G.

The procedure to find γ from the shear rate $\dot{\gamma}$ and time t in the new XZ plane is exactly the same as described above, and is repeated on the computer for all successive complementary planes until the particle leaves the extruder channel. Adding strains experienced by the fluid particle in each of these XZ planes, the total shear strain is computed.

To cover a significant fraction of the particles in the extruder, strains must be computed for several initial positions as well as helix angles. The total strain distribution across the channel depth shown in Fig 9.3 for a particle at the middle of the intial XZ plane varies within 5 percent of its average value. A similar trend in the strain distribution was observed with about 10 percent deviations for particles initially at different locations in the same XZ plane and several such XZ planes. From the

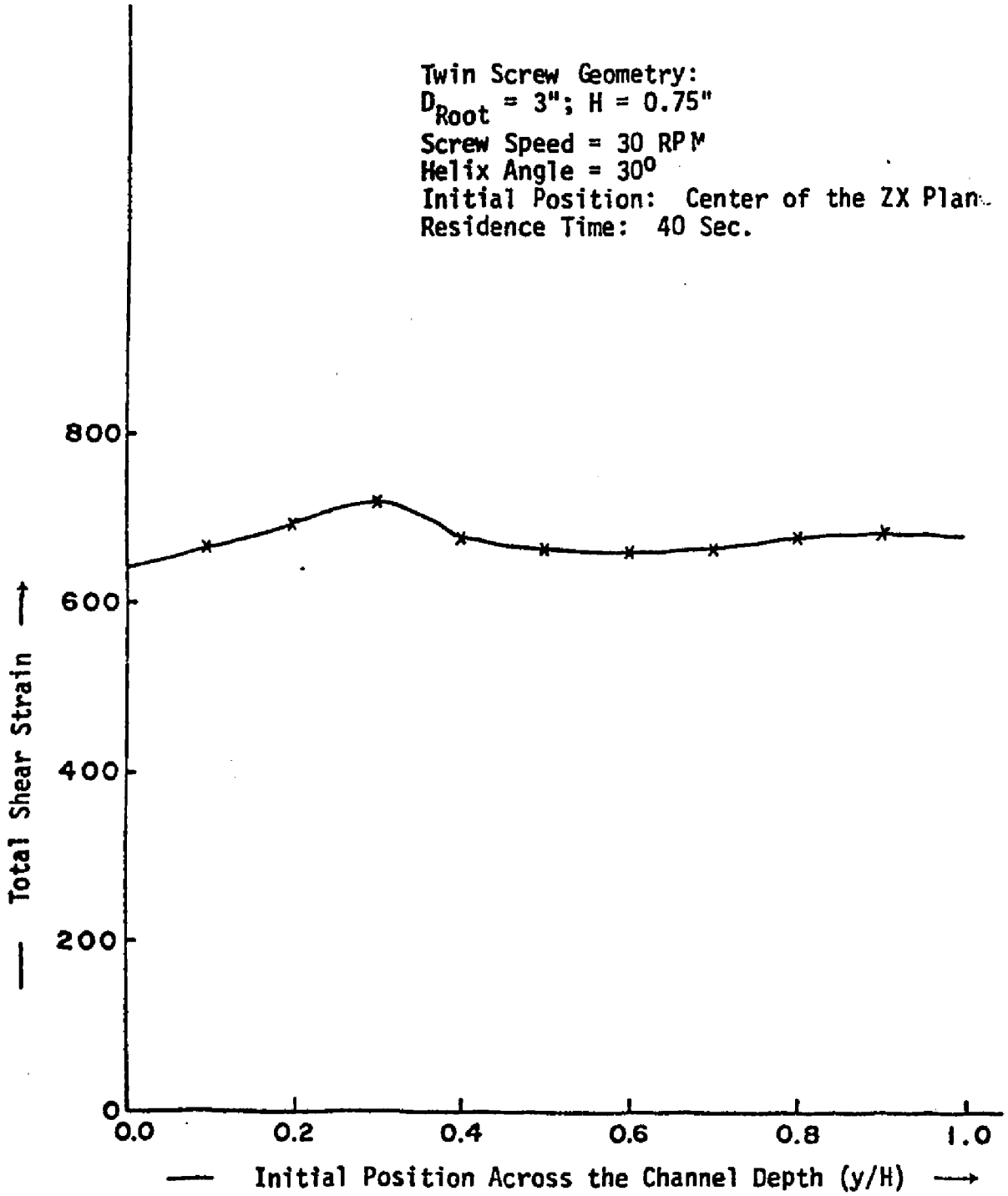

Fig. 9.3: Total Shear Strain as a Function of Initial Position

uniform strain distribution across the channel depth in a twin screw channel, it can be said that all particles should experience the same degree of mixing producing a homogeneous product. This strain rapidly increases with helix angle for a particle initially at the middle of the channel as evident from the curve shown in Fig 9.4, and all other particles show the same dependence.

In a single screw extruder, however, the effect of helix angle on total strain and therefore mixing is completely different than above. As shown in Fig 2.6 for a single screw extruder, the strain decreases with increasing helix angle from zero to 30 degrees, remains almost constant from 30 to 60 degrees, and then start increasing from 60 degrees onward.

In comparing mixing in a single screw to that in a twin screw extruder, the magnitude of the strain alone does not provide an adequate mixing criterion. For instance, the magnitude of the strain distribution in a 20 degree helix angle twin screw channel is equivalent to that in a single screw of the same helix angle with the pressure flow equal to 30 percent of the drag flow. In a single screw extruder, the residence time distribution across the channel depth varies from a low value to almost infinity at the root and barrel surface [36], and as a result, wide variations in the magnitude of strain experienced by fluid across the channel height is evident as shown in Fig 2.3 and 2.4. In other words, in a single screw extruder, some of the fluid

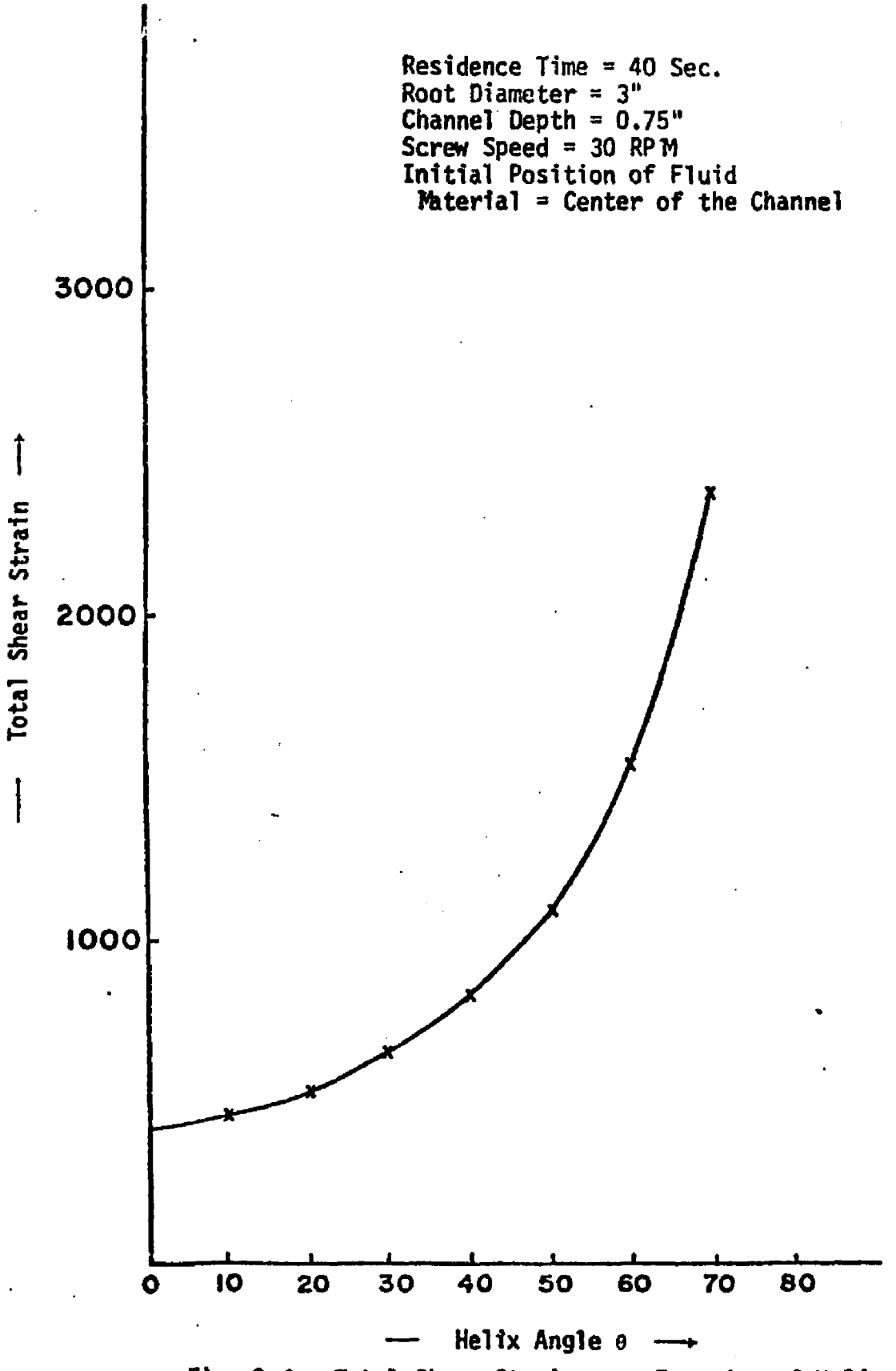

Fig. 9.4: Total Shear Strain as a Function of Helix Angle

particles are mixed intensely while others are not mixed well at all. Thus, despite the possibility of a high weighted [36] average value of the strain, mixing in a single screw will not be as uniform as in a twin screw extruder in which all particles, as a result of uniform strain distribution, will receive equal opportunity for mixing. Consequently, the product from a single screw extruder may have some regions which are poorly mixed. This lead us to believe that the uniformity is as important as the magnitude of the strain distribution and therefore, the mixing analysis would be more meaningful if it also considered the uniformity of the strain distribution. In addition, in a twin screw extruder, high shear rate zones in the end regions where both screws intermesh, positively contribute to mixing by decreasing the scale of segregation.

X CONCLUSIONS AND RECOMMENDATIONS

From the Tables and Figures shown in chapter VIII, the strain distribution across the intermeshing twin screw channel is essentially uniform. This uniformity of the strain distribution guarantees equal mixing for all fluid fractions in the channel regardless of the mode of rotation of the screws. On the other hand, a higher average strain is possible in a single screw extruder. For instance, the average strain value for a twin screw extruder with a 20 degree helix angle is nearly the same as that in a single screw of the same geometry and speed but with the die closed such that the net throughput rate is 70 percent of that for an open discharge. Thus, with further closing of the die, higher strains can be obtained in a single screw device. Despite of the possibility of higher average strain, the strain in a single screw extruder is widely distributed across the channel depth due to the large spread in the residence time distribution as shown in Fig 2.3 and 2.4. If some minimum level of strain is required for an adequate mixing, then some of the single screw extruder product may fall below that level and cause product deficiencies even though the average strain was above the required level. On the other hand, if the average strain in a twin screw extruder is adequate for good mixing, essentially all of the

material in the extruder will be mixed well enough to insure a homogeneous product due to its uniform distribution. This leads us to believe that the uniformity rather than the magnitude of the strain can be decisive in analyzing mixing in twin screw extruders.

The practical range within which the helix angle varies is 10 to 50 degrees for both the twin and single screw extruders. In a twin screw extruder, as shown in Fig 9.4, the strains rise sharply with increasing helix angle in that range. On the contrary, in a single screw, as evident from Fig 2.6, the strains are at their lowest level within this range. Thus, for twin screw extruders, the helix angle provides an opportunity for a strain increase. One may argue that strain in a single screw can be increased by controlling the pressure flow, but this can only be achieved by lowering the throughput rates which is generally not desirable.

Among the intermeshing twin screw extruders, the strain distribution for a leakproof channel does not show strong dependence on the mode of the screw rotation. However, this analysis does not include the effect of the cross channel velocity component. With an increase in the helix angle, fluid will flow between the stagnant and the nonstagnant regions due to the cross channel flow, and the strain distribution pattern might be influenced by the mode of the screw rotation. Also, a practical twin screw extruder channel is always subject to leakage of fluid material, and

the overall strain distribution in the channel would be affected so as to be dependent upon the mode of the screw rotation [26,27]. Nonetheless, the uniformity of the strain distribution should not be influenced since in both cases mixing should be improved further.

In the future, the effect of leakage and the cross channel component of velocity should be considered to get a more accurate picture of mixing in intermeshing twin screw extruders. In addition, the equation of motion should be solved for the actual helical channel geometry. In this study, a technique is successfully used to transform the results of the curved boundary flat plate model into cylindrical coordinates for a zero helix angle case. However, this procedure is questionable for a nonzero helix angle case, and the exact helical flow solution would provide more definitive results. Furthermore, in order to make the analysis complete, nonisothermal, nonNewtonian flow of fluid should be considered, and the direction of shear should be taken into account in the strain distribution if possible.

The experimental analysis for the present work is limited to a hypothetical zero helix angle case. However, the nonzero helix angle results were found to be quite different from the zero helix angle case; and it would be useful to experimentally observe this behavior. To include the cross channel component of velocity, simplified methods that provide simulations of an actual nonzero twin screw

extruder channel are desirable, but a procedure to experimentally obtain the velocity profiles for the three components of velocity would probably be extremely difficult.

In order to obtain the velocity profiles which were in turn used to compute the shear strain, the biharmonic equation was solved by numerical methods. For this, as described in chapter IV, two approaches were critically examined. In the first, the coupled pair of Poisson equation method, 750 iterations were required before the convergence was obtained while 400 iterations were enough for the other, the direct iterative method. The total times on DEC10 computer were 85 seconds for the first method as opposed to only 64 seconds for the latter. The accuracy of the convergence for the direct iterative method was 99.99 percent while that in the coupled pair method was 99.7 percent. Although the direct iterative method is found to be better than the coupled pair of Poisson equations in these ways, the determination of the optimum accelerating factor is not as simple. From a programming point of view, the direct iterative method is not nearly as straightforward as evident from Appendix E-1 and E-2.

BIBLIOGRAPHY

1. Adams R.L.,Soc. Plast. Eng. Reg. Tech. Conf. Paper, March 13 (1974).
2. Bigg D., Middleman S., Ind. Eng. Chem., Fundam., 13, 66 (1974).
3. Bigg D., Middleman S., Ind. Eng. Chem., Fundam., 13, 184 (1974).
4. Bigg D., Polym. Eng. Sci., 15, 684 (1975).
5. Bird R.B., Stewart W.E., Lightfoot E.N., "Transport Phenomena", John Wiley & Sons., Inc. New York, N.Y. (1960).
6. Boguslawski J.J., Rubber Chem. Tech., 45, 1421 (1972).
7. Buzbee B.L., Dorr F.W., SIAM J. Num. Anal., 11, 753 (1974).
8. Campbell W.B., Soc. Plast. Eng., Tech. Pap., 21, 510, 1975.
9. Carre' B.A., Computer J., 4, 73 (1961).
10. Ehrlich L.W., Gupta M.M., SIAM J. Num. Anal., 12, 773 (1975)
11. Ehrlich L.W. Communications of the ACM, 16, 711 (1973).
12. Ehrlich L.W., SIAM J. Anal., 8, 278 (1971).
13. Fox L., 1949 Phil. Trans. A242, 345-378 [268] (1950).
14. Gras D., Plast. Tech., 18, 40 (1972).
15. Hadjidimos A., Num. Math., 17, 301 (1971).
16. Inouye K., Journal de Mecanique, 12, 609 (1973).

17. Jewmenow S.D., Kim W.S., Plaste und Kautschuk, 20, 356 (1973).

18. Kaplan A., Tadmor Z., Polym. Eng. Sci., 14, 58 (1974).

19. Kim W.S., Skatschkow W.W., Jewmenow S.D., Plaste und Kautschuk, 22, 730 (1975).

20. Kim W.S., Skatschkow W.W., Jewmenow S.D., Plaste und Kautschuk, 20, 696 (1973)

21. Kuo S.S., "Computer Application of Numerical Methods", Addison-Wesley Publishing Co., Philippines (1972).

22. Lidor G., Tadmor Z., Polym. Eng. Sci., 16, 450 (1976).

23. Mack A., Plast. Tech., 21, 45 (1975).

24. Mckelvey J.M., "Polymer Processing", John Wiley, New York, N.Y. (1962).

25. McLaurin J.W.,SIAM J. Num. Anal., 11, 14 (1974).

26. Prause J.J., Plast. Tech., 13, 41 (1967).

27. Prause J.J., Plast. Tech., 14, 29 (1968).

28. Prause J.J., Plast. Tech., 14, 52 (1968).

29. Riley M.W., Plast. Tech., 22, 47 (1976).

30. Salvadcri M.G., Baron M. L., "Numerical Methods in Engineering", Prentice-Hall, Inc., Englewood Cliffs, N.J. (1961).

31. Sheridan I.A., Chem. Eng. Prog., 71, 83 (1975).

32. Sier-Bath Pump Division/Gilbarco, Inc., Tech. Info. Bulletin, 1-1001 (1975).

33. Smith J., SIAM J. Num. Anal., 10, 967 (1973).

34. Smith J., SIAM J. Num. Anal., 7, 104 (1970).

35. Smith J., SIAM J. Num. Anal., 5, 323 (1968).

36. Tadmor Z., Klein I., "Engineering Principles of Plasticating Extrusion", Van Nostrand Reinhold, New York, N.Y. (1970).

37. Todd D.B., Soc. Plast. Eng. Tech. Pap., 22, 354 (1976).

38. Todd D.B., Polym. Eng. Sci., 15, 437 (1975).

39. Todd D.B., Chem. Eng. Prog., 71, 81 (1975).

40. Wyman C.E., Polym. Eng. Sci., 15, 606 (1975).

41. Zlamal M., SIAM J. Num. Anal., 4, 626 (1967).

42. Zlamal M., SIAM J. Num. Anal., 2, 337 (1965).

43. Mohr W.C., Saxton R. L., Jepson C. H., Ind. Eng. Chem., 49, 1805 (1957).

44. Fromm J.E., Los Alamos Scientific Laboratory Report LA-2910 (1963).

45. Golub G.H., An algorithm for the discrete biharmonic equation, unpublished.

46. Walker I., M.S. Thesis, Computer Science Dept., Stanford University (1970).

47. Bauer L., Reiss E.L., Math. Comp., 26, 311 (1972).

48. Angel E., Bellman R., "Dynamic Programming and Partial Differential Equations", Academic Press, New York (1972).

49. Fairweather G., Gourlay A.R., Mitchell A.R., Numer. Math., 10, 56 (1967).

50. Tung T.T., Laurence R.L., Polym. Eng. Sci., 15, 401 (1975).

51. Greenspan D., Schultz D., Comm. ACM, 15, 347 (1972).

52. Gupta M.M., Doctoral Thesis, University of

Saskatchewan, Saskatcon (1971).

53. Gupta M.K., Manohar R., Proc. Manitoba Conf. on Numerical Math., University of Manitoba, Winnipeg, 345 (1971).

54. Wyman C.E., Doctoral Thesis, Princeton University, (1971).

APPENDIX A

Transformation of Point Locations between the Reduced Rectangular Coordinate System and the Cylindrical Coordinate System

In Chapter III, the model of flat plate with curved boundaries was developed to describe flow in the down channel direction involving the velocity components Vy and Vz. According to this model, the confined channel of a zero helix angle twin screw extruder with its moving barrel and the stationary screw root are represented as flat plates, such that the barrel length is shrunk while the screw root lenght in the down channel direction remains unchanged. The channel depth is also shrunk to half its normal size while the size of the lands of the second screw represented by the curved boundaries remain unchanged after unwinding (Fig 3.2). As a result of this model, lines of constant angle ϕ on r-ϕ diagram do not represent lines of constant z on the y-z diagram; and therefore, a relationship between the two coordinate systems is desired. Since the channel is symmetrical, only the left half will be considered. Thus, the desired relationships are derived for ϕ less than or equal to π and greater than or equal to 0.

In Fig A-1a, the channel geometry is shown. The screw root with center B and radius b is surrounded by the cocentric barrel of radius a. The lands of the second screw

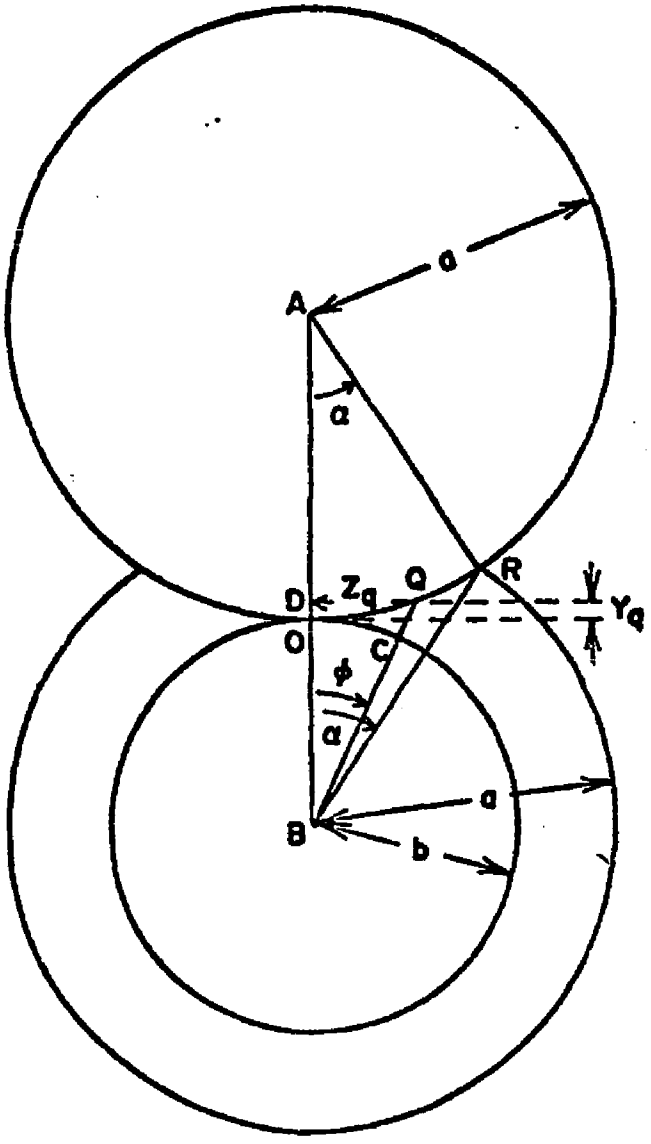

(a)

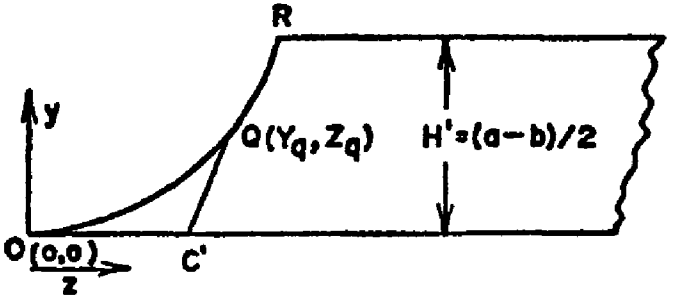

(b)

Fig. A-1: Determination of the Locus of a Point $Q(Y_q, Z_q)$ on the Curved Boundary OR. Fig(a) represents the axial projection of the Channel in Cylindrical Coordinates while Fig(b) is in the Rectangular Coordinate System

with center A and radius a just touch the first screw root at point O. R is the point at which the barrel touches the second screw land. Therefore, the angle α as shown in Fig A-1a is given by:

$$\alpha = \cos^{-1}\left[\frac{a+b}{2a}\right] \qquad (A-1)$$

According to the model developed in chapter III, the channel will become as shown in Fig A-1b (only a part of it is shown) after unwinding and will be described by the rectangular coordinates y and z. Consider any point Q with rectangular coordinate Yq and Zq on the curved boundary as shown in Fig C-1b. The distances Yq and Zq from the point O are represented by the distances OD and DQ respectively in Fig A-1a. Let the angle between lines OB and BQ in Fig A-1a be ϕ and let S be equal to $\tan\phi$ so that:

$$z_q = S(b+Y_q) \qquad (A-2)$$

Also, from the triangle ADQ in Fig A-1a,

$$z_q^2 + (a-Y_q)^2 = a^2 \qquad (A-3)$$

Eliminating Zq from equations A-2 and A-3, the expression for Yq can be obtained as:

$$Y_q = \frac{a - bS^2 - (a^2 - 2abS^2 - b^2S^2)^{0.5}}{(1+S^2)} \qquad (A-4)$$

Since from Fig A-1a, BQ is equal to the sum of b and CQ while from triangle BQD $\sin\phi$ is equal to Zq/BQ, therefore,

$$CQ = \left(\frac{zq}{\sin\phi}\right) - b \qquad (A\text{-}5)$$

Equations A-2, A-4 and A-5 will be used in subsequent derivations.

Consider a point P(y,z) lying on the line C'Q in Fig A-2b so that its corresponding location P(r,ϕ) in cylindrical coordinates lies on the line of constant angle ϕ, CQ, as shown in Fig A-2a with ϕ less than or equal to the angle α (equation A-1). Now the line TPR in Fig A-2b, which is parallel to the Y axis passing through the point P(y,z), meets the curve in R(Ym,z). The y coordinate of the point R, i.e. Ym, is known from the following relation:

$$Y_m = a - (a^2 - z^2)^{0.5} \qquad (A\text{-}6a)$$

Therefore, the line of constant angle ϕ_R passing through the point R, from equation A-2, becomes,

$$\phi_R = \tan^{-1}\left[\frac{z}{b+Y_m}\right] \qquad (A\text{-}6b)$$

Also, the line of constant angle ϕ_T passing through the point T is,

$$\phi_T = z/b \qquad (A\text{-}6c)$$

Now, the desired line of constant angle ϕ passing through the point P should lie between lines of constant angles ϕ_R and ϕ_T. Using a linear approximation, the expression for ϕ can be shown to yield:

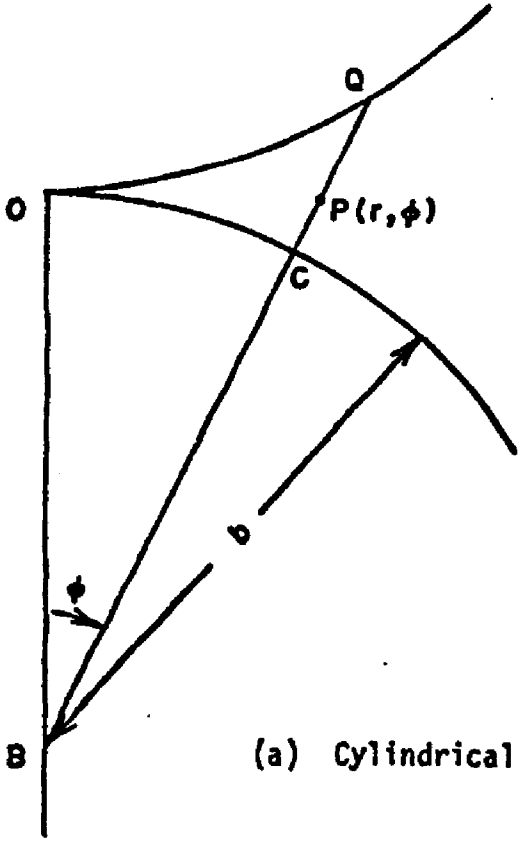

(a) Cylindrical Coordinate System

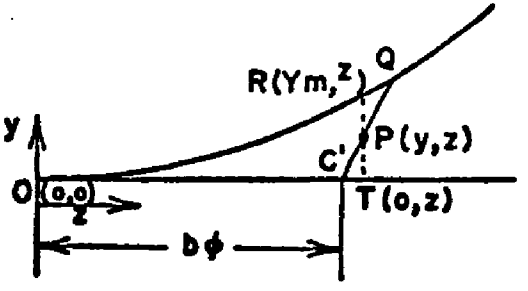

(b) Rectangular Coordinate System

Fig. A-2: Transformation of a Point P(y,z) to P(r,ϕ) for $\phi \leq \alpha$

$$\phi = \phi_R + (\phi_T - \phi_R)\left(\frac{Y_m - y}{Y_m}\right) \qquad b\alpha \geq z \qquad (A\text{-}6d)$$

$$\phi = \phi_R + (\alpha - \phi_R)\frac{(Y_m - y)}{(Y_m - Y_L)} \qquad z_r \geq z \geq b\alpha \qquad (A\text{-}6e)$$

where $Y_L = H'(b\alpha - z)/(b\alpha - z_r)$,

and Zr is defined in equation A-10. Thus, the angle ϕ is determined.

Now, from Fig A-2a, the r coordinate is found as follows:

$$r = BP = BC + CP = b + CP \qquad (A\text{-}7)$$

The distance CP can be expressed as a fraction of the distance CQ, the fraction being C'P/C'Q from Fig A-2b. From Fig A-2b, this fraction can be shown to be equal to y/Yq, and hence the distance CP in Fig A-2a becomes:

$$CP = (y/Y_q)\,CQ \qquad (A\text{-}8)$$

Thus, from equations A-7 and A-8, the expression for r is:

$$r = b + (y/Y_q)\,CQ \qquad (A\text{-}9)$$

where Yq and CQ are given by equations A-4 and A-5 respectively. Equations A-6d or A-6e, and A-9 form the pair of equations required for the desired transformation of a point P(y,z) to the point P(r,ϕ) for a case of ϕ less than or equal to α.

When ϕ is greater than the angle α, the transformation

of a point P(y,z) to its corresponding location on r-ϕ diagram, i.e. P(r,ϕ), can be derived as follows. In Fig A-3, the point P(y,z) is shown lying on a line AB which would represent a line of constant ϕ on r-ϕ diagram. If H' represents the channel depth on the y-z diagram, the length Zr, i.e. the z coordinate of the point R, from the equation A-3, is then,

$$Z_r = \sqrt{H'(2a-H')} \qquad (A-10)$$

Now, the equation of line AB is given as:

$$y/H' = \frac{z - Z_a}{Z_b - Z_a} \qquad (A-11)$$

Since the length of the screw root remains unchanged after unwinding of the channel, Za can be expressed as:

$$Z_a = b\phi \qquad (A-12)$$

The z coordinate of point B, Zb, is Zr plus RB (Fig A-3) where RB is the length of the barrel arc after unwinding which must be determined.

The length of the barrel around the screw under consideration is $2a(\pi-\alpha)$ and after unwinding this becomes $2\pi b-2Zr$. Therefore, the shrinkage factor by which the actual barrel length must be multiplied to obtain the barrel length after unwinding is $(\pi b-Zr)/a(\pi-\alpha)$; and, the length RB is given as:

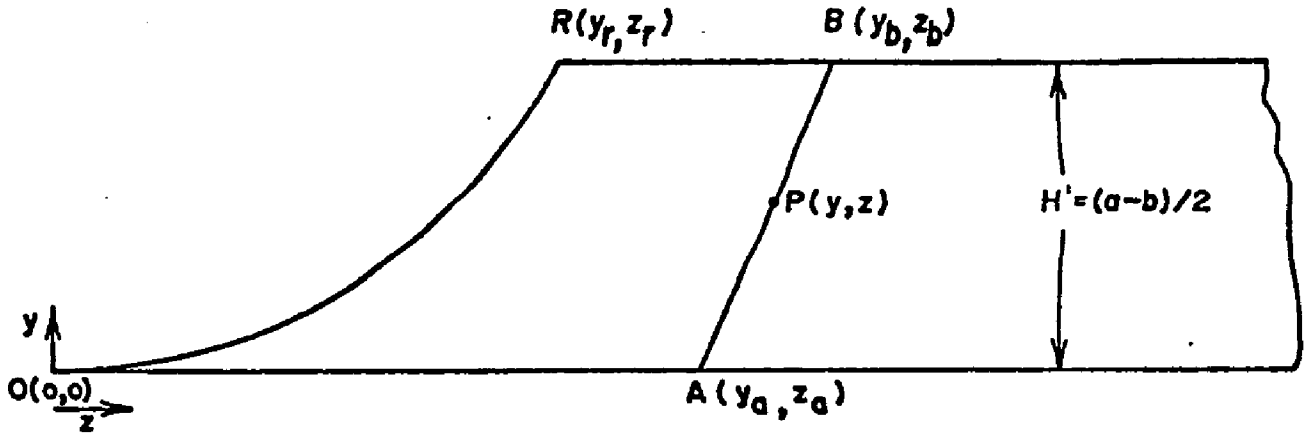

Fig. A-3: Transformation of a Point P(y,z) to P(r,ϕ) for $\phi > \alpha$

$$RB = (\phi-\alpha)(\pi b - Z_r)/(\pi-\alpha) \qquad (A-13)$$

Now, the z coordinate of the point B in Fig A-3, becomes:

$$Z_b = Z_r + \frac{(\phi-\alpha)}{(\pi-\alpha)}(\pi b - Z_r) \qquad (A-14)$$

Combining equations A-11, A-12 and A-14 and eliminating Za and Zb in terms of ϕ, the final expression for ϕ is,

$$\phi = \frac{z(H'/y) - Z_r + \alpha\left(\frac{\pi b - Z_r}{\pi-\alpha}\right)}{\left[\left(\frac{\pi b - Z_r}{\pi-\alpha}\right) - b + b(H'/y)\right]} \qquad (A-15)$$

where Zr and α are given by equations A-10 and A-11 respectively. Since the channel depth is half its original size, the r coordinate of the point $P(r,\phi)$ on $r-\phi$ diagram for ϕ greater than α, simply becomes,

$$r = b + 2y \qquad (A-16)$$

Thus, equations A-15 and A-16 form the pair of equations relating the two coordinate systems for ϕ greater than α.

Before transforming a point in rectangular coordinates, P(y,z) to its corresponding location in cylindrical coordinates, $P(r,\phi)$, ϕ is not known; and therefore it remains uncertain as to which pair of transformation equations is to be applied. However, it can be seen that if the slope of the line passing through the given point P(y,z) and the point $(0,b\alpha)$ is less than that of the line passing

through the points (H', Zr) and $(0, b\alpha)$, ϕ is greater than the angle α and vice versa. Hence the desired pair of transformation equations is known for those cases. Further, for ϕ less than α, equation A-6d is used to find ϕ if z is less than $b\alpha$, or equation A-6e is used otherwise.

For transforming a point $P(r, \phi)$ from cylindrical coordinate system to $P(y, z)$ in the rectangular coordinate system the following relations can be derived. Thus, for ϕ greater than α,

$$y = (r - b)/2 \qquad \text{(A-17a)}$$

$$z = b\phi + (y/H')\left(Z_r - b\phi + \frac{(\pi - 2r)}{2(\pi - \alpha)}(\phi - \alpha)\right) \qquad \text{(A-17b)}$$

and for ϕ less than α,

$$y = (r - b)\, Y_q / cQ \qquad \text{(A-18a)}$$

$$z = b\phi + (r - b)(Z_q - b\phi)/cQ \qquad \text{(A-18b)}$$

APPENDIX B

Elimination of the Fictitious Mesh Points

The computational molecule of equation 4.14 with its center mesh point surrounded by twelve other mesh points is shown in Fig B-1. The center point is indicated by a circled asterisk ⊛, while the other mesh points involved in the 13 point formula are represented by an asterisk or by an asterisk in a square. The y and z distances of a mesh point from the curved boundary AB, as shown in Fig B-1, are represented by Pn, where n is an integer subscript. When n is odd, Pn represents the y distance of the mesh point from the curved boundary while if n is even, Pn is the z distance of the mesh point from the curved boundary. The y and z distances as represented by the corresponding Pn's are made dimensionless in terms of the respective mesh dimensions as follows:

$$R_n = P_n / \Delta y \qquad \text{if } n \text{ is odd}$$

$$R_n = P_n / \Delta z \qquad \text{if } n \text{ is even}$$

where y and z are the mesh lengths in the y and z directions respectively. Thus, Rn represents the number of mesh spaces of a point from the curved boundary and it may be a fraction.

In the computer program, "TWIN" (Appendix E-3), the

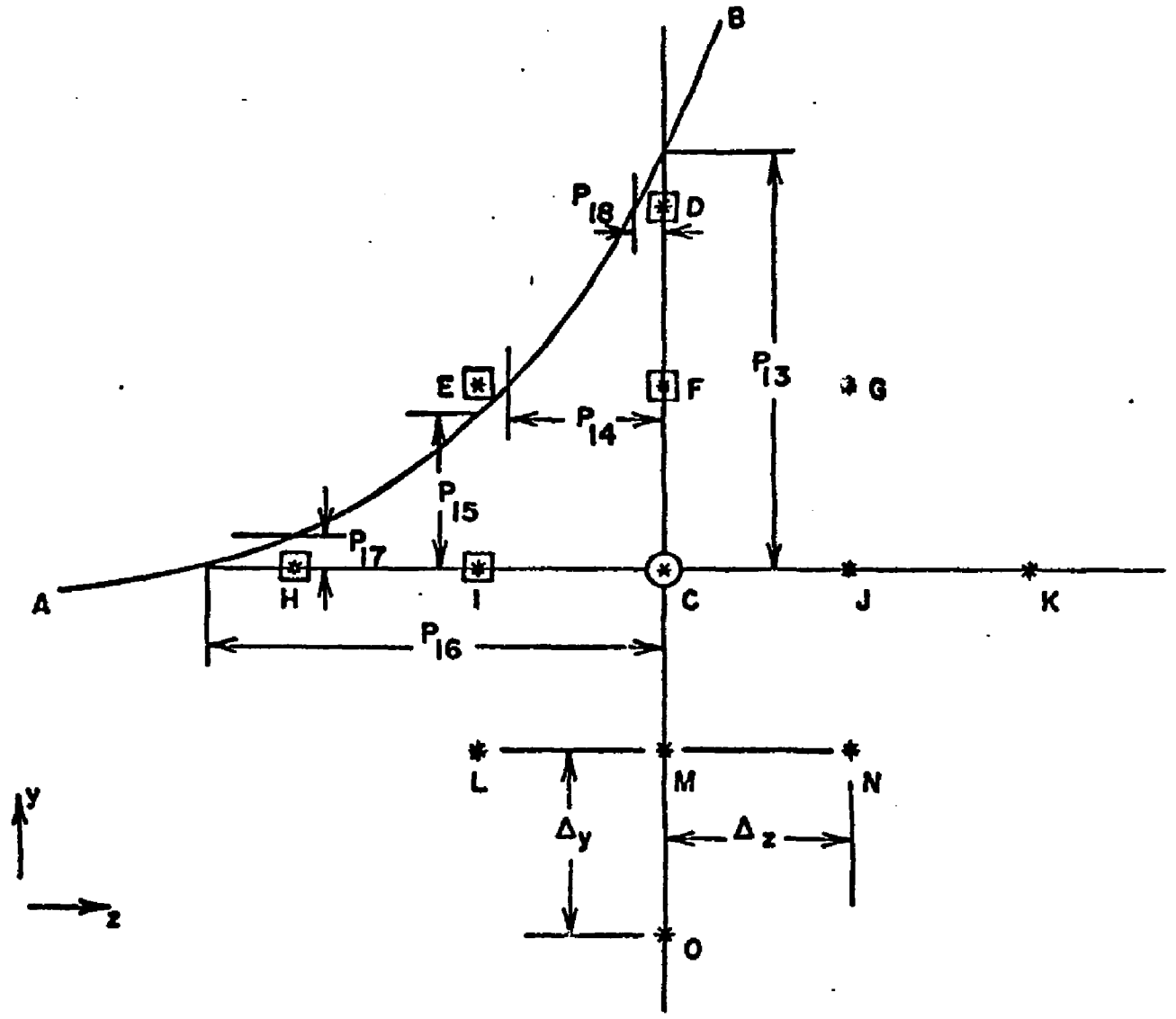

Fig. B-1: A Molecule Representation of the 13 Point Formula Involving Fictitious Mesh Points

dimensionless distances Rn's play an important role in setting up the mathematical relations that must be met for elimination of fictitious mesh points which may be beyond the curved boundary or less than one mesh length inside it. Fictitious points are eliminated in terms of a specific set of internal mesh points. Some of these internal mesh points may be fictitious ones so that they must be further eliminated in terms of nonfictitious mesh points. In Fig B-1 initial fictitious mesh points are represented by asterisks in a square while those fictitious mesh points which appear due to elimination of the initial fictitious mesh points are represented by an x in a square as shown in Fig B-2 and B-3.

In the computer program, "TWIN", the computational procedure for elimination of fictitious mesh points is described in detail in six sets. Sets 1 and 2 deal with the initial fictitious mesh points involved in the 13 point formula, equation 4.14. In set 1, the complete elimination is performed for fictitious mesh points lying on the line of constant z passing through the center point C while the desired partial or complete elimination is accomplished for the fictitious mesh points lying on the line of constant z one mesh length to the left of point C. The procedure for the partial or complete elimination of the fictitious mesh points will be explained later with an example. In set 2, the fictitious mesh points lying on the line of constant y passing through the center point C are completely eliminated

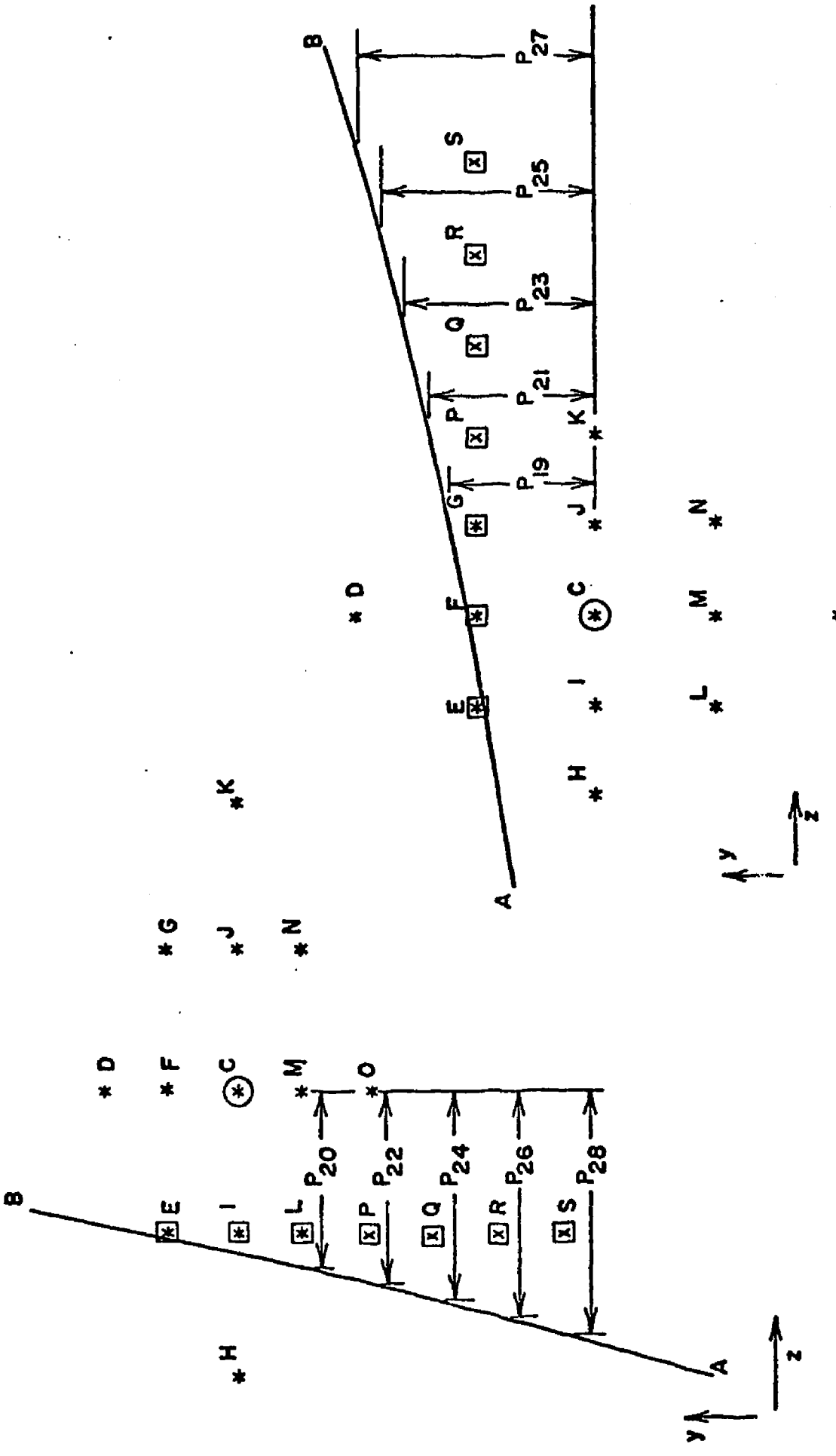
B
A
P27
P25
P23
P21
P19
S
R
Q
P
G
K
J
D
F
C
M
O
E
I
L
N
H
K
G
J
N
z
y

Fig. B-3

B
A
P20
P22
P24
P26
P28
D
F
C
M
O
E
I
L
P
Q
R
S
H
z
y

Fig. B-2

while those lying on the constant y line one mesh distance above the center mesh point are eliminated partially or completely as required. Sets 3 and 4 deal with the initial fictitious mesh points which are at one or two mesh lengths from the top (the barrel) or the bottom boundary (the screw root) respectively. Sets 5 and 6 deals with the initial fictitious mesh points which are yet to be eliminated or appear due to elimination of the initial fictitious mesh points as described in sets 1 and 2.

To clarify this explaination, in Fig B-1 the fictitious mesh points D,F,E,H and I are eliminated using sets 1 and 2; and in Fig B-2 the fictitious mesh points D,E,H, and I are eliminated using sets 1 and 2. Fictitious points P,Q,R and S in Fig B-2 are now introduced due to partial elimination of the initial fictitious mesh point E in the negative y direction and must be eliminated along with the point L using set 5. The fictitious mesh points D,E,F,H, and I in Fig B-3 are eliminated using sets 1 and 2, while the fictitious mesh points P,Q,R and S which result due to partial elimination of the initial fictitious mesh point E are eliminated along with the point G by set 6. The equations governing the elimination of the fictitious mesh points based upon the Gregory-Newton's interpolation formulae are discussed in chapter IV and V. The step by step details of this elimination procedure are presented in the computer program "TWIN", in Appendix E-3.

APPENDIX C

Estimation of the Roller length

The axial length of the rollers used for the experimental analysis should be great enough so that the velocity profiles in the middle region of the roller axis are unchanged in the direction of the roller axis. This criteria ensures that ends of the experimental apparatus do not affect the velocity profiles in the region of interest. An estimate of the required roller length is obtained by examining a similar case of tangential laminar flow (couette flow) of an incompressible fluid of viscosity μ, between two horizontal coaxial cylinders of length L, the inner one of which is rotating with an angular velocity Ω while the outer one is stationary [5]. The ends of the cylinders are against the stationary walls as shown in Fig C-1.

Using the cylindrical coordinate system with the z direction lying along the roller axis, the r direction directed radially outward, and the θ direction projecting tangentially, it can be seen that the r and z components of velocity are zero in this system, i.e. Vr=0; Vz=0; and there is no pressure gradient in the θ direction. Viscous effects are so predominant that gravitational and inertial effects can be neglected, and the equation of motion for steady flow reduces to [5]:

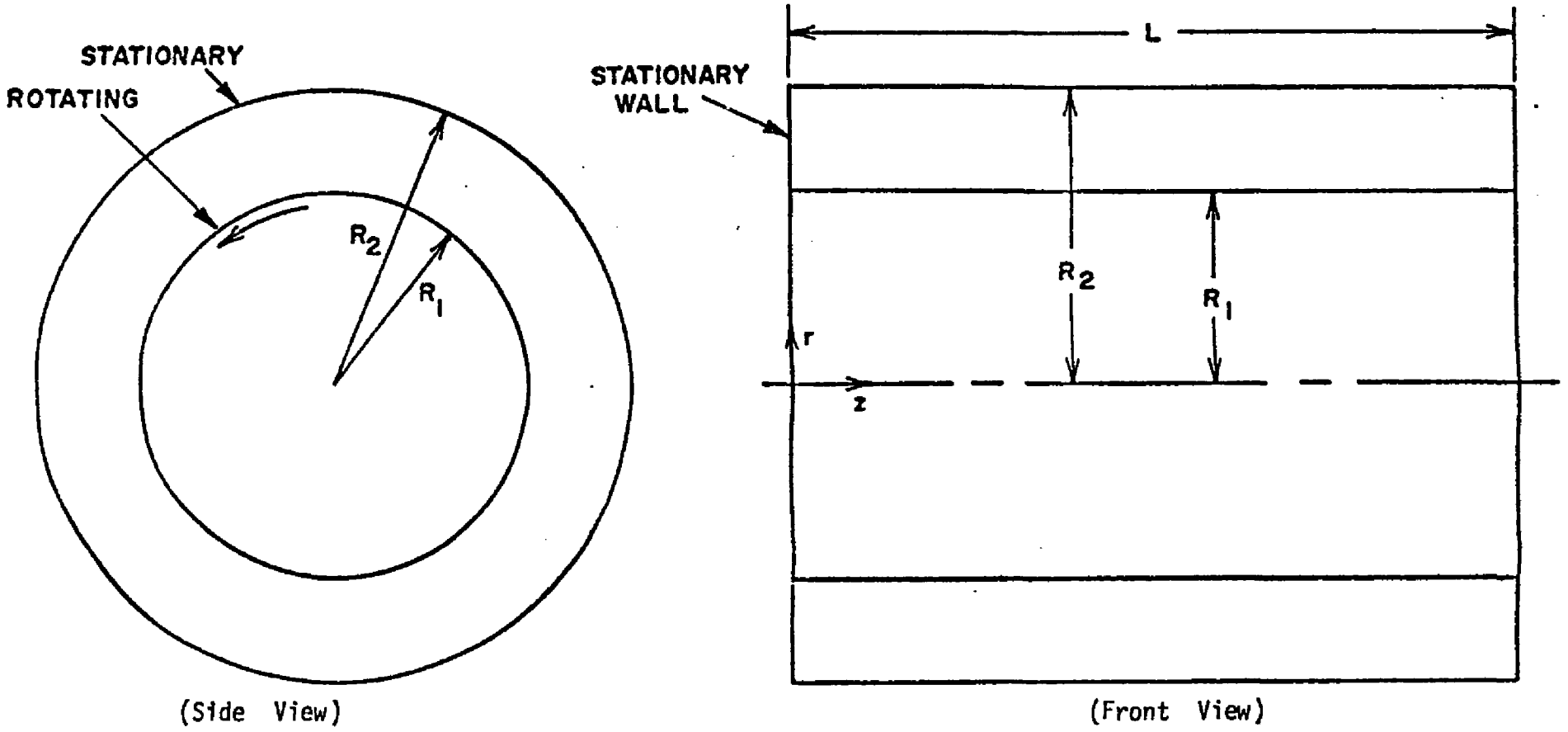

Fig. C-1: Tangential Laminar Flow of an Incompressible Fluid Between Two Horizontal Coaxial Cylinders, the Inner one of which is Rotating with an Angular Velocity Ω

$$\mu\left[\frac{\partial}{\partial r}\left(\frac{1}{r}\frac{\partial}{\partial r}(rV_\theta)\right)+\frac{1}{r^2}\frac{\partial^2 V_\theta}{\partial\theta^2}+\frac{\partial^2 V_\theta}{\partial z^2}\right]=0 \qquad (c\text{-}1)$$

From the equation of continuity for an incompressible fluid with Vr and Vz equal zero, $\partial V_\theta/\partial\theta$ equals zero, and therefore, the equation C-1 becomes:

$$\frac{\partial}{\partial r}\left(\frac{1}{r}\frac{\partial}{\partial r}(rV_\theta)\right)+\frac{\partial^2 V_\theta}{\partial z^2}=0 \qquad (c\text{-}2)$$

The boundary conditions for the present problem can be stated as follows:

$$V_\theta = 0 \quad \text{at} \quad z=0, L \qquad (c\text{-}3.1)$$

$$V_\theta = 0 \quad \text{at} \quad r=R_2 \qquad (c\text{-}3.2)$$

$$V_\theta = -\Omega R_1 \quad \text{at} \quad r=R_1 \qquad (c\text{-}3.3)$$

where R_1 and R_2 are the radii of the inner and the outer cylinders respectively as shown in Fig C-1.

Equation C-2 can be solved by separation of variables. Let R be a function of r only and Z be a function of z only so that V_θ can be expressed as:

$$V_\theta = RZ \qquad (c\text{-}4)$$

With this, equation C-2 becomes:

$$\frac{R''}{R}+\frac{R'}{rR}-\frac{1}{r^2}=\frac{-Z''}{Z} \qquad (c\text{-}5)$$

where R', R" and Z" are $\partial R/\partial r$, $\partial^2 R/\partial r^2$, and $\partial^2 Z/\partial z^2$ respectively. Since the left hand side of the equation C-5

is a function of r alone while the right hand side of the same equation is a function of only z, both sides are independent of each other and therefore must be equal to a constant C^2. Thus,

$$-\frac{Z''}{Z} = C^2 \qquad (C-6)$$

The solution of the equation C-6, using the boundary conditions given by equation C-3.1 is,

$$Z = B \sin \frac{n\pi z}{L} \qquad (C-7)$$

where B is a constant and n is an integer constant such that the constant C is equal to n /L. Now, considering the left hand side of the equation C-5 and equating it to C^2, the general solution for R is,

$$R = A' I_1(n\pi r/L) + B' K_1(n\pi r/L) \qquad (C-8)$$

where A', B' are constants and I_1 and K_1 are the first order modified Bessel functions. Combining equations C-4, C-7, and C-8 and using boundary conditions C-3.2 and C-3.3, the solution for V_θ is:

$$\frac{V_\theta}{V_{max}} = \frac{4}{\pi} \sum_{n=1,3,5,\cdots}^{\infty} \frac{1}{n} \frac{\left[I_1(n\pi r/L) - \frac{I_1(n\pi R_2/L)}{K_1(n\pi R_2/L)} K_1(n\pi r/L) \right]}{\left[I_1(n\pi R_1/L) - \frac{I_1(n\pi R_2/L)}{K_1(n\pi R_2/L)} K_1(n\pi R_1/L) \right]} \qquad (C-9)$$

where Vmax equals ΩR_1.

In order to estimate the axial lenght of the rollers

for which the velocity distribution V_θ is independent of z over a sufficient middle portion of the roller axis, first the velocity distribution V_θ is computed across the radial gap at the midpoint of the roller length, i.e. at $z=L/2$. In Fig C-2, this velocity distribution V_θ is plotted against the radial distance across the gap for different values of roller lengths L. From these plots, it can be seen that the deviation in V_θ from its linear profile without end effects is a maximum at the midpoint along the radial gap, i.e. at $r=(R_1+R_2)/2$, for all axial lengths. Thus, the value of r in equation C-9 is set equal to $(R_1+R_2)/2$; and the velocity distribution V_θ is computed as a function of the axial distance z for different axial lengths L. In Fig C-3, plots of the velocity distribution V_θ vs the fractional axial length z/L are shown for different values of L. From these plots, it can be seen that the velocity distribution in the middle portion of the roller axis remains unchanged over approximately 80% of the total axial length for L=5 inches. To be even more certain of fully developed flow in the center, the length of the roller for the experimental simulation unit was chosen to be six inches.

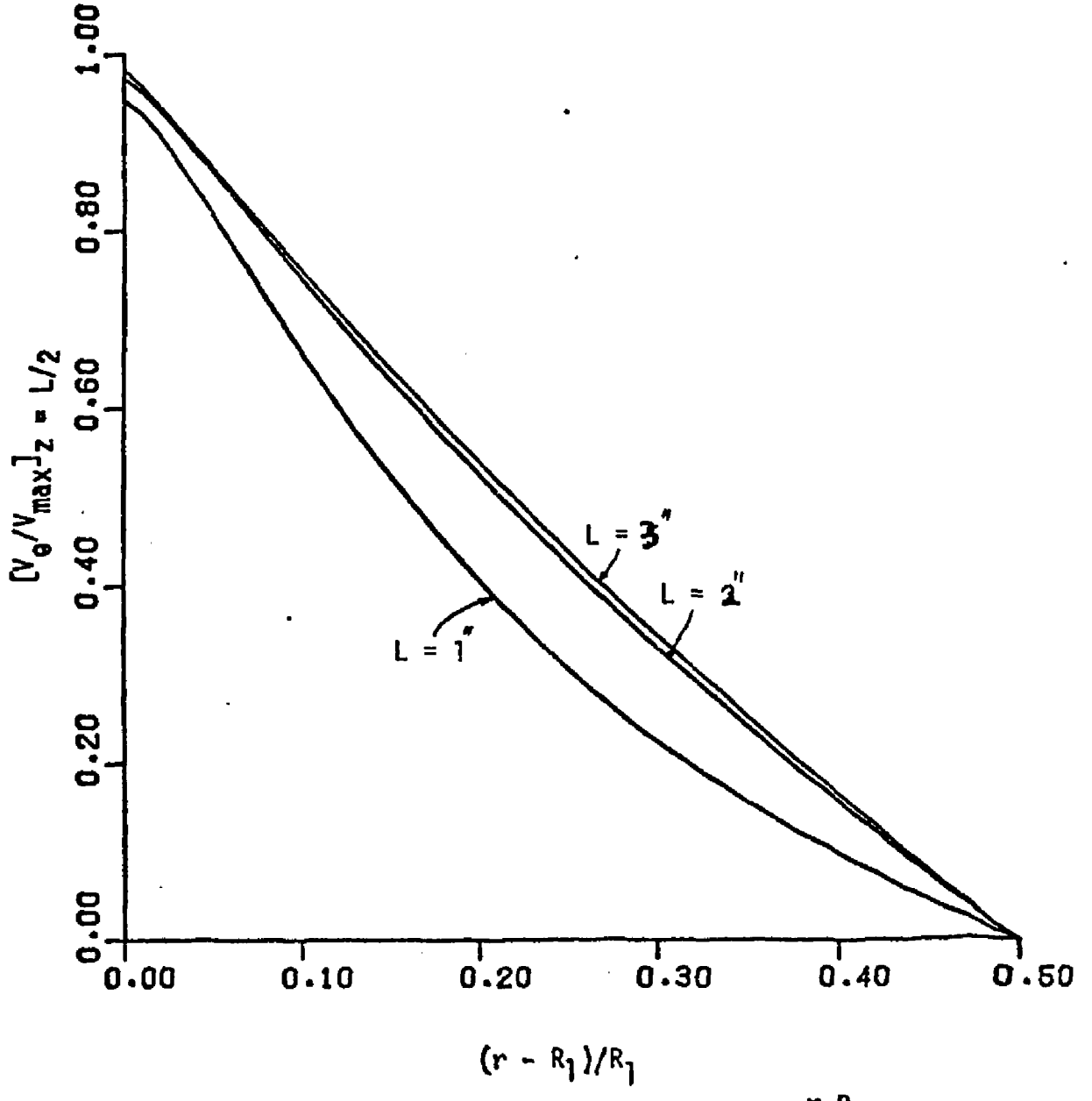

FIGURE C-2: A plot of $[V_\theta/V_{max}]_{z = L/2}$ Vs $(\frac{r-R_1}{R_1})$

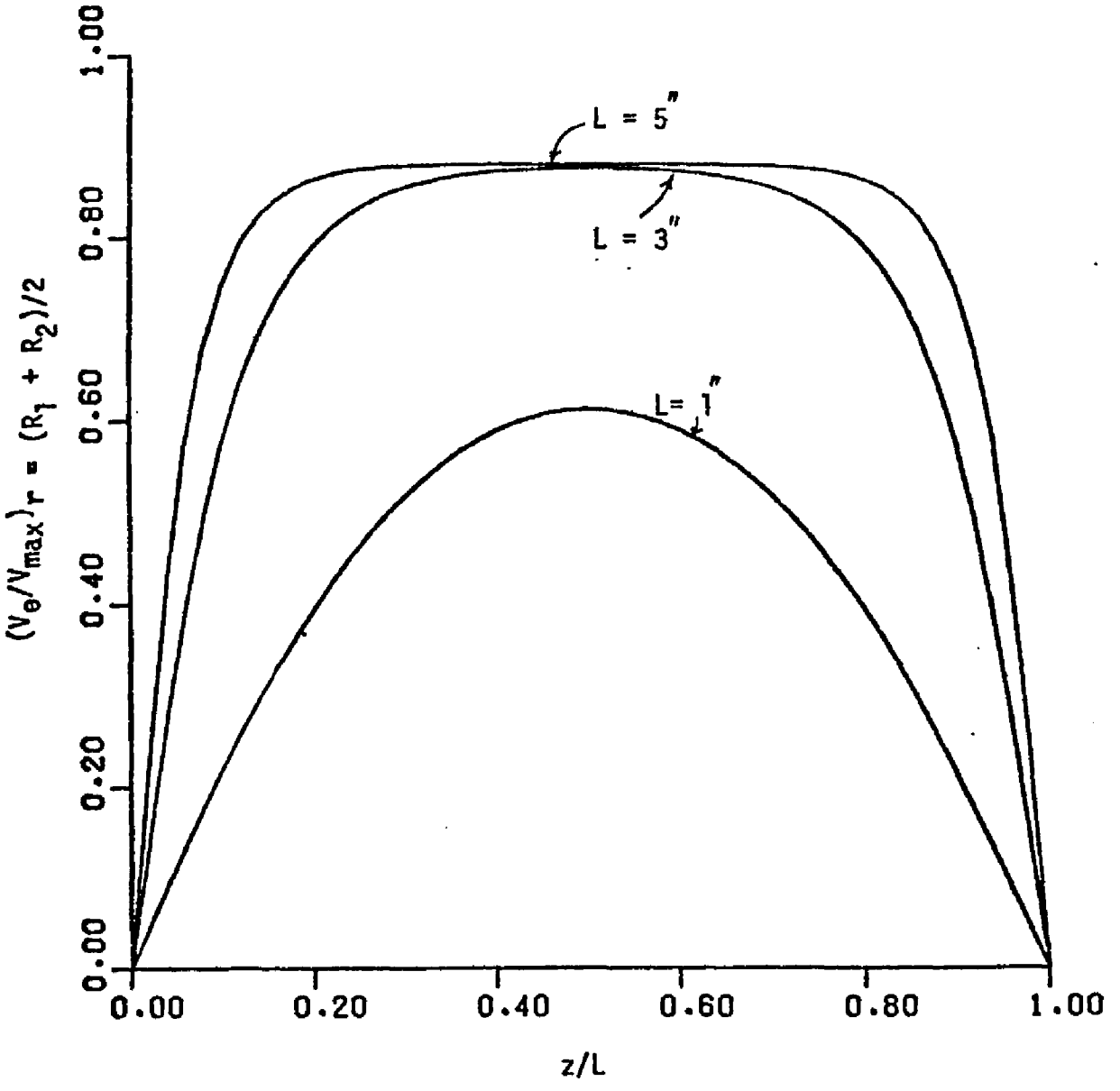

FIGURE C-3: A plot of $(V_e/V_{max})_r = \frac{(R_1+R_2)}{2}$ V_s z/L

APPENDIX D

Torque and Power Required for the Experimental Simulation Unit

An estimation of torques required to turn the rollers used in the experimental simulation unit can be approximately determined by considering a similar case of tangential laminar flow of an incompressible fluid of viscosity μ, between two horizontal coaxial cylinders of length L, the inner one of which is rotating with an angular speed Ω while the outer one is stationary as shown in Fig C-1. If R_1 and R_2 are the radii of the inner and the outer cylinders respectively, then the tangential velocity distribution (V_θ) for such a case can be expressed as [5]:

$$V_\theta = \Omega r (1 - R_2^2/r^2)/(1 - R_2^2/R_1^2) \qquad (D-1)$$

where r is the radial distance and V_θ is the tangential velocity. The shear stress distribution $Tr\theta$, can be determined from the tangential velocity as [5],

$$T_{r\theta} = -\mu \left[r \frac{\partial}{\partial r} (V_\theta / r) \right] \qquad (D-2)$$

Therefore, combining equations D-1 and D-2 gives,

$$T_{r\theta} = -2\mu \frac{\Omega}{r^2} \frac{R_2^2}{(1 - R_2^2/R_1^2)} \qquad (D-3)$$

Then, the total torque T required to turn the inner shaft is

determined by taking the product of the force times the lever arm,

$$T = (2\pi R_1 L)\,(\tau_{r\theta})|_{r=R_1} \cdot R_1$$

or,
$$T = 4\pi\mu L\Omega \left[\frac{R_2^2}{(R_2^2/R_1^2 - 1)}\right] \qquad (D\text{-}4)$$

For the experimental design purposes, the torque and horse power will be estimated for conditions which make them each a maximum. Thus, for a fluid having a 30,000 cps viscosity with the lower roller turning at an angular velocity of 120 revolutions per minute and R_1, R_2 and L being equal to 1.5, 2.25 and 6 inches respectively, the estimated value of the torque T according to equation D-4 is approximately 50 inch-lbf. For the present case, Zeromax drives capable of providing 100 inch-lbf torque for the lower roller and 25 inch-lbf torque for the upper roller were selected, because the upper roller was not totally enclosed (the free fluid surface at the top). Since the power required equals the torque times the angular velocity, the power requirement for the lower roller is 0.2 HP under the given conditions. In order to allow for frictional losses occurring in the drives, chains, couplings, sprockets, bushings, etc., a 3/4 HP motor was selected for the lower roller and a 1/3 HP motor for the upper roller. These motors proved more than adequate for the experimental device since a total power of 0.4 HP was measured with a 1000 cp fluid viscosity and the rollers turning at 40 RPM.

APPENDIX E-1

TWOSEC

```
CCCCCCCCCCCCCCCCCCCCCCCCCCCCCCCCCCCCCCCCCCCCCCCCCCCCCCCCCCCCCCCCCCCCCCCCCC
C                                                                      C
C                                                                      C
C                                                                      C
C     THE FOLLOWINGS THINGS SHOULD BE CHECKED BEFORE PROCEDING         C
C     TO RUN THIS PROGRAM:                                             C
C                                                                      C
C       1.THE OPEN STATEMENT IF ANY                                    C
C       2.NUMBER OF ITERATIONS DESIRED                                 C
C       3.THE ACCELERATING FACTORS, ALPHA1 AND ALPHA2                  C
C                                                                      C
CCCCCCCCCCCCCCCCCCCCCCCCCCCCCCCCCCCCCCCCCCCCCCCCCCCCCCCCCCCCCCCCCCCCCCCCCC
C
C
C
C
C     THIS PROGRAM COMPUTES VELOCITY PROFILES IN Y AND Z DIRECTIONS
C     IN A SCREW CHANNEL OF A TWIN SCREW EXTRUDER BY
C     THE METHOD OF A COUPLED PAIR OF POISSON EQUATIONS
C
C
C                    DESCRIPTION OF PARAMETERS:
C
C     ALL VELOCITIES ARE DIMENSIONLESS BASED ON
C     THE SCREW ROOT LINEAR VELOCITY PI D1 N.
C     ALL DISTANCES ARE DIMENSIONLESS BASED ON THE ROOT
C     DIAMETER D1.
C     THE CHANNEL IS DIVIDED INTO 30 BY 30 MESH POINTS,
C     EACH MESH OF DY BY DZ SIZE.
C
C     D1=ROOT DIAMETER  IN FT.
C     D2=BARREL DIAMETER IN FT.
C     H1=CHANNEL DEPTH
C
C     THE 33 BY 33 PSI MATRIX REPRESENTS THE STREAM FUNCTION
C     MATRIX
C
      DIMENSION PSI(33,33),OMEGA(33,33),UZ(33,33),UY(33,33),UYZ(33,33)
     1,SAI(33),P(1000,29),ANGLE(33,33),SSS(33,33)
      PI=3.1415927
      D1=0.25
      D2=0.375
      H=(D2-D1)/(4.*D1)
      VZR=1.0
      VZB=0.0
      NJ=30
      NI=30
      DY=H/NI
      DZ=PI/NJ
      II=NI+3
      JJ=NJ+3
      II1=II-1
      JJ1=JJ-1
      IN=NI-1
```

```
      JN=NJ-1
      F=300.
      N3=3
      IND='I'
      CALL PLOTS(IND,15.,11.)
      CALL NEWPEN(N3)
      CALL PLOT(2.,0.,3)
      CALL PLOT(2.,10.75,-2)
      CALL FACTOR(F)
      DO 7 I=2,II1
      AS=(I-2)/30.
      BS=AS-1.
      SIA=-AS*BS*BS*H
      SAI(I)=SIA
      CALL PLOT(0.,SIA,3)
      CALL PLOT(0.020,SIA,2)
    7 CONTINUE
      CALL STRMFN(DY,DZ,IN,JN,IN2,JN2,II1,JJ1,II,JJ,VZR,VZB,PSI)
      CALL VELCTY(UZ,UY,VZR,VZB,IN2,JN2,II1,JJ1,DY,DZ,UYZ,ANGLE,PSI)
      WRITE(6,54)
   54 FORMAT(4X,'I',5X,'ANALYTICAL',3X,'NUMERICAL',5X,'DIFFERENCE',
     12X,'% DIFFERENCE',///)
      DO 55 I=3,IN2
      DIFF=SAI(I)-PSI(I,17)
      PER=(DIFF/SAI(I))*100.
      WRITE(6,56) I,SAI(I),PSI(I,17),DIFF,PER
   56 FORMAT(1X,I3,5X,4G13.6)
   55 CONTINUE
      STOP
      END
      SUBROUTINE TPRINT (JJ1,II1,SSS,N)
      DIMENSION SSS(33,33)
      NCOL=JJ1-1
      NPGS=(NCOL-1)/10+1
      DO 82 I=1,NPGS
      WRITE(N,16)
   16 FORMAT(1X,///////)
      J1=(I-1)*10+2
      J2=J1+9
      IF(I.EQ.NPGS) J2=JJ1
      DO 83 K=2,II1
      M=II1+2-K
      WRITE(N,81) (SSS(M,J),J=J1,J2)
   81 FORMAT(1X,10G13.6)
   83 CONTINUE
   82 CONTINUE
      RETURN
      END
      SUBROUTINE STRMFN(DY,DZ,IN,JN,IN2,JN2,II1,JJ1,II,JJ,VZR,VZB,PSI)
      DIMENSION PSI(33,33),P(1000,29),OMEGA(33,33)
      ITR=790
      ITR10=ITR-10
      RATIO=(DY/DZ)**2
      IN2=IN+2
      JN2=JN+2
      DN=2.*(1.+RATIO)
      ALPHA1=0.90
      ALPHA2=0.90
      VYL=-1.5
      VYR=1.5
```

```
      DO 9 I=3,IN2
      DO 9 J=3,JN2
      PSI(I,J)=-0.01
    9 OMEGA(I,J)=50.0
      DO 31 K=2,II1
      PSI(K,2)=0.0
   31 PSI(K,JJ1)=0.0
      DO 32 K=2,JJ1
      PSI(2,K)=0.0
   32 PSI(II1,K)=0.0
      DO 10 MM=1,ITR
      DO 21 I=3,IN2
      IM2=I-2
      IM1=I-1
      IP1=I+1
      IP2=I+2
      DO 21 J=3,JN2
      JM2=J-2
      JM1=J-1
      JP1=J+1
      JP2=J+2
      IF(IM2.EQ.1) CALL SUBIM2(PSI,OMEGA,I,J,VZR,DY)
      IF(IP2.EQ.II) CALL SUBIP2(PSI,OMEGA,I,J,VZB,DY)
      IF(JM2.EQ.1) CALL SUBJM2(PSI,OMEGA,I,J,VYL,DZ)
      IF(JP2.EQ.JJ) CALL SUBJP2(PSI,OMEGA,I,J,VYR,DZ)
      OMEGAN=RATIO*(OMEGA(I,JP1)+OMEGA(I,JM1))+OMEGA(IP1,J)+OMEGA(IM1,J)
      OMEGA(I,J)=(OMEGAN*ALPHA2/DN)+(1.-ALPHA2)*OMEGA(I,J)
      PSINEW=RATIO*(PSI(I,JP1)+PSI(I,JM1))+PSI(IP1,J)+PSI(IM1,J)
     1-DY*DY*OMEGA(I,J)
      PSI(I,J)=(ALPHA1*PSINEW/DN)+(1.-ALPHA1)*PSI(I,J)
   21 CONTINUE
      DO 11 I=3,IN2
      I2=I-2
   11 P(MM,I2)=PSI(I,17)
   10 CONTINUE
      IPEN2=2
      IPEN1=1
      CALL NEWPEN(IPEN2)
      DO 13 I=1,29
      IF(I.EQ.11) CALL NEWPEN(IPEN1)
      DO 12 J=25,ITR
      X=0.000025*J
      Y=P(J,I)
      IF(J.EQ.25) CALL PLOT(X,Y,3)
      IF(J.EQ.25) GO TO 12
      CALL PLOT(X,Y,2)
   12 CONTINUE
   13 CONTINUE
      RETURN
      END
      SUBROUTINE SUBIM2(PSI,OMEGA,I,J,VZR,DY)
      DIMENSION PSI(33,33),OMEGA(33,33)
      IM1=I-1
      OMEGA(IM1,J)=2.*(PSI(I,J)+DY*VZR)/(DY*DY)
      RETURN
      END
      SUBROUTINE SUBIP2(PSI,OMEGA,I,J,VZB,DY)
      DIMENSION PSI(33,33),OMEGA(33,33)
      IP1=I+1
      OMEGA(IP1,J)=2.*(PSI(I,J)-DY*VZB)/(DY*DY)
```

```
      RETURN
      END
      SUBROUTINE SUBJM2(PSI,OMEGA,I,J,VY,DZ)
      DIMENSION PSI(33,33),OMEGA(33,33)
      JM1=J-1
      OMEGA(I,JM1)=2.*(PSI(I,J)-DZ*VY)/(DZ*DZ)
      RETURN
      END
      SUBROUTINE SUBJP2(PSI,OMEGA,I,J,VY,DZ)
      DIMENSION PSI(33,33),OMEGA(33,33)
      JP1=J+1
      OMEGA(I,JP1)=2.*(PSI(I,J)+DZ*VY)/(DZ*DZ)
      RETURN
      END
      SUBROUTINE VELCTY (UZ,UY,VZR,VZB,IN2,JN2,II1,JJ1,DY,DZ,UYZ,ANGLE,
     2PSI)
      DIMENSION PSI(33,33),UZ(33,33),UY(33,33),UYZ(33,33),ANGLE(33,33)
      VYL=-1.5
      VYR=1.5
      EPS=10.**(-35.)
      DO 10 K=2,JJ1
      UZ(2,K)=VZR
      UY(2,K)=0.0
      UYZ(2,K)=ABS(VZR)
      ANGLE(2,K)=0.0
      UZ(II1,K)=VZB
      UY(II1,K)=0.0
      UYZ(II1,K)=ABS(VZB)
   10 ANGLE(II1,K)=0.0
      DO 15 K=2,II1
      UZ(K,2)=0.0
      UY(K,2)=VYL
      UYZ(K,2)=ABS(VYL)
      ANGLE(K,2)=-90.
      UZ(K,JJ1)=0.0
      UY(K,JJ1)=VYR
      UYZ(K,JJ1)=ABS(VYR)
   15  ANGLE(K,JJ1)=90.
      DO 30 I=3,IN2
      IP1=I+1
      IP2=I+2
      IP3=I+3
      IP4=I+4
      IP5=I+5
      IM1=I-1
      IM2=I-2
      IM3=I-3
      IM4=I-4
      IM5=I-5
      DO 30 J=3,JN2
      JM5=J-5
      JM4=J-4
      JM3=J-3
      JM2=J-2
      JM1=J-1
      JP1=J+1
      JP2=J+2
      JP3=J+3
      JP4=J+4
      JP5=J+5
```

```
      IF(JP5.LE.JJ1)   UY(I,J)=(-PSI(I,JM1)-7.7*PSI(I,J)+15.*PSI(I,JP1)-
     110.*PSI(I,JP2)+5.*PSI(I,JP3)-1.5*PSI(I,JP4)+0.2*PSI(I,JP5))/(6.*DZ
     2)
      IF(JP5.GT.JJ1)  UY(I,J)=(PSI(I,JP1)+7.7*PSI(I,J)-15.*PSI(I,JM1)+10.
     1*PSI(I,JM2)-5.*PSI(I,JM3)+1.5*PSI(I,JM4)-0.2*PSI(I,JM5))/(6.*DZ)
      IF(IP5.LE.II1)  UZ(I,J)=(PSI(IM1,J)+7.7*PSI(I,J)-15.*PSI(IP1,J)+10.
     1*PSI(IP2,J)-5.*PSI(IP3,J)+1.5*PSI(IP4,J)-0.2*PSI(IP5,J))/(6.*DY)
      IF(IP5.GT.II1)  UZ(I,J)=(-PSI(IP1,J)-7.7*PSI(I,J)+15.*PSI(IM1,J)-
     110.*PSI(IM2,J)+5.*PSI(IM3,J)-1.5*PSI(IM4,J)+0.2*PSI(IM5,J))/(6.*DY
     2)
      UYZ(I,J)=(UZ(I,J)**2+UY(I,J)**2)**0.5
      IF(ABS(UZ(I,J)).LT.EPS) GO TO 30
      ANGLE(I,J)=ATAN(UY(I,J)/UZ(I,J))*(180./3.1415)
   30 CONTINUE
      WRITE(6,40)
   40 FORMAT('1',10X,'Z-DIRECTIONAL VELOCITY',///)
      CALL TPRINT(JJ1,II1,UZ,6)
      WRITE(6,47)
   47 FORMAT('1',10X,'NET FLOW IN Z DIRECTION',///)
      DO 50 J=3,JN2
      SUMZ=0.0
      DO 51 I=3,IN2
   51 SUMZ=SUMZ+UZ(I,J)
      SUMZ=SUMZ+UZ(II1,J)/2.+UZ(2,J)/2.
      SUMZ=SUMZ*DY
      WRITE(6,61) SUMZ
   61 FORMAT(10X,G13.6,//)
   50 CONTINUE
      RETURN
      END
```

FOURTH

```
CCCCCCCCCCCCCCCCCCCCCCCCCCCCCCCCCCCCCCCCCCCCCCCCCCCCCCCCCCCCCCCCCCCCCCC
C                                                                      C
C                                                                      C
C     THE FOLLOWINGS THINGS SHOULD BE CHECKED BEFORE PROCEDING         C
C     TO RUN THIS PROGRAM:                                             C
C                                                                      C
C       1.THE OPEN STATEMENT IF ANY                                    C
C       2.NUMBER OF ITERATIONS DESIRED                                 C
C       3.THE ACCELERATING FACTOR, ALPHA                               C
C                                                                      C
CCCCCCCCCCCCCCCCCCCCCCCCCCCCCCCCCCCCCCCCCCCCCCCCCCCCCCCCCCCCCCCCCCCCCCC
C
C
C
C     THIS PROGRAM COMPUTES VELOCITY PROFILES IN Y AND Z DIRECTIONS
C     IN A SCREW CHANNEL OF A TWIN SCREW EXTRUDER
C     BY THE DIRECT ITERATIVE METHOD.
C
C                    DESCRIPTION OF PARAMETERS:
C
C     ALL VELOCITIES ARE DIMENSIONLESS BASED ON
C     THE SCREW ROOT LINEAR VELOCITY PI D1 N.
C     ALL DISTANCES ARE DIMENSIONLESS BASED ON THE ROOT
C     DIAMETER D1.
C     THE CHANNEL IS DIVIDED INTO 30 BY 30 MESH POINTS,
C     EACH MESH OF DY BY DZ SIZE.
C
C     D1=ROOT DIAMETER  IN FT.
C     D2=BARREL DIAMETER IN FT.
C     H1=CHANNEL DEPTH
C
C     THE 33 BY 33 UZ MATRIX FIRST REPRESENTS STREAM FUNCTION
C     MATRIX.LATER,BEFORE THE VELOCITY COMPONENTS ARE COMPUTED,
C     IT REPRESENTS THE Z-DIRECTIONAL VELOCITY COMPONENT MATRIX.
C
C
C     THE PSI MATRIX FIRST REPRESENTS A COEFFICIENT MATRIX AND LATER
C     BEFORE IT IS PASSED TO THE SUBROUTINE FOR COMPUTING VELOCITY
C     COMPONENTS,IT BECOMES THE STREAM FUNCTION MATRIX.
C
C
      DIMENSION PSI(33,33),UZ(33,33),UY(33,33),UYZ(33,33),ANGLE(33,33)
     1,SSS(33,33),P(500,29),VEL(33),B(216),G(216,21)
      PI=3.1415927
      D1=0.25
      D2=0.375
      VR=1.0
      VB=0.0
      H=(D2-D1)/(4.*D1)
      NJ=30
      NI=30
      DY=H/NI
      DZ=PI/NJ
      RATIO=(DY/DZ)**2
```

```
      II=NI+3
      JJ=NJ+3
      II1=II-1
      JJ1=JJ-1
      IN=NI-1
      JN=NJ-1
      F=400.0
      IND='I'
      N3=3
      CALL PLOTS(IND,15.,10.)
      CALL NEWPEN(N3)
      CALL PLOT(2.,0.,3)
      CALL PLOT(2.,9.5,-2)
      CALL FACTOR(F)
      DO 7 I=2,II1
      AS=(I-2)/30.
      BS=AS-1.
      SIA=-AS*BS*BS*H
      VEL(I)=SIA
      CALL PLOT(0.,SIA,3)
      CALL PLOT(0.015,SIA,2)
    7 CONTINUE
      CALL PLOT(0.,-0.01,3)
      DO 8 I=1,II
      DO 8 J=1,JJ
      UZ(I,J) = -0.01
    8 PSI(I,J)=0.0
      CALL STRMFN(PSI,II,JJ,RATIO,IN,JN,DY,DZ,VR,VB,IN2,JN2,II1,JJ1,B,UZ
     1)
      DO 70 I=1,II
      DO 70 J=1,JJ
      PSI(I,J)=UZ(I,J)
   70 UZ(I,J)=0.0
      CALL VELCTY(UZ,UY,VR,VB,IN2,JN2,II1,JJ1,DY,DZ,UYZ,ANGLE,PSI)
      WRITE(6,54)
   54 FORMAT(4X,'I',5X,'ANALYTICAL',3X,'NUMERICAL',5X,'DIFFERENCE',
     12X,'% DIFFERENCE',///)
      DO 55 I=3,IN2
      DIFF=VEL(I)-PSI(I,17)
      PER=(DIFF/VEL(I))*100.
      WRITE(6,56) I,VEL(I),PSI(I,17),DIFF,PER
   56 FORMAT(1X,I3,5X,4G13.6)
   55 CONTINUE
      STOP
      END
      SUBROUTINE TPRINT (JJ1,II1,SSS,N)
      DIMENSION SSS(33,33)
      NCOL=JJ1-1
      NPGS=(NCOL-1)/10+1
      DO 82 I=1,NPGS
      WRITE(N,16)
   16 FORMAT(1X,///////)
      J1=(I-1)*10+2
      J2=J1+9
      IF(I.EQ.NPGS) J2=JJ1
      DO 83 K=2,II1
      M=II1+2-K
      WRITE(N,81) (SSS(M,J),J=J1,J2)
   81 FORMAT(1X,10G13.6)
   83 CONTINUE
```

```
 82 CONTINUE
    RETURN
    END
    SUBROUTINE STRMFN(PSI,II,JJ,RATIO,IN,JN,DY,DZ,VR,VB,IN2,JN2,
   1II1,JJ1,B,UZ)
    DIMENSION PSI(33,33),UZ(33,33),B(216),G(216,21)
   1,P(500,29)
    VYL=-1.5
    VYR=1.5
    ITR=500
    IN2=IN+2
    JN2=JN+2
    RATIO2=RATIO**2
    RATIOS=4.*(1.+RATIO)
    RATIOT=4.*(RATIO2+RATIO)
    C=-1./9.
    A1=1.-C*6.
    A2=RATIO2*A1
    A3=A2
    A4=A1
    A5=2.*RATIO
    A6=-RATIOS+C*15.
    A7=A5
    A8=-RATIOT+C*15.*RATIO2
    A9=6.+6.*RATIO2+8.*RATIO-C*20.*(1.+RATIO2)
    A10=A8
    A11=A7
    A12=A6
    A13=A5
    A14=C
    A15=C
    A16=C*RATIO2
    A17=C*RATIO2
    B1=0.70925
    D1=0.085
    C1=(8.-3.*D1)/(11.*D1)
    WRITE(6,2) B1,C1,D1
  2 FORMAT(1X,'B1=',F7.4,'C1=',F7.4,'D1=',F7.4,////)
    DO 31 K=2,II1
    UZ(K,JJ1)=0.0
    UZ(K,JJ)=0.0
    UZ(K,1)=0.0
 31 UZ(K,2)=0.0
    DO 32 K=2,JJ1
    UZ(2,K)=0.0
    UZ(1,K)=0.0
    UZ(II1,K)=0.0
 32 UZ(II,K)=0.0
    DO 10 MM=1,ITR
    L=0
    DO 21 I=3,IN2
    IM2=I-2
    IM1=I-1
    IM3=I-3
    IM4=I-4
    IP1=I+1
    IP2=I+2
    IP3=I+3
    IP4=I+4
    IF(I.LE.12) ALPHA=2.-B1*(IM2/10.)**C1
```

```
      IF(I.GT.12) ALPHA=2.-B1+B1*((I-12)/20.)**D1
      DO 21 J=3,JN2
      JM2=J-2
      JM1=J-1
      JP1=J+1
      JP2=J+2
      JP3=J+3
      JM3=J-3
      JM4=J-4
      JP4=J+4
      IF(J.LE.4.OR.J.GE.30.OR.I.LE.4.OR.I.GE.30) GO TO 25
      TOTAL=-(A1*UZ(IM2,J)+A2*UZ(I,JM2)+A3*UZ(I,JP2)+A4*UZ(IP2,J)+A5*
     1UZ(IM1,JM1)+A6*UZ(IM1,J)+A7*UZ(IM1,JP1)+A8*UZ(I,JM1)+A10*UZ(I,JP1)
     2+A11*UZ(IP1,JM1)+A12*UZ(IP1,J)+A13*UZ(IP1,JP1)+A14*UZ(IM3,J)+A15*
     3UZ(IP3,J)+A16*UZ(I,JM3)+A17*UZ(I,JP3))/A9
      GO TO 26
   20 SUM=G(L,1)*UZ(IP2,J)+G(L,2)*UZ(IP1,JM1)+G(L,3)*UZ(IP1,J)+
     1G(L,4)*UZ(IP1,JP1)+G(L,5)*UZ(I,JM2)+G(L,6)*UZ(I,JM1)+
     2G(L,8)*UZ(I,JP1)+G(L,9)*UZ(I,JP2)+G(L,10)*UZ(IM1,JM1)+
     3G(L,11)*UZ(IM1,J)+G(L,12)*UZ(IM1,JP1)+G(L,13)*UZ(IM2,J)
      IF(IM2.EQ.1.AND.JM2.EQ.1) GO TO 171
      IF(IP2.EQ.II.AND.JM2.EQ.1) GO TO 172
      IF(IM2.EQ.1.AND.JP2.EQ.JJ) GO TO 173
      IF(IP2.EQ.II.AND.JP2.EQ.JJ) GO TO 174
      IF(IM2.EQ.1) SUM=SUM+G(L,14)*UZ(IP3,J)+G(L,18)*UZ(IP4,J)
     1+G(L,17)*UZ(I,JP3)+G(L,15)*UZ(I,JM3)
      IF(IP2.EQ.II) SUM=SUM+G(L,16)*UZ(IM3,J)+G(L,20)*UZ(IM4,J)
     1+G(L,17)*UZ(I,JP3)+G(L,15)*UZ(I,JM3)
      IF(JM2.EQ.1) SUM=SUM+G(L,17)*UZ(I,JP3)+G(L,21)*UZ(I,JP4)
     1+G(L,14)*UZ(IP3,J)+G(L,16)*UZ(IM3,J)
      IF(JP2.EQ.JJ) SUM=SUM+G(L,15)*UZ(I,JM3)+G(L,19)*UZ(I,JM4)
     1+G(L,14)*UZ(IP3,J)+G(L,16)*UZ(IM3,J)
      IF(IM2.NE.1.AND.IP2.NE.II.AND.JM2.NE.1.AND.JP2.NE.JJ) SUM=
     1SUM+G(L,16)*UZ(IM3,J)+G(L,14)*UZ(IP3,J)+G(L,15)*
     2UZ(I,JM3)+G(L,17)*UZ(I,JP3)
      GO TO 129
  171 SUM=SUM+G(L,14)*UZ(IP3,J)+G(L,18)*UZ(IP4,J)
     1+G(L,17)*UZ(I,JP3)+G(L,21)*UZ(I,JP4)
      GO TO 129
  172 SUM=SUM+G(L,16)*UZ(IM3,J)+G(L,20)*UZ(IM4,J)
     1+G(L,17)*UZ(I,JP3)+G(L,21)*UZ(I,JP4)
      GO TO 129
  173 SUM=SUM+G(L,14)*UZ(IP3,J)+G(L,18)*UZ(IP4,J)
     1+G(L,15)*UZ(I,JM3)+G(L,19)*UZ(I,JM4)
      GO TO 129
  174 SUM=SUM+G(L,16)*UZ(IM3,J)+G(L,20)*UZ(IM4,J)
     1+G(L,15)*UZ(I,JM3)+G(L,19)*UZ(I,JM4)
  129 TOTAL=(B(L)-SUM)/G(L,7)
      GO TO 26
   25 L=L+1
      IF(MM.GT.1) GO TO 20
      PSI(IM2,J)=A1
      PSI(I,JM2)=A2
      PSI(I,JP2)=A3
      PSI(IP2,J)=A4
      PSI(IM1,JM1)=A5
      PSI(IM1,J)=A6
      PSI(IM1,JP1)=A7
      PSI(I,JM1)=A8
      PSI(I,J)=A9
```

```
      PSI(I,JP1)=A10
      PSI(IP1,JM1)=A11
      PSI(IP1,J)=A12
      PSI(IP1,JP1)=A13
      IF(IM2.NE.1) PSI(IM3,J)=A14
      IF(IP2.NE.II) PSI(IP3,J)=A15
      IF(JM2.NE.1) PSI(I,JM3)=A16
      IF(JP2.NE.JJ) PSI(I,JP3)=A17
      B(L)=0.0
      IR=I
      JR=J
      IF(IM2.EQ.1)CALL SUBIM2(PSI,IR,JR,B,L,VR,DY,C,
     1IM2,IM1,IP1,IP2,IP3,IP4)
      IF(IP2.EQ.II) CALL SUBIP2(PSI,IR,JR,B,L,VB,DY,C,
     1IP2,IP1,IM1,IM2,IM3,IM4)
      IF(JM2.EQ.1)  CALL  SUBJM2 (PSI,IR,JR,B,L,VYL,DZ,RATIO2,C,
     1JM2,JM1,JP1,JP2,JP3,JP4)
      IF(JP2.EQ.JJ) CALL SUBJP2(PSI,IR,JR,B,L,VYR,DZ,RATIO2,C,
     1JP1,JP2,JM1,JM2,JM3,JM4)
      IF(IM3.EQ.1) CALL SUBIM3 (PSI,IR,JR,B,L,VR,DY,
     1IM3,IM2,IM1,IP1,IP2,IP3)
      IF(IP3.EQ.II) CALL SUBIP3(PSI,IR,JR,B,L,VB,DY,
     1IP3,IP2,IP1,IM1,IM2,IM3)
      IF(JM3.EQ.1)  CALL  SUBJM3 (PSI,IR,JR,B,L,VYL,DZ,
     1JM3,JM2,JM1,JP1,JP2,JP3)
      IF(JP3.EQ.JJ) CALL SUBJP3(PSI,IR,JR,B,L,VYR,DZ,
     1JP3,JP2,JP1,JM1,JM2,JM3)
      SUM=PSI(IM2,J)*UZ(IM2,J) +PSI(I,JM2)*UZ(I,JM2)+PSI(I,JP2)*UZ(I,JP2
     1)+PSI(IM1,JM1)*UZ(IM1,JM1)+PSI(IM1,J)*UZ(IM1,J)+PSI(IM1,JP1)*
     2UZ(IM1,JP1)+PSI(I,JM1)*UZ(I,JM1)+PSI(I,JP1)*UZ(I,JP1)+PSI(IP1,JM1)
     3*UZ(IP1,JM1)+PSI(IP2,J)*UZ(IP2,J)+PSI(IP1,J)*UZ(IP1,J)
     4+PSI(IP1,JP1)*UZ(IP1,JP1)
      G(L,1)=PSI(IP2,J)
      G(L,2)=PSI(IP1,JM1)
      G(L,3)=PSI(IP1,J)
      G(L,4)=PSI(IP1,JP1)
      G(L,5)=PSI(I,JM2)
      G(L,6)=PSI(I,JM1)
      G(L,7)=PSI(I,J)
      G(L,8)=PSI(I,JP1)
      G(L,9)=PSI(I,JP2)
      G(L,10)=PSI(IM1,JM1)
      G(L,11)=PSI(IM1,J)
      G(L,12)=PSI(IM1,JP1)
      G(L,13)=PSI(IM2,J)
      IF(IM2.EQ.1.AND.JM2.EQ.1) GO TO 71
      IF(IP2.EQ.II.AND.JM2.EQ.1) GO TO 72
      IF(IM2.EQ.1.AND.JP2.EQ.JJ) GO TO 73
      IF(IP2.EQ.II.AND.JP2.EQ.JJ) GO TO 74
      IF(IM2.EQ.1) SUM=SUM+PSI(IP3,J)*UZ(IP3,J)+PSI(IP4,J)*UZ(IP4,J)
     1+PSI(I,JP3)*UZ(I,JP3)+PSI(I,JM3)*UZ(I,JM3)
      IF(IM2.NE.1) GO TO 61
      G(L,14)=PSI(IP3,J)
      G(L,18)=PSI(IP4,J)
      G(L,17)=PSI(I,JP3)
      G(L,15)=PSI(I,JM3)
   61 IF(IP2.EQ.II) SUM=SUM+PSI(IM3,J)*UZ(IM3,J)+PSI(IM4,J)*UZ(IM4,J)
     1+PSI(I,JP3)*UZ(I,JP3)+PSI(I,JM3)*UZ(I,JM3)
      IF(IP2.NE.II) GO TO 62
      G(L,16)=PSI(IM3,J)
```

```
      G(L,20)=PSI(IM4,J)
      G(L,17)=PSI(I,JP3)
      G(L,15)=PSI(I,JM3)
   62 IF(JM2.EQ.1) SUM=SUM+PSI(I,JP3)*UZ(I,JP3)+PSI(I,JP4)*UZ(I,JP4)
     1+PSI(IP3,J)*UZ(IP3,J)+PSI(IM3,J)*UZ(IM3,J)
      IF(JM2.NE.1) GO TO 63
      G(L,17)=PSI(I,JP3)
      G(L,21)=PSI(I,JP4)
      G(L,14)=PSI(IP3,J)
      G(L,16)=PSI(IM3,J)
   63 IF(JP2.EQ.JJ) SUM=SUM+PSI(I,JM3)*UZ(I,JM3)+PSI(I,JM4)*UZ(I,JM4)
     1+PSI(IP3,J)*UZ(IP3,J)+PSI(IM3,J)*UZ(IM3,J)
      IF(JP2.NE.JJ) GO TO 64
      G(L,15)=PSI(I,JM3)
      G(L,19)=PSI(I,JM4)
      G(L,14)=PSI(IP3,J)
      G(L,16)=PSI(IM3,J)
   64 IF(IM2.NE.1.AND.IP2.NE.II.AND.JM2.NE.1.AND.JP2.NE.JJ) SUM=
     1SUM+PSI(IM3,J)*UZ(IM3,J)+PSI(IP3,J)*UZ(IP3,J)+PSI(I,JM3)*
     2UZ(I,JM3)+PSI(I,JP3)*UZ(I,JP3)
      IF(IM2.NE.1.AND.IP2.NE.II.AND.JM2.NE.1.AND.JP2.NE.JJ) GO TO 65
      GO TO 29
   65 G(L,14)=PSI(IP3,J)
      G(L,15)=PSI(I,JM3)
      G(L,16)=PSI(IM3,J)
      G(L,17)=PSI(I,JP3)
      GO TO 29
   71 SUM=SUM+PSI(IP3,J)*UZ(IP3,J)+PSI(IP4,J)*UZ(IP4,J)
     1+PSI(I,JP3)*UZ(I,JP3)+PSI(I,JP4)*UZ(I,JP4)
      G(L,14)=PSI(IP3,J)
      G(L,18)=PSI(IP4,J)
      G(L,17)=PSI(I,JP3)
      G(L,21)=PSI(I,JP4)
      GO TO 29
   72 SUM=SUM+PSI(IM3,J)*UZ(IM3,J)+PSI(IM4,J)*UZ(IM4,J)
     1+PSI(I,JP3)*UZ(I,JP3)+PSI(I,JP4)*UZ(I,JP4)
      G(L,16)=PSI(IM3,J)
      G(L,20)=PSI(IM4,J)
      G(L,17)=PSI(I,JP3)
      G(L,21)=PSI(I,JP4)
      GO TO 29
   73 SUM=SUM+PSI(IP3,J)*UZ(IP3,J)+PSI(IP4,J)*UZ(IP4,J)
     1+PSI(I,JM3)*UZ(I,JM3)+PSI(I,JM4)*UZ(I,JM4)
      G(L,14)=PSI(IP3,J)
      G(L,18)=PSI(IP4,J)
      G(L,15)=PSI(I,JM3)
      G(L,19)=PSI(I,JM4)
      GO TO 29
   74 SUM=SUM+PSI(IM3,J)*UZ(IM3,J)+PSI(IM4,J)*UZ(IM4,J)
     1+PSI(I,JM3)*UZ(I,JM3)+PSI(I,JM4)*UZ(I,JM4)
      G(L,16)=PSI(IM3,J)
      G(L,20)=PSI(IM4,J)
      G(L,15)=PSI(I,JM3)
      G(L,19)=PSI(I,JM4)
   29 TOTAL=(B(L)-SUM)/PSI(I,J)
   26 UZ(I,J)=ALPHA*TOTAL+(1.-ALPHA)*UZ(I,J)
   21 CONTINUE
      DO 11 I=3,IN2
      I2=I-2
   11 P(MM,I2)=UZ(I,17)
```

```
 10 CONTINUE
    IPEN2=2
    IPEN1=1
    CALL NEWPEN(IPEN2)
    DO 13 I=1,29
    IF(I.EQ.11) CALL NEWPEN(IPEN1)
    DO 12 J=50,ITR
    X=0.000030*J
    Y=P(J,I)
    IF(J.EQ.50) CALL PLOT(X,Y,3)
    IF(J.EQ.50) GO TO 12
    CALL PLOT(X,Y,2)
 12 CONTINUE
 13 CONTINUE
    RETURN
    END
    SUBROUTINE  SUBIM2 (PSI,I,J,B,L,VZ,DY,C,IM2,IM1,IP1,IP2,IP3,IP4)
    DIMENSION PSI(33,33),B(216)
    A1=PSI(IM2,J) +4.*C
    PSI(IM1,J)=PSI(IM1,J)-7.7*A1-6.*C
    PSI(I,J)=PSI(I,J) +15.*A1 +4.*C
    PSI(IP1,J)=PSI(IP1,J)-10.*A1-C
    PSI(IP2,J)=PSI(IP2,J)+5.*A1
    PSI(IP3,J)=PSI(IP3,J)-1.5*A1
    PSI(IP4,J)=     0.2*A1
    B(L)=B(L)-6.*DY*VZ*A1
    RETURN
    END
    SUBROUTINE  SUBIP2 (PSI,I,J,B,L,VZ,DY,C,IP2,IP1,IM1,IM2,IM3,IM4)
    DIMENSION PSI(33,33),B(216)
    A2=PSI(IP2,J)+4.*C
    PSI(IP1,J)=PSI(IP1,J)-7.7*A2-6.*C
    PSI(I,J)=PSI(I,J) +15.*A2 +4.*C
    PSI(IM1,J)=PSI(IM1,J)-10.*A2-C
    PSI(IM2,J)=PSI(IM2,J)+5.*A2
    PSI(IM3,J)=PSI(IM3,J)-1.5*A2
    PSI(IM4,J)=0.2*A2
    B(L)=B(L)+6.*DY*VZ*A2
    RETURN
    END
    SUBROUTINE  SUBJM2 (PSI,I,J,B,L,VY,DZ,RATIO2,C,
   1JM2,JM1,JP1,JP2,JP3,JP4)
    DIMENSION PSI(33,33),B(216)
    A3=PSI(I,JM2)+4.*C*RATIO2
    PSI(I,JM1)=PSI(I,JM1)-7.7*A3-6.*C*RATIO2
    PSI(I,J)=PSI(I,J) +15.*A3+4.*C*RATIO2
    PSI(I,JP1)=PSI(I,JP1)-10.*A3 -C*RATIO2
    PSI(I,JP2)=PSI(I,JP2)+5.*A3
    PSI(I,JP3)=PSI(I,JP3)-1.5*A3
    PSI(I,JP4)=0.2*A3
    B(L)=B(L)+6.*DZ*VY*A3
    RETURN
    END
    SUBROUTINE SUBJP2 (PSI,I,J,B,L,VY,DZ,RATIO2,C,
   1JP1,JP2,JM1,JM2,JM3,JM4)
    DIMENSION PSI(33,33),B(216)
    A4=PSI(I,JP2)+4.*C*RATIO2
    PSI(I,JP1)=PSI(I,JP1)-7.7*A4-6.*C*RATIO2
    PSI(I,J)=PSI(I,J) +15.*A4 +4.*C*RATIO2
    PSI(I,JM1)=PSI(I,JM1)-10.*A4 -C*RATIO2
```

```
PSI(I,JM2)=PSI(I,JM2)+5.*A4
PSI(I,JM3)=PSI(I,JM3)-1.5*A4
PSI(I,JM4)=0.2*A4
B(L)=B(L)-6.*DZ*VY*A4
RETURN
END
SUBROUTINE SUBIM3 (PSI,I,J,B,L,VZ,DY,IM3,IM2,IM1,IP1,IP2,IP3)
DIMENSION PSI(33,33),B(216)
A1=PSI(IM3,J)
PSI(IM2,J)=PSI(IM2,J)-7.7*A1
PSI(IM1,J)=PSI(IM1,J)+15.*A1
PSI(I,J)=PSI(I,J)-10.*A1
PSI(IP1,J)=PSI(IP1,J)+5.*A1
PSI(IP2,J)=PSI(IP2,J)-1.5*A1
PSI(IP3,J)=PSI(IP3,J)+0.2*A1
B(L)=B(L)-6.*DY*VZ*A1
RETURN
END
SUBROUTINE SUBIP3 (PSI,I,J,B,L,VZ,DY,IP3,IP2,IP1,IM1,IM2,IM3)
DIMENSION PSI(33,33),B(216)
A2=PSI(IP3,J)
PSI(IP2,J)=PSI(IP2,J)-7.7*A2
PSI(IP1,J)=PSI(IP1,J)+15.*A2
PSI(I,J)=PSI(I ,J)-10.*A2
PSI(IM1,J)=PSI(IM1,J)+5.*A2
PSI(IM2,J)=PSI(IM2,J)-1.5*A2
PSI(IM3,J)=PSI(IM3,J)+0.2*A2
B(L)=B(L)+6.*DY*VZ*A2
RETURN
END
SUBROUTINE SUBJM3 (PSI,I,J,B,L,VY,DZ,JM3,JM2,JM1,JP1,JP2,JP3)
DIMENSION PSI(33,33),B(216)
A3=PSI(I,JM3)
PSI(I,JM2)=PSI(I,JM2)-7.7*A3
PSI(I,JM1)=PSI(I,JM1)+15.*A3
PSI(I,J)=PSI(I ,J)-10.*A3
PSI(I,JP1)=PSI(I,JP1)+5.*A3
PSI(I,JP2)=PSI(I,JP2)-1.5*A3
PSI(I,JP3)=PSI(I,JP3)+0.2*A3
B(L)=B(L)+6.*DZ*VY*A3
RETURN
END
SUBROUTINE SUBJP3 (PSI,I,J,B,L,VY,DZ,JP3,JP2,JP1,JM1,JM2,JM3)
DIMENSION PSI(33,33),B(216)
A4=PSI(I,JP3)
PSI(I,J P1)=PSI(I,JP1)+15.*A4
PSI(I,JP2)=PSI(I,JP2)-7.7*A4
PSI(I,J)=PSI(I ,J)-10.*A4
PSI(I,J M1)=PSI(I,JM1)+5.*A4
PSI(I,J M2)=PSI(I,JM2)-1.5*A4
PSI(I,J M3)=PSI(I,JM3)+0.2*A4
B(L)=B(L)-6.*DZ*VY*A4
RETURN
END
SUBROUTINE VELCTY(UZ,UY,VR,VB,IN2,JN2,II1,JJ1,DY,DZ,UYZ,ANGLE,PSI)
DIMENSION PSI(33,33),UZ(33,33),UY(33,33),UYZ(33,33),ANGLE(33,33)
VY=1.5
EPS=10.**(-38.)
DO 10 K=2,JJ1
UZ(2,K)=VR
```

```
      UY(2,K)=0.0
      UYZ(2,K)=ABS(VR)
      ANGLE(2,K)=0.0
      UZ(II1,K)=VB
      UY(II1,K)=0.0
      UYZ(II1,K)=ABS(VB)
   10 ANGLE(II1,K)=0.0
      DO 20 K=2,II1
      UZ(K,2)=0.0
      UY(K,2)=-VY
      UYZ(K,2)=ABS(VY)
      ANGLE(K,2)=-90.0
      UZ(K,JJ1)=0.0
      UY(K,JJ1)=VY
      UYZ(K,JJ1)=ABS(VY)
   20 ANGLE(K,JJ1)=90.0
      DO 30 I=3,IN2
      IP1=I+1
      IP2=I+2
      IP3=I+3
      IP4=I+4
      IP5=I+5
      IM1=I-1
      IM2=I-2
      IM3=I-3
      IM4=I-4
      IM5=I-5
      DO 30 J=3,JN2
      JM5=J-5
      JM4=J-4
      JM3=J-3
      JM2=J-2
      JM1=J-1
      JP1=J+1
      JP2=J+2
      JP3=J+3
      JP4=J+4
      JP5=J+5
      IF(IP5.LE.II1) UZ(I,J)=(PSI(IM1,J)+7.7*PSI(I,J)-15.*PSI(IP1,J)+10.
     1*PSI(IP2,J)-5.*PSI(IP3,J)+1.5*PSI(IP4,J)-0.2*PSI(IP5,J))/(6.*DY)
      IF(IP5.GT.II1) UZ(I,J)=(-PSI(IP1,J)-7.7*PSI(I,J)+15.*PSI(IM1,J)-
     110.*PSI(IM2,J)+5.*PSI(IM3,J)-1.5*PSI(IM4,J)+0.2*PSI(IM5,J))/(6.*DY
     2)
   30 CONTINUE
      WRITE(6,40)
   40 FORMAT('1',10X,'Z-DIRECTIONAL VELOCITY',///)
      CALL TPRINT(JJ1,II1,UZ,6)
      WRITE(6,47)
   47 FORMAT('1',10X,'NET FLOW IN Z DIRECTION',///)
      DO 50 J=3,JN2
      SUMZ=0.0
      DO 51 I=3,IN2
   51 SUMZ=SUMZ+UZ(I,J)
      SUMZ=SUMZ+UZ(II1,J)/2.+UZ(2,J)/2.
      SUMZ=SUMZ*DY
      WRITE(6,61) SUMZ
   61 FORMAT(10X,G13.6)
   50 CONTINUE
      RETURN
      END
```

TWIN

```
CCCCCCCCCCCCCCCCCCCCCCCCCCCCCCCCCCCCCCCCCCCCCCCCCCCCCCCCCCCCCCCCCCCCCCCCCCCC
C                                                                            C
C                                                                            C
C                                                                            C
C     THE FOLLOWINGS THINGS SECULD EE CHECKED BEFORE PROCEDING               C
C     TO RUN THIS PROGRAM:                                                   C
C                                                                            C
C       1.THE OPEN STATEMENT                                                 C
C       2.THE VELCCITY VR (CCROTATING CR COUNTER ROTATING)                   C
C       3.IDZ                                                                C
C       4.NUMBER OF ITERATICNS DESIRED                                       C
C       5.THE ACCELERATING FACTCR, AIPHA                                     C
C       6.THE VELOCITY CCMPCNENT UY AT THE RIGHT HAND SIDE BOUNDARY          C
C         IS ASSUMED TO BE ZERO WHEN IDZ>1.HOWEVER FOR ACCURACY,             C
C         THE VELCCITY UY AT THE RIGHT HAND SIDE BOUNDARY FOR IDZ>1          C
C         CAN BE SUBSTITUTED WITH THE KNCWN VELOCITY COMPONENT UY.           C
C         UYR REPRESENTS THE Y-CCMPCNENT VELOCITY AT                         C
C         THE RIGHT HAND SIDE BCUNDARY.                                      C
C                                                                            C
CCCCCCCCCCCCCCCCCCCCCCCCCCCCCCCCCCCCCCCCCCCCCCCCCCCCCCCCCCCCCCCCCCCCCCCCCCCC
C
C
C
C
C     THIS PROGRAM COMPUTES VELOCITY PROFILES IN Y AND Z DIRECTIONS,
C     AND THE CORRESPONDING PRESSURE GRADIENTS IN A SCREW CHANNEL OF
C     A TWIN SCREW EXTRUDER BY THE DIRECT ITERATIVE METHOD.
C
C
C                    DESCRIPTICN OF PARAMETERS:
C
C     ALL VELOCITIES ARE DIMENSICNLESS BASED CN
C     THE SCREW RCCT LINEAR VELOCITY PI D1 N.
C     ALL DISTANCES ARE DIMENSICNLESS BASED ON THE ROOT
C     DIAMETER D1.
C     THE CHANNEL IS DIVIDED INTO 30 BY 30 MESH POINTS,
C     EACH MESH OF DY BY DZ SIZE.
C
C     D1=ROOT DIAMETER  IN FT.
C     D2=BARREL DIAMETER IN FT.
C     VZR=ROOT VELOCITY;+VE WHEN CLOCKWISE.
C     VZB=BARREL VELOCITY
C     VR=FLIGHT VELOCITY OF THE CTHER SCREW,+VE WHEN CLOCKWISE.
C     H1=CHANNEL DEPTH
C
C     THE 33 BY 33 UZ MATRIX FIRST REPRESENTS STREAM FUNCTION
C     MATRIX.LATER,BEFORE THE VELOCITY COMPONENTS ARE COMPUTED,
C     IT REPRESENTS THE Z-DIRECTICNAL VELOCITY COMPONENT MATRIX.
C
C     THE 33 BY 33 ANGLE MATRIX IS FIRST USED TO FIND OUT
C     FICTICIOUS POINTS AND LATER IT BECOMES A MATRIX REPRESENTING
```

```
C     THE ANGLE OF THE RESULTANT VELOCITY AT ALL MESH POINTS.
C
C     THE PSI MATRIX FIRST REPRESENTS A COEFFICIENT MATRIX AND LATER
C     BEFORE IT IS PASSED TO THE SUBROUTINE FOR COMPUTING VELOCITY
C     COMPONENTS,IT BECOMES THE STREAM FUNCTION MATRIX.
C
C
      DIMENSION PSI(33,33),U2(33,33),UY(33,33),UYZ(33,33),ANGLE(33,33)
     1,SSS(33,33),RR(122,16),G(6),H(6),E(156),C(156,59),VEL(33)
     2,STRFN(33)
      COMMON/ELK/CESTRF,I,D22
      OPEN(UNIT=8,DEVICE='TAPE',ACCESS='SEQINOUT',FILE='NC045.DAT')
      PI=3.1415927
      D1=0.25
      D2=0.375
      VR=D2/D1
      VR=-VR
      D22=ABS(VR)
      T=PI/4.
      C1=(D2/D1)*SIN(T)*SIN(T)/COS(T)
      VZR=-1./COS(T)
      VZB=-C1
      R=1./COS(T)
      PP=C1+R
      Q=-(PP+R)
      H1=((D2/D1)-1.)/4.
C
C     WHEN IDZ=1 VELOCITY PROFILE FOR THE ENTIRE CHANNEL IS COMPUTED;
C     OTHERWISE JUST A PART OF IT.
C
      IDZ=1
C
      NI=30
      NJ=30
      DY=H1/NI
      DZ=PI/(NJ*COS(T))
      DZ=DZ/IDZ
      II=NI+3
      JJ=NJ+3
      II1=II-1
      JJ1=JJ-1
      IN=NI-1
      JN=NJ-1
      DO 7 I=2,II1
      AS=(I-2)/30.
      BS=1.-AS
      STRFN(I)=AS*H1*(PP*AS*AS+Q*AS+R)
      VEL(I)=AS*(2.-3.*AS)*C1+BS*(3.*AS-1.)*R
    7 CONTINUE
C
C
C     STREAM FUNCTION VALUE AT ALL MESH POINTS ARE INITIALLY
C     SET TO -0.01
C
C
C
      DO 10 I=1,II
      DO 10 J=1,JJ
      UZ(I,J)=0.01
      ANGLE(I,J)=0.0
   10 PSI(I,J)=0.0
```

```
C
CC
C     CBSTRF IS A KNOWN VALUE OF STREAM FUNCTION ON CURVE BOUNDARIES
C     WHICH TAKES CARE CF IEAKAGE CCCUBING IN THE CHANNEL.IT IS +VE
C     FOR COROTATING CASE WHILE -VE FOR THE CCUNTER ROTATING CASE.
CC
C
      CBSTRF=0.0
C
C
      DO 11 I=2,II1
   11 UZ(I,JJ1)=STRFN(I)
      CALL STRMFN(PSI,II,JJ,IN,JN,DY,DZ,VR,VZB,VZB,IN2,JN2,II1,JJ1,R1,PI
     1,ANGLE,ZR,ZI,ZMAX,UZ,E,I,IDZ)
      DO 70 I=1,II
      DO 70 J=1,JJ
      PSI(I,J)=UZ(I,J)
   70 UZ(I,J)=0.0
C
CC
C     COMPUTATION OF STREAM FUNCTICN VALUES OF FICTICIOUS
C     MESH POINTS
CC
C
      DO 74 KK=1,2
      LL=0
      DO 75 IR=3,IN2
      DO 75 JR=3,JN2
      I=IR
      J=JR
      JM2=J-2
      Z=JM2*DZ
      IF(ANGLE(I,J).GT.5)CALL CURVE(I,J,2,Y,ZI,ZR,ZMAX,DY,DZ,VZR,VZB,VR,
     1R13,R16,PSI,N1,PI,II,R1,10,JJ,E,I,LL)
   75 CONTINUE
   74 CONTINUE
      WRITE(6,80)
   80 FORMAT('1',10X,'STREAM FUNCTICN MATRIX PSI',///)
      CALL TPRINT(JJ1,II1,PSI,6)
      WRITE(8,80)
      CALL TPRINT(JJ1,II1,PSI,8)
      DO 82 I=1,II
      DO 82 J=1,JJ
   82 ANGLE(I,J)=0.0
      DO 81 I=2,II1
   81 UZ(I,JJ1)=VEI(I)
      CALL VELCTY(UZ,UY,VZR,VZB,IN2,JN2,II1,JJ1,DY,DZ,UYZ,ANGLE,PSI,ZMAX
     1,PI,IDZ)
      WRITE(6,54)
   54 FORMAT(4X,'I',5X,'ANALYTICAL',3X,'NUMERICAL',5X,'DIFFERENCE',
     12X,'% DIFFERENCE',///)
      JN1=JN2
      IF(IDZ.EQ.1) JN1=17
      DO 55 I=3,IN2
      DIFF=STRFN(I)-PSI(I,JN1)
      PER=(DIFF/STRFN(I))*10C.
      WRITE(6,56) I,STRFN(I),PSI(I,JN1),DIFF,PER
   56 FORMAT(1X,I3,5X,4G13.6)
   55 CONTINUE
      DO 57 I=3,IN2
```

```
      UYZ(I,JJ1)=0.0
   57 PSI(I,JJ1)=0.0
      CALL PRESRE(PSI,UYZ,UZ,UY,DZ,DY,II,JJ,IN2,JN2,ZMAX)
      END FILE 8
      STOP
      END
C
C
C     SUBROUTINE STRMFN COMPUTES THE STREAM FUNCTION VALUES AT ALL
C     MESH POINTS BY ITERATIVE METHODS.
C
C
C
C     ITR=NUMBER OF ITERATIONS PERFORMED
C     ALPHA=THE ACCELERATING FACTOR
C
C     THE CONSTANTS A1 THRU A13 REPRESENT STREAM FUNCTION
C     COEFFICIENTS.
C
      SUBROUTINE STRMFN(PSI,II,JJ,IN,JN,DY,DZ,VR,VZR,VZB,IN2,JN2,II1,
     1JJ1,H1,PI,ANGLE,ZB,ZL,ZMAX,UZ,E,L,IDZ)
      DIMENSION PSI(33,33),UZ(33,33),B(156),ANGLE(33,33),C(156,59)
      COMMON/ELK/CESTRF,T,D22
      ITR=4500
      ITR5=ITR-5
      IN2=IN+2
      JN2=JN+2
      RATIO=(DY/DZ)**2
      RATIO2=RATIO**2
      RATIOS=4.*(1.+RATIO)
      RATIOT=4.*(RATIO2+RATIO)
      CALL  ZZZ(H1,ZMAX)
      ZL=ZMAX+3.*DZ
      ZB=PI/COS(T)-ZL
      EPS=10.**(-15)
      A1=1.
      A2=RATIO2
      A3=A2
      A4=A1
      A5=2.*RATIO
      A6=-RATIOS
      A7=A5
      A8=-RATIOT
      A9=6.+6.*RATIO2+8.*RATIO
      A10=A8
      A11=A7
      A12=A6
      A13=A5
C
C
C     THE VELOCITY COMPONENT UY AT THE RIGHT HAND SIDE BOUNDARY
C     WHEN IDZ>1 IS ASSUMED TO BE ZERO (IT CAN,HOWEVER BE
C     REPLACED BY ANY DESIRED VALUE OR VECTOR).
C
C
      UYR=0.0
C
C
C     BOUNDARY CONDITIONS:
C
```

```
C     ON THE BOUNDARY STREAM FUNCTION VALUE IS ZERO.
C     WHEN IDZ>1,THE RIGHT HAND SIDE BOUNDARY IS REPLACED BY
C     THE KNOWN VELOCITY PROFILE OF STREAM FUNCTION.
C
C
C
      DO 32 K=2,JJ1
      UZ(2,K)=0.0
      UZ(1,K)=0.0
      UZ(II,K)=0.0
   32 UZ(II1,K)=0.0
      DO 31 K=2,II1
      UZ(K,2)=0.0
      UZ(K,1)=0.0
      IF(IDZ.EQ.1) UZ(K,JJ1)=0.0
   31 UZ(K,JJ)=0.0
      LL=0
      L=0
      K1=5
C
C     COMPUTATION OF THE DESIRED MESH POINTS
C     (THE MESH POINTS TO BE ITERATED)
C
      DO 8 IR=3,IN2
      DO 8 JR=3,JN2
      I=IR
      J=JR
      Z=(J-2)*DZ
      IF(Z.GE.ZL.AND.Z.LE.ZR) GO TO 8
      CALL CURVE(I,J,Z,Y,ZI,ZR,ZMAX,DY,DZ,VZR,VZB,VR,R13,R16,
     1UZ,N1,PI,II,H1,K1,JJ,E,I,II)
      IF(ABS(R16).LT.N1.OR.ABS(R13).LT.N1) ANGLE(I,J)=10.0
      IF(R13.LT.N1.OR.R16.LT.N1)UZ(I,J)=0.0
      IF(K1.EQ.6) ANGLE(I,J)=-2.0
    8 CONTINUE
      NM1=-1
C
C
C     ITERATION LOOP BEGINS HERE
C
C
      DO 10 MM=1,ITR
      LL=0
      L=0
      DO 21 I=3,IN2
      IM1=I-1
      IM2=I-2
      IM3=I-3
      IM4=I-4
      IM5=I-5
      IP1=I+1
      IP2=I+2
      IP3=I+3
      IP4=I+4
      IP5=I+5
      DO 21 J=3,JN2
      IF(ABS(UZ(I,J)).LE.EPS) GO TO 21
      JM2=J-2
      JM1=J-1
      JP1=J+1
```

```
      JP2=J+2
      JP3=J+3
      JM3=J-3
      JM4=J-4
      JP4=J+4
      JP5=J+5
      JM5=J-5
      ALPHA=2.-15.*ABS(UZ(I,J))
      Z=JM2*DZ
      IF(IM2.EQ.1.OR.IP2.EQ.II.OR.JP2.EQ.JJ) GO TO 25
      IF(Z.LT.ZL.OR.Z.GT.ZR) GO TO 24
   23 TOTAL=-(A1*UZ(IM2,J)+A2*UZ(I,JM2)+A3*UZ(I,JP2)+A4*UZ(IP2,J)
     1+A5*UZ(IM1,JM1)+A6*UZ(IM1,J)+A7*UZ(IM1,JP1)+A8*UZ(I,JM1)+
     2A10*UZ(I,JP1)+A11*UZ(IP1,JM1)+A12*UZ(IP1,J)+A13*UZ(IP1,JP1))/A9
      GO TO 38
   24 IF(ANGLE(I,J).LT.NM1) GO TO 23
   25 L=L+1
      IF(MM.GT.1) GO TO 20
C
C
C     THE FIRST ITERATION STEP BEGINS HERE
C
C     IN THE FIRST ITERATION STEP ALL THE COEFFICIENTS ARE
C     STORED IN THE MATRIX C AND TEUS THRU THE SUCCESSIVE ITERATIONS
C     THE MATRIX C IS USED.
C
C
C     THE VECTOR B REPRESENTS THE RIGHT HAND SIDE CONSTANT VECTOR
C
C
      PSI(IM2,J)=A1
      PSI(I,JM2)=A2
      PSI(I,JP2)=A3
      PSI(IP2,J)=A4
      PSI(IM1,JM1)=A5
      PSI(IM1,J)=A6
      PSI(IM1,JP1)=A7
      PSI(I,JM1)=A8
      PSI(I,J)=A9
      PSI(I,JP1)=A10
      PSI(IP1,JM1)=A11
      PSI(IP1,J)=A12
      PSI(IP1,JP1)=A13
      B(L)=0.0
      IR=I
      JR=J
      IF(Z.LT.ZL.OR.Z.GT.ZR) GO TO 33
      R13=IN
      R15=IN
      IF(IM2.EQ.1) CALL SUBIM2(PSI,IR,JR,VZR,DY,R13,R15,B,L)
      IF(IP2.EQ.II) CALL SUBIP2(PSI,IR,JR,VZR,DY,B,L)
      IF(JP2.EQ.JJ) CALL SUBJP2(PSI,IR,JR,UYR,DZ,B,L,UZ,DY)
      GO TO 37
   33 CALL CURVE(IR,JR,2,Y,ZL,ZR,ZMAX,DY,DZ,VZR,VZB,VR,R13,R16,PSI,
     1N1,PI,II,H1,7,JJ,B,L,II)
      GO TO 95
   37 SUM=PSI(IM2,J)*UZ(IM2,J)+PSI(IP2,J)*UZ(IP2,J)+PSI(I,JP2)*UZ(I,JP2)
     1+PSI(I,JM2)*UZ(I,JM2)+PSI(IP1,JP1)*UZ(IP1,JP1)
     2+PSI(IM1,JM1)*UZ(IP1,JM1)+PSI(IM1,JP1)*UZ(IM1,JP1)
     3+PSI(I,JM1)*UZ(I,JM1)+PSI(IM1,J)*UZ(IM1,J)+PSI(IP1,J)*UZ(IP1,J)
```

```
   4+PSI(IP1,JM1)*UZ(IP1,JM1)+PSI(I,JP1)*UZ(I,JP1)
    C(L,1)=PSI(IP2,J)
    C(L,7)=PSI(IP1,JM1)
    C(L,8)=PSI(IP1,J)
    C(L,9)=PSI(IP1,JP1)
    C(L,14)=PSI(I,JM2)
    C(L,15)=PSI(I,JM1)
    C(L,16)=PSI(I,J)
    C(L,17)=PSI(I,JP1)
    C(L,18)=PSI(I,JP2)
    C(L,22)=PSI(IM1,JM1)
    C(L,23)=PSI(IM1,J)
    C(L,24)=PSI(IM1,JP1)
    C(L,30)=PSI(IM2,J)
    PSI(I,JM2)=0.0
    PSI(I,JM1)=0.0
    PSI(I,JP1)=0.0
    PSI(I,JP2)=0.0
    PSI(IP1,JM1)=0.0
    PSI(IP1,J)=0.0
    PSI(IP1,JP1)=0.0
    PSI(IM1,JM1)=0.0
    PSI(IM1,J)=0.0
    PSI(IM1,JP1)=0.0
     PSI(IP2,J)=0.0
    PSI(IM2,J)=0.0
46  IF(IM2.EQ.1)SUM=SUM+PSI(IP3,J)*UZ(IP3,J)+PSI(IP4,J)*
   1UZ(IP4,J)
    IF(IP2.EQ.II)  SUM=SUM+PSI(IM3,J)*UZ(IM3,J)+PSI(IM4,J)*
   1UZ(IM4,J)
    IF(JP2.EQ.JJ)  SUM=SUM+PSI(I,JM3)*UZ(I,JM3)+PSI(I,JM4)*UZ(I,JM4)
    IF(IM2.EQ.1)  GO TO 67
    IF(IP2.EQ.II)  GO TO 68
    IF(JP2.EQ.JJ)  GO TO 69
    GO TO 39
67  C(L,56)=PSI(IP3,J)
    C(L,57)=PSI(IP4,J)
    PSI(IP3,J)=0.0
    PSI(IP4,J)=0.0
    GO TO 39
68  IF(Z.LT.ZL.OR.Z.GT.ZR)  GO TO 39
    C(L,37)=PSI(IM3,J)
    C(L,44)=PSI(IM4,J)
    PSI(IM3,J)=0.0
    PSI(IM4,J)=0.0
    GO TO 39
69  C(L,58)=PSI(I,JM3)
    C(L,59)=PSI(I,JM4)
    PSI(I,JM3)=0.0
    PSI(I,JM4)=0.0
    GO TO 39
95  SUMIP1=0.0
    SUMI=0.0
    SUMIM1=0.0
    SUMIM2=0.0
    SUMIM3=0.0
    SUMIM4=0.0
    SUMIM5=0.0
    SUMIP2=0.0
    C(L,1)=PSI(IP2,J)
```

```
      C(L,8)=PSI(IP1,J)
      C(L,16)=PSI(I,J)
      C(L,23)=PSI(IM1,J)
      C(L,30)=PSI(IM2,J)
      IF(Z.GT.ZR) GO TO 97
C
C
C     LEFT END REGION
C
C
      C(L,2)=PSI(IP2,JP1)
      C(L,3)=PSI(IP2,JP2)
      C(L,4)=PSI(IP2,JP3)
      C(L,5)=PSI(IP2,JP4)
      C(L,6)=PSI(IP2,JP5)
      C(L,7)=PSI(IP1,JM1)
      C(L,9)=PSI(IP1,JP1)
      C(L,10)=PSI(IP1,JP2)
      C(L,11)=PSI(IP1,JP3)
      C(L,12)=PSI(IP1,JP4)
      C(L,13)=PSI(IP1,JP5)
      C(L,14)=PSI(I,JM2)
      C(L,15)=PSI(I,JM1)
      C(L,17)=PSI(I,JP1)
      C(L,18)=PSI(I,JP2)
      C(L,19)=PSI(I,JP3)
      C(L,20)=PSI(I,JP4)
      C(L,21)=PSI(IM1,JM2)
      C(L,22)=PSI(IM1,JM1)
      C(L,24)=PSI(IM1,JP1)
      C(L,25)=PSI(IM1,JP2)
      C(L,26)=PSI(IM1,JP3)
      C(L,27)=PSI(IM1,JP4)
   79 DO 81 M1=JM1,JP5
      SUMIP1=SUMIP1+UZ(IP1,M1)*PSI(IP1,M1)
   81 PSI(IP1,M1)=0.0
      DO 80 M1=J,JP5
      SUMIP2=SUMIP2+UZ(IP2,M1)*PSI(IP2,M1)
   80 PSI(IP2,M1)=0.0
      DO 82 M1=JM2,JP4
      IF(M1.EQ.J) GO TO 82
      SUMI=SUMI+UZ(I,M1)*PSI(I,M1)
      PSI(I,M1)=0.0
   82 CONTINUE
      DO 83 M1=JM2,JP4
      SUMIM1=SUMIM1+PSI(IM1,M1)*UZ(IM1,M1)
   83 PSI(IM1,M1)=0.0
      IF(IM1.EQ.2) GO TO 87
      C(L,28)=PSI(IM2,JM2)
      C(L,29)=PSI(IM2,JM1)
      C(L,31)=PSI(IM2,JP1)
      C(L,32)=PSI(IM2,JP2)
      C(L,33)=PSI(IM2,JP3)
      C(L,34)=PSI(IM2,JP4)
      IF(IM1.LE.3) GO TO 96
      C(L,35)=PSI(IM3,JM2)
      C(L,36)=PSI(IM3,JM1)
      C(L,37)=PSI(IM3,J)
      C(L,38)=PSI(IM3,JP1)
      C(L,39)=PSI(IM3,JP2)
```

```
      C(L,40)=PSI(IM3,JP3)
      C(L,41)=PSI(IM3,JP4)
      IF(IM1.LE.4) GO TO 96
      C(L,42)=PSI(IM4,JM2)
      C(L,43)=PSI(IM4,JM1)
      C(L,44)=PSI(IM4,J)
      C(L,45)=PSI(IM4,JP1)
      C(L,46)=PSI(IM4,JP2)
      C(L,47)=PSI(IM4,JP3)
      C(L,48)=PSI(IM4,JP4)
      IF(IM1.LE.5) GO TO 96
      C(L,49)=PSI(IM5,JM2)
      C(L,50)=PSI(IM5,JM1)
      C(L,51)=PSI(IM5,J)
      C(L,52)=PSI(IM5,JP1)
      C(L,53)=PSI(IM5,JP2)
      C(L,54)=PSI(IM5,JP3)
      C(L,55)=PSI(IM5,JP4)
   96 DO 86 M1=JM2,JP4
      SUMIM2=SUMIM2+PSI(IM2,M1)*UZ(IM2,M1)
      IF(IM1.LE.3) GO TO 84
      SUMIM3=SUMIM3+PSI(IM3,M1)*UZ(IM3,M1)
      IF(IM1.LE.4) GO TO 85
      SUMIM4=SUMIM4+UZ(IM4,M1)*PSI(IM4,M1)
      IF(IM1.LE.5) GO TO 88
      SUMIM5=SUMIM5+UZ(IM5,M1)*PSI(IM5,M1)
      PSI(IM2,M1)=0.0
      PSI(IM3,M1)=0.0
      PSI(IM4,M1)=0.0
      PSI(IM5,M1)=0.0
      GO TO 86
   88 PSI(IM2,M1)=0.0
      PSI(IM3,M1)=0.0
      PSI(IM4,M1)=0.0
      GO TO 86
   84 PSI(IM2,M1)=0.0
      GO TO 86
   85 PSI(IM2,M1)=0.0
      PSI(IM3,M1)=0.0
   86 CONTINUE
   87 SUM=SUMIP1+SUMI+SUMIM1+SUMIM2+SUMIM3+SUMIM4+SUMIM5+SUMIP2
      GO TO 46
C
C
C     RIGHT END REGION
C
C
   97 C(L,2)=PSI(IP2,JM1)
      C(L,3)=PSI(IP2,JM2)
      C(L,4)=PSI(IP2,JM3)
      C(L,5)=PSI(IP2,JM4)
      C(L,6)=PSI(IP2,JM5)
      C(L,7)=PSI(IP1,JP1)
      C(L,9)=PSI(IP1,JM1)
      C(L,10)=PSI(IP1,JM2)
      C(L,11)=PSI(IP1,JM3)
      C(L,12)=PSI(IP1,JM4)
      C(L,13)=PSI(IP1,JM5)
      C(L,14)=PSI(I,JP2)
      C(L,15)=PSI(I,JP1)
```

```
      C(L,17)=PSI(I,JM1)
      C(L,18)=PSI(I,JM2)
      C(L,19)=PSI(I,JM3)
      C(L,20)=PSI(I,JM4)
      C(L,21)=PSI(IM1,JP2)
      C(L,22)=PSI(IM1,JP1)
      C(L,24)=PSI(IM1,JM1)
      C(L,25)=PSI(IM1,JM2)
      C(L,26)=PSI(IM1,JM3)
      C(L,27)=PSI(IM1,JM4)
   91 DO 51 M1=JM5,JP1
      SUMIP1=SUMIP1+UZ(IP1,M1)*PSI(IP1,M1)
   51 PSI(IP1,M1)=0.0
      DO 50 M1=JM5,J
      SUMIP2=SUMIP2+UZ(IP2,M1)*PSI(IP2,M1)
   50 PSI(IP2,M1)=0.0
      DO 52 M1=JM4,JP2
      IF(M1.EQ.J) GO TO 52
      SUMI=SUMI+UZ(I,M1)*PSI(I,M1)
      PSI(I,M1)=0.0
   52 CONTINUE
      DO 53 M1=JM4,JP2
      SUMIM1=SUMIM1+PSI(IM1,M1)*UZ(IM1,M1)
   53 PSI(IM1,M1)=0.0
      IF(IM1.EQ.2) GO TO 87
      C(L,28)=PSI(IM2,JP2)
      C(L,29)=PSI(IM2,JP1)
      C(L,31)=PSI(IM2,JM1)
      C(L,32)=PSI(IM2,JM2)
      C(L,33)=PSI(IM2,JM3)
      C(L,34)=PSI(IM2,JM4)
      IF(IM1.LE.3) GO TO 98
      C(L,35)=PSI(IM3,JP2)
      C(L,36)=PSI(IM3,JP1)
      C(L,37)=PSI(IM3,J)
      C(L,38)=PSI(IM3,JM1)
      C(L,39)=PSI(IM3,JM2)
      C(L,40)=PSI(IM3,JM3)
      C(L,41)=PSI(IM3,JM4)
      IF(IM1.LE.4) GO TO 98
      C(L,42)=PSI(IM4,JP2)
      C(L,43)=PSI(IM4,JP1)
      C(L,44)=PSI(IM4,J)
      C(L,45)=PSI(IM4,JM1)
      C(L,46)=PSI(IM4,JM2)
      C(L,47)=PSI(IM4,JM3)
      C(L,48)=PSI(IM4,JM4)
      IF(IM1.LE.5) GO TO 98
      C(L,49)=PSI(IM5,JP2)
      C(L,50)=PSI(IM5,JP1)
      C(L,51)=PSI(IM5,J)
      C(L,52)=PSI(IM5,JM1)
      C(L,53)=PSI(IM5,JM2)
      C(L,54)=PSI(IM5,JM3)
      C(L,55)=PSI(IM5,JM4)
   98 DO 56 M1=JM4,JP2
      SUMIM2=SUMIM2+PSI(IM2,M1)*UZ(IM2,M1)
      IF(IM1.LE.3) GO TO 54
      SUMIM3=SUMIM3+PSI(IM3,M1)*UZ(IM3,M1)
      IF(IM1.LE.4) GO TO 55
```

```
      SUMIM4=SUMIM4+UZ(IM4,M1)*PSI(IM4,M1)
      IF(IM1.LE.5) GO TO 58
      SUMIM5=SUMIM5+UZ(IM5,M1)*PSI(IM5,M1)
      PSI(IM2,M1)=0.0
      PSI(IM3,M1)=0.0
      PSI(IM4,M1)=0.0
      PSI(IM5,M1)=0.0
      GO TO 56
   58 PSI(IM2,M1)=0.0
      PSI(IM3,M1)=0.0
      PSI(IM4,M1)=0.0
      GO TO 56
   54 PSI(IM2,M1)=0.0
      GO TO 56
   55 PSI(IM2,M1)=0.0
      PSI(IM3,M1)=0.0
   56 CONTINUE
      GO TO 87
C
C
C
C     SUCCESSIVE ITERATIONS BEGIN HERE
C
C
   20 IF(Z.LT.ZL) GO TO 133
      IF(Z.GT.ZR) GO TO 143
      IF(IM2.EQ.1.OR.IP2.EQ.II.OR.JP2.EQ.JJ) GO TO 137
      GO TO 21
  133 SUM=C(L,1)*UZ(IP2,J)+C(I,2)*UZ(IP2,JP1)+C(L,3)*UZ(IP2,JP2)
     1+UZ(IP2,JP3)*C(I,4)+UZ(IP2,JP4)*C(L,5)+C(L,6)*UZ(IP2,JP5)
     2+UZ(IP1,JM1)*C(L,7)+UZ(IP1,J)*C(L,8)+UZ(IP1,JP1)*C(L,9)
     3+UZ(IP1,JP2)*C(L,10)+UZ(IP1,JP3)*C(L,11)+UZ(IP1,JP4)*C(L,12)
     4+UZ(IP1,JP5)*C(L,13)+UZ(I,JM2)*C(I,14)+UZ(I,JM1)*C(L,15)+
     5UZ(I,JP1)*C(L,17)+UZ(I,JP2)*C(I,18)+UZ(I,JP3)
     6*C(L,19)+UZ(I,JP4)*C(I,20)+UZ(IM1,JM2)*C(L,21)+UZ(IM1,JM1)*C(L,22)
     7+UZ(IM1,J)*C(L,23)+UZ(IM1,JP1)*C(L,24)+UZ(IM1,JP2)*C(L,25)+
     8UZ(IM1,JP3)*C(L,26)+UZ(IM1,JP4)*C(L,27)+UZ(IM2,JM2)*C(L,28)
     9+UZ(IM2,JM1)*C(L,29)+UZ(IM2,J)*C(I,30)+UZ(IM2,JP1)*C(L,31)
     8+UZ(IM2,JP2)*C(L,32)+UZ(IM2,JP3)*C(L,33)+UZ(IM2,JP4)*C(L,34)
      IF(IM1.LE.3) GO TO 153
      SUM=SUM+UZ(IM3,JM2)*C(I,35)+UZ(IM3,JM1)*C(L,36)+UZ(IM3,J)*
     1C(L,37)+UZ(IM3,JP1)*C(I,38)+UZ(IM3,JP2)*C(L,39)
     2+UZ(IM3,JP3)*C(L,40)+UZ(IM3,JP4)*C(L,41)
      IF(IM1.LE.4) GO TO 153
      SUM=SUM+UZ(IM4,JM2)*C(I,42)+UZ(IM4,JM1)*C(L,43)+UZ(IM4,J)*
     1C(L,44)+UZ(IM4,JP1)*C(I,45)+UZ(IM4,JP2)*C(L,46)+UZ(IM4,JP3)
     2*C(L,47)+UZ(IM4,JP4)*C(I,48)
      IF(IM1.LE.5) GO TO 153
      SUM=SUM+UZ(IM5,JM2)*C(I,49)+UZ(IM5,JM1)*C(L,50)+UZ(IM5,J)*
     1C(L,51)+UZ(IM5,JP1)*C(I,52)+UZ(IM5,JP2)*C(L,53)+UZ(IM5,JP3)*
     2C(L,54)+UZ(IM5,JP4)*C(I,55)
      GO TO 153
  143 SUM=UZ(IP2,J)*C(L,1)+UZ(IP2,JM1)*C(L,2)+UZ(IP2,JM2)*C(L,3)
     1+UZ(IP2,JM3)*C(L,4)+UZ(IP2,JM4)*C(L,5)+C(L,6)*UZ(IP2,JM5)
     2+UZ(IP1,JP1)*C(L,7)+UZ(IP1,J)*C(L,8)+UZ(IP1,JM1)*C(L,9)
     3+UZ(IP1,JM2)*C(L,10)+UZ(IP1,JM3)*C(L,11)+UZ(IP1,JM4)*C(L,12)
     4+UZ(IP1,JM5)*C(L,13)+UZ(I,JP2)*C(I,14)+UZ(I,JP1)*C(L,15)+
     5UZ(I,JM1)*C(L,17)+UZ(I,JM2)*C(I,18)+UZ(I,JM3)
     6*C(L,19)+UZ(I,JM4)*C(I,20)+UZ(IM1,JP2)*C(L,21)+UZ(IM1,JP1)*C(L,22)
     7+UZ(IM1,J)*C(L,23)+UZ(IM1,JM1)*C(I,24)+UZ(IM1,JM2)*C(L,25)+
```

```
     8UZ(IM1,JM3)*C(L,26)+UZ(IM1,JM4)*C(L,27)+UZ(IM2,JP2)*C(L,28)
     9+UZ(IM2,JP1)*C(L,29)+UZ(IM2,J)*C(L,30)+UZ(IM2,JM1)*C(L,31)
     8+UZ(IM2,JM2)*C(L,32)+UZ(IM2,JM3)*C(L,33)+UZ(IM2,JM4)*C(L,34)
      IF(IM1.LE.3) GO TO 153
      SUM=SUM+UZ(IM3,JP2)*C(L,35)+UZ(IM3,JP1)*C(L,36)+
     1UZ(IM3,J)*C(L,37)+UZ(IM3,JM1)*C(L,38)+UZ(IM3,JM2)*C(L,39)+
     2UZ(IM3,JM3)*C(L,40)+UZ(IM3,JM4)*C(L,41)
      IF(IM1.LE.4) GO TO 153
      SUM=SUM+UZ(IM4,JP2)*C(L,42)+UZ(IM4,JP1)*C(L,43)+UZ(IM4,J)*
     1C(L,44)+UZ(IM4,JM1)*C(L,45)+UZ(IM4,JM2)*C(L,46)+
     2UZ(IM4,JM3)*C(L,47)+UZ(IM4,JM4)*C(L,48)
      IF(IM1.LE.5) GO TO 153
      SUM=SUM+UZ(IM5,JP2)*C(L,49)+UZ(IM5,JP1)*C(L,50)+UZ(IM5,J)*
     1C(L,51)+UZ(IM5,JM1)*C(L,52)+UZ(IM5,JM2)*C(L,53)+UZ(IM5,JM3)*
     2C(L,54)+UZ(IM5,JM4)*C(L,55)
      GO TO 153
  137 SUM=C(L,1)*UZ(IP2,J)+UZ(IP1,JM1)*C(L,7)
     1+UZ(IP1,J)*C(L,8)+UZ(IP1,JP1)*C(L,9)+UZ(I,JM2)*C(L,14)
     2+UZ(I,JM1)*C(L,15)+UZ(I,JP1)*C(I,17)
     3+UZ(I,JP2)*C(L,18)+UZ(IM1,JM1)*C(L,22)+UZ(IM1,J)*C(L,23)+
     4UZ(IM1,JP1)*C(L,24)+UZ(IM2,J)*C(I,30)
  153 IF(IM2.EQ.1) SUM=SUM+C(I,56)*UZ(IP3,J)+C(L,57)*UZ(IP4,J)
      IF(JP2.EQ.JJ) SUM=SUM+C(L,58)*UZ(I,JM3)+C(L,59)*UZ(I,JM4)
      IF(Z.LT.ZL.OR.Z.GT.ZR) GO TO 154
      IF(IP2.EQ.II) SUM=SUM+C(I,37)*UZ(IM3,J)+UZ(IM4,J)*C(L,44)
  154 TOTAL=(E(L)-SUM)/C(L,16)
      GO TO 38
   39 TOTAL=(E(L)-SUM)/PSI(I,J)
      PSI(I,J)=0.0
   38 UZ(I,J)=ALPHA*TOTAL+(1.-ALPHA)*UZ(I,J)
   21 CONTINUE
      IF(MM.LT.ITB5) GO TO 10
      WRITE(6,16) MM
   16 FORMAT(1X,'ITERATION # =',I4,//////)
      CALL TPRINT(JJ1,II1,UZ,6)
   10 CONTINUE
      RETURN
      END
C
C
C     THIS SUBROUTINE COMPUTES Z COORDINATE ON THE CURVE FOR
C     A GIVEN Y COORDINATE
C
C     D22=THE DIMENSIONLESS BARREL DIAMETER
C
C
      SUBROUTINE ZZ2(YY,ZZ)
      COMMON/ELK/CESTRF,T,D22
      ZZ=(YY*(D22-YY))**0.5
      ZZ=ZZ/COS(T)
      RETURN
      END
C
C
C
C     THIS SUBROUTINE COMPUTES Y COORDINATE ON THE CURVE FOR
C     A GIVEN Z COORDINATE.
C
C     R2=DIMENSIONLESS BARREL RADIUS
C
```

```
C
      SUBROUTINE YMAX(YY,ZZ)
      COMMON/ELK/CESTRF,T,D22
      R2=D22/2.
      Z=ZZ*COS(T)
      YY=R2-((R2+Z)*(R2-Z))**C.5
      RETURN
      END
C
C
C     THE FOLLOWING SUBROUTINES CURVE3,CURVE4,CURVE5,AND
C     CURVE6 HELP TO SHIFT THE POINT (I,J) AT THE DESIRED LOCATION
C     SO THAT THE FICTICIOUS POINTS CAN BE ELIMINATED IN TERMS OF
C     NON-FICTICIOUS POINTS.
C
C
C
      SUBROUTINE CURVE3(I,J,Z,ZR)
      I=I+1
      IF(Z.LT.ZR) J=J+1
      IF(Z.GT.ZR) J=J-1
      RETURN
      END
      SUBROUTINE CURVE4(I,J,Z,ZR)
      I=I-1
      IF(Z.LT.ZR) J=J-1
      IF(Z.GT.ZR) J=J+1
      RETURN
      END
      SUBROUTINE CURVE5(I,J,Z,ZR)
      I=I+2
      IF(Z.LT.ZR) J=J+1
      IF(Z.GT.ZR) J=J-1
      RETURN
      END
      SUBROUTINE CURVE6 (I,J,Z,ZR)
      I=I-1
      IF(Z.LT.ZR) J=J-2
      IF(Z.GT.ZR) J=J+2
      RETURN
      END
C
C
C     THIS SUBROUTINE PRINTSOUT THE MATRIX SSS IN THE DESIRED FORMAT
C
C
      SUBROUTINE IPRINT(JJ1,II1,SSS,N)
      DIMENSION SSS(33,33)
      NCOL=JJ1-1
      NPGS=(NCOL-1)/10+1
      DO 82 I=1,NPGS
      WRITE(N,16)
   16 FORMAT(1X,///////)
      J1=(I-1)*10+2
      J2=J1+9
      IF(I.EQ.NPGS) J2=JJ1
      DO 83 K=2,II1
      M=II1+2-K
      WRITE(N,81) (SSS(M,J),J=J1,J2)
   81 FORMAT(1X,10G13.6)
```

```
   83 CONTINUE
   82 CONTINUE
      RETURN
      END
C
CC
CC
C     THE SUBROUTINE CURVE1 ELIMINATES FICTICIOUS POINTS IN
C     TERMS OF THE NON-FICTICIOUS POINTS OF THE SAME COLUMN OR
C     OF THOSE WITH THE SAME Z-COORDINATE VALUE IMPLICITLY.
CC
C     POINTS A1 AND A2 ARE FICTICIOUS POINTS.
CC
CC
C
      SUBROUTINE CURVE1 (R13,Y13,VR,DY,Y,I,J,PSI,N2,N3,R2,R16,M,B,L)
      DIMENSION PSI(33,33),H(6),G(6),B(156)
      COMMON/ELK/CESIRF,T,D22
      IR=I
      JR=J
      IF(R13.LE.N2) F=N2-R13
      IF(R13.GT.N2) F=N3-R13
      TANT2=((2.*R2-Y13)*Y13)/((R2-Y13)/COS(T))**2
      COSN13=1./(1.+TANT2)**0.5
      EC=DY*VR*COSN13*COS(T)
      IF(R13.GE.N2) I=I+1
      IM1=I-1
      IM2=I-2
      IM3=I-3
      CALL CALGH(F,EC,G,H,IM3,IM2)
      IM4=I-4
      IP1=I+1
      IP2=I+2
      A1=PSI(IP1,J)
      A2=PSI(IP2,J)
      IF(N2.EQ.1) GO TO 12
      IF(R13.GE.N2) A2=0.0
      IF(M.EQ.7) A2=0.0
      GO TO 13
   12 IF(R16.GE.N3) GO TO 14
      IF(R13.LT.N2) A2=A2/2.
      IF(R13.LT.N2) A1=0.0
      IF(R13.LT.N2.AND.M.EQ.5) A1=PSI(IP1,J)
      IF(R13.GE.N2) A2=0.0
      IF(R13.GE.N2) A1=A1/2.
      GO TO 13
   14 IF(R13.LT.N2.AND.M.EQ.5) GO TO 17
      IF(R13.LT.N2) A2=A2/2.
      IF(R13.GE.N2) A2=0.0
      IF(R13.GE.N2) A1=A1/2.
      IF(R13.GE.N2.AND.M.EQ.5) A1=PSI(IP1,J)
   13 PSI(I,J)=PSI(I,J)+A1*G(1)-A2*H(1)
      PSI(IM1,J)=PSI(IM1,J)+A1*G(2)-A2*H(2)
      PSI(IM2,J)=PSI(IM2,J)+A1*G(3)-A2*H(3)
      IF(I.LE.3) GO TO 10
      PSI(IM3,J)=PSI(IM3,J)+A1*G(4)-A2*H(4)
      IF(I.LE.4) GO TO 10
      PSI(IM4,J)=PSI(IM4,J)+A1*G(5)-A2*H(5)
   10 B(L)=B(L)-A1*G(6)+A2*H(6)
      GO TO 20
```

```
   17 A2=0.0
      GO TO 13
   20 PSI(IP1,J)=0.0
      PSI(IP2,J)=0.0
      I=IR
      J=JR
      RETURN
      END
C
C
C
C     THIS SUBROUTINE ELIMINATES FICTICIOUS POINTS IN TERMS OF
C     NON-FICTICICUS POINTS OF THE SAME ROW OR OF THE Y COORDINATE
C     VALUE IMPLICITLY.
C
C     POINTS A1 AND A2 ARE FICTICICUS POINTS.
C
C
C
      SUBROUTINE CURVE2 (R16,Z16,VF,DZ,Z,ZR,I,J,PSI,N2,N3,R2,R13,M,K1,
     1K2,B,L)
      DIMENSION PSI(33,33),E(156),H(6),G(6)
      COMMON/ELK/CESIRF,T,D22
      IF(R16.LE.N2) F=N2-R16
      IF(R16.GT.N2) F=N3-R16
      TANT2=(Z16*COS(T)*COS(I))**2/(R2*R2-(Z16*COS(T))**2)
      SINE16=(TANT2/(1.+TANT2))**0.5
      EC=DZ*VF*SINE16
      N5=150
      CALL CALGH(F,EC,G,H,N5,N5)
      IR=I
      JR=J
      IF(R16.GE.N2.AND.Z.GT.ZR) J=J+1
      IF(R16.GE.N2.AND.Z.LT.ZR) J=J-1
      IF(Z.GT.ZR) GO TO 10
      JP1=J+1
      JP2=J+2
      JP3=J+3
      JP4=J+4
      JM1=J-1
      JM2=J-2
   11 A1=PSI(I,JM1)
      A2=PSI(I,JM2)
      IF(N2.EQ.1) GO TO 12
      IF(R16.GE.N2) A2=0.0
      IF(K2.EQ.7) A2=0.0
      GO TO 13
   12 IF(R13.GE.N3) GO TO 14
      IF(R16.LT.N2) A2=A2/2.
      IF(R16.LT.N2.AND.M.EQ.9) GO TO 13
      IF(R16.LT.N2) A1=0.0
      IF(R16.GE.N2) A2=0.0
      IF(R16.GE.N2) A1=A1/2.
      IF(R16.GE.N2.AND.M.EQ.5) A1=PSI(I,JM1)
      GO TO 13
   14 IF(R16.LT.N2.AND.M.EQ.5) GO TO 16
      IF(R16.LT.N2) A2=A2/2.
      IF(R16.GE.N2) A2=0.0
      IF(R16.GE.N2) A1=A1/2.
      IF(R16.GE.N2.AND.M.EQ.5) A1=PSI(I,JM1)
```

```
   13 PSI(I,J)=PSI(I,J)+A1*G(1)-A2*H(1)
      PSI(I,JP1)=PSI(I,JP1)+A1*G(2)-A2*H(2)
      PSI(I,JP2)=PSI(I,JP2)+A1*G(3)-A2*H(3)
      PSI(I,JP3)=PSI(I,JP3)+A1*G(4)-A2*H(4)
      PSI(I,JP4)=PSI(I,JP4)+A1*G(5)-A2*H(5)
      B(L)=B(I)-A1*G(6)+A2*E(6)
      GO TO 20
   10 JP1=J-1
      JP2=J-2
      JP3=J-3
      JP4=J-4
      JM1=J+1
      JM2=J+2
      GO TO 11
   16 A2=0.0
      GO TO 13
   20 IF(K1.EQ.5) GO TO 30
      PSI(I,JM1)=0.0
      PSI(I,JM2)=0.0
   30 IF(K2.EQ.6) PSI(I,JM1)=0.0
      I=IR
      J=JR
      RETURN
      END
C
C
C
C
C     SUBROUTINE CURVE DEALS WITH FICTICICUS AS WELL AS
C     NON-FICTICICUS POINTS LYING IN THE END REGIONS.
C     THIS SUBROUTINE SYSTEMATICALLY FIGURES OUT THE WAY THE
C     FICTICICUS POINTS TO BE ELIMINATED
C      IMPLICITLY AND ACCORDINGLY DOES IT WITH
C     THE HELP OF SUBROUTINES CURVE1,CURVE2,CURVE3,CURVE4,CURVE5,CURVE6.
C
C
C     R13,R15,R17,R19,R21,R23,R25 ARE DIMENSIONLESS Y DISTANCES
C     OF MESH POINTS SURROUNDING THE CENTER POINT FROM THE CURVE
C     BOUNDARY.
C
C     R14,R16,R18,R20,R22,R24,R26,R28 ARE DIMENSIONLESS
C     Z DISTANCES OF MESH POINTS SURROUNDING THE CENTER POINT FROM THE
C     CURVE BOUNDARY.
C
C
C
      SUBROUTINE CURVE(I,J,Z,Y,ZI,ZR,ZMAX,DY,DZ,VZR,VZE,VR,R13,R16,PSI,
     1N1,PI,II,H1,K1,JJ,E,I,KK)
      DIMENSION PSI(33,33),E(156),H(6),G(6),RR(122,16)
      COMMON/ELK/CESTRF,T,D22
      N1=1
      N2=2
      N3=3
      N4=4
      NO=0
      N6=II-I-1
      II2=II-2
      II3=II-3
      R2=D22/2.
      ZMAX1=ZMAX+DZ
```

```
      ZMAX2=ZMAX+2.*DZ
      IM2=I-2
      IP2=I+2
      Y=IM2*DY
      IF(K1.EQ.7) GO TO 29
      ZOLD=Z
      IF(Z.GT.ZB) Z=PI/CCS(T)-Z
      CALL ZZZ(Y,Z16)
      P16=Z-Z16
      R16=P16/DZ
      Y14=Y+DY
      CALL ZZZ(Y14,Z14)
      P14=Z-Z14
      R14=P14/DZ
      Y18=Y14+DY
      CALL ZZZ(Y18,Z18)
      P18=Z-Z18
      R18=P18/DZ
      Y20=Y-DY
      CALL ZZZ(Y20,Z20)
      P20=Z-Z20
      R20=P20/DZ
      Y22=Y20-DY
      IF(Y22.LT.N0) GO TO 24
      CALL ZZZ(Y22,Z22)
      R22=(Z-Z22)/DZ
      Y24=Y22-DY
      IF(Y24.LT.N0) GO TO 25
      CALL ZZZ(Y24,Z24)
      R24=(Z-Z24)/DZ
      Y26=Y24-DY
      IF(Y26.LT.N0) GO TO 26
      CALL ZZZ(Y26,Z26)
      R26=(Z-Z26)/DZ
      Y28=Y26-DY
      IF(Y28.LT.N0) GO TO 27
      CALL ZZZ(Y28,Z28)
      R28=(Z-Z28)/DZ
      GO TO 19
   27 R28=N2+0.1
      GO TO 19
   26 R28=N2+0.1
      R26=R28
      GO TO 19
   25 R28=N2+0.1
      R26=R28
      R24=R28
      GO TO 19
   24 R28=N2+0.1
      R26=R28
      R24=R28
      R22=R28
   19 IF(Z.GE.ZMAX2) GO TO 20
      Z17=Z-2.*DZ
      CALL YMAX(Y17,Z17)
      P17=Y17-Y
      R17=P17/DY
      IF(Z.GE.ZMAX1) GO TO 21
      Z15=Z-DZ
      CALL YMAX(Y15,Z15)
```

```
      P15=Y15-Y
      R15=P15/DY
      IF(Z.GE.ZMAX) GO TO 22
      CALL YMAX(Y13,Z)
      P13=Y13-Y
      R13=P13/DY
      Z19=Z+DZ
      IF(Z19.GE.ZMAX) GO TO 23
      CALL YMAX(Y19,Z19)
      P19=Y19-Y
      R19=P19/DY
      Z21=Z19+DZ
      IF(Z21.GE.ZMAX) GO TO 11
      CALL YMAX(Y21,Z21)
      R21=(Y21-Y)/DY
      Z23=Z21+DZ
      IF(Z23.GE.ZMAX) GO TO 12
      CALL YMAX(Y23,Z23)
      R23=(Y23-Y)/DY
      Z25=Z23+DZ
      IF(Z25.GE.ZMAX) GO TO 13
      CALL YMAX(Y25,Z25)
      R25=(Y25-Y)/DY
      GO TO 30
   11 R21=N6+0.1
      R23=R21
      R25=R21
      GO TO 30
   12 R23=N6+0.1
      R25=R23
      GO TO 30
   13 R25=N6+C.1
      GO TO 30
   23 R19=N6+C.1
      R21=R19
      R23=R19
      R25=R19
      GO TO 30
   22 R13=N6+0.1
      R19=R13
      R21=R13
      R23=R13
      R25=R13
      GO TO 30
   21 R13=N6+0.1
      R15=R13
      R19=R13
      R21=R13
      R23=R13
      R25=R13
      GO TO 30
   20 R13=N6+C.1
      R15=R13
      R17=R13
      R19=R13
      R21=R13
      R23=R13
      R25=R13
   30 Z=ZOLD
      IF(K1.EQ.10) GO TO 31
```

```
      K1=5
      IF(R16.LT.N1.OR.R13.LT.N1) GO TO 100
      IF(R16.GE.N3.AND.R13.GE.N3.AND.R17.GE.N1.AND.R18.GE.N1
     1.AND.IM2.NE.N1) GO TO 28
      KK=KK+1
      RR(KK,1)=R13
      RR(KK,2)=R14
      RR(KK,3)=R15
      RR(KK,4)=R16
      RR(KK,5)=R17
      RR(KK,6)=R18
      RR(KK,7)=R19
      RR(KK,8)=R20
      RR(KK,9)=R21
      RR(KK,10)=R22
      RR(KK,11)=R23
      RR(KK,12)=R24
      RR(KK,13)=R25
      RR(KK,14)=R26
      RR(KK,15)=0.0
      RR(KK,16)=R28
      GO TO 100
   28 K1=6
      GO TO 100
   29 KK=KK+1
      R13=RR(KK,1)
      R14=RR(KK,2)
      R15=RR(KK,3)
      R16=RR(KK,4)
      R17=RR(KK,5)
      R18=RR(KK,6)
      R19=RR(KK,7)
      R20=RR(KK,8)
      R21=RR(KK,9)
      R22=RR(KK,10)
      R23=RR(KK,11)
      R24=RR(KK,12)
      R25=RR(KK,13)
      R26=RR(KK,14)
      R27=RR(KK,15)
      R28=RR(KK,16)
      I1=I
      J1=J
   31 IF(R16.LT.N1.OR.R13.LT.N1) GO TO 50
      IF(I.GE.II3.AND.R13.GE.N6) GO TO 36
C
C  SET #1 BEGINS HERE
C
C    (1)
C
      IF(R13.GE.N3.AND.R18.GE.N1.AND.R14.GE.N2) GO TO 35
C
C    (2)
C
      IF(R13.GE.N3.AND.R18.GE.N1) CALL CURVE3(I,J,Z,ZR)
      IF(R13.GE.N3.AND.R18.GE.N1) CALL CURVE2(R14,Z14,VR,DZ,Z,ZR,I,J,
     1PSI,N1,N2,R2,R13,5,4,4,B,L)
      I=I1
      J=J1
      IF(R13.GE.N3.AND.R18.GE.N1) GO TO 35
```

```
C
C    (3)
C
      IF(R13.GE.N3.AND.R14.GE.N2) CALL CURVE5 (I,J,Z,ZR)
      IF(R13.GE.N3.AND.R14.GE.N2) CALL CURVE2(R18,Z18,VR,DZ,Z,ZR,I,J,
     1PSI,N1,N2,R2,R13,5,4,4,E,L)
      I=I1
      J=J1
      IF(R13.GE.N3.AND.R18.GE.N2) GO TO 35
C
C    (4)
C
      IF(R13.GE.N3.AND.R14.GE.N1) CALL CURVE5 (I,J,Z,ZR)
      IF(R13.GE.N3.AND.R14.GE.N1) CALL CURVE2(R18,Z18,VR,DZ,Z,ZR,I,J,
     1PSI,N1,N2,R2,R13,5,4,4,E,L)
      I=I1
      J=J1
      IF(R13.GE.N3.AND.R14.GE.N1) CALL CURVE3(I,J,Z,ZR)
      IF(R13.GE.N3.AND.R14.GE.N1) CALL CURVE2(R14,Z14,VR,DZ,Z,ZR,I,J,
     1PSI,N1,N2,R2,R13,4,5,4,E,L)
      I=I1
      J=J1
C
C    (5)
C
      IF(R13.GE.N3.AND.R14.LT.N1) CALL CURVE5(I,J,Z,ZR)
      IF(R13.GE.N3.AND.R14.LT.N1) CALL CURVE2(R18,Z18,VR,DZ,Z,ZR,I,J,
     1PSI,N1,N2,R2,R13,5,4,4,E,L)
      I=I1
      J=J1
      IF(R13.GE.N3.AND.R14.LT.N1) CALL CURVE3(I,J,Z,ZR)
      IF(R13.GE.N3.AND.R14.LT.N1) CALL CURVE2(R14,Z14,VR,DZ,Z,ZR,I,J,
     1PSI,N1,N2,R2,R13,4,5,6,E,L)
      I=I1
      J=J1
      IF(R13.GE.N3) GO TO 35
C
C    (6)
C
      IF(R13.GE.N2.AND.R14.GE.N2) CALL CURVE1(R13,Y13,VR,DY,Y,I,J,
     1PSI,N2,N3,R2,R16,4,B,L)
      IF(R13.GE.N2.AND.R14.GE.N2) GO TO 35
C
C    (7)
C
      IF(R13.GE.N2.AND.R18.GE.N1.AND.R14.GE.N1) CALL CURVE1
     1(R13,Y13,VR,DY,Y,I,J,PSI,N2,N3,R2,R16,4,B,L)
      IF(R13.GE.N2.AND.R18.GE.N1.AND.R14.GE.N1) CALL CURVE3(I,J,Z,ZR)
      IF(R13.GE.N2.AND.R18.GE.N1.AND.R14.GE.N1) CALL CURVE2
     1(R14,Z14,VR,DZ,Z,ZR,I,J,PSI,N1,N2,R2,R13,5,4,4,B,L)
      I=I1
      J=J1
C
C    (8)
C
      IF(R13.GE.N2.AND.R18.LT.N1.AND.R14.GE.N1) CALL CURVE1
     1(R13,Y13,VR,DY,Y,I,J,PSI,N2,N3,R2,R16,4,B,L)
      IF(R13.GE.N2.AND.R18.LT.N1.AND.R14.GE.N1) CALL CURVE3(I,J,Z,ZR)
      IF(R13.GE.N2.AND.R18.LT.N1.AND.R14.GE.N1) CALL CURVE2
     1(R14,Z14,VR,DZ,Z,ZR,I,J,PSI,N1,N2,R2,R13,4,5,4,B,L)
```

```
      I=I1
      J=J1
C
C    (9)
C
      IF(R13.GE.N2.AND.R14.LT.N1)CALL CURVE1
     1(R13,Y13,VR,DY,Y,I,J,PSI,N2,N3,R2,R16,4,B,L)
      IF(R13.GE.N2.AND.R14.LT.N1) CALL CURVE3(I,J,Z,ZR)
      IF(R13.GE.N2.AND.R14.LT.N1) CALL CURVE2
     1(R14,Z14,VR,DZ,Z,ZR,I,J,PSI,N1,N2,R2,R13,9,5,6,B,L)
      I=I1
      J=J1
      IF(R13.GE.N2) GO TO 35
C
C    (10)
C
      IF(R14.GE.N2) CALL CURVE1
     1(R13,Y13,VR,DY,Y,I,J,PSI,N2,N3,R2,R16,4,B,L)
      IF(R14.GE.N2) GO TO 35
C
C    (11)
C
      IF(R14.GE.N1) CALL CURVE3(I,J,Z,ZR)
      IF(R14.GE.N1) CALL CURVE2
     1(R14,Z14,VR,DZ,Z,ZR,I,J,PSI,N1,N2,R2,R13,4,5,4,B,L)
      I=I1
      J=J1
      IF(R14.GE.N1) CALL CURVE1
     1(R13,Y13,VR,DY,Y,I,J,PSI,N2,N3,R2,R16,4,B,L)
C
C    (12)
C
      IF(R14.LT.N1) CALL CURVE1
     1(R13,Y13,VR,DY,Y,I,J,PSI,N2,N3,R2,R16,4,B,L)
      IF(R14.LT.N1) CALL CURVE3(I,J,Z,ZR)
      IF(R14.LT.N1) CALL CURVE2
     1(R14,Z14,VR,DZ,Z,ZR,I,J,PSI,N1,N2,R2,R13,4,5,6,B,L)
      I=I1
      J=J1
C
C    SET#1 ENDS HERE
C
C    SET#2 BEGINS HERE
C
C    (1)
C
   35 IF(R16.GE.N3.AND.R17.GE.N1.AND.R15.GE.N2) GO TO 37
C
C    (2)
C
   41 IF(R16.GE.N3.AND.R17.GE.N1) CALL CURVE4(I,J,Z,ZR)
      IF(R16.GE.N3.AND.R17.GE.N1) CALL CURVE1
     1(R15,Y15,VR,DY,Y,I,J,PSI,N1,N2,R2,R16,5,B,L)
      I=I1
      J=J1
      IF(R16.GE.N3.AND.R17.GE.N1) GO TO 37
C
C    (3)
C
      IF(R16.GE.N3.AND.R15.GE.N2) CALL CURVE6(I,J,Z,ZR)
```

```
      IF(R16.GE.N3.AND.R15.GE.N2) CALL CURVE1
     1(R17,Y17,VR,DY,Y,I,J,PSI,N1,N2,R2,R16,5,B,L)
      I=I1
      J=J1
      IF(R16.GE.N3.AND.R15.GE.N2) GO TO 37
C
C    (4)
C
   42 IF(R16.GE.N3.AND.R15.GE.N1) CALL CURVE6(I,J,Z,ZR)
      IF(R16.GE.N3.AND.R15.GE.N1) CALL CURVE1
     1(R17,Y17,VR,DY,Y,I,J,PSI,N1,N2,R2,R16,5,B,L)
      I=I1
      J=J1
      IF(I.EQ.II2) GO TO 37
      IF(R16.GE.N3.AND.R15.GE.N1) CALL CURVE4(I,J,Z,ZR)
      IF(R16.GE.N3.AND.R15.GE.N1) CALL CURVE1
     1(R15,Y15,VR,DY,Y,I,J,PSI,N1,N2,R2,R16,4,B,L)
      I=I1
      J=J1
C
C    (5)
C
   43 IF(R16.GE.N3.AND.R15.LT.N1) CALL CURVE6(I,J,Z,ZR)
      IF(R16.GE.N3.AND.R15.LT.N1) CALL CURVE1
     1(R17,Y17,VR,DY,Y,I,J,PSI,N1,N2,R2,R16,5,B,L)
      I=I1
      J=J1
      IF(R16.GE.N3.AND.R15.LT.N1) CALL CURVE4(I,J,Z,ZR)
      IF(R16.GE.N3.AND.R15.LT.N1) CALL CURVE1
     1(R15,Y15,VR,DY,Y,I,J,PSI,N1,N2,R2,R16,4,B,L)
      I=I1
      J=J1
      IF(R16.GE.N3) GO TO 37
C
C    (6)
C
   44 IF(R16.GE.N2.AND.R15.GE.N2) CALL CURVE2(R16,Z16,VR,DZ,Z,ZR,I,J,
     1PSI,N2,N3,R2,R13,4,4,4,B,L)
      IF(R16.GE.N2.AND.R15.GE.N2) GO TO 37
C
C    (7)
C
   49 IF(R16.GE.N2.AND.R15.GE.N1.AND.R17.GE.N1) CALL CURVE2
     1(R16,Z16,VR,DZ,Z,ZR,I,J,PSI,N2,N3,R2,R13,4,4,4,B,L)
      IF(I.EQ.II2) GO TO 37
      IF(R16.GE.N2.AND.R15.GE.N1.AND.R17.GE.N1) CALL CURVE4(I,J,Z,ZR)
      IF(R16.GE.N2.AND.R15.GE.N1.AND.R17.GE.N1) CALL CURVE1
     1(R15,Y15,VR,DY,Y,I,J,PSI,N1,N2,R2,R16,5,B,L)
      I=I1
      J=J1
C
C    (8)
C
   45 IF(R16.GE.N2.AND.R15.GE.N1.AND. R17.LT.1)CALL CURVE2
     1(R16,Z16,VR,DZ,Z,ZR,I,J,PSI,N2,N3,R2,R13,4,4,4,B,L)
      IF(I.EQ.II2) GO TO 37
      IF(R16.GE.N2.AND.R15.GE.N1.AND. R17.LT.1)CALL CURVE4(I,J,Z,ZR)
      IF(R16.GE.N2.AND.R15.GE.N1.AND. R17.LT.1)CALL CURVE1
     1(R15,Y15,VR,DY,Y,I,J,PSI,N1,N2,R2,R16,4,B,L)
      I=I1
```

```
      J=J1
C
C    (9)
C
   71 IF(R16.GE.N2.AND.R15.LT.N1) CALL CURVE2
     1(R16,Z16,VR,DZ,Z,ZR,I,J,PSI,N2,N3,R2,R13,4,4,4,B,L)
   46 IF(R16.GE.N2.AND.R15.LT.N1) CALL CURVE4(I,J,Z,ZR)
      IF(R16.GE.N2.AND.R15.LT.N1) CALL CURVE1
     1(R15,Y15,VR,DY,Y,I,J,PSI,N1,N2,R2,R16,4,B,L)
      I=I1
      J=J1
      IF(R16.GE.N2) GO TO 37
C
C    (10)
C
      IF(R15.GE.N2) CALL CURVE2
     1(R16,Z16,VR,DZ,Z,ZR,I,J,PSI,N2,N3,R2,R13,4,4,4,B,L)
      IF(R15.GE.N2) GO TO 37
C
C    (11)
C
   33 IF(R15.GE.N1) CALL CURVE4(I,J,Z,ZR)
      IF(R15.GE.N1) CALL CURVE1
     1(R15,Y15,VR,DY,Y,I,J,PSI,N1,N2,R2,R16,4,B,L)
      I=I1
      J=J1
   47 IF(R15.GE.N1) CALL CURVE2
     1(R16,Z16,VR,DZ,Z,ZR,I,J,PSI,N2,N3,R2,R13,4,4,4,B,L)
      IF(I.EQ.II2) GO TO 37
C
C    (12)
C
   72 IF(R15.LT.N1) CALL CURVE2
     1(R16,Z16,VR,DZ,Z,ZR,I,J,PSI,N2,N3,R2,R13,4,4,4,B,L)
   48 IF(R15.LT.N1) CALL CURVE4(I,J,Z,ZR)
      IF(R15.LT.N1) CALL CURVE1
     1(R15,Y15,VR,DY,Y,I,J,PSI,N1,N2,R2,R16,4,B,L)
      I=I1
      J=J1
      GO TO 37
C
C    SET #2 ENDS HERE
C
   36 IF(I.EQ.II2) GO TO 38
C
C    SET#3 BEGINS HERE
C
C    (1)
C
      IF(R16.GE.N3.AND.R17.GE.N1.AND.R15.GE.N2) GO TO 37
C
C    (2)
C
      IF(R16.GE.N3.AND.R17.GE.N1) GO TO 41
C
C    (3)
C
      IF(R16.GE.N3.AND.R15.GE.N2) CALL CURVE3(I,J,Z,ZR)
      IF(R16.GE.N3.AND.R15.GE.N2) CALL CURVE2
     1(R14,Z14,VR,DZ,Z,ZR,I,J,PSI,N1,N2,R2,R13,5,4,4,B,L)
```

```
      I=I1
      J=J1
      IF(R16.GE.N3.AND.B15.GE.N2) CALL CURVE6(I,J,Z,ZR)
      IF(R16.GE.N3.AND.B15.GE.N2) CALL CURVE1
     1(R17,Y17,VR,DY,Y,I,J,PSI,N1,N2,B2,R16,5,B,L)
      I=I1
      J=J1
      IF(R16.GE.N3.AND.B15.GE.N2) GC TC 37
C
C     (4)
C
      IF(R16.GE.N3) CALL CURVE3(I,J,Z,ZR)
      IF(R16.GE.N3) CALL CURVE2
     1(R14,Z14,VR,DZ,Z,ZR,I,J,PSI,N1,N2,R2,R13,4,5,4,B,L)
      I=I1
      J=J1
      IF(R16.GE.N3.AND.B15.GE.N1) GC TO 42
C
C     (5)
C
      IF(R16.GE.N3.AND.B15.LT.N1) CALL CURVE3(I,J,Z,ZR)
      IF(R16.GE.N3.AND.B15.LT.N1) CALL CURVE2
     1(R14,Z14,VR,DZ,Z,ZR,I,J,PSI,N1,N2,R2,R13,4,5,6,B,L)
      I=I1
      J=J1
      IF(R16.GE.N3.AND.B15.LT.N1) GC TO 43
      IF(R16.GE.N3) GO TO 37
C
C     (6)
C
      IF(R17.GE.N1) CALL CURVE2
     1(R16,Z16,VR,DZ,Z,ZR,I,J,PSI,N2,N3,R2,R13,4,4,4,B,L)
      IF(R17.GE.N1) GO TO 37
C
C     (7)
C
      IF(R16.GE.N2.AND.B15.GE.N2) CALL CURVE3 (I,J,Z,ZR)
      IF(R16.GE.N2.AND.B15.GE.N2) CALL CURVE2
     1(R14,Z14,VR,DZ,Z,ZR,I,J,PSI,N1,N2,R2,R13,5,4,4,B,L)
      I=I1
      J=J1
      IF(R16.GE.N2.AND.B15.GE.N2) GC TO 44
C
C     (8) & (9)
C
      IF(R16.GE.N2) CALL CURVE3 (I,J,Z,ZR)
      IF(R16.GE.N2.AND.B15.GE.N1) CALL CURVE2
     1(R14,Z14,VR,DZ,Z,ZR,I,J,PSI,N1,N2,R2,R13,4,5,4,B,L)
      IF(R16.GE.N2.AND.B15.LT.N1) CALL CURVE2
     1(R14,Z14,VR,DZ,Z,ZR,I,J,PSI,N1,N2,R2,R13,4,5,6,B,L)
      I=I1
      J=J1
      IF(R16.GE.N2.AND.B15.GE.N1) GC TO 45
      IF(R16.GE.N2.AND.B15.LT.N1) GC TO 71
      IF(R16.GE.N2) GO TO 37
C
C     (10)
C
      IF(R15.GE.N2) CALL CURVE2
     1(R16,Z16,VR,DZ,Z,ZR,I,J,PSI,N2,N3,R2,R13,4,4,4,B,L)
```

```
      IF(R15.GE.N2) CALL CURVE3 (I,J,Z,ZR)
      IF(R15.GE.N2) CALL CURVE2
     1(R14,Z14,VR,DZ,Z,ZR,I,J,PSI,N1,N2,R2,R13,5,4,4,B,L)
      I=I1
      J=J1
      IF(R15.GE.N2) GO TO 37
C
C    (11) & (12)
C
      CALL CURVE3(I,J,Z,ZR)
      IF(R15.GE.N1) CALL CURVE2
     1(R14,Z14,VR,DZ,Z,ZR,I,J,PSI,N1,N2,R2,R13,4,5,4,B,L)
      IF(R15.LT.N1) CALL CURVE2
     1(R14,Z14,VR,DZ,Z,ZR,I,J,PSI,N1,N2,R2,R13,4,5,6,B,L)
      I=I1
      J=J1
      IF(R15.GE.N1) GO TO 38
      IF(R15.LT.N1) GO TO 72
C
C    SET #3 ENDS HERE
C
C    SET #4 BEGINS HERE
C
C    (1)
C
   38 IF(R16.GE.N3.AND.R17.GE.N1) GO TO 37
C
C    (2)
C
      IF(R16.GE.N3.AND.R15.GE.N1) GO TO 42
C
C    (3)
C
      IF(R16.GE.N3.AND.R15.LT.N1) GO TO 43
      IF(R16.GE.N3) GO TO 37
C
C    (4)
C
      IF(R16.GE.N2.AND.R17.GE.N1) GO TO 49
      IF(R17.GE.N1) GO TO 37
C
C    (5)
C
      IF(R16.GE.N2.AND.R15.GE.N1) GO TO 45
C
C    (6)
C
      IF(R16.GE.N2.AND.R15.LT.N1) GO TO 71
      IF(R16.GE.N2) GO TO 37
C
C    (7)
C
      IF(R15.GE.N1) GO TO 47
C
C    (8)
C
      IF(R15.LT.N1) GO TO 72
C
C    SET #4 ENDS HERE
C
```

```
C    SET #5 BEGINS HERE
C
   37 IF(R20.GE.N2) GO TO 99
      I=I-1
      CALL CURVE2(R20,Z20,VR,DZ,Z,ZR,I,J,PSI,N2,N3,R2,R13,4,4,7,B,L)
      I=I1
      IF(R22.GE.N2) GO TO 99
      I=I-2
      CALL CURVE2(R22,Z22,VR,DZ,Z,ZR,I,J,PSI,N2,N3,R2,R13,4,4,7,B,L)
      I=I1
      IF(R24.GE.N2) GO TO 99
      I=I-3
      CALL CURVE2(R24,Z24,VR,DZ,Z,ZR,I,J,PSI,N2,N3,R2,R13,4,4,7,B,L)
      I=I1
      IF(R26.GE.N2) GO TO 99
      I=I-4
      CALL CURVE2(R26,Z26,VR,DZ,Z,ZR,I,J,PSI,N2,N3,R2,R13,4,4,7,B,L)
      I=I1
      IF(R28.GE.N2) GO TO 99
      I=I-5
      CALL CURVE2(R28,Z28,VR,DZ,Z,ZR,I,J,PSI,N2,N3,R2,R13,4,4,7,B,L)
      I=I1
C
C    SET #5 ENDS HERE
C
C    SET #6 BEGINS HERE
C
   99 IF(I.EQ.II2) GO TO 39
      IF(R19.GE.N2) GO TO 39
      IF(Z.LT.ZL) J=J+1
      IF(Z.GT.ZR) J=J-1
      CALL CURVE1(R19,Y19,VR,DY,Y,I,J,PSI,N2,N3,R2,R16,7,B,L)
      J=J1
      IF(R21.GE.N2) GO TO 39
      IF(Z.LT.ZL) J=J+2
      IF(Z.GT.ZR) J=J-2
      CALL CURVE1(R21,Y21,VR,DY,Y,I,J,PSI,N2,N3,R2,R16,7,B,L)
      J=J1
      IF(R23.GE.N2) GO TO 39
      IF(Z.LT.ZL) J=J+3
      IF(Z.GT.ZR) J=J-3
      CALL CURVE1(R23,Y23,VR,DY,Y,I,J,PSI,N2,N3,R2,R16,7,B,L)
      J=J1
      IF(R25.GE.N2) GO TO 39
      IF(Z.LT.ZL) J=J+4
      IF(Z.GT.ZR) J=J-4
      CALL CURVE1(R25,Y25,VR,DY,Y,I,J,PSI,N2,N3,R2,R16,7,B,L)
      J=J1
C
C    SET #6 ENDS HERE
C
   39 IF(IM2.EQ.1) CALL SUBIM2(PSI,I,J,VZB,DY,R13,R15,B,L)
      IF(IP2.EQ.II) CALL SUBIP2(PSI,I,J,VZB,DY,B,L)
   50 IF(K1.EQ.10) GO TO 60
      GO TO 100
   60 IF(ABS(R16).GE.N1.AND.ABS(R13).GE.N1) GO TO 100
C
C
C
C
```

```
C     COMPUTATION OF STREAM FUNCTION VALUES OF THE FICTICIOUS POINTS
C     WHICH ARE WITH IN ONE MESH LENGTH FROM THE BOUNDARY.
C
C     THIS COMPUTATION BEGINS AFTER ALL NON-FICTICIOUS POINTS
C     ARE COMPUTED BY ITERATIVE METHODS USING THE SUBROUTINE STRMFN.
C
C
C
      I1=I
      J1=J
      NO=0
      IF(ABS(R16).GE.N1) SUMZ=0.0
      IF(ABS(R16).GE.N1) GO TO 81
      IF(R16.GT.NO.AND.Z.LT.ZR) J=J+1
      IF(R16.GT.NO.AND.Z.GT.ZR) J=J-1
      IF(R16.LE.NO.AND.Z.LT.ZR) J=J+2
      IF(R16.LE.NO.AND.Z.GT.ZR) J=J-2
      JP4=J+4
      TANT2=(Z16*COS(T)*COS(T))**2/(R2*R2-(Z16*COS(T))**2)
      SINE16=(TANT2/(1.+TANT2))**0.5
      EC=DZ*VR*SINE16
      IF(R16.GT.NO) F=1.-R16
      IF(R16.LE.NO) F=-R16
      N5=150
      CALL CALGH(F,EC,G,H,N5,N5)
      IF(Z.GT.ZR) GO TO 70
   59 SUMZ=0.0
      DO 61 K=J,JP4
      N=K-J+1
      IF(Z.GT.ZR) N=JP4-K+1
      IF(R16.GT.NO) SUMZ=SUMZ+G(N)*PSI(I,K)
      IF(R16.LE.NO) SUMZ=SUMZ-H(N)*PSI(I,K)
   61 CONTINUE
      IF(R16.GT.NO) SUMZ=SUMZ+G(6)
      IF(R16.LE.NO) SUMZ=SUMZ-H(6)
      SUMZ=SUMZ/2.
      GO TO 81
   70 JP4=J
      J=J-4
      GO TO 59
   81 J=J1
      IF(ABS(R13).GE.N1) SUMY=0.0
      IF(ABS(R13).GE.N1) GO TO 86
      IF(R13.GT.NO) I=I-1
      IF(R13.LE.NO) I=I-2
      IM4=I-4
      IM3=I-3
      IM2=I-2
      IM1=I-1
      TANT2=((2.*R2-Y13)*Y13)/((R2-Y13)/COS(T))**2
      COSN13=1./(1.+TANT2)**0.5
      EC=DY*VR*COSN13*COS(T)
      IF(R13.GT.NO) F=1.-R13
      IF(R13.LE.NO) F=-R13
      IF(IM2.LT.1) GO TO 80
      CALL CALGH(F,EC,G,H,IM3,IM2)
      SUMY=0.0
      IF(IM2.EQ.1) PSI(IM2,J)=2.*DY*VZR+PSI(I,J)
      IF(IM3.EQ.1) PSI(IM3,J)=3.*DY*VZR+3.*PSI(IM1,J)-0.5*PSI(I,J)
      IF(IM4.EQ.1) PSI(IM4,J)=4.*DY*VZR+6.*PSI(IM2,J)-2.*PSI(IM1,J)+0.33
```

```
     1*PSI(I,J)
      IF(IM2.EQ.1) IM4=IM2
      IF(IM3.EQ.1) IM4=IM3
      DO 85 K=IM4,I
      N=I-K+1
      IF(R13.GT.NC) SUMY=SUMY+G(N)*PSI(K,J)
      IF(R13.LE.NC) SUMY=SUMY-H(N)*PSI(K,J)
   85 CONTINUE
      IF(R13.GT.NO) SUMY=SUMY+G(6)
      IF(R13.LE.NC) SUMY=SUMY-H(6)
      SUMY=SUMY/2.
      I=I1
      IF(ABS(R16).GE.N1) SUMY=2.*SUMY
      PSI(I,J)=SUMY+SUM2
      GO TO 100
   80 I=I1
      IF(R13.GE.NO) SUMY=-DY*VZR/2.
      IF(R13.LT.NC) SUMY=-R13*VR*CCS(T)*CCSN13/2.
      IF(ABS(R16).GT.N1) SUMY=2.*SUMY
      PSI(I,J)=(SUMZ+SUMY)
      GO TO 100
   86 PSI(I,J)=2.*(SUMY+SUM2)
  100 RETURN
      END
C
C
C
      SUBROUTINE CALGH (F,EC,G,H,IM3,IM2)
C
C
      DIMENSION G(6),H(6)
      COMMON/ELK/CESTRF,T,D22
      EPS=10.**(-38)
      F1=F-1.
      F2=F-2.
      F3=F-3.
      F4=F-4.
      F5=F-5.
      A1=F
      A2=F*F1/2.
      A3=A2*F2/3.
      A4=A3*F3/4.
      A5=A4*F4/5.
      A6=A5*F5/6.
      IF(IM2.EQ.1) A5=0.
      IF(IM3.EQ.1.OR.IM2.EQ.1) A6=0.
      B1=1.-A1+A2-A3+A4-A5+A6
      B2=A1-2.*A2+3.*A3-4.*A4+5.*A5-6.*A6
      B3=A2-3.*A3+6.*A4-10.*A5+15.*A6
      B4=A3-4.*A4+10.*A5-20.*A6
      B5=A4-5.*A5+15.*A6
      B6=A5-6.*A6
      B7=A6
      C1=(F+F1)/2.
      C2=(F*F1+F*F2+F1*F2)/6.
      C3=(F*F1*F2+F*F1*F3+F*F2*F3+F1*F2*F3)/24.
      C4=(F*F1*F2*F3+F*F1*F2*F4+F*F1*F3*F4+F*F2*F3*F4+F1*F2*F3*F4)/120.
      C5=(F*F1*F2*F3*F4+F*F1*F2*F3*F5+F*F1*F2*F4*F5+F*F1*F3*F4*F5+
     1F*F2*F3*F4*F5+F1*F2*F3*F4*F5)/720.
      IF(IM3.EQ.1.OR.IM2.EQ.1)C5=0.0
```

```
      IF(IM2.EQ.1) C4=0.0
      D1=-1.+C1-C2+C3-C4+C5
      D2=1.-2.*C1+3.*C2-4.*C3+5.*C4-6.*C5
      D3=C1-3.*C2+6.*C3-10.*C4+15.*C5
      D4=C2-4.*C3+10.*C4-20.*C5
      D5=C3-5.*C4+15.*C5
      D6=C4-6.*C5
      D7=C5
      IF(ABS(F1).LT.EPS) GO TO 10
      EO=B2/B1-D2/D1
   11 E1=D3/D1-B3/B1
      E2=D4/D1-B4/B1
      E3=D5/D1-B5/B1
      E4=D6/D1-B6/B1
      E5=D7/D1-B7/B1
      E6=EC/D1+CBSTRF/B1
      IF(ABS(F1).LT.EPS) E6=EC/D1+(D2/D1)*CBSTRF
      GG=B2/B1
      IF(ABS(F1).LT.EPS) GO TO 12
      G(1)=E1/EO
      G(2)=E2/EO
      G(3)=E3/EO
      G(4)=E4/EO
      G(5)=E5/EO
      G(6)=E6/EO
      H(1)=B3/B1+GG*G(1)
      H(2)=B4/B1+GG*G(2)
      H(3)=B5/B1+GG*G(3)
      H(4)=B6/B1+GG*G(4)
      H(5)=B7/B1+GG*G(5)
      H(6)=GG*G(6)-CBSTRF/E1
      GO TO 13
   10 B1=1.0
      B2=0.0
      B3=0.0
      B4=0.0
      B5=0.0
      B6=0.0
      B7=0.0
      GO TO 11
   12 H(1)=E1
      H(2)=E2
      H(3)=E3
      H(4)=E4
      H(5)=E5
      H(6)=E6
      DO 6 I=1,6
    6 G(I)=0.0
   13 RETURN
      END
C
C
C
      SUBROUTINE SUBIM2(PSI,I,J,VZ,DY,R13,R15,B,L)
C
C
C     THIS SUBROUTINE ELIMINATES FICTICIOUS POINTS WHICH ARE
C     OUTSIDE THE LOWER BOUNDARY(SCREW ROOT) IMPLICITLY.
C
C
```

```
      DIMENSION PSI(33,33),E(156)
      IM2=I-2
      IM1=I-1
      IP1=I+1
      IP2=I+2
      IP3=I+3
      IP4=I+4
      N1=1
      N2=2
      N3=3
      N4=4
      N5=5
      A1=PSI(IM2,J)
      IF(R13.LT.N5) GO TO 10
      IF(R15.LT.N4) GO TO 10
      PSI(IM1,J)=PSI(IM1,J)-7.7*A1
      PSI(I,J)=PSI(I,J)+15.*A1
      PSI(IP1,J)=PSI(IP1,J)-10.*A1
      PSI(IP2,J)=PSI(IP2,J)+5.*A1
      PSI(IP3,J)=PSI(IP3,J)-1.5*A1
      PSI(IP4,J)=PSI(IP4,J)+0.2*A1
      B(L)=B(I)-6.*DY*VZ*A1
      GO TO 20
   10 IF(R13.LT.N4) GO TO 11
      IF(R15.LT.N3) GO TO 11
        PSI(IM1,J)=PSI(IM1,J)-5.416*A1
      PSI(I,J)=PSI(I,J)+10.*A1
      PSI(IP1,J)=PSI(IP1,J)-5.*A1
      PSI(IP2,J)=PSI(IP2,J)+1.666*A1
      PSI(IP3,J)=PSI(IP3,J)-0.25*A1
      B(L)=B(L)-5.*DY*VZ*A1
      GO TO 20
   11 IF(R13.LT.N3) GO TO 12
      IF(R15.LT.N2) GO TO 12
      PSI(IM1,J)=PSI(IM1,J)-3.333*A1
      PSI(I,J)=PSI(I,J)+6.*A1
      PSI(IP1,J)=PSI(IP1,J)-2.*A1
      PSI(IP2,J)=PSI(IP2,J)+0.333*A1
      B(L)=B(L)-4.*DY*VZ*A1
      GO TO 20
   12 IF(R13.LT.N2) GO TO 13
      IF(R15.LT.N1) GO TO 13
      PSI(IM1,J)=PSI(IM1,J)-1.5*A1
      PSI(I,J)=PSI(I,J)+3.*A1
      PSI(IP1,J)=PSI(IP1,J)-0.5*A1
      B(L)=B(L)-3.*DY*VZ*A1
      GO TO 20
   13 PSI(I,J)=PSI(I,J)+A1
      B(L)=B(L)-2.*DY*VZ*A1
   20 PSI(IM2,J)=0.0
      RETURN
      END
C
CC
CC
      SUBROUTINE  SUBIP2 (PSI,I,J,VZ,DY,B,L)
C
CC
CC
C     FICTICIOUS POINTS LYING OUTSIDE THE UPPER BOUNDARY(BARREL)
```

```
C     ARE ELIMINATED IMPLICITLY IN TERMS OF THOSE LYING INSIDE THE
CC    BOUNDARY.
C
C
C
      DIMENSION PSI(33,33),B(156)
      IP2=I+2
      IP1=I+1
      IM1=I-1
      IM2=I-2
      IM3=I-3
      IM4=I-4
      A2=PSI(IP2,J)
      PSI(IP1,J)=PSI(IP1,J)-7.7*A2
      PSI(I,J)=PSI(I,J)+15.*A2
      PSI(IM1,J)=PSI(IM1,J)-10.*A2
      PSI(IM2,J)=PSI(IM2,J)+5.*A2
      PSI(IM3,J)=PSI(IM3,J)-1.5*A2
      PSI(IM4,J)=PSI(IM4,J)+0.2*A2
      B(L)=B(I)+6.*DY*VZ*A2
      PSI(IP2,J)=0.0
      RETURN
      END
C
CC
      SUBROUTINE SUBJP2(PSI,I,J,DY,DZ,B,L,UZ,DY)
C
CC
C
      DIMENSION PSI(33,33),B(156),UZ(33,33)
      N1=1
      N2=2
      N3=3
      N4=4
      N5=5
      JP1=J+1
      JP2=J+2
      JM1=J-1
      JM2=J-2
      JM3=J-3
      JM4=J-4
      Z=JM2*DZ
      Y=(I-2)*DY
      CALL ZZZ(Y,Z16)
      R16=(Z-Z16)/DZ
      Y14=Y+DY
      CALL ZZZ(Y14,Z14)
      R14=(Z-Z14)/DZ
      A4=PSI(I,JP2)
      IF(R16.LT.N5) GO TO 10
      IF(R14.LT.N4) GO TO 10
      PSI(I,J)=PSI(I,J)+15.*A4
      PSI(I,JM1)=PSI(I,JM1)-10.*A4
      PSI(I,JM2)=PSI(I,JM2)+5.*A4
      PSI(I,JM3)=PSI(I,JM3)-1.5*A4
      PSI(I,JM4)=PSI(I,JM4)+0.2*A4
      B(L)=B(I)-6.*DZ*DY*A4+7.7*UZ(I,JP1)*A4
      GO TO 20
   10 IF(R16.LT.N4) GO TO 11
```

```
      IF(R14.IT.N3) GO TO 11
      PSI(I,J)=PSI(I,J)+10.*A4
      PSI(I,JM1)=PSI(I,JM1)-5.*A4
      PSI(I,JM2)=PSI(I,JM2)+1.666*A4
      PSI(I,JM3)=PSI(I,JM3)-0.25*A4
      B(L)=B(L)-5.*DZ*UY*A4+5.416*UZ(I,JP1)*A4
      GO TO 20
   11 IF(R16.IT.N3) GO TO 12
      IF(R14.IT.N2) GO TO 12
      PSI(I,J)=PSI(I,J)+6.*A4
      PSI(I,JM1)=PSI(I,JM1)-2.*A4
      PSI(I,JM2)=PSI(I,JM2)+0.333*A4
      B(L)=B(L)-4.*DZ*UY*A4+3.3333*UZ(I,JP1)*A4
      GO TO 20
   12 IF(R16.IT.N2) GO TO 13
      IF(R14.IT.N1) GO TO 13
      PSI(I,J)=PSI(I,J)+3.*A4
      PSI(I,JM1)=PSI(I,JM1)-0.5*A4
      B(L)=B(L)-3.*DZ*UY*A4+1.5*UZ(I,JP1)*A4
      GO TO 20
   13 PSI(I,J)=PSI(I,J)+A4
      B(L)=B(L)-2.*DZ*UY*A4
   20 PSI(I,JP2)=0.0
      RETURN
      END
C
C
C
C
      SUBROUTINE VELCTY(UZ,UY,VZR,VZB,IN2,JN2,II1,JJ1,DY,DZ,UYZ,ANGLE,
     1PSI,ZMAX,PI,IDZ)
C
C
C     THE VELOCITY COMPONENTS UZ,UY AT EACH MESH POINT ARE COMPUTED
C     FROM THE KNOWN STREAM FUNCTION VALUES AT THOSE POINTS.
C
C     FURTHER THE RESULTANT VELOCITY AND ITS DIRECTION AT EACH MESH
C     POINT IS COMPUTED.
C
C
      DIMENSION PSI(33,33),UZ(33,33),UY(33,33),UYZ(33,33),ANGLE(33,33)
      COMMON/ELK/CESTRF,I,I22
      EPS=10.**(-20)
      DO 10 K=2,JJ1
      UZ(2,K)=VZR
      UY(2,K)=0.0
      UYZ(2,K)=VZR
      ANGLE(2,K)=0.0
      UZ(II1,K)=VZB
      UY(II1,K)=0.0
      UYZ(II1,K)=VZB
   10 ANGLE(II1,K)=0.0
      IF(IDZ.NE.1) GO TO 12
      DO 11 I=2,II1
   11 UZ(I,JJ1)=0.0
      GO TO 14
   12 DO 13 I=2,II1
      UYZ(I,JJ1)=UZ(I,JJ1)
   13 ANGLE(I,JJ1)=0.0
   14 NO=0
```

```
      JJR=JJ1
      N1=1
      R2=0.75
      NM1=-1
      ZR=PI/CCS(T)-ZMAX
      J1=ZMAX/DZ
      DO 30 I=3,IN2
      IP1=I+1
      IP2=I+2
      IP3=I+3
      IP4=I+4
      IP5=I+5
      IM1=I-1
      IM2=I-2
      IM3=I-3
      IM4=I-4
      IM5=I-5
      DO 30 J=3,JN2
      JM5=J-5
      JM4=J-4
      JM3=J-3
      JM2=J-2
      JM1=J-1
      JP1=J+1
      JP2=J+2
      JP3=J+3
      JP4=J+4
      JP5=J+5
      Z=JM2*DZ
      Y=IM2*DY
      IF(Z.GT.ZR) Z=PI/CCS(T)-Z
      IF(Z.GE.ZMAX) GO TO 25
      CALL ZZZ(Y,Z16)
      P16=Z-Z16
      R16=P16/DZ
      CALL YMAX(Y13,Z)
      P13=Y13-Y
      R13=P13/DY
      NR13=R13+1
      IF(R13.LE.NM1.AND.R16.LE.NM1) GO TO 30
      IF(IDZ.NE.N1) GO TO 24
      IF(R16.LE.NC.AND.R16.GT.NM1) JJR=JJ1-J+2
   24 IF(R16.LT.NC.AND.R13.LT.NC) GO TO 30
      IF(R13.GT.NO) IIR=I+NR13
   25 IF(JP5.LE.JJR) UY(I,J)=(-PSI(I,JM1)-7.7*PSI(I,J)+15.*PSI(I,JP1)-
     110.*PSI(I,JP2)+5.*PSI(I,JP3)-1.5*PSI(I,JP4)+0.2*PSI(I,JP5))/(6.*DZ
     2)
      IF(JP5.GT.JJR) UY(I,J)=(PSI(I,JP1)+7.7*PSI(I,J)-15.*PSI(I,JM1)+10.
     1*PSI(I,JM2)-5.*PSI(I,JM3)+1.5*PSI(I,JM4)-0.2*PSI(I,JM5))/(6.*DZ)
      IF(Z.LT.ZMAX) GO TO 31
   32 IF(IP5.LE.II1) UZ(I,J)=(PSI(IM1,J)+7.7*PSI(I,J)-15.*PSI(IP1,J)+10.
     1*PSI(IP2,J)-5.*PSI(IP3,J)+1.5*PSI(IP4,J)-0.2*PSI(IP5,J))/(6.*DY)
      IF(IP5.GT.II1) UZ(I,J)=(-PSI(IP1,J)-7.7*PSI(I,J)+15.*PSI(IM1,J)-
     110.*PSI(IM2,J)+5.*PSI(IM3,J)-1.5*PSI(IM4,J)+0.2*PSI(IM5,J))/(6.*DY
     2)
      GO TO 38
   31 IF(IP5.LT.IIR) GO TO 32
      IF(IM5.GE.2) UZ(I,J)=(-PSI(IP1,J)-7.7*PSI(I,J)+15.*PSI(IM1,J)-
     110.*PSI(IM2,J)+5.*PSI(IM3,J)-1.5*PSI(IM4,J)+0.2*PSI(IM5,J))/(6.*DY
     2)
```

```
      IF(IM5.GE.2) GO TC 38
      IUP=IIR-I
      IDOWN=I-2
      IF(IUP.GT.IDOWN) GC TO 36
      IF(IM2.EQ.1) UZ(I,J)=(-PSI(IP1,J)+PSI(IM1,J))/(2.*DY)
      IF(IM3.EQ.1) UZ(I,J)=(-PSI(IP1,J)-1.5*PSI(I,J)+3.*PSI(IM1,J)-
     10.5*PSI(IM2,J))/(3.*DY)
      IF(IM4.EQ.1) UZ(I,J)=(-PSI(IP1,J)-3.333*PSI(I,J)+6.*PSI(IM1,J)
     1-2.*PSI(IM2,J)+0.333*PSI(IM3,J))/(4.*DY)
      IF(IM5.EQ.1) UZ(I,J)=(-PSI(IP1,J)-(65./12.)*PSI(I,J)+10.*PSI(IM1,J
     1)-5.*PSI(IM2,J)+1.666*PSI(IM3,J)-C.25*PSI(IM4,J))/(5.*DY)
      GO TO 38
   36 IF(IP2.EQ.IIR) UZ(I,J)=(PSI(IM1,J)-PSI(IP1,J))/(2.*DY)
      IF(IP3.EQ.IIR) UZ(I,J)=(PSI(IM1,J)+1.5*PSI(I,J)-3.*PSI(IP1,J)+0.5*
     1PSI(IP2,J))/(3.*DY)
      IF(IP4.EQ.IIR) UZ(I,J)=(PSI(IM1,J)+3.333*PSI(I,J)-6.*PSI(IP1,J)+
     12.*PSI(IP2,J)-0.333*PSI(IP3,J))/(4.*DY)
      IF(IP5.EQ.IIR) UZ(I,J)=(PSI(IM1,J)+(65./12.)*PSI(I,J)-10.*PSI(IP1,
     1J)+5.*PSI(IP2,J)-1.666*PSI(IP3,J)+0.25*PSI(IP4,J))/(5.*DY)
   38 UYZ(I,J)=(UZ(I,J)**2+UY(I,J)**2)**0.5
      IF(ABS(UZ(I,J)).LT.EPS) GC TO 30
      ANGLE(I,J)=ATAN(UY(I,J)/UZ(I,J))*(180./3.1415)
   30 CONTINUE
      WRITE(6,40)
   40 FORMAT('1',10X,'Z-DIRECTICNAI VELCCITY',///)
      CALL TPRINT(JJ1,II1,UZ,6)
      WRITE(8,40)
      CALL TPRINT(JJ1,II1,UZ,8)
      WRITE(6,41)
   41 FORMAT('1',10X,'Y-DIRECTICNAI VELOCITY',///)
      CALL TPRINT(JJ1,II1,UY,6)
      WRITE(8,41)
      CALL TPRINT(JJ1,II1,UY,8)
      WRITE(6,42)
   42 FORMAT('1',10X,'RESULTANT VELCCITY',///)
      CALL TPRINT(JJ1,II1,UYZ,6)
      WRITE(6,43)
   43 FORMAT('1',10X,'DIRECTICN OF RESULTANT VELOCITY',///)
      CALL TPRINT(JJ1,II1,ANGLE,6)
      WRITE(6,47)
   47 FORMAT('1',10X,'NET FICW IN Z DIRECTION',///)
      DO 50 J=3,JM2
      SUMZ=0.0
      Z=(J-2)*DZ
      IF(Z.GE.ZMAX) ITOP=IM2
      IF(Z.GE.ZMAX) GO TO 53
      CALL YMAX(Y13,Z)
      TANT2=((2.*R2-Y13)*Y13)/((R2-Y13)/COS(T))**2
      COSN13=1./(1.+TANT2)**0.5
      TOP=(Y13-DY)/DY
      TOP=TOP+2.
      ITOP=TOP
      R13=TOP-ITOP
   53 ITOP1=ITOP+N1
      IF(ITOP.LT.3) GO TO 52
      DO 51 I=3,ITOP
   51 SUMZ=SUMZ+UZ(I,J)
   52 IF(Z.LT.ZMAX) GO TO 54
      SUMZ=SUMZ+UZ(II1,J)/2.+UZ(2,J)/2.
      GO TO 56
```

```
   54 IF(ITOP.LT.2) SUMZ=SUMZ+UZ(2,J)/2.-R13*COS(T)*VR*COSN13/2.
      IF(ITOP.LT.2) GO TO 56
      SUMZ=SUMZ+UZ(ITOP1,J)*(R1+R13)/2.+
     1UZ(2,J)/2.-R13*COS(T)*VR*COSN13/2.
   56 SUMZ=SUMZ*DY
      WRITE(6,61) SUMZ
   61 FORMAT(10X,G13.6)
   50 CONTINUE
      RETURN
      END
C
CC
      SUBROUTINE PRESRE(PSI,UYZ,UZ,UY,DZ,DY,II,JJ,IN2,JN2,ZMAX)
C
CCC   THIS SUBROUTINE COMPUTES THE PRESSURE GRADIENT IN
CC    Z-DIRECTION AS WELL AS IN Y-DIRECTION AT EACH MESH POINT.
C
C
      DIMENSION PSI(33,33),UYZ(33,33),UZ(33,33),UY(33,33)
      COMMON/ELK/CESTRF,T,D22
      PI=3.1415927
      II1=II-1
      JJ1=JJ-1
      ZMAX1=ZMAX+DZ
      ZR=PI/COS(T)-ZMAX1
      N1=1
      DO 21 I=3,IN2
      DO 21 J=3,JN2
      JP1=J+1
      JM1=J-1
      IP1=I+1
      IM1=I-1
      Z=(J-2)*DZ
      Y=(I-2)*DY
      IF(Z.GT.ZR) Z=PI/COS(T)-2
      IF(Z.GE.ZMAX1) GO TO 20
      CALL ZZZ(Y,Z16)
      P16=Z-Z16
      R16=P16/DZ
      IF(Z.GT.ZMAX) R13=5.
      IF(Z.GT.ZMAX) GO TO 19
      CALL YMAX(Y13,Z)
      P13=Y13-Y
      R13=P13/DY
   19 IF(R13.LT.N1.OR.R16.LT.N1) GO TO 21
   20 PSI(I,J)=   (UZ(IP1,J)-2.*UZ(I,J)+UZ(IM1,J))/(DY**2)
     1+   (UZ(I,JP1)-2.*UZ(I,J)+UZ(I,JM1))/(DZ**2)
      UYZ(I,J)=   (UY(IP1,J)-2.*UY(I,J)+UY(IM1,J))/(DY**2)
     1+   (UY(I,JP1)-2.*UY(I,J)+UY(I,JM1))/(DZ**2)
   21 CONTINUE
      WRITE(6,10)
   10 FORMAT('1',10X,'PRESSURE GRADIENT IN Z-DIRECTION',///)
      CALL TPRINT(JJ1,II1,PSI,6)
      WRITE(6,25)
   25 FORMAT('1',10X,'PRESSURE GRADIENT IN Y-DIRECTION',///)
      CALL TPRINT(JJ1,II1,UYZ,6)
      RETURN
      END
```

APPENDIX F-1

Experimental Data For The Middle Part of the Channel

Run #1: all data points
Mode of Rotation: co-rotating
Number of Particles: 10
Total Data Points: 92

Particle Number	Data Point	Fractional Height*	Dimensionless Velocity**	
			Experimental	Numerical
1	1	0.0465	0.855	0.801
	2	0.0465	0.849	
	3	0.0465	0.8315	
2	1	0.1465	0.389	0.441
	2	0.1465	0.401	
	3	0.1465	0.412	
3	1	0.186	0.218	0.318
	2	0.186	0.206	
	3	0.186	0.206	
4	1	0.290	0.1328	0.0568
	2	0.290	0.129	
	3	0.290	0.1328	
	4	0.290	0.1328	
	5	0.290	0.106	

* Fractional Height is (r-R1)/(R2-R1)
** Dimensionless Velocity is based upon the root velocity

	6	0.290	0.118	
	7	0.290	0.1269	
	8	0.290	0.129	
	9	0.290	0.118	
	10	0.290	0.118	
	11	0.290	0.118	
	12	0.290	0.124	
	13	0.290	0.127	
	14	0.290	0.129	
	15	0.290	0.132	
	16	0.290	0.135	
	17	0.290	0.135	
	18	0.290	0.124	
	19	0.290	0.118	
	20	0.290	0.127	
	21	0.290	0.129	
	22	0.290	0.132	
	23	0.290	0.141	
5	1	0.367	-0.106	-0.084
	2	0.367	-0.0796	
6	1	0.403	-0.1415	-0.1405
	2	0.403	-0.1357	
	3	0.403	-0.1239	
	4	0.403	-0.1178	
	5	0.403	-0.1239	

	6	0.403	-0.1239	
	7	0.403	-0.1178	
	8	0.403	-0.1357	
	9	0.403	-0.1357	
	10	0.403	-0.1239	
	11	0.403	-0.1357	
	12	0.403	-0.1178	
	13	0.403	-0.1119	
	14	0.403	-0.1300	
	15	0.403	-0.1326	
	16	0.403	-0.1446	
	17	0.403	-0.1326	
	18	0.403	-0.1090	
7	1	0.450	-0.1889	-0.199
	2	0.450	-0.177	
	3	0.450	-0.166	
	4	0.450	-0.166	
	5	0.450	-0.168	
	6	0.450	-0.186	
	7	0.450	-0.180	
	8	0.450	-0.177	
	9	0.450	-0.186	
8	1	0.581	-0.323	-0.2925
	2	0.581	-0.305	
	3	0.581	-0.2919	

	4	0.581	-0.3008	
	5	0.581	-0.313	
	6	0.581	-0.310	
	7	0.581	-0.3008	
	8	0.581	-0.310	
9	1	0.760	-0.28	-0.269
	2	0.760	-0.289	
	3	0.760	-0.283	
	4	0.760	-0.292	
	5	0.760	-0.286	
10	1	0.860	-0.1533	-0.1877
	2	0.860	-0.170	
	3	0.860	-0.170	
	4	0.860	-0.1533	
	5	0.860	-0.1533	
	6	0.860	-0.1346	
	7	0.860	-0.1297	
	8	0.860	-0.1413	
	9	0.860	-0.1591	
	10	0.860	-0.1533	
	11	0.860	-0.1466	
	12	0.860	-0.1533	
	13	0.860	-0.1413	
	14	0.860	-0.1466	
	15	0.860	-0.1466	

16	0.860	-0.1297
17	0.860	-0.1413
18	0.860	-0.1640

Run #2: summarized data points
Mode of Rotation: co-rotating
Number of Particles: 9
Total Data Points: 74

Particle Number	Data Points	Fractional Height	Dimensionless Velocity	
			Experimental (average)	Numerical
1	3	0.1163	0.5733	0.54
2	3	0.1535	0.4482	0.42
3	8	0.233	0.2217	0.192
4	6	0.335	-0.0530	-0.032
5	10	0.472	-0.2353	-0.223
6	7	0.536	-0.2876	-0.272
7	5	0.593	-0.3146	-0.295
8	9	0.638	-0.3241	-0.303
9	23	0.744	-0.1256	-0.270

Run #3: summarized data points
Mode of Rotation: counter-rotating
Number of Particles: 8
Total Data Points: 58

Particle Number	Data Points	Fractional Height	Dimensionless Velocity	
			Experimental (average)	Numerical
1	3	0.070	0.661	0.709
2	5	0.151	0.459	0.425
3	11	0.43	-0.193	-0.176
4	9	0.470	-0.25	-0.22
5	6	0.500	-0.202	-0.246
6	6	0.651	-0.1795	-0.30
7	13	0.815	-0.079	-0.23
8	5	0.93	-0.1436	-0.104

Run #4: summarized data points
Mode of Rotation: counter-rotating
Number of Particles: 9
Total Data Points: 85

Particle Number	Data Points	Fractional Height	Dimensionless Velocity	
			Experimental (average)	Numerical
1	7	0.142	0.512	0.456
2	6	0.216	0.254	0.236
3	6	0.388	-0.132	-0.118
4	10	0.455	-0.179	-0.204
5	9	0.479	-0.219	-0.229
6	8	0.539	-0.276	-0.2734
7	5	0.618	-0.250	-0.300
8	6	0.679	-0.298	-0.299
9	28	0.942	-0.133	-0.092

APPENDIX F-2

Experimental Data For An End Region of the Channel

TABLE-1

Mode of Rotation: co-rotating
Particle: C
Total Data Points: 14
Particle Location: non-stagnant region

Data Point	Angle* degree	Fractional Height	Dimensionless Velocity**	
			Experimental (average)	Numerical
1	58.85	0.49		
2	53.9	0.486	0.251	0.248
3	52.6	0.49	0.265	0.249
4	51.5	0.5	0.274	0.253
5	50.25	0.5	0.28	0.258
6	49.05	0.51	0.29	0.27
7	47.65	0.52	0.30	0.285
8	46.5	0.54	0.32	0.31
9	44.9	0.555	0.366	0.349
10	43.4	0.57	0.366	0.36
11	41.8	0.60	0.41	0.399
12	40.0	0.625	0.472	0.43
13	38.1	0.666	0.487	0.461
14	36.25	0.695		

* angle is measured from the second screw land along the channel
** absolute value of the dimensionless velocity is used.

TABLE-2

Mode of Rotation: co-rotating
Particle: F
Total Data Points: 18
Particle Location: stagnant region

Data Point	Angle degree	Fractional Height	Dimensionless Velocity	
			Experimental (average)	Numerical
1	47.3	0.3225	0.1712	0.153
2	44	0.34	0.130	0.129
3	44	0.37	0.112	0.115
4	43.8	0.387	0.112	0.116
5	43.5	0.407	0.124	0.140
6	43	0.426	0.183	0.180
7	42.3	0.455	0.236	0.215
8	41.3	0.48	0.283	0.255
9	40.1	0.51	0.336	0.272
10	38.85	0.5483	0.36	0.34
11	37.3	0.58	0.384	0.335
12	35.75	0.606	0.40	0.355
13	34.0	0.622	0.39	0.40
14	32.5	0.606	0.43	0.42
15	31.05	0.537	0.53	0.77
16	29.5	0.447	0.53	0.61
17	28.55	0.36	0.436	0.59
18	28.0	0.286	0.33	0.325

TABLE-3

Mode of Rotation: counter-rotating
Particle: J
Total Data Points: 13
Particle Location: non-stagnant region

Data Point	Angle degree	Fractional Height	Dimensionless Velocity	
			Experimental (average)	Numerical
1	43.9	0.46		
2	43.2	0.44	0.221	0.394
3	42.5	0.40	0.246	0.41
4	41.8	0.37	0.246	0.41
5	41.0	0.333	0.253	0.42
6	40.5	0.295	0.246	0.38
7	39.6	0.26	0.215	0.355
8	39.0	0.23	0.196	0.28
9	38.6	0.20	0.170	0.25
10	38.4	0.172	0.145	0.146
11	39.0	0.155	0.145	0.146
12	39.6	0.137	0.196	0.179
13	40.7	0.125		

TABLE-4

Mode of Rotation: counter-rotating
Particle: R
Total Data Points: 8
Particle Location: stagnant region

Data Point	Angle degree	Fractional Height	Dimensionless Velocity	
			Experimental (average)	Numerical
1	35.2	0.49		
2	34.25	0.43	0.436	0.465
3	32.8	0.365	0.487	0.525
4	31.0	0.31	0.48	0.505
5	29.15	0.27	0.48	0.605
6	27.2	0.24	0.461	0.56
7	25	0.2175	0.404	0.435
8	21.5	0.20		

APPENDIX G

Complementary Planes for the Down Channel Velocity Profile

In chapter IX an expression for the down channel velocity, Vzs, with respect to the stationary second screw lands was developed, and is given by equation 9.8:

$$V_{zs} = a(2-3a)\,V_b \sin\theta\tan\theta + (1-a)(3a-1)V_r/\cos\theta \qquad (9.8)$$

where a is the fractional height of a plane of interest measured from the screw root; Vb and Vr are the linear speeds $\pi D_2 N$ and $\pi D_1 N$ respectively; D_1 and D_2 are the root and barrel diameters respectively; and N is the angular velocity.

Equation 9.8 can be represented in dimensionless form as:

$$\bar{V}_{zs} = \frac{V_{zs}}{V_r} = a(2-3a)\frac{V_b}{V_r}\sin\theta\tan\theta + \frac{(1-a)(3a-1)}{\cos\theta} \qquad (G-1)$$

Simplifying further yields:

$$\bar{V}_{zs} = -(3pa^3 + 2qa + r) \qquad (G-2)$$

where constants p, q, and r are:

$$p = \frac{V_b}{V_r}\sin\theta\tan\theta + \frac{1}{\cos\theta} \qquad (G-3)$$

$$q = -\left(\frac{V_b}{V_r}\sin\theta\tan\theta + \frac{2}{\cos\theta}\right) \qquad (G-4)$$

$$r = 1/\cos\theta \qquad (G-5)$$

Consider a particle in Fig 9.1b at a fractional height a_ℓ from the screw root such that a_ℓ is less than a_D Let a_ℓ^* be the fractional height of its complementary plane as shown in the same figure. Since the net flow in the down channel direction is zero and for laminar flow the streamlines do not cross each other, the flow rate from the screw root to the fractional level a_ℓ must be equal to the flow rate between the fractional levels a_ℓ^* and a_F; or mathematically,

$$HW \int_0^{a_\ell} \bar{V}_{zs}\, da = - HW \int_{a_\ell^*}^{a_F} \bar{V}_{zs}\, da \qquad (G-6)$$

where W is the channel width. The streamline corresponding the level a_F is the same as for the screw root, and separates the lower region from the upper. Now, from equations G-2 and G-6, it can be shown that,

$$p a_\ell^{*3} + q a_\ell^{*2} + r a_\ell^* = p a_F^3 + q a_F^2 + r a_F + p a_\ell^3 + q a_\ell^2 + r a_\ell \qquad (G-7)$$

The only unknown in equation G-7 is the fractional height a_F, and it can be determined by equating the flow rate from the screw root to the level a_F to zero; or mathematically,

$$\int_0^{a_F} \bar{V}_{zs}\, da = 0 \qquad (G-8)$$

The resulting integration can be shown to yield:

$$a_F = \frac{1}{1+\frac{V_b}{V_r}\sin^2\theta} \qquad (G\text{-}8a)$$

Similarly expressions for a_D and a_B can be obtaind to yield:

$$a_D = \frac{2+\frac{V_b}{V_r}\sin^2\theta - \left(\left(\frac{V_b}{V_r}\sin^2\theta\right)^2 + \frac{V_b}{V_r}\sin^2\theta + 1\right)^{0.5}}{3\left(1+\frac{V_b}{V_r}\sin^2\theta\right)} \qquad (G\text{-}8b)$$

$$a_B = \frac{2+\frac{V_b}{V_r}\sin^2\theta + \left(\left(\frac{V_b}{V_r}\sin^2\theta\right)^2 + \frac{V_b}{V_r}\sin^2\theta + 1\right)^{0.5}}{3\left(1+\frac{V_b}{V_r}\sin^2\theta\right)} \qquad (G\text{-}8c)$$

Thus, with a_F known, the cubic equation G-7 can be solved for a_l^*. Conversely, for any given a_l^*, a_l can be determined using the same equation.

For a particle at a fractional height a_u, the net flow from the level a_F to a_u must be equated to that from the fractional height a_u^* to the barrel surface, or,

$$\int_{a_F}^{a_u} \bar{V}_{zs}\, da = -\int_{a_u^*}^{1} \bar{V}_{zs}\, da \qquad (G\text{-}9)$$

and the resulting cubic equation in a_u^* in this case becomes:

$$p a_u^{*3} + q a_u^{*2} + r a_u^* = (p a_u^3 + q a_u^2 + r a_u + p + q + r) - (p a_F^3 + q a_F^2 + r a_F) \qquad (G\text{-}10)$$

The equation G-10 can also be used to determine a_u if a_u^* is given.